E-16-653

NASA LANGLEY FINAL TECHNICAL REPORT
NAG 1-133 (3/1/81 - 2/28/82)

DEVELOPMENT OF ANALYTICAL TECHNIQUE FOR THE OPTIMIZATION OF JET ENGINE AND DUCT ACOUSTIC LINERS

By
Ben T. Zinn
and
William L. Meyer

GEORGIA INSTITUTE OF TECHNOLOGY
A UNIT OF THE UNIVERSITY SYSTEM OF GEORGIA
SCHOOL OF AEROSPACE ENGINEERING
ATLANTA, GEORGIA 30332

1982

NASA LANGLEY FINAL TECHNICAL REPORT
NAG 1-133 (3/1/81 - 2/28/82)

DEVELOPMENT OF AN ANALYTICAL TECHNIQUE FOR THE OPTIMIZATION OF JET ENGINE AND DUCT ACOUSTIC LINERS

BY

Ben T. Zinn

and

William L. Meyer

SCHOOL OF AEROSPACE ENGINEERING
GEORGIA INSTITUTE OF TECHNOLOGY
Atlanta, GA 30332

ABSTRACT

This report summarizes the work performed during the NASA LANGLEY research program entitled "Development of an Analytical Technique for the Optimization of Jet Engine and Duct Acoustic Liners." This research program ran for one year (3/1/81-2/28/82) and carries the NASA number NAG 1-133. Detailed results of the work performed during the first six months of this contract are presented in the NASA LANGLEY SEMI-ANNUAL STATUS REPORT (3/1/81-8/31/81) for NAG 1-133 and thus will not be repeated here in its entirety.

During the past six months, a new method was developed for the calculation of optimum constant admittance solutions for the minimization of the sound radiated from an arbitrary axisymmetric body. This method utilizes both the integral equation technique used in the calculation of the optimum non-constant admittance liners and the independent solutions generated as a by product of these calculations. The results generated by both these methods are presented for three duct geometries: (1) a straight duct; (2) the QCSEE inlet; and (3) the QCSEE inlet less its centerbody.

TABLE OF CONTENTS

I. INTRODUCTION

The object of this research program was the development of an analytical technique for the determination of the optimum admittance distribution along the wall of an axisymmetric duct for the minimization of sound radiated from the duct given a specific source of acoustic radiation in the duct. The results of this method were to be checked against calculations performed for constant admittance liners to see if better results could be obtained with the new method. Finally, a parametric study was to be done, based on wave number, for at least two geometries in which the optimum constant and distributed admittance liners were to be calculated.

The formulation of the problem which has been used in the parametric study is presented in detail in Chapter IV of the previous six month status report for this grant (See Reference 1.). This being the case, the precise mathematical formulation of the method will not be repeated. Instead, only a brief overview of the method will be presented here.

The method itself is based upon a special integral formulation of the external solutions of the Helmholtz equation. The basic formulation of the governing equations for three dimensions is given in great detail in Reference 2. This formulation can be specialized for axisymmetric bodies[3] and it is this form of the equations which is used in this study.

These integral equations govern the acoustic quantities on the surface of the body and take into account the Sommerfeld radiation conditions at infinity in the field so that only outgoing, decaying solutions are considered. To solve these equations, the surface of the body is discretized into many small areas and since

the problem is elliptic in nature a boundary condition is applied over each small area. The boundary condition specified may be either the acoustic potential which is directly related to the acoustic pressure, the normal acoustic velocity, or a ratio of these two quantities referred to as the effective acoustic admittance at each point.

When this is done, a system of linear equations can be developed in which the acoustic potential or the normal acoustic velocity is the unknown at each point on the body depending on which boundary condition is specified there. The boundary conditions themselves contribute to the inhomogeneous term in each equation and in some cases the diagonal term of the matrix.

Since the resulting equations are linear, the solutions may be superimposed. Also, if the boundary conditions are chosen appropriately they do not effect the matrix coefficients, only the inhomogeneous vector terms. It is these two characteristics of this formulation which are exploited in both the calculation of the optimum varying admittance for a duct and the optimum constant admittance.

Normally to find the optimum constant admittance for a duct, a parametric study must be done in which the real and imaginary parts of the admittance of the liner are varied. Usually, this means that a complete, separate solution must be generated for each admittance value; however, a method has been developed which utilizes the same independent solutions on the admittance surface which were generated for the calculation of the optimum varying admittance solution. This new method greatly reduces the amount of computing time required for the generation of constant admittance solutions and is presented in detail in the following section of this report.

Having developed both the theory and the computer codes for the generation of both optimum constant and varying admittance liners for general finite axisymmetric ducts, a parametric study was performed on three separate duct geometries. The three duct geometries are: (1) a straight duct with a rounded lip; (2) the NASA QCSEE inlet of Reference 4; and (3) the NASA QCSEE inlet less its centerbody. The results of this parametric study are presented at six wave numbers for each geometry at which both the constant and varying optimum admittance liners are calculated for both constant acoustic potential and constant normal acoustic velocity drivers.

II. CALCULATION OF OPTIMUM CONSTANT ADMITTANCE LINERS

In this section, we will briefly go over the generation of the independent solutions on the surface of the body. Then, the development of constant admittance solutions will be discussed in detail. Since the development of the special integral formulation of the external solutions of the Helmholtz equation is given in References 1-3, only the final form of the equations will be presented here. It will be noted that although this form of the equations has been specialized for axisymmetric geometries, that any cylindrically symmetric acoustic mode may be calculated.

Firstly, let us define the geometrical variables that we will use on a surface of revolution. In Fig. 1, the coordinate system employed on the body S is given (ρ , Z,Θ) along with an outward normal from the body, $\vec{n}$, and an element of area on the surface of the body, $\rho\, ds\, d\Theta$. The variable s is the distance along the generating line of the surface of revolution and is assumed to go from o at one end of the body to ℓ at the other.

We now assume that the acoustic potential on the surface of a body of revolution can be written as

$$\Phi(\rho, Z, \Theta) = \phi(s) \cos(m\Theta)$$

and similarly that the normal acoustic velotiy on the surface of the body can be written as

$$\frac{\partial \Phi(\rho, Z, \Theta)}{\partial \vec{n}} = V(s) \cos(m\Theta)$$

In doing this we have incurred no loss in generality. Since all of the equations are linear, any acoustic radiation pattern may be generated as a sum of these simple, cylindrically symmetric patterns. Also, the variable m is commonly referred to as the tangential acoustic mode number.

In order to write the equation in compact form we now define three sets of functions:

Influence functions:

$$I_1(r_{pq}) = 2\int_o^{\pi} G(P, Q) \cos(m\theta_q)\, d\theta_q$$

$$I_2(r_{pq}) = 2\alpha\int_o^{\pi} \frac{\partial G(P, Q)}{\partial \vec{n}_p} \cos(m\theta_q)\, d\theta_q \qquad (3)$$

Kernel Functions:

$$K_1(r_{pq}) = 2\int_o^{\pi} \frac{\partial G(P, Q)}{\partial \vec{n}_q} \cos(m\theta_q)\, d\theta_q$$

$$K_2(r_{pq}) = 2\alpha\int_o^{\pi} \frac{\partial^2 G(P, Q)}{\partial \vec{n}_p\, \partial \vec{n}_q} \cos(m\theta_q)\, d\theta_q, \qquad (4)$$

$$\theta_q \neq \theta_p$$

Forcing functions:

$$F_1(r_{pq}) = 2\alpha\int_o^{\pi} G(P,Q)\,(ik)^2(\vec{n}_p \cdot \vec{n}_q)\, d\theta_q$$

$$F_2(r_{pq}) = 2\alpha\int_o^{\pi} \frac{\partial^2 G(P,Q)}{\partial \vec{n}_p\, \partial \vec{n}_q}\, d\theta_q, \qquad (5)$$

$$\theta_q \neq \theta_p$$

where r_{pq} is the distance between points P and Q and $\vec{n}_p$ and $\vec{n}_q$ are the outward normals from the points P and Q, respectively (See Fig. 2.). Also, G(P,Q) is the free space Green's function

$$G(P,Q) = \frac{e^{ikr_{pq}}}{r_{pq}} \tag{6}$$

where k is the wave number and α is the complex coupling constant for this particular formulation which is found to be

$$\alpha = i/k \tag{7}$$

It will be noted that in evaluating K_2 and F_2 the point at which $\Theta_p = \Theta_q$ is excluded from the integration as it constitutes a strong sigularity.

Using the above definitions and equations, the special integral formulation of the external solutions of the Helmholtz equation may be written as

$$\int_o^{\ell} \phi(s_q)\left[K_1(r_{pq}) + K_2(r_{pq})\right]\rho_q\, ds_q$$

$$- \phi(s_p)\int_o^{\ell} \left[F_1(r_{pq}) + F_2(r_{pq})\right]\rho_q\, ds_q$$

$$-\int_o^{\ell} V(s_q)\left[I_1(r_{pq}) + I_2(r_{pq})\right]\rho_q\, ds_q \tag{8}$$

$$= 2\pi\left[\phi(s_p) + \alpha V(s_p)\right]$$

In this particular formulation of the problem the s and θ coordinate directions have been uncoupled so that the solution of the problem has been reduced to the evaluation of line integrals on the surface of the body.

Equation (8) represents a relationship between the acoustic pressure and normal acoustic velocity at any given point on a body (i.e., point P) to all of the values everywhere else on the body (i.e., at the Q points). If this equation is applied at each point on the body, along with the boundary condition at each point, a system of linear algebraic equations is obtained for the unknown variables at each point on the body. Thus, if there are N points on the body, a system of N complex equations in N complex unknowns is developed.

In the numerical integration of the functions (See Eqns. (3)-(5).) a Gauss-Legendre integration formula is used. For the integration in the s direction, a simple two point integration is employed such that the point P is never actually equal to any of the integration points (i.e., the Q points). Also, when the body is divided into N points in the s direction, both the acoustic potential ϕ and the normal acoustic velocity V are assumed to be constant over each element even though there are two integration points per element.

For the development of the independent solutions on the surface of the body let us assume that the body is divided into three distinct regions as in Fig. 3. These regions do not necessarily have to be contiguous however, for the sake of clarity they are presented as such here. The first solution which we must consider is the driver solution. To calculate it we must solve for the acoustic quantities on the surface of the body subject to the boundary conditions

$$\phi(Q) = \tilde{\phi}_D(Q) \qquad \text{on } S_D$$

$$V(Q) = 0 \qquad \text{on } S_H \text{ and } S_L \tag{9}$$

where $\tilde{\phi}_D$ (Q) is some specified function of the acoustic potential on the driver. Solving this problem, we obtain the driver solution

$$\begin{aligned} & V_D(Q) \qquad \text{on } S_D \\ & \phi_D(Q) \qquad \text{on } S_H \text{ and } S_L \end{aligned} \tag{10}$$

Next, the liner surface(s) is divided up into M finite regions as in Fig. 4. Then M independent solutions are generated which represent the effect of M simple acoustic velocity sources on the liner using the boundary conditions given below

$$\begin{aligned} & \phi\,(Q) = 0 \quad \text{on } S_D \\ & V(Q) = 0 \text{ on } S_H \\ & \left.\begin{aligned} V(Q_j) &= 1 \qquad j = 1,\ldots, M \\ V(Q_i) &= 0 \qquad i \neq j \end{aligned}\right\} \text{ on } S_L \end{aligned} \tag{11}$$

The M solutions thus generated are given by

$$\begin{aligned} &V_j(Q) && \text{on } S_D \\ &\phi_j(Q) && \text{on } S_H \\ &\phi_j(Q) && \text{on } S_L \end{aligned} \tag{12}$$

If we now sum these solutions multiplied by some arbitrary coupling constants designated by a_j, which we can do as the problem is linear,we generate a general solution which has the form

$$\begin{aligned} &\phi(Q) = \tilde{\phi}(Q) \\ &V(Q) = V_D(Q) + \sum_{j=1}^{M} a_j V_j(Q) && \text{on } S_D \end{aligned} \tag{13}$$

$$\begin{aligned} &\phi(Q) = \phi_D(Q) + \sum_{j=1}^{M} a_j \phi_j(Q) \\ &V(Q) = 0 && \text{on } S_H \end{aligned} \tag{14}$$

$$\begin{aligned} &\phi(Q) = \phi_D(Q) + \sum_{j=1}^{M} a_j \phi_j(Q) \\ &V(Q_j) = a_j \qquad j=1,\ldots,M \qquad \text{on } S_L \\ &V(Q_j) = 0 \qquad i \neq j \end{aligned} \tag{15}$$

It will be noted here that the above solution has some interesting properties in that the acoustic potential on the driver surface (See Eqn. (13).) and the normal acoustic velocity on the hard walled surface (See Eqn. (14).) are not dependent upon the choice of the coupling constants a_j.

In this study we are interested in the effective acoustic admittance Y which is defined as

$$Y = \frac{\frac{\partial \Phi}{\partial \vec{n}}}{\Phi} = \frac{V}{\Phi} \tag{16}$$

This being the case, we can now represent the effective acoustic admittance at any point on the admittance surface as

$$Y(Q_j) = \frac{a_j}{\phi_D(Q_j) + \sum_{i=1}^{M} a_i \phi_i(Q_j)} \tag{17}$$

If we now specify that the effective acoustic admittance at all points on the admittance surface is to be the complex number C we obtain

$$\sum_{i=1}^{M} a_i \phi_i(Q_j) - \frac{1}{C} a_j = \phi_D(Q_j), \tag{18}$$

$$j = 1, \ldots, M$$

which represents a system of M linear complex equations for the M complex coupling constants, a_j. Using this method many constant admittance solutions can be generated very economically once the independent solutions on the surface of the body are known. Since the independent solutions have already been calculated for the generation of the optimum varying admittance, a relatively small amount of extra computing time is required for the determination of the optimum constant admittance solution.

To find the optimum constant admittance solution for a specified geometry, driver and wave number, the values of C are chosen in a grid pattern and a solution is generated for each value. Once the surface solution is known it is an easy job to calculate the acoustic power radiated from the driver and the acoustic power lost to the admittance surface using[1,5]

$$E \propto \iint_{S_L} \left[\phi^R(Q)\, v^I(Q) - \phi^I(Q)\, v^R(Q) \right] dS(Q) \tag{19}$$

where E is the acoustic energy radiated out of a surface and the superscripts R and I refer to the "real and imaginary part of", respectively. When the solution having the minimum radiated power is found, the region may be further subdivided to "home in" on the optimal value of the admittance.

It is of interest to note here that strictly speaking all possible values of the effective admittance Y are not possible at each point on the liner surface. To demonstrate this, let us look at the point j=1 on the liner surface where

$$\bar{Y}(Q_1) = \frac{a_1}{\phi_D(Q_1) + \sum_{i=1}^{M} a_i\, \phi_i(Q_1)} \tag{20}$$

Solving for a_1 we obtain

$$a_1 = \frac{Y(Q_1) \sum_{i=2}^{M} a_i \phi_i (Q_1)}{1 - Y(Q_1) \phi_1 (Q_1)} \qquad (21)$$

where it can be seen that if we want $Y(Q_1) = \frac{1}{\phi_j(Q_j)}$ we must hava $a_1 \to \infty$. Thus, we cannot generate the solution where the effective admittance $Y(Q_j) = \frac{1}{\phi_j (Q_j)}$ with a finite value for the complex coupling constant, a_j.

III. SOME GENERAL COMMENTS

The problem of acoustic radiation from a duct, as formulated for this study, is strictly elliptic so that only one boundary condition may be specified on any part of the body. Thus, either the acoustic potential (i.e., pressure) or the normal acoustic velocity may be specified on the driver but not both. This leads us to an interesting problem when trying to compare the results of this method to any other as other methods utilize the mathematical artifice of a semi-infinite duct.[6] This artifice allows them to keep the driver power and modal input constant while varying the acoustic properties of a liner. This tends to neglect any possible effect the acoustic properties of the liner could have on the amount or modal content of the power coming out of the driver.

In the problem, as formulated for this study, the driver power and more importantly the radial modal output of the driver cannot be fixed as this would overspecify the problem. This being the case, there are two possible optimum constant admittance liners possible, one a relative measure of the percent of the driver power attenuated by the liner and the other an absolute measure of the power coming out of the duct. Both were calculated at each wave number for each geometry and are presented as such (i.e., Relative and Absolute optimum constant admittances). Also, since either the acoustic potential or the normal acoustic velocity could be specified on the driver runs were done with each and are noted as such. For the runs where the normal acoustic velocity is specified on the driver, the acoustic potential is specified on the admittance (i.e., liner) surface and vice versa (See Eqns. (9) and (11).).

IV. NUMERICAL CONSIDERATIONS

The special integral formulation of the external solutions of the Helmholtz equation[2,3] which is used as the basis for all of the calculations done in this study requires a closed body. Thus, all three of the ducts used in this study: the straight duct with the rounded lip; the NASA QCSEE inlet; and, the NASA QCSEE inlet less its centerbody were terminated with a 2:1 ellipse (See Figs. 5-7.). Also, for the three geometries investigated the total height to the inner wall of the duct at the driver plane was normalized to one and the outer wall of the duct was 1.15. All of the ducts have an L/a of 2.0

For the numerical calculations , points were spaced evenly along the inner walls of the ducts with a nominal spacing of 0.05a. On the outer walls of the ducts, the points were systematically spaced at larger and larger intervals as it has been found that the outer walls of ducts and their terminations have little effect on the total power radiated and the radiation pattern in the forward half plane. The total number of points used on the three geometries in the s direction for the calculations performed for this study were: 92 points for the straight duct; 108 points for the NASA QCSEE inlet; and, 100 points for the NASA QCSEE inlet less its centerbody. For the Θ integration, a 32-point Gauss-Legendre integration formula was used in all cases.

For all three of the ducts, the admittance surface consisted of 25 points or intervals over which the optimum admittance distributions were to be generated and ran from 0.4a to 1.6a in the Z direction along the inner walls of the ducts.

Thus, a hard wall or driver solution and 25 independent source solutions were calculated for each geometry, wave number and type of driver specified (i.e., potential or velocity).

V. RESULTS

Each of the geometries was run with a plane wave as input on the driver for non-dimensional wave numbers of 1, 2, 3, 5, 7, and 10. That is, in all of the cases run, the tangential mode number was taken as zero. Although a plane wave was input, a plane wave driver did not necessarily result since only one variable could be specified at a time.

The results for all of the straight duct runs are presented in Tables I-VI and in Figs. 8-13. In the Tables, the power radiated out of the driver and the power radiated into the field are tabulated along with their values, for the optimum distributed admittance and for the optimum absolute and relative constant admittances. In all the Tables, the power values are relative as they have been normalized by the power out of the hard walled configuration. Also, each table contains the results for one wave number for both the constant acoustic pressure and normal acoustic velocity drivers.

It will be of interest to note here that for the lower wave numbers, the power out of the driver is negative (i.e., it is damping). This necessarily means that the liner surface is driving since the formulation of the integral equations only allows for the case where there is a net flow of power out of the body (i.e., no incoming waves). If the imaginary part of the effective admittance Y (See Eqn. (16).) is positive, this denotes driving; that is, an active suppressor. The relative optimum constant admittance must always be a damping admittance since it is determined as the smallest ratio of power out of the driver, to the power lost to the admittance surface.

In general, it is found that the lowest power output is obtained from the optimum admittance distribution. Also, the relative constant admittance usually has the highest power output as measured in the field surrounding the duct.

Each Figure constitutes a set of 6 plots for each wave number. The first group of three plots in each set are for the case where a constant acoustic pressure is specified on the driver and the second group is for the case where a constant normal acoustic velocity was specified. The first plot in each group (e.g., Figs. 8a & d), contains a plot of the optimum admittance distribution on the inner wall of the duct from the driver end Z=0.4a (inner), to the open end, Z=1.6a (outer). As can be seen even at the low wave numbers where there are a more than sufficient number of points on the body to generate an accurate solution, the effective admittance distribution is not very smooth. This is because it is a ratio of two functions on the surface of the body which tends to make it less continuous than either generating function. Of course, more points could be taken on the surface of the body to obtain a smoother function for the effective admittance; however, this would not substantially change the overall accuracy of the solution (i.e., the power output). At the higher wave numbers, the solution does become suspect however, and more points should probably have been used for the cases where ka=7 and 10. This should not detract from the overall validity of the method however.

It will be noted that at the lower wave numbers, the distributed admittance found for the minimum power out of the body is totally driving. As the wave number gets higher, the optimum admittance distribution becomes mixed (i.e., some of the liner surface drives and some of it damps) and finally at some of the higher wave numbers, the distributed admittance is almost totally passive. This

is probably due to the fact that at the higher wave numbers, the wave structure in the duct becomes more complicated so that interference patterns are more difficult to set up. Since an active suppressor damps out sound through the setting up of interference patterns, these types of suppressors are probably only useful at lower wave numbers where the wave patterns are less complicated. Also, since it is more difficult to set up interference patterns with the constraint of a constant admittance liner, the optimum absolute constant admittance liner transition from driving to damping occurs sooner.

In the second plot in each group of three, is a plot of the absolute power out of the duct as a function of the admittance (constant) on the liner surface which is expressed in dB. The admittance value for which the minimum power out of the duct is obtained is marked with a large dot. Again, these values are tabulated in the tables (See Tables I-VI.).

In the final plot in each group of three, is a plot of the relative power out of the duct as a function of admittance (constant) on the liner which is also expressed in dB. Only negative values of the imaginary part of the admittance are considered in this case as the power out of the duct is referrenced to the power out of the driver. As with the previous plot, the admittance value, for which the minimum percent power is radiated, is marked with a large dot and those values also are tabulated in the Tables.

The results for the QCSEE inlet are presented in Tables VII-XII and in Figs. 14-19. As with the straight duct, the tables contain the results for the six wave numbers run, one wave number per table. The results at a non-dimensional wave number of ka=7.0 for the case where the acoustic potential is specified on the driver are not included since the optimum values for the absolute and relative

constant admittances fell outside of the initial search pattern. This pattern ran from -10 to 10 in increments of 1 for both the real and imaginary parts of the admittance. This is not to imply that they couldn't be calculated, just that they were not, since this would have required modification of the computer programs used for all of the other cases run.

As with the straight duct, each figure for this geometry consists of the six plots done for each wave number. As before, the optimum admittance distribution for both the constant acoustic pressure and the constant normal acoustic velocity drivers are presented along with the contour power plots for the constant absolute and relative admittance liners. Again, the optimum values are marked with dots in these plots and are tabulated in the Tables. It will be noted in Fig. 18a and b that these points are not marked since they fell outside the range of the plots.

The results for the QCSEE inlet less its centerbody are presented in Tables XIII-XVIII and in Figs. 20-25. The reason for running the cases for this particular geometry was to see if any trends could be established in going from the straight duct geometry to the full inlet geometry. At the lower wave numbers, the optimum admittance values calculated for it, seem to fall between those for the other two geometries as one would intuitively expect; however, this trend is not maintained at the higher wave numbers.

VI. SUMMARY AND CONCLUSIONS

During the past year, a method was developed for the calculation of optimum distributed admittance duct liners. This method is based upon a special integral representaiton of the external solutions of the Helmholtz equation which is valid (i.e., can be used to generate the correct, unique solutions) at all wave numbers. The equations used had been specialized for axisymmetric geometries but this is not a restriction on the method itself.

As a by-product of this method, a procedure was developed for the identification of optimum constant admittance duct liners. This procedure utilizes solutions already developed for the optimum distributed admittance calculation. At present, it entails the use of a simple search pattern for the optimum constant admittance; however, it is believed that this could be refined if time allowed.

To give some idea of the time involved in calculating these results , some typical computing times are presented below. These runs were done on the Georgia Tech CDC CYBER 760 and the programs are written in Fortran V. For the case where 100 points were used on the body in the s direction, a 32 point Gauss-Legendre integration formula was used in the Θ direction (See Fig. 1.), and there were 25 points on the liner surface, the calculation of the 26 independent solutions required for the optimization procedure took 185 seconds of CPU time. The generation of the optimum distributed admittance then took an additional 10 seconds and the identification of the optimum constant admittances took 390 seconds. As can be seen, the calculation of the constant admittance solutions is slow compared to the calculation of the optimum distributed admittance. The contour plots of the sound radiated for each constant admittance chosen on the

liner surface were done with the GPCP (General Purpose Contour Plotting) package which we have available here at Georgia Tech. It was developed originally for plotting contour maps but was found to be very useful in this research program.

In conclusion, an effective, efficient method has been developed for the calculation of both optimum distributed and constant admittance liners for general geometries. It was found through the use of this method that even very similar geometries may have vastly different optimum liners associated with them. Also, it was found that at low wave numbers often the most efficient liners for the reduction of the sound radiated are active and not passive. At the higher wave numbers, the optimum distributed admittances are found to be almost always a combination of both active and passive elements.

REFERENCES

1. Zinn, B.T. and Meyer, W.L., "Development of an Analytical Technique for the Optimization of Jet Engine and Duct Acoustic Liners," NASA Langley Semi-Annual Status Report for grant NAG 1-133, (3/1/81-8/31/81).

2. Meyer, W.L., Bell, W.A., Stallybrass, M.P. and Zinn, B.T., "Boundary Integral Solutions of Three Dimensional Acoustic Radiation Problems," Journal of Sound and Vibration, Vol. 59, No. 2, July 1978, pp. 245-262.

3. Meyer, W.L., Bell, W.A., Stallybrass, M.P. and Zinn, B.T., "Prediction of the Sound Field Radiated from Axisymmetric Surfaces," Journal of the Acoustical Society of America, Vol. 65, No. 3, March 1979, pp. 631-638.

4. Miller, B.A., Dastoli, B.J. and Wesoky, H.L., "Effect of Entry-Lip Design on Aerodynamics and Acoustics of High-Throat-Mach-Number Inlets for the Quiet, Clean, Short-Haul Experimental Engine," NASA TM X-3222, May 1975.

5. Morse, P.M. and Ingard, K.U., Theoretical Acoustics, McGraw-Hill, New York, 1969.

6. Rice, E.J., "Spinning Mode Sound Propagation in Ducts with Acoustic Treatment and Sheared Flow," NASA TM X-71672, March 1975.

TABLE I

STRAIGHT DUCT

Relative power normalized with respect to the hard walled radiated power

ka = 1.0

	Constant Phi on the Driver	Constant Velocity on the Driver
OPTIMUM ADMITTANCE DISTRIBUTION		
POWER OUT OF THE DRIVER	-0.57	-0.67
TOTAL POWER IN FAR FIELD	0.000017	0.000042
ABSOLUTE CONSTANT ADMITTANCE	(-0.18, 4.88i)	(-1.32, 4.60i)
POWER OUT OF THE DRIVER	-0.64	-0.53
TOTAL POWER IN FAR FIELD	0.0014	0.00063
RELATIVE CONSTANT ADMITTANCE	(-1.30, -3.40i)	(-1.34, -3.33i)
POWER OUT OF THE DPIVER	0.87	0.65
TOTAL POWER IN FAR FIELD	0.0015	0.0012

TABLE II

STRAIGHT DUCT

Relative power normalized with respect to the hard walled radiated power

ka = 2.0

	Constant Phi on the Driver	Constant Velocity on the Driver
OPTIMUM ADMITTANCE DISTRIBUTION		
POWER OUT OF THE DRIVER	-0.65	-0.61
TOTAL POWER IN FAR FIELD	0.00012	0.00014
ABSOLUTE CONSTANT ADMITTANCE	(-2.95, 3.05i)	(-2.70, -2.90i)
POWER OUT OF THE DRIVER	-0.89	0.75
TOTAL POWER IN FAR FIELD	0.00034	0.00054
RELATIVE CONSTANT ADMITTANCE	(-2.64, -3.14i)	(-2.65, -3.13i)
POWER OUT OF THE DRIVER	0.91	0.78
TOTAL POWER IN FAR FIELD	0.00088	0.00068

TABLE III

STRAIGHT DUCT

Relative power normalized with respect to the hard walled radiated power

ka = 3.0

	Constant Phi on the Driver	Constant Velocity on the Driver
OPTIMUM ADMITTANCE DISTRIBUTION		
POWER OUT OF THE DRIVER	-0.23	-0.016
TOTAL POWER IN FAR FIELD	0.000075	0.00011
ABSOLUTE CONSTANT ADMITTANCE	(-2.71, -2.38i)	(-2.65, -2.33i)
POWER OUT OF THE DRIVER	0.77	0.13
TOTAL POWER IN FAR FIELD	0.00072	0.00014
RELATIVE CONSTANT ADMITTANCE	(-2.70, -2.39i)	(-2.65, -2.32i)
POWER OUT OF THE DRIVER	0.77	0.13
TOTAL POWER IN FAR FIELD	0.00079	0.00013

TABLE IV

STRAIGHT DUCT

Relative power normalized with respect to the hard walled radiated power

ka = 5.0

	Constant Phi on the Driver	Constant Velocity on the Driver
OPTIMUM ADMITTANCE DISTRIBUTION		
POWER OUT OF THE DRIVER	-0.0011	0.0075
TOTAL POWER IN FAR FIELD	0.00084	0.000011
ABSOLUTE CONSTANT ADMITTANCE	(-3.48, -1.66i)	(-4.61, -2.29i)
POWER OUT OF THE DRIVER	1.00	0.043
TOTAL POWER IN FAR FIELD	0.37	0.010
RELATIVE CONSTANT ADMITTANCE	(-4.13, -1.77i)	(-4.44, -2.38i)
POWER OUT OF THE DRIVER	1.06	0.043
TOTAL POWER IN FAR FIELD	0.37	0.010

TABLE V

STRAIGHT DUCT

Relative power normalized with respect to the hard walled radiated power

ka = 7.0

	Constant Phi on the Driver	Constant Velocity on the Driver
OPTIMUM ADMITTANCE DISTRIBUTION		
POWER OUT OF THE DRIVER	0.066	0.014
TOTAL POWER IN FAR FIELD	0.00064	0.054
ABSOLUTE CONSTANT ADMITTANCE	(-5.17, -1.95i)	(-4.72, -0.89i)
POWER OUT OF THE DRIVER	1.29	0.016
TOTAL POWER IN FAR FIELD	0.43	0.0078
RELATIVE CONSTANT ADMITTANCE	(-5.56, -1.30i)	(-3.97, -1.76i)
POWER OUT OF THE DRIVER	1.42	0.019
TOTAL POWER IN FAR FIELD	0.42	0.0086

TABLE VI

STRAIGHT DUCT

Relative power normalized with respect to the hard walled radiated power

ka = 10.0

	Constant Phi on the Driver	Constant Velocity on the Driver
OPTIMUM ADMITTANCE DISTRIBUTION		
POWER OUT OF THE DRIVER	0.050	0.00066
TOTAL POWER IN FAR FIELD	0.0049	0.00016
ABSOLUTE CONSTANT ADMITTANCE	(-5.65, -2.80i)	(-4.89, -2.69i)
POWER OUT OF THE DRIVER	1.02	0.010
TOTAL POWER IN FAR FIELD	0.48	0.0051
RELATIVE CONSTANT ADMITTANCE	(-5.41, -2.75i)	(-5.02, -2.83i)
POWER OUT OF THE DRIVER	1.02	0.010
TOTAL POWER IN FAR FIELD	0.48	0.0051

TABLE VII

NASA QCSEE INLET

Relative power normalized with respect to the hard walled radiated power

ka = 1.0

	Constant Phi on the Driver	Constant Velocity on the Driver
OPTIMUM ADMITTANCE DISTRIBUTION		
POWER OUT OF THE DRIVER	-1.91	-2.45
TOTAL POWER IN FAR FIELD	0.00012	0.00012
ABSOLUTE CONSTANT ADMITTANCE	(-0.64, 4.03i)	(-0.65, 4.11i)
POWER OUT OF THE DRIVER	-1.25	-0.74
TOTAL POWER IN FAR FIELD	0.0015	0.00082
RELATIVE CONSTANT ADMITTANCE	(-0.47, -3.78i)	(-0.53, -3.77i)
POWER OUT OF THE DRIVER	1.27	0.79
TOTAL POWER IN FAR FIELD	0.0019	0.0011

TABLE VIII

NASA QCSEE INLET

Relative power normalized with respect to tne hard walled radiated power

ka = 2.0

	Constant Phi on the Driver	Constant Velocity on the Driver
OPTIMUM ADMITTANCE DISTRIBUTION		
POWER OUT OF THE DRIVER	-1.11	-0.70
TOTAL POWER IN FAR FIELD	0.00011	0.000060
ABSOLUTE CONSTANT ADMITTANCE	(-2.99, 3.91i)	(-3.06, 3.58i)
POWER OUT OF THE DRIVER	-0.79	-0.53
TOTAL POWER IN FAR FIELD	0.00074	0.00025
RELATIVE CONSTANT ADMITTANCE	(-2.35, -3.91i)	(-2.36, -3.93i)
POWER OUT OF THE DRIVER	0.82	0.59
TOTAL POWER IN FAR FIELD	0.0013	0.00094

TABLE IX

NASA QCSEE INLET

Relative power normalized with respect to the hard walled radiated power

ka = 3.0

	Constant Phi on the Driver	Constant Velocity on the Driver
OPTIMUM ADMITTANCE DISTRIBUTION		
POWER OUT OF THE DRIVER	-3.69	-0.050
TOTAL POWER IN FAR FIELD	0.0096	0.000049
ABSOLUTE CONSTANT ADMITTANCE	(-3.10, -3.20i)	(-3.00, -3.19i)
POWER OUT OF THE DRIVER	0.69	0.18
TOTAL POWER IN FAR FIELD	0.00045	0.00020
RELATIVE CONSTANT ADMITTANCE	(-3.04, -3.20i)	(-3.05, -3.18i)
POWER OUT OF THE DRIVER	0.69	0.18
TOTAL POWER IN FAR FIELD	0.00061	0.00015

TABLE X

NASA QCSEE INLET

Relative power normalized with respect to the hard walled radiated power

ka = 5.0

	Constant Phi on the Driver	Constant Velocity on the Driver
OPTIMUM ADMITTANCE DISTRIBUTION		
POWER OUT OF THE DRIVER	-0.023	0.00059
TOTAL POWER IN FAR FIELD	0.00040	0.000031
ABSOLUTE CONSTANT ADMITTANCE	(-4.20, -1.80i)	(-4.57, -1.89i)
POWER OUT OF THE DRIVER	0.80	0.040
TOTAL POWER IN FAR FIELD	0.13	0.0065
RELATIVE CONSTANT ADMITTANCE	(-4.26, -1.96i)	(-4.37, -1.87i)
POWER OUT OF THE DRIVER	0.81	0.041
TOTAL POWER IN FAR FIELD	0.13	0.0066

TABLE XI

NASA QCSEE INLET

Relative power normalized with respect to the hard walled radiated power

ka = 7.0

	Constant Phi on the Driver	Constant Velocity on the Driver
OPTIMUM ADMITTANCE DISTRIBUTION		
POWER OUT OF THE DRIVER	0.56	0.0066
TOTAL POWER IN FAR FIELD	0.13	0.00013
ABSOLUTE CONSTANT ADMITTANCE	(-----, -----i)	(-5.42, -2.57i)
POWER OUT OF THE DRIVER	----	0.018
TOTAL POWER IN FAR FIELD	----	0.0022
RELATIVE CONSTANT ADMITTANCE	(-----, -----i)	(-5.28, -2.56i)
POWER OUT OF THE DRIVER	----	0.018
TOTAL POWER IN FAR FIELD	----	0.0022

TABLE XII

NASA QCSEE INLET

Relative power normalized with respect to the hard walled radiated power

ka = 10.0

	Constant Phi on the Driver	Constant Velocity on the Driver
OPTIMUM ADMITTANCE DISTRIBUTION		
POWER OUT OF THE DRIVER	0.29	0.010
TOTAL POWER IN FAR FIELD	0.00075	0.000064
ABSOLUTE CONSTANT ADMITTANCE	(-4.32, -3.83i)	(-4.02, -3.56i)
POWER OUT OF THE DRIVER	0.94	0.010
TOTAL POWER IN FAR FIELD	0.22	0.0026
RELATIVE CONSTANT ADMITTANCE	(-4.27, -3.78i)	(-4.05, -3.60i)
POWER OUT OF THE DRIVER	0.94	0.010
TOTAL POWER IN FAR FIELD	0.22	0.0026

TABLE XIII

QCSEE INLET LESS CENTERBODY

Relative power normalized with respect to the hard walled radiated power

ka = 1.0

	Constant Phi on the Driver	Constant Velocity on the Driver
OPTIMUM ADMITTANCE DISTRIBUTION		
POWER OUT OF THE DRIVER	-1.20	-1.78
TOTAL POWER IN FAR FIELD	0.000025	0.000072
ABSOLUTE CONSTANT ADMITTANCE	(0.81, 4.68i)	(-0.75, 4.72i)
POWER OUT OF THE DRIVER	-1.19	-1.06
TOTAL POWER IN FAR FIELD	0.0021	0.00091
RELATIVE CONSTANT ADMITTANCE	(-0.73, -3.49i)	(-0.79, -3.44i)
POWER OUT OF THE DRIVER	1.71	1.33
TOTAL POWER IN FAR FIELD	0.0029	0.0023

TABLE XIV

QCSEE INLET LESS CENTERBODY

Relative power normalized with respect to the hard walled radiated power

ka = 2.0

	Constant Phi on the Driver	Constant Velocity on the Driver
OPTIMUM ADMITTANCE DISTRIBUTION		
POWER OUT OF THE DRIVER	-0.56	-0.50
TOTAL POWER IN FAR FIELD	0.000044	0.000049
ABSOLUTE CONSTANT ADMITTANCE	(-2.99, 3.73i)	(-2.99, 3.41i)
POWER OUT OF THE DRIVER	-0.74	-0.65
TOTAL POWER IN FAR FIELD	0.00058	0.00025
RELATIVE CONSTANT ADMITTANCE	(-2.42, -3.78i)	(-2.45, -3.79i)
POWER OUT OF THE DRIVER	0.76	0.71
TOTAL POWER IN FAR FIELD	0.0011	0.00093

TABLE XV

QCSEE INLET LESS CENTERBODY

Relative power normalized with respect to the hard walled radiated power

ka = 3.0

	Constant Phi on the Driver	Constant Velocity on the Driver
OPTIMUM ADMITTANCE DISTRIBUTION		
POWER OUT OF THE DRIVER	-0.41	-0.024
TOTAL POWER IN FAR FIELD	0.000084	0.000032
ABSOLUTE CONSTANT ADMITTANCE	(-3.06, 2.94i)	(-2.88, -3.02i)
POWER OUT OF THE DRIVER	-0.67	0.13
TOTAL POWER IN FAR FIELD	0.000087	0.000094
RELATIVE CONSTANT ADMITTANCE	(-2.90, -3.07i)	(-2.91, -2.97i)
POWER OUT OF THE DRIVER	0.69	0.13
TOTAL POWER IN FAR FIELD	0.00047	0.000063

TABLE XVI

QCSEE INLET LESS CENTERBODY

Relative power normalized with respect to the hard walled radiated power

ka = 5.0

	Constant Phi on the Driver	Constant velocity on the Driver
OPTIMUM ADMITTANCE DISTRIBUTION		
POWER OUT OF THE DRIVER	0.098	0.0069
TOTAL POWER IN FAR FIELD	0.00077	0.0000071
ABSOLUTE CONSTANT ADMITTANCE	(-3.89, -1.65i)	(-3.93, -2.39i)
POWER OUT OF THE DRIVER	0.74	0.044
TOTAL POWER IN FAR FIELD	0.20	0.0042
RELATIVE CONSTANT ADMITTANCE	(-3.87, -1.98i)	(-3.88, -2.24i)
POWER OUT OF THE DRIVER	0.77	0.044
TOTAL POWER IN FAR FIELD	0.21	0.0042

TABLE XVII

QCSEE INLET LESS CENTERBODY

Relative power normalized with respect to the hard walled radiated power

ka = 7.0

	Constant Phi on the Driver	Constant Velocity on the Driver
OPTIMUM ADMITTANCE DISTRIBUTION		
POWER OUT OF THE DRIVER	0.14	0.0091
TOTAL POWER IN FAR FIELD	0.0016	0.00028
ABSOLUTE CONSTANT ADMITTANCE	(-4.77, -2.07i)	(-7.32, -1.67i)
POWER OUT OF THE DRIVER	1.02	0.020
TOTAL POWER IN FAR FIELD	0.29	0.0058
RELATIVE CONSTANT ADMITTANCE	(-4.87, -2.06i)	(-6.84, -1.57i)
POWER OUT OF THE DRIVER	1.02	0.021
TOTAL POWER IN FAR FIELD	0.29	0.0062

TABLE XVIII

QCSEE INLET LESS CENTERBODY

Relative power normalized with respect to the hard walled radiated power

ka = 10.0

	Constant Phi on the Driver	Constant Velocity on the Driver
OPTIMUM ADMITTANCE DISTRIBUTION		
POWER OUT OF THE DRIVER	0.33	0.00060
TOTAL POWER IN FAR FIELD	0.16	0.000060
ABSOLUTE CONSTANT ADMITTANCE	(-5.27, -3.01i)	(-4.38, -3.18i)
POWER OUT OF THE DRIVER	0.97	0.010
TOTAL POWER IN FAR FIELD	0.36	0.0039
RELATIVE CONSTANT ADMITTANCE	(-5.05, -2.91i)	(-4.49, -3.30i)
POWER OUT OF THE DRIVER	0.98	0.010
TOTAL POWER IN FAR FIELD	0.36	0.0039

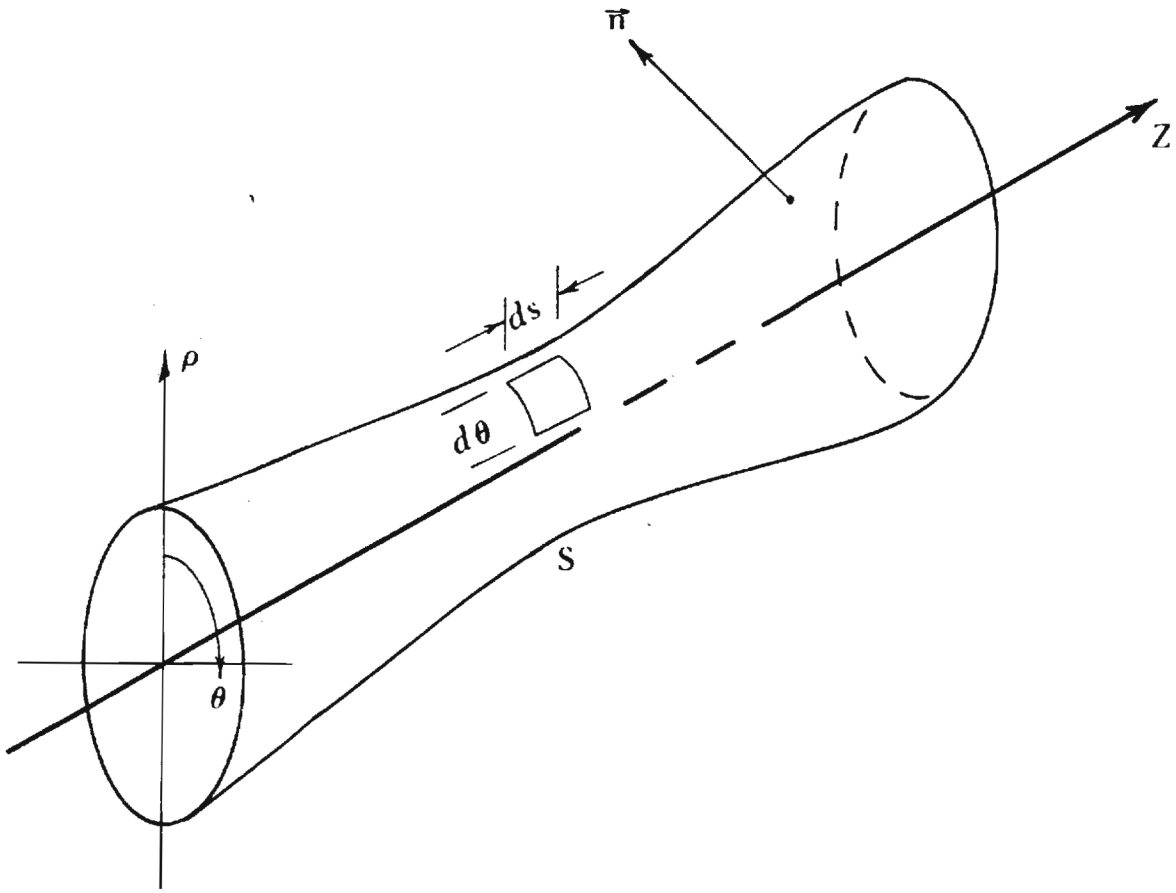

Figure 1. (ρ, Z, θ) coordinate system for a body of revolution

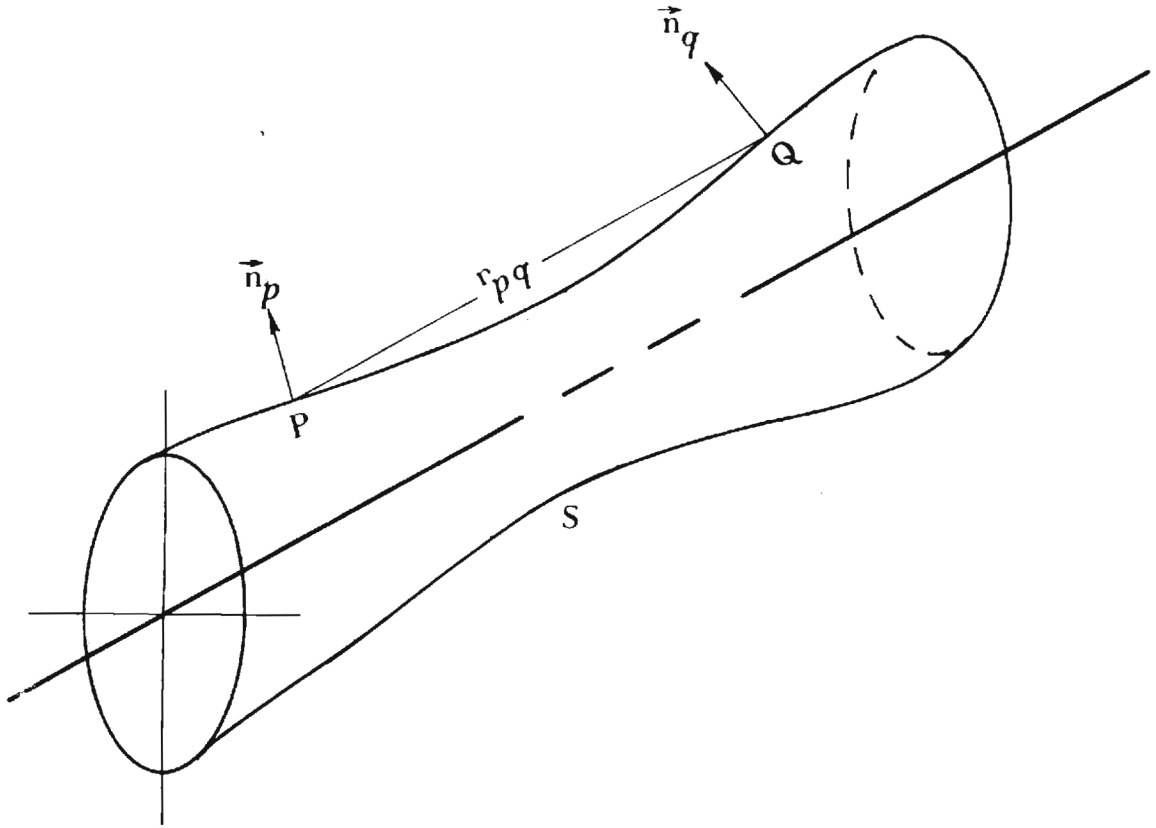

Figure 2. Body S showing P and Q points, the distance between them r_{pq} and their outward normals

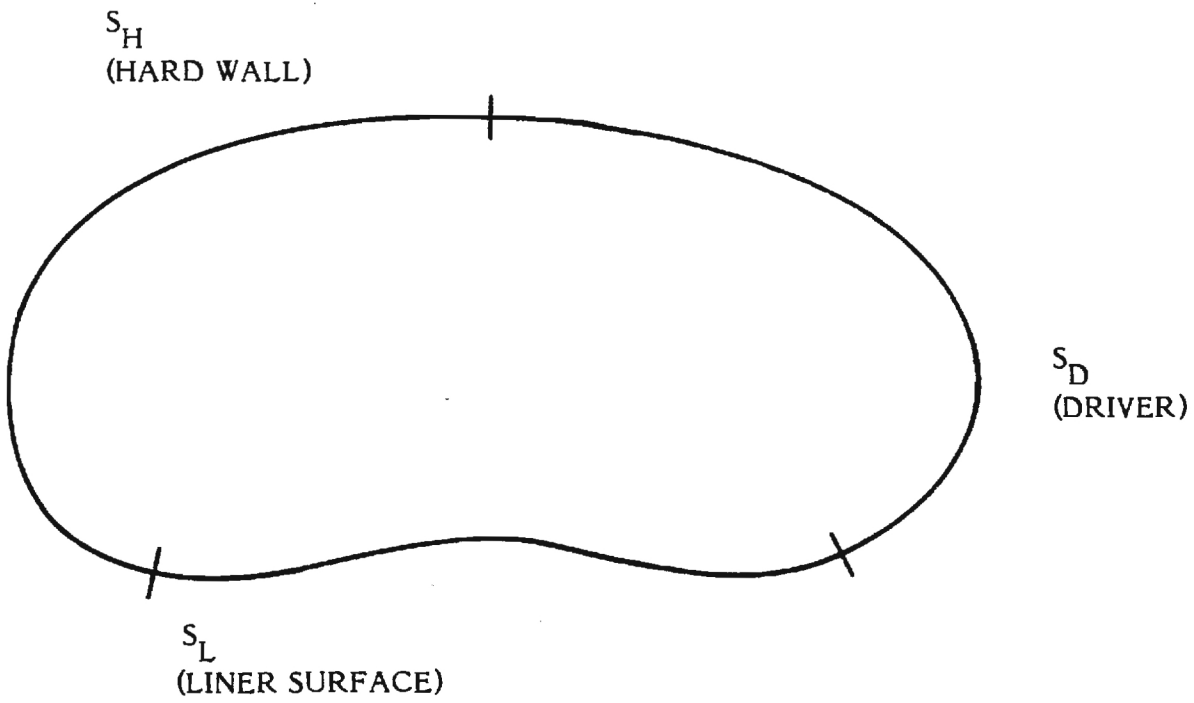

Figure 3. The three types of regions on the body

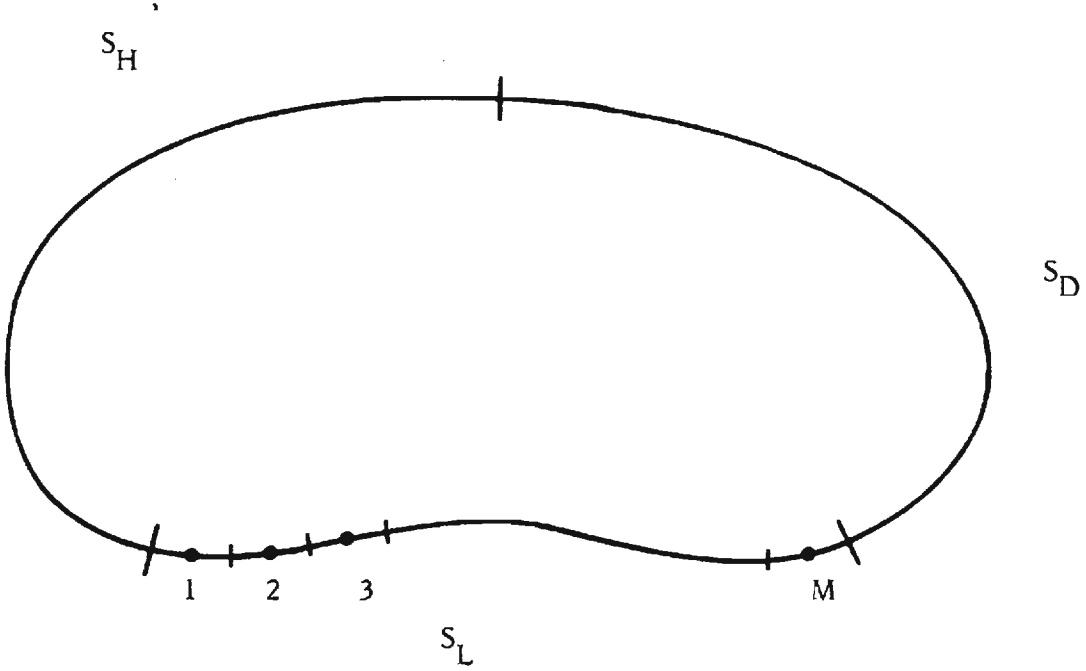

Figure 4. Liner surface divided into M finite regions.

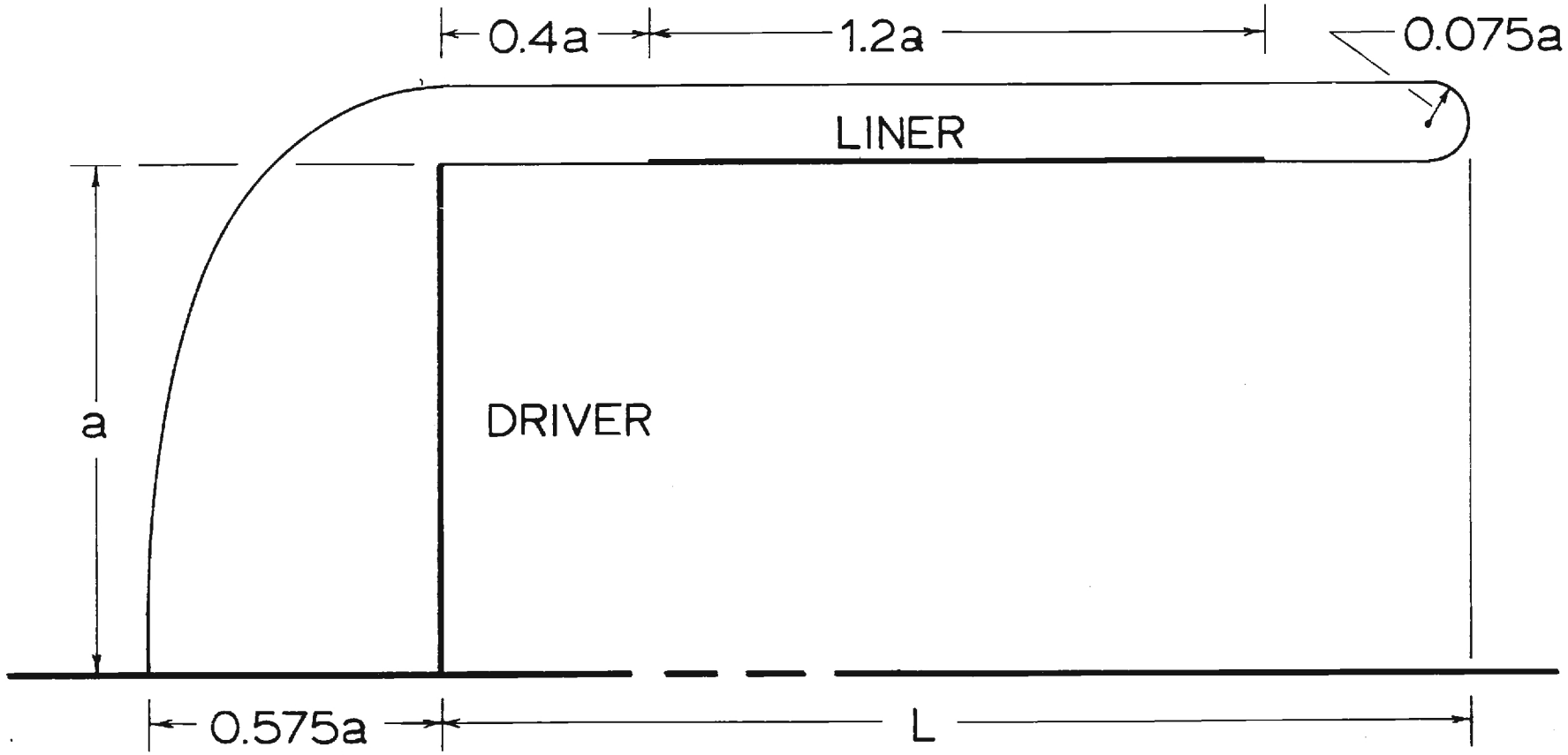

Figure 5. Straight Duct

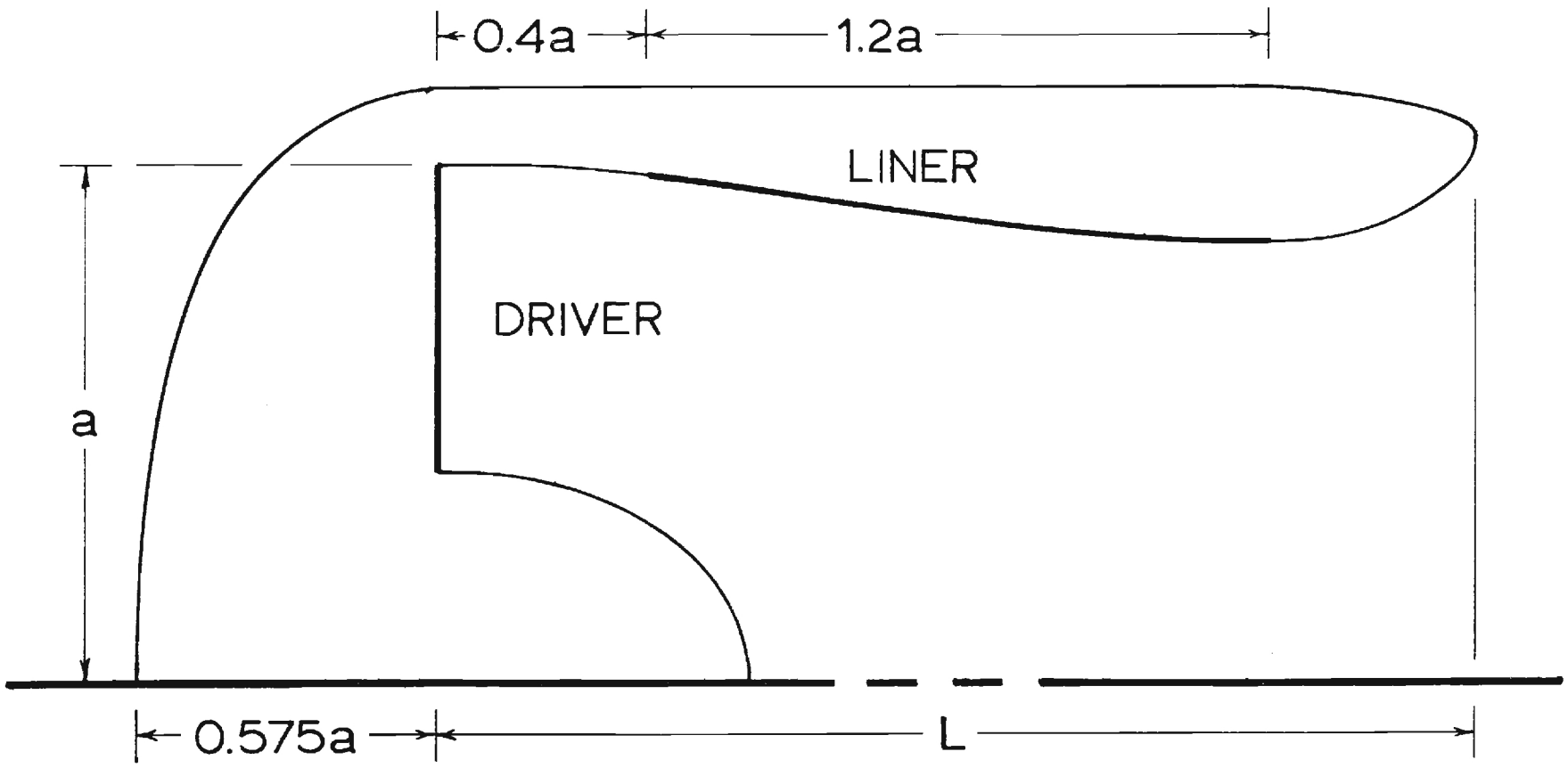

Figure 6. QCSEE Inlet

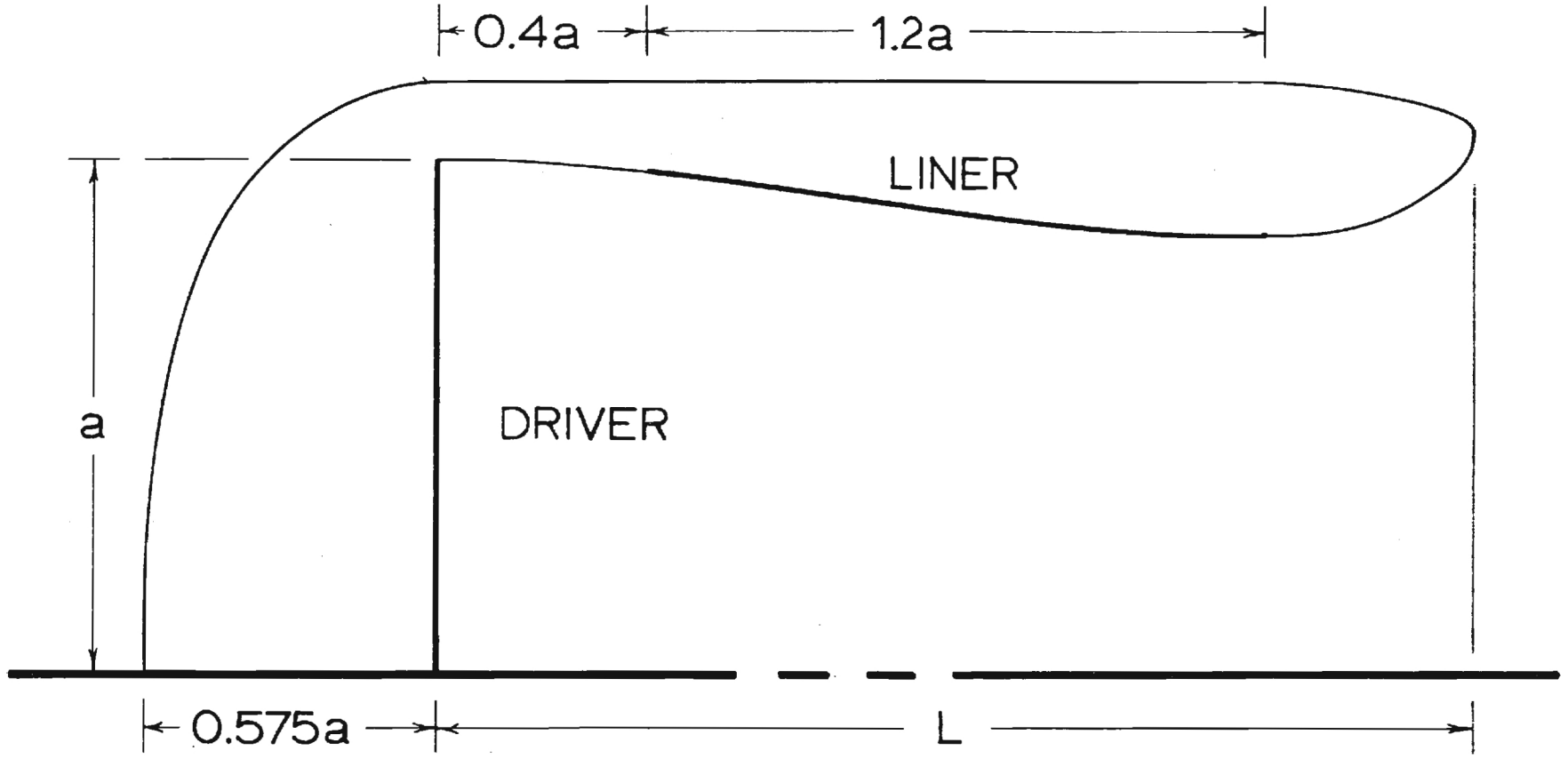

Figure 7. QCSEE inlet less centerbody

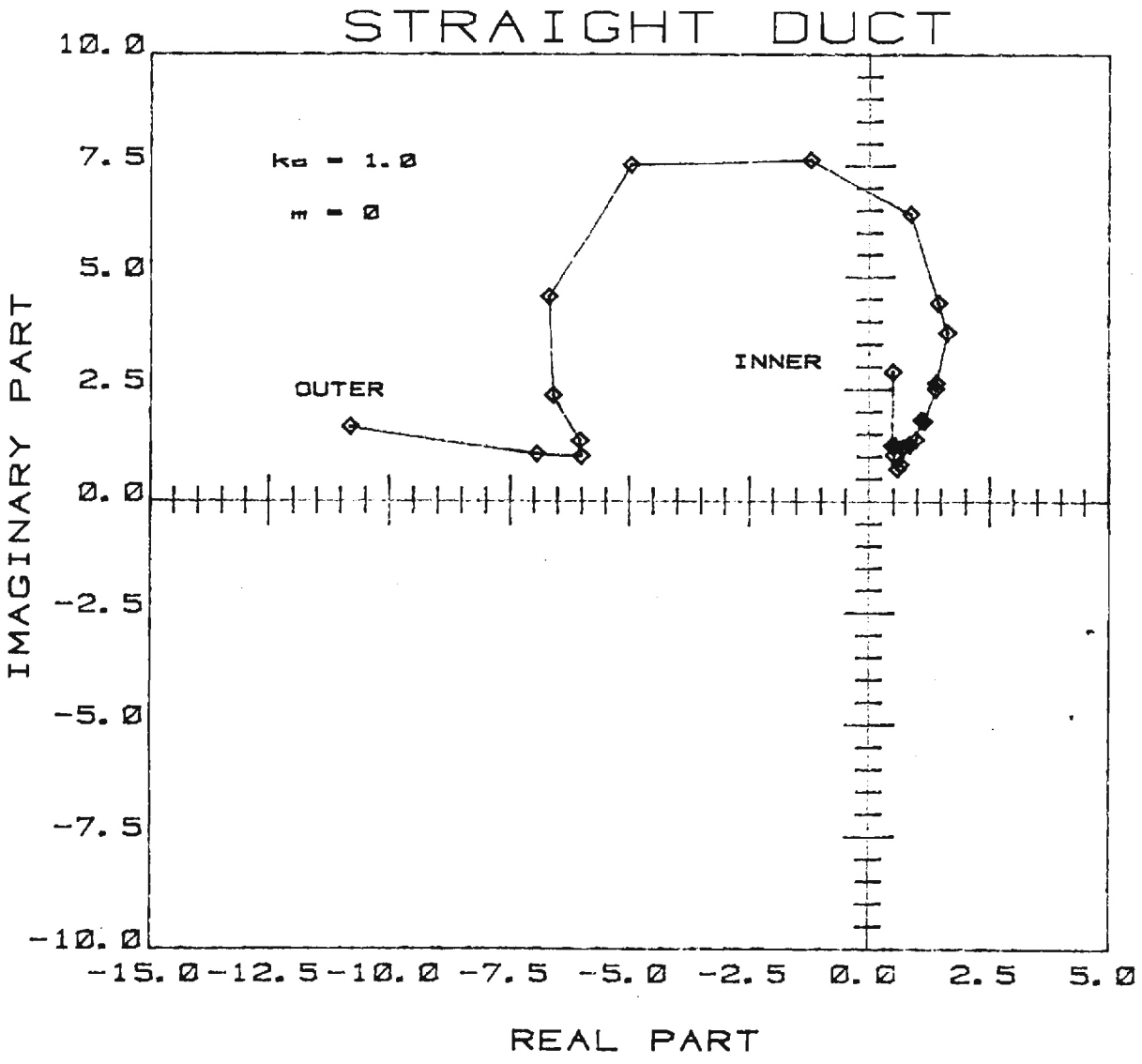

OPTIMUM ADMITTANCE DISTRIBUTION

Conetant Phi on the Driver

Figure 8a

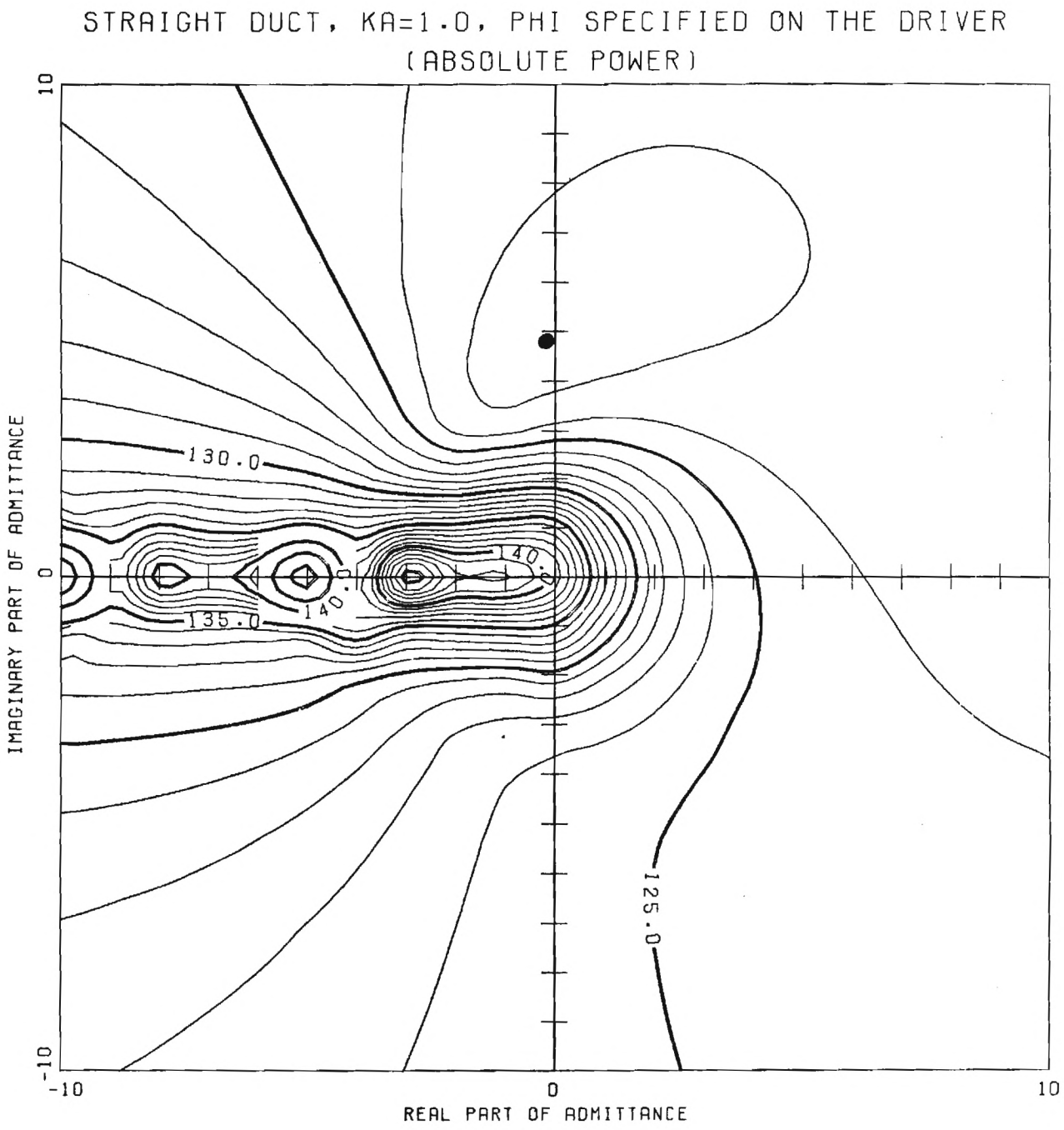
STRAIGHT DUCT, KA=1.0, PHI SPECIFIED ON THE DRIVER
(ABSOLUTE POWER)
IMAGINARY PART OF ADMITTANCE
REAL PART OF ADMITTANCE
10
0
-10
-10
0
10
130.0
140.0
135.0
140.0
125.0

Figure 8b

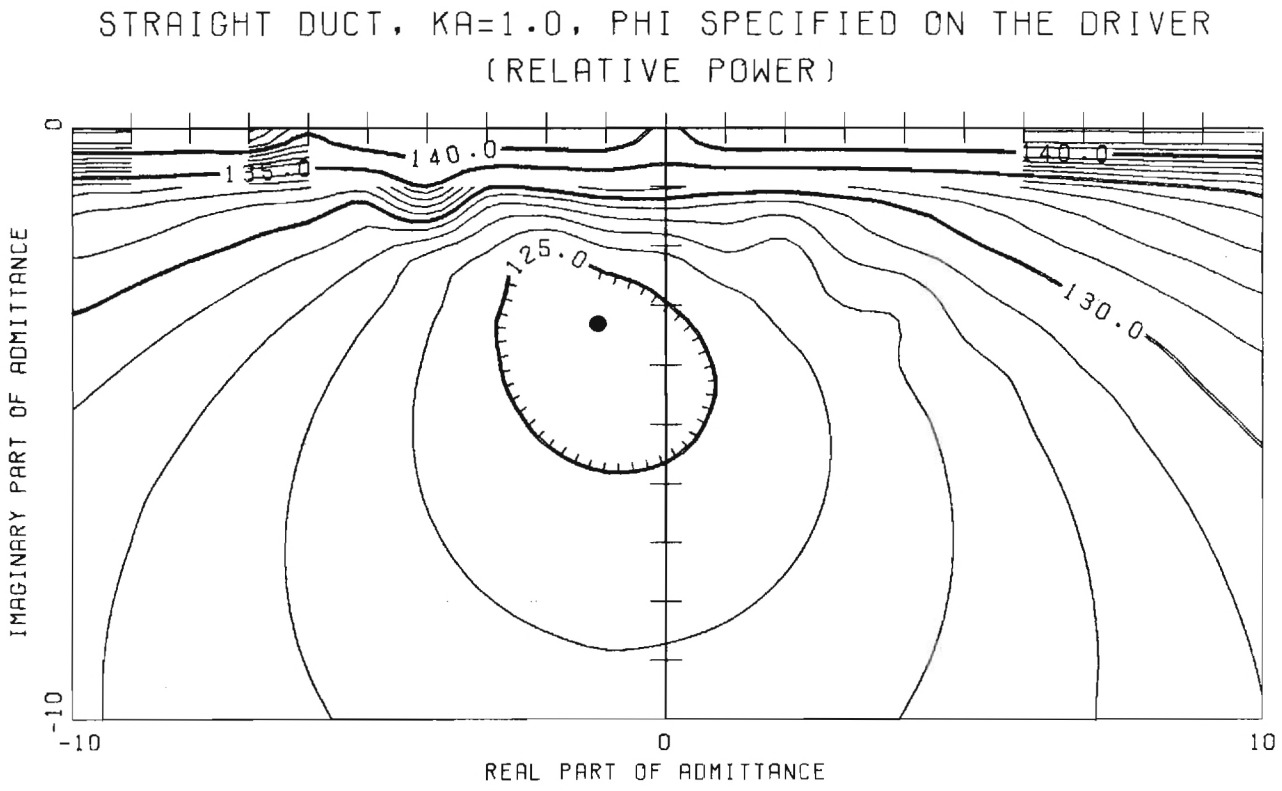
STRAIGHT DUCT, KA=1.0, PHI SPECIFIED ON THE DRIVER
(RELATIVE POWER)
135.0
140.0
140.0
125.0
130.0
IMAGINARY PART OF ADMITTANCE
0
-10
-10
0
10
REAL PART OF ADMITTANCE

Figure 8c

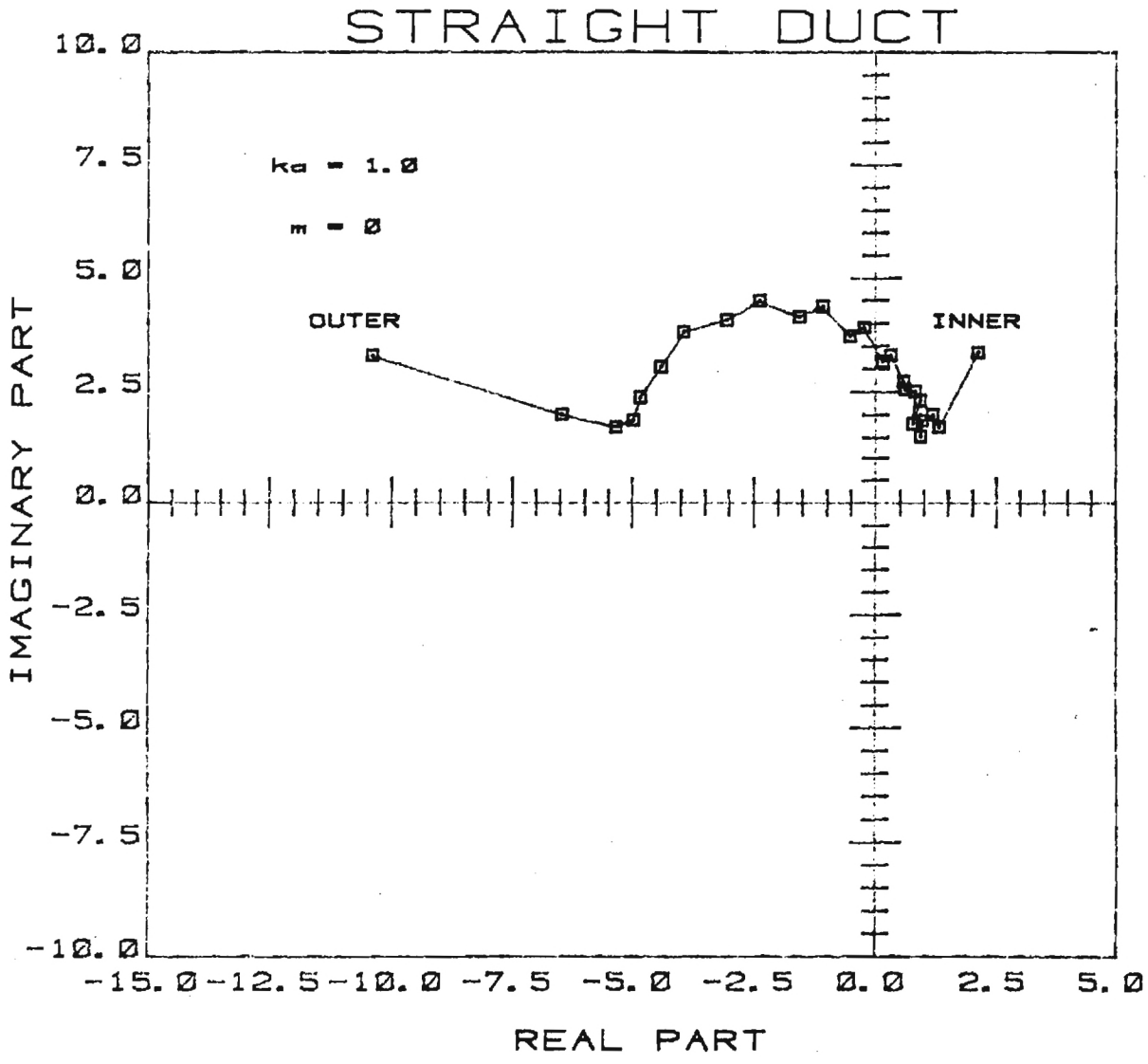

OPTIMUM ADMITTANCE DISTRIBUTION

Constant Velocity on the Driver

Figure 8d

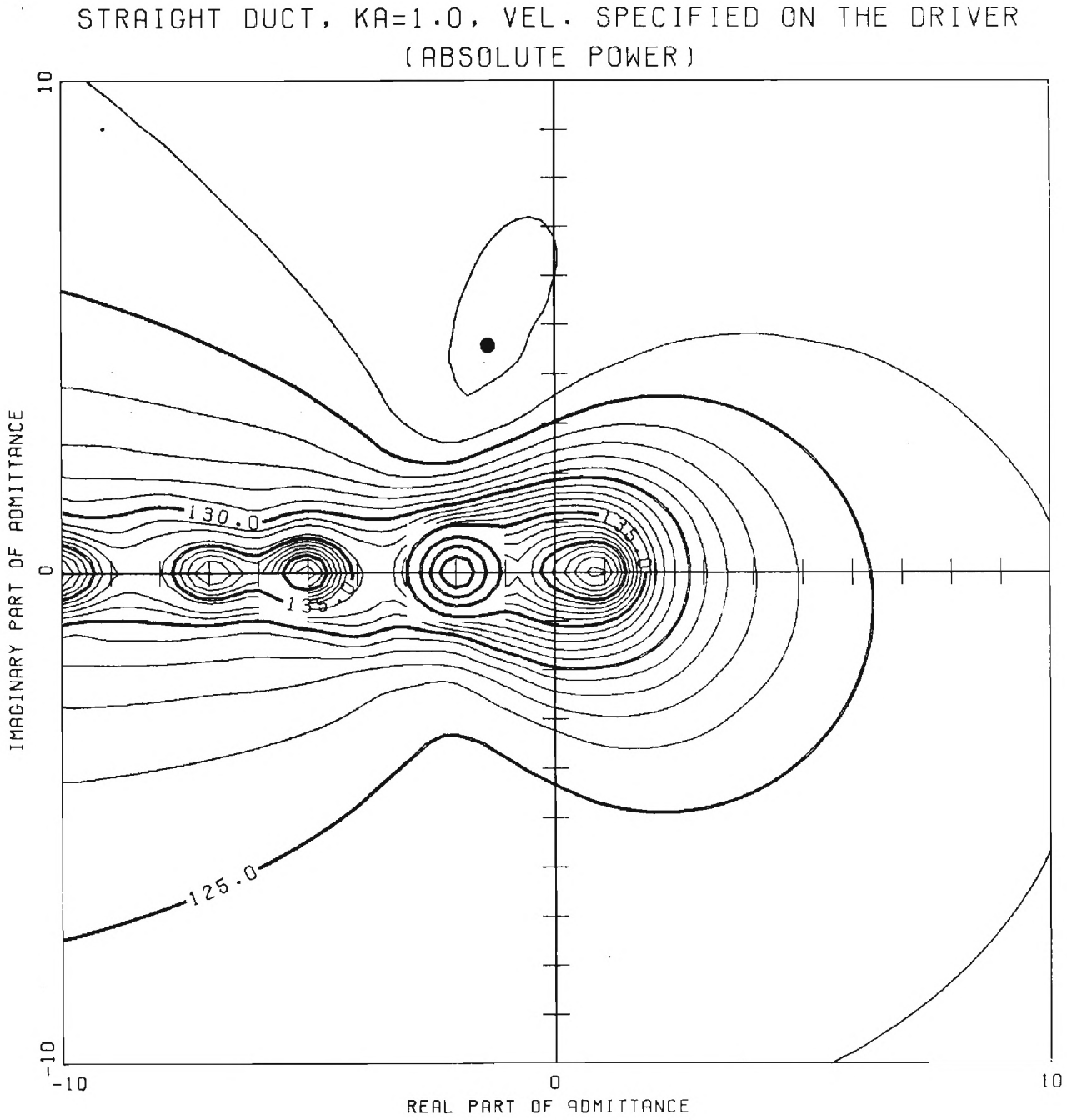
STRAIGHT DUCT, KA=1.0, VEL. SPECIFIED ON THE DRIVER
(ABSOLUTE POWER)
IMAGINARY PART OF ADMITTANCE
REAL PART OF ADMITTANCE
10
0
-10
-10
0
10
130.0
135.0
135.0
125.0

Figure 8e

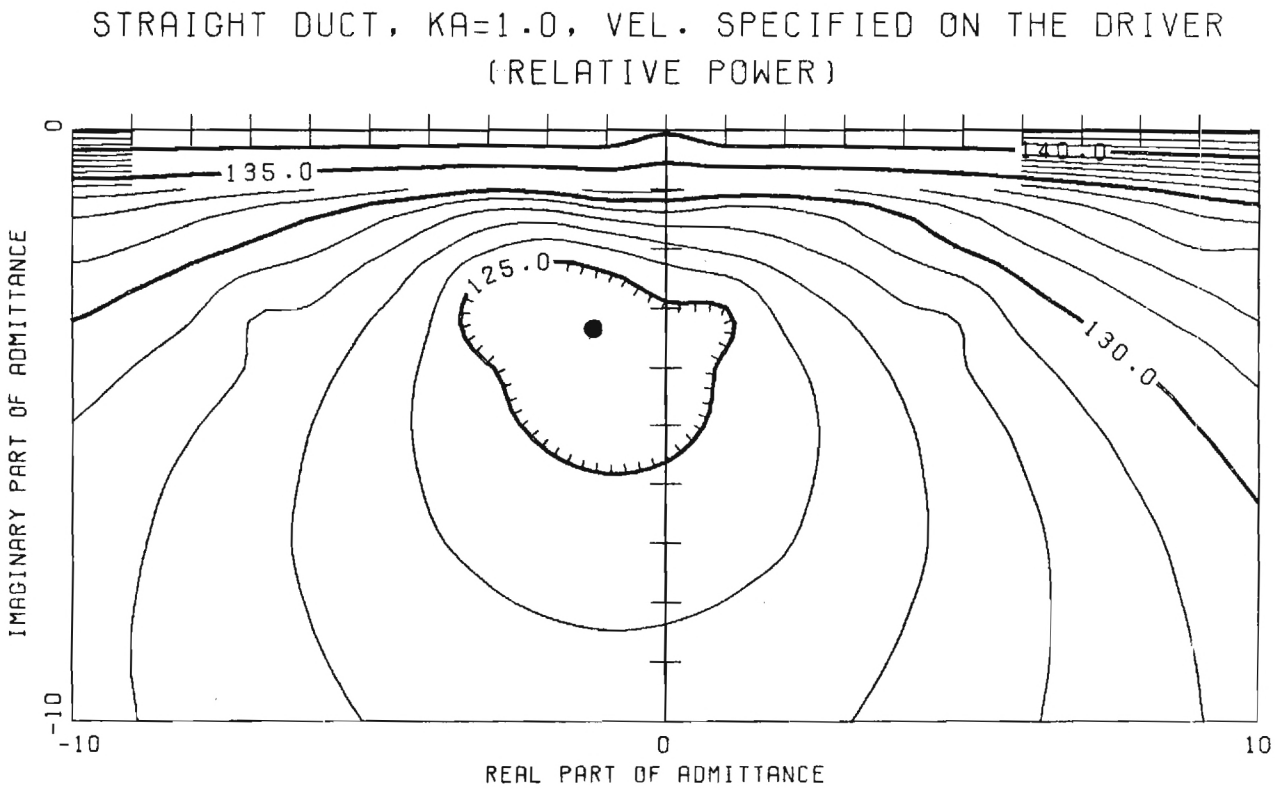
STRAIGHT DUCT, KA=1.0, VEL. SPECIFIED ON THE DRIVER
(RELATIVE POWER)
135.0
140.0
125.0
130.0
0
-10
-10
0
10
IMAGINARY PART OF ADMITTANCE
REAL PART OF ADMITTANCE

Figure 8f

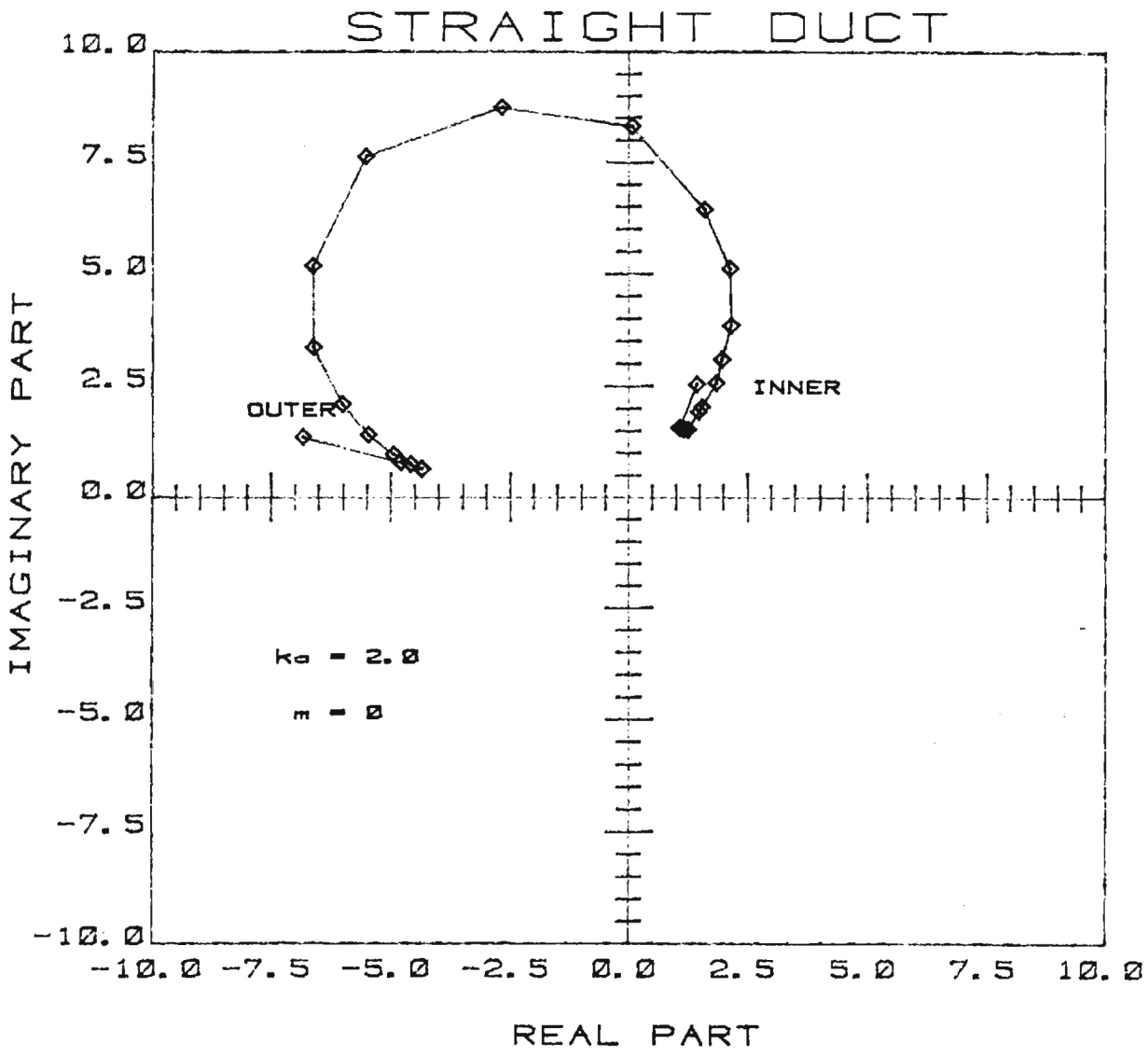

OPTIMUM ADMITTANCE DISTRIBUTION

Constant Phi on the Driver

Figure 9a

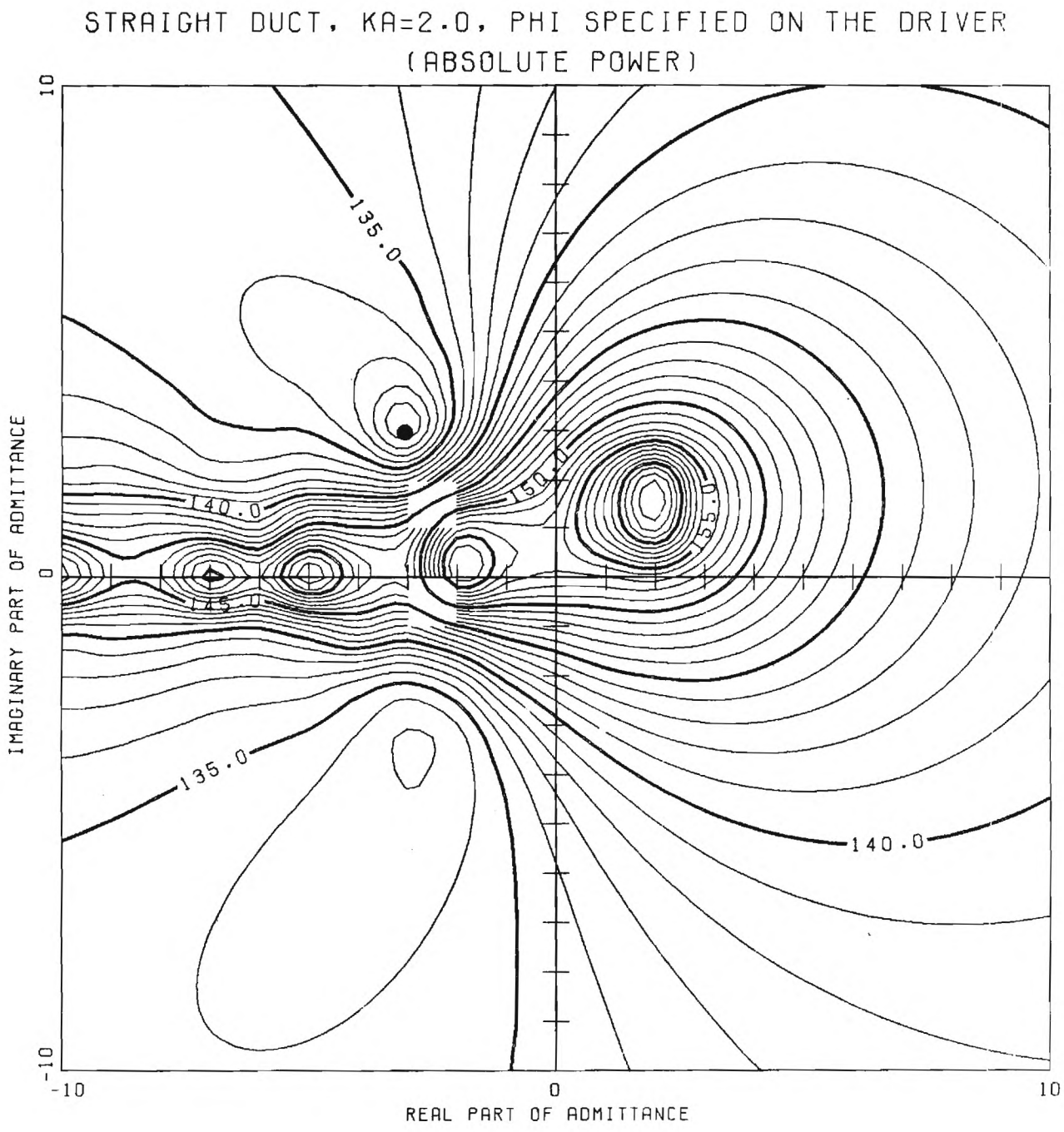
STRAIGHT DUCT, KA=2.0, PHI SPECIFIED ON THE DRIVER
(ABSOLUTE POWER)
IMAGINARY PART OF ADMITTANCE
REAL PART OF ADMITTANCE
10
0
-10
-10
0
10
135.0
140.0
145.0
150.0
155.0
135.0
140.0

Figure 9b

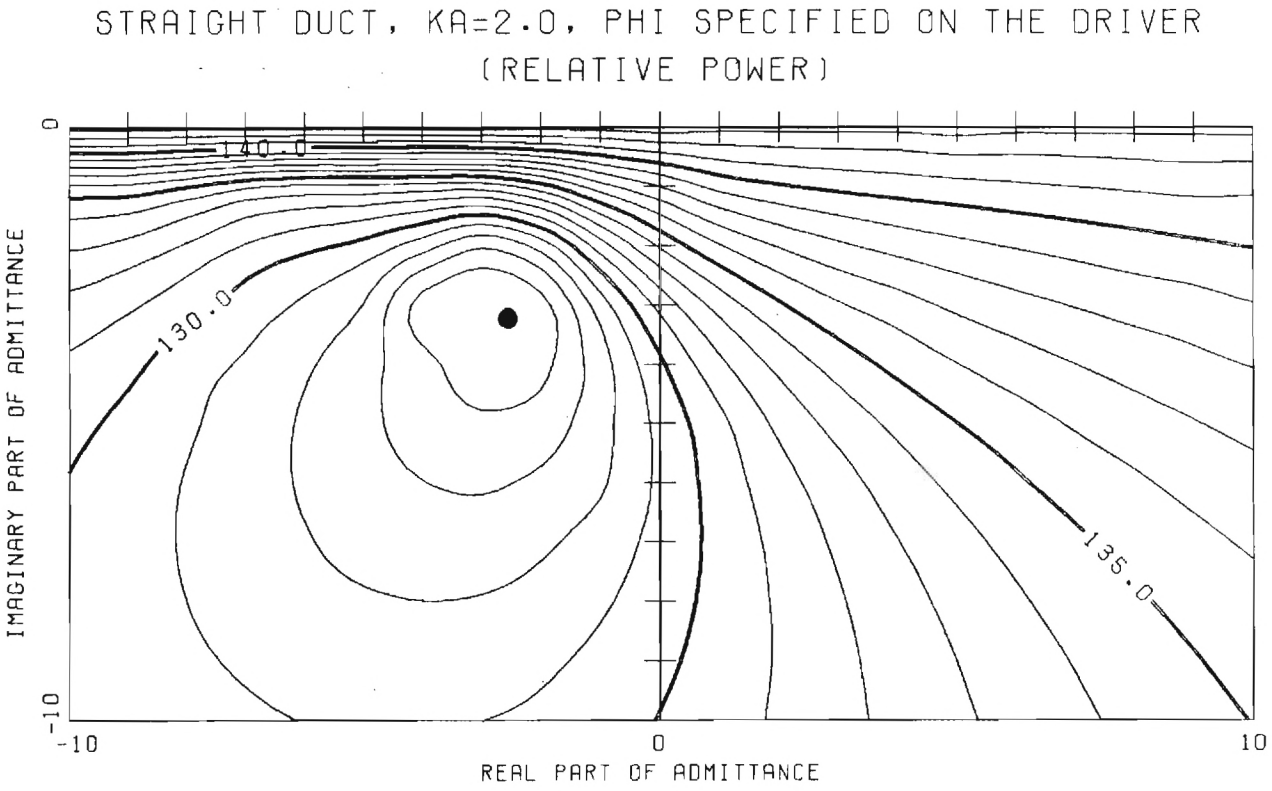
STRAIGHT DUCT, KA=2.0, PHI SPECIFIED ON THE DRIVER
(RELATIVE POWER)
IMAGINARY PART OF ADMITTANCE
REAL PART OF ADMITTANCE
0
-10
-10
0
10
140.0
130.0
135.0

Figure 9c

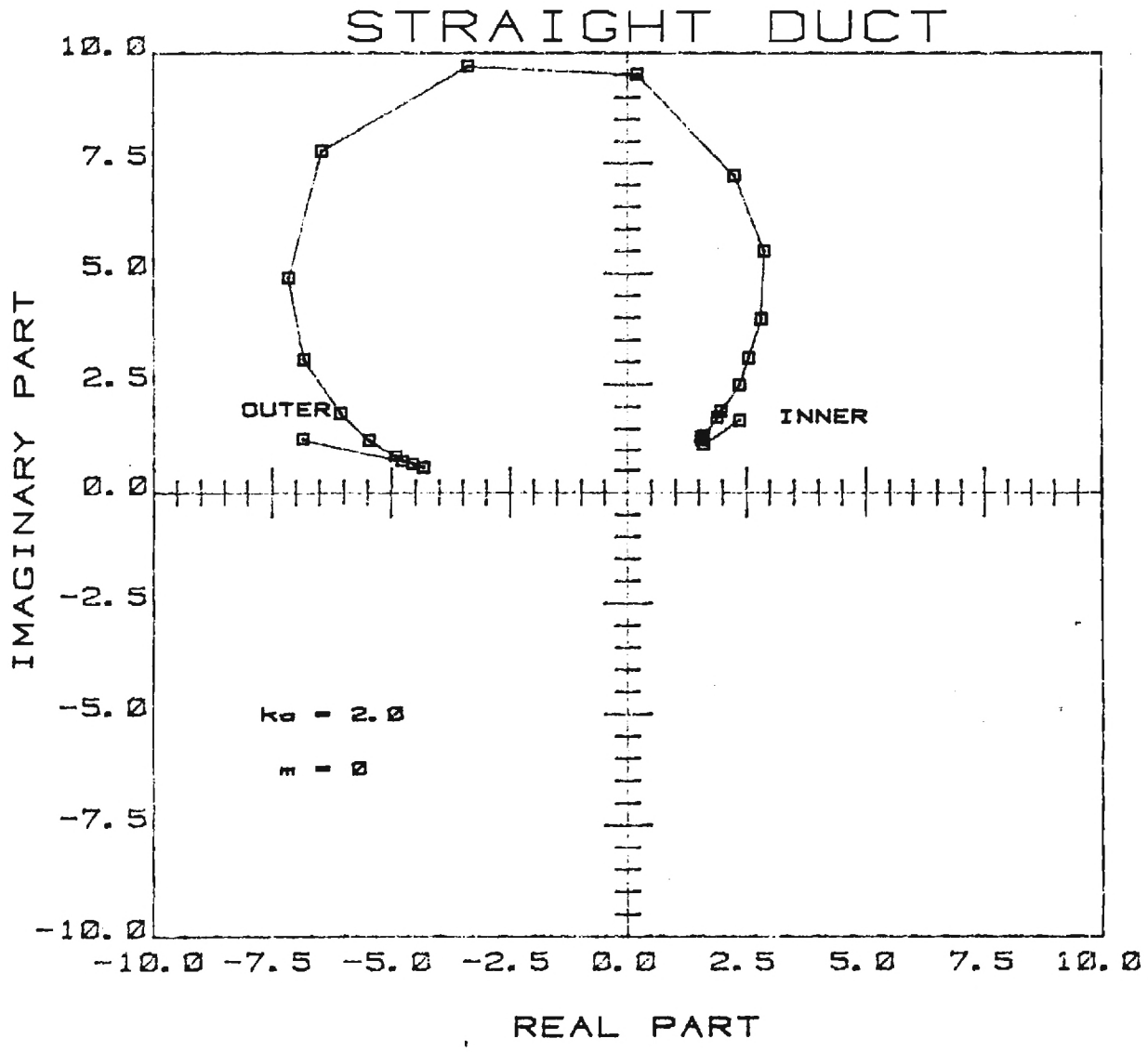

OPTIMUM ADMITTANCE DISTRIBUTION

Constant Velocity on the Driver

Figure 9d

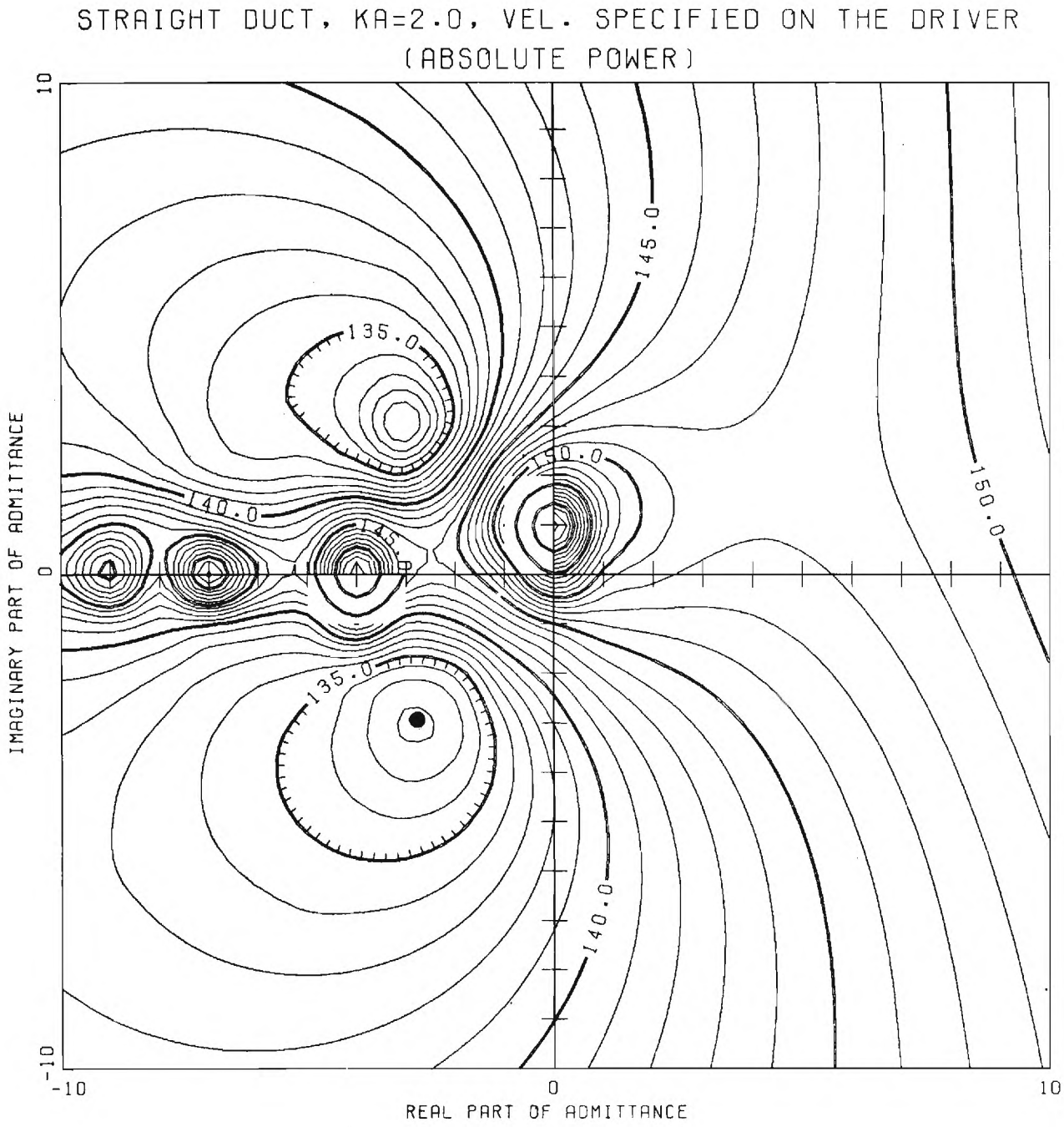
STRAIGHT DUCT, KA=2.0, VEL. SPECIFIED ON THE DRIVER
(ABSOLUTE POWER)
IMAGINARY PART OF ADMITTANCE
REAL PART OF ADMITTANCE
10
0
-10
-10
0
10
145.0
135.0
150.0
140.0
145.
150.0
135.0
140.0

Figure 9e

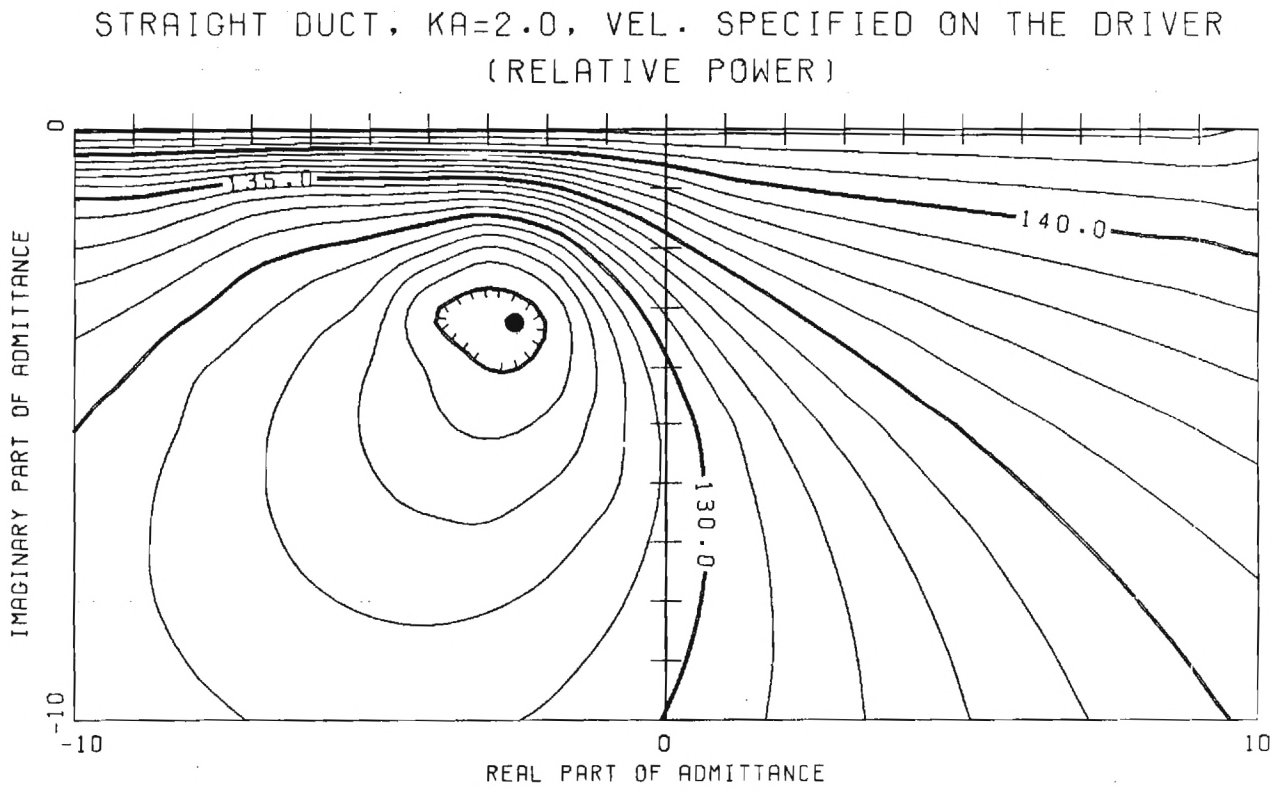
STRAIGHT DUCT, KA=2.0, VEL. SPECIFIED ON THE DRIVER
(RELATIVE POWER)
IMAGINARY PART OF ADMITTANCE
REAL PART OF ADMITTANCE
0
-10
-10
0
10
135.0
140.0
130.0

Figure 9f

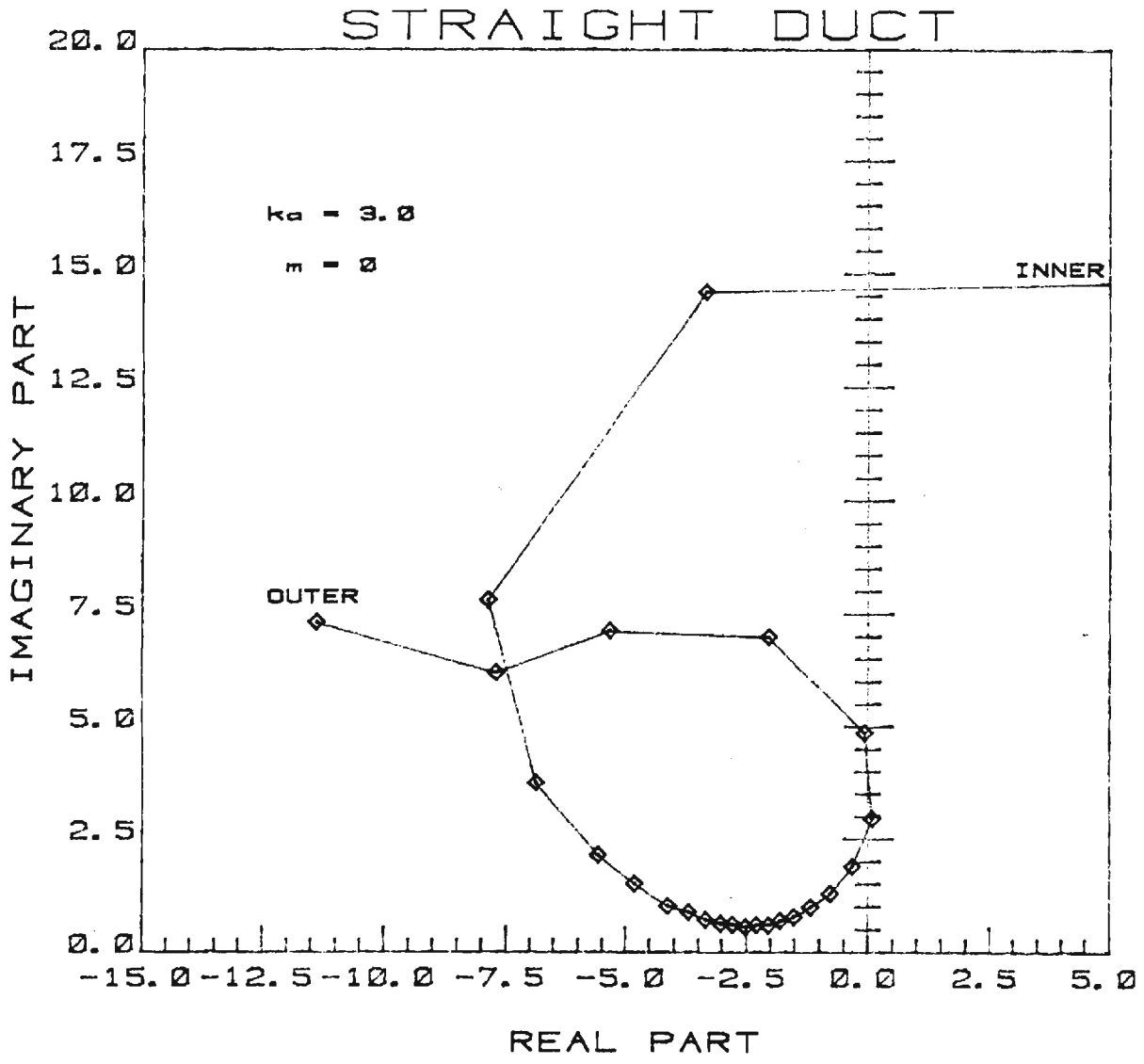

OPTIMUM ADMITTANCE DISTRIBUTION

Conetant Phi on the Driver

Figure 10a

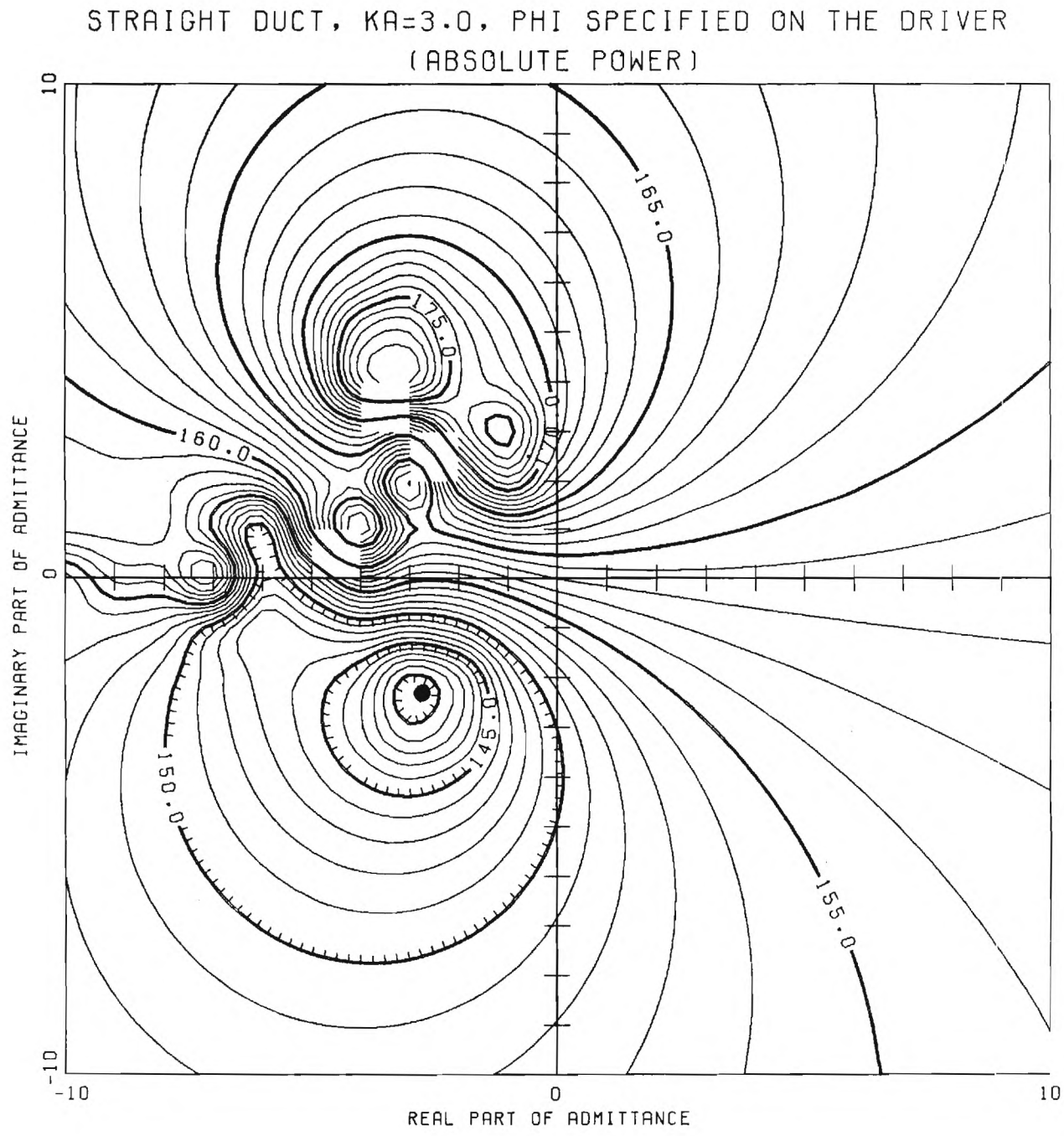
STRAIGHT DUCT, KA=3.0, PHI SPECIFIED ON THE DRIVER
(ABSOLUTE POWER)
IMAGINARY PART OF ADMITTANCE
REAL PART OF ADMITTANCE
10
0
-10
-10
0
10
165.0
175.0
160.0
170.0
145.0
150.0
155.0

Figure 10b

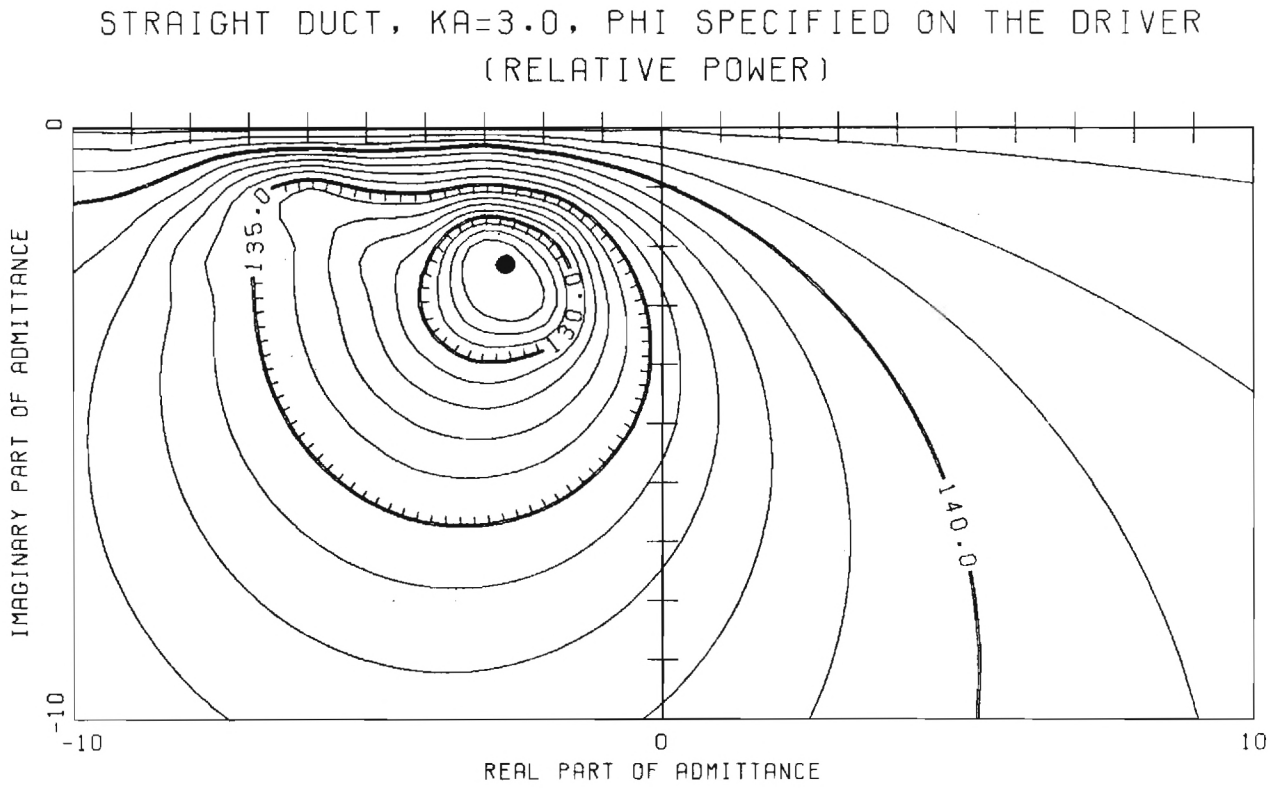
STRAIGHT DUCT, KA=3.0, PHI SPECIFIED ON THE DRIVER
(RELATIVE POWER)
IMAGINARY PART OF ADMITTANCE
REAL PART OF ADMITTANCE
0
-10
-10
0
10
135.0
130.0
140.0

Figure 10c

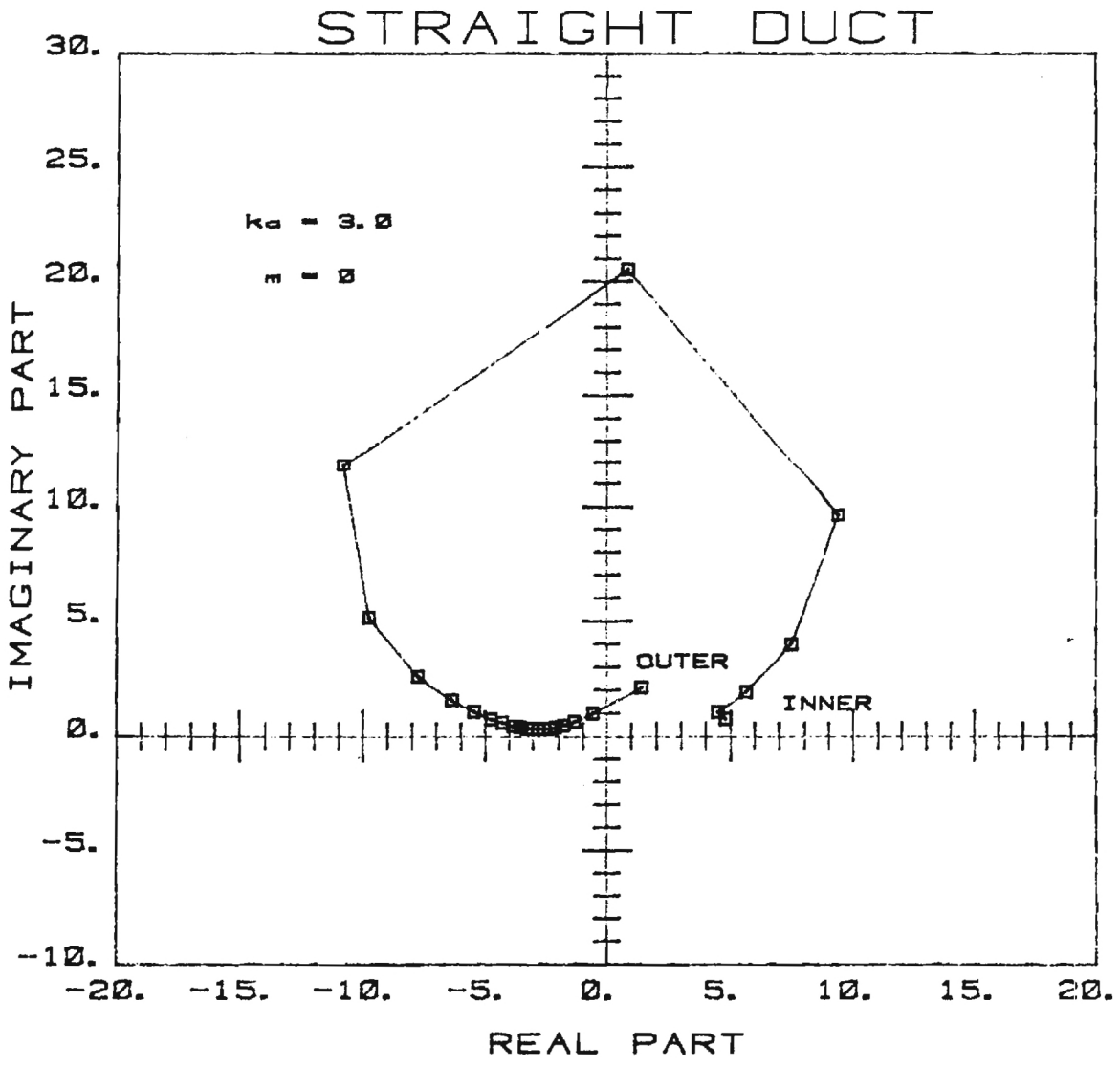

OPTIMUM ADMITTANCE DISTRIBUTION

Constant Velocity on the Driver

Figure 10d

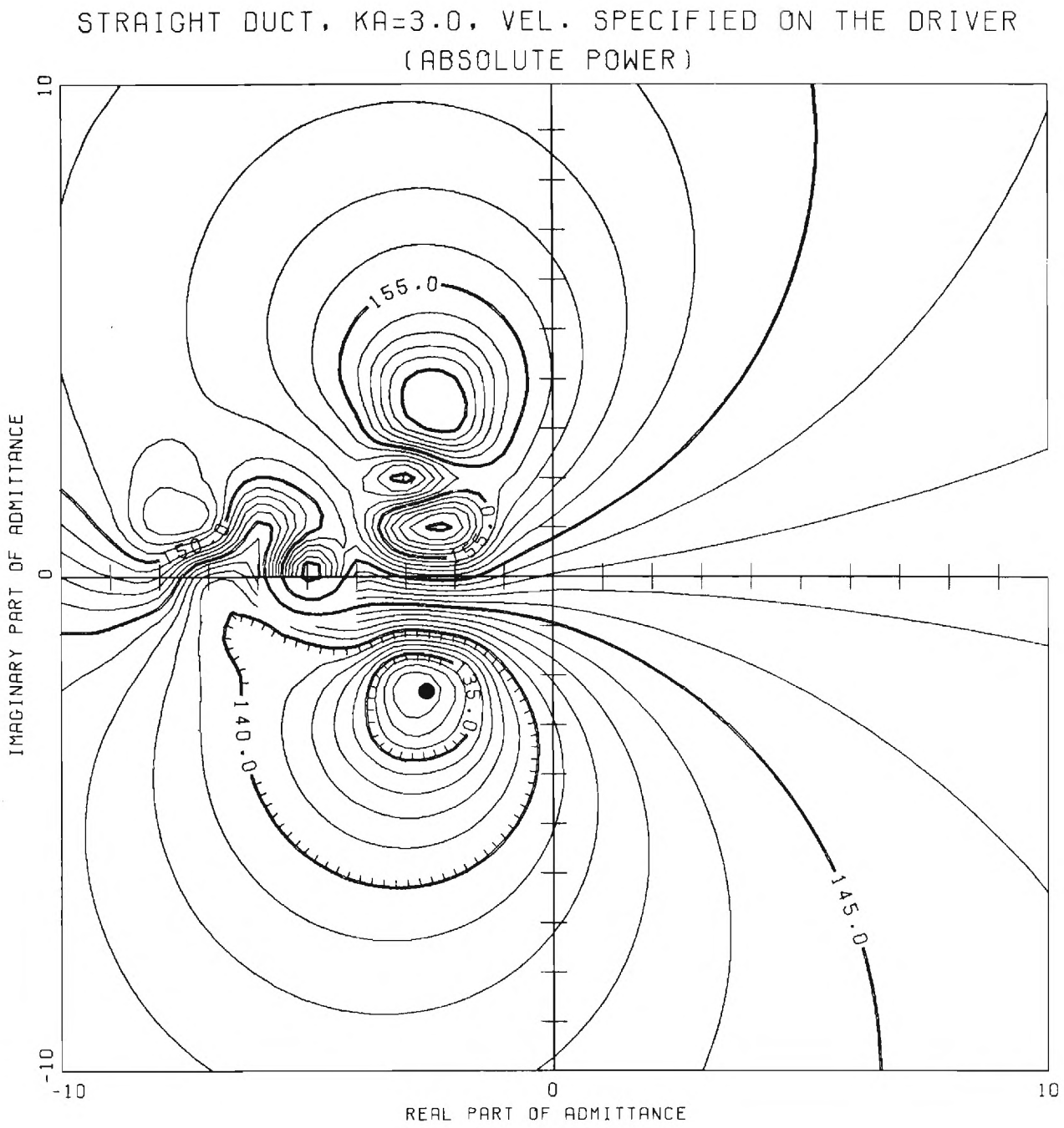
STRAIGHT DUCT, KA=3.0, VEL. SPECIFIED ON THE DRIVER
(ABSOLUTE POWER)
IMAGINARY PART OF ADMITTANCE
REAL PART OF ADMITTANCE
10
0
-10
-10
0
10
155.0
150.0
155.0
140.0
135.0
145.0

Figure 10e

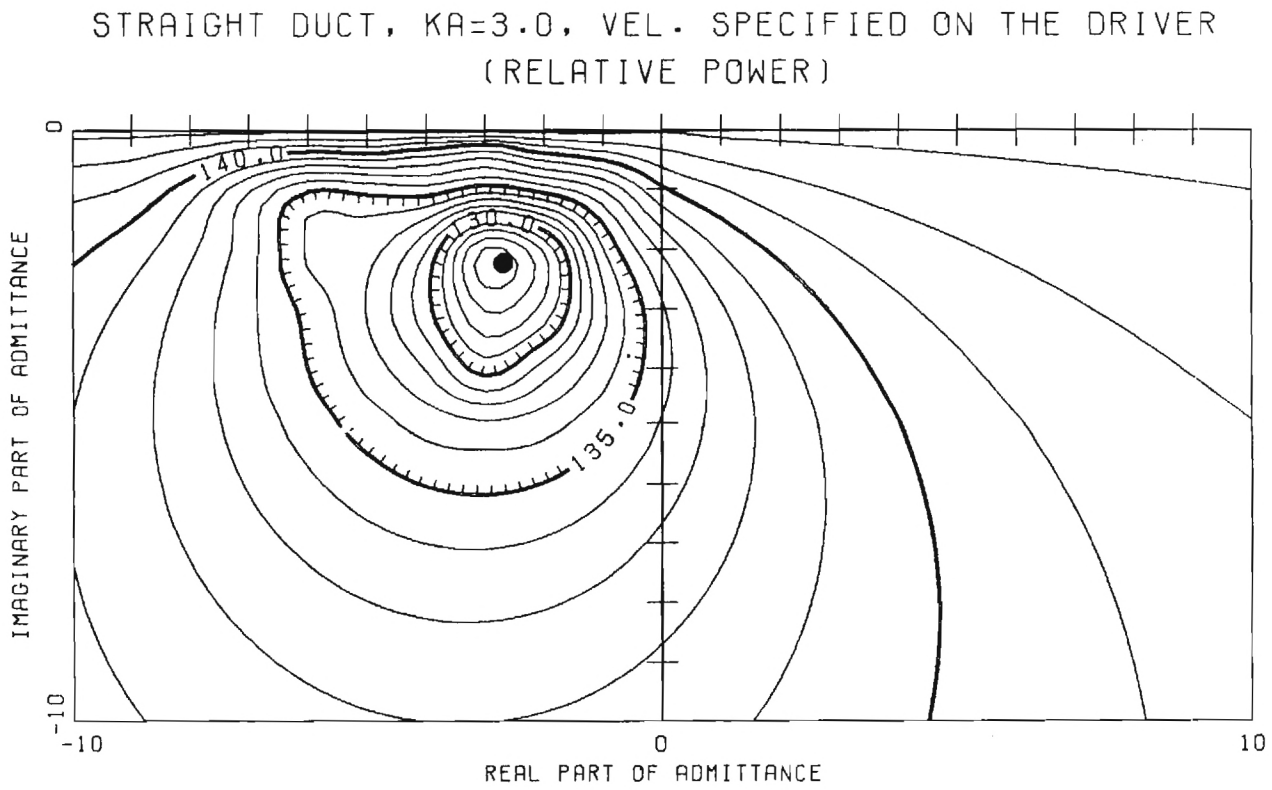
STRAIGHT DUCT, KA=3.0, VEL. SPECIFIED ON THE DRIVER
(RELATIVE POWER)
IMAGINARY PART OF ADMITTANCE
REAL PART OF ADMITTANCE
0
-10
-10
0
10
140.0
130.0
135.0

Figure 10f

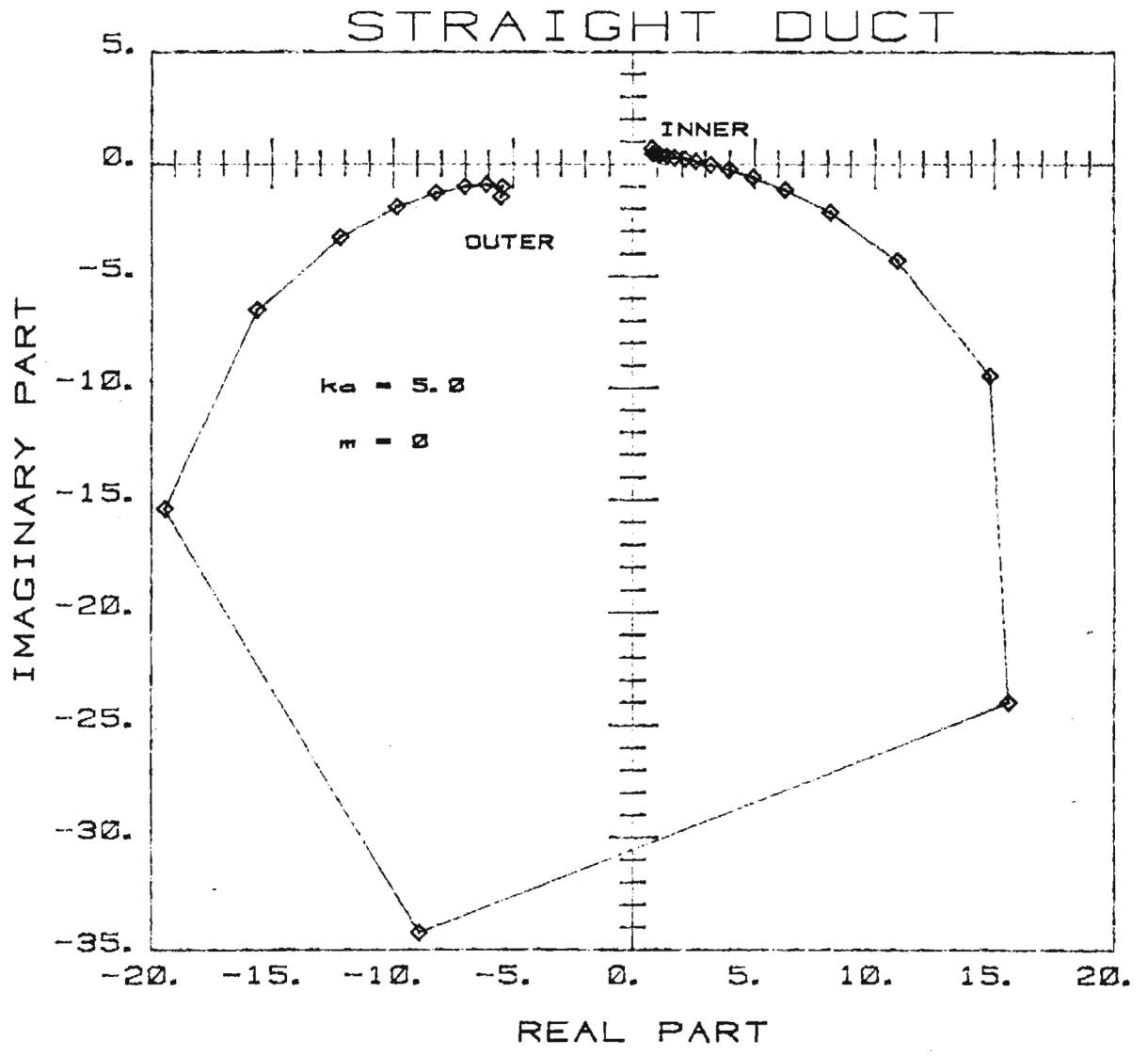

OPTIMUM ADMITTANCE DISTRIBUTION

Conetant Phi on the Driver

Figure 11a

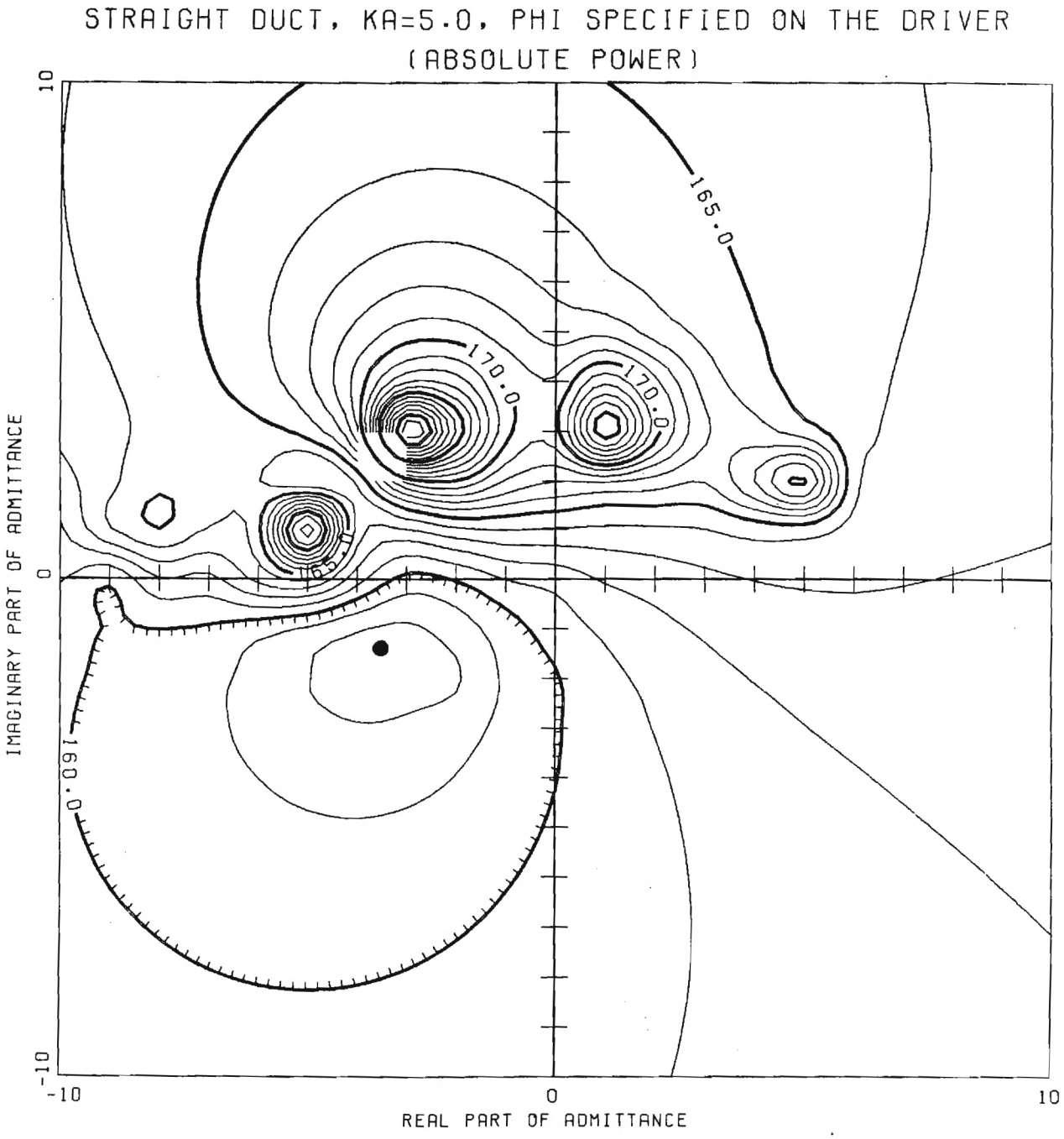
STRAIGHT DUCT, KA=5.0, PHI SPECIFIED ON THE DRIVER
(ABSOLUTE POWER)
IMAGINARY PART OF ADMITTANCE
REAL PART OF ADMITTANCE
10
0
-10
-10
0
10
165.0
170.0
170.0
165.0
160.0

Figure 11b

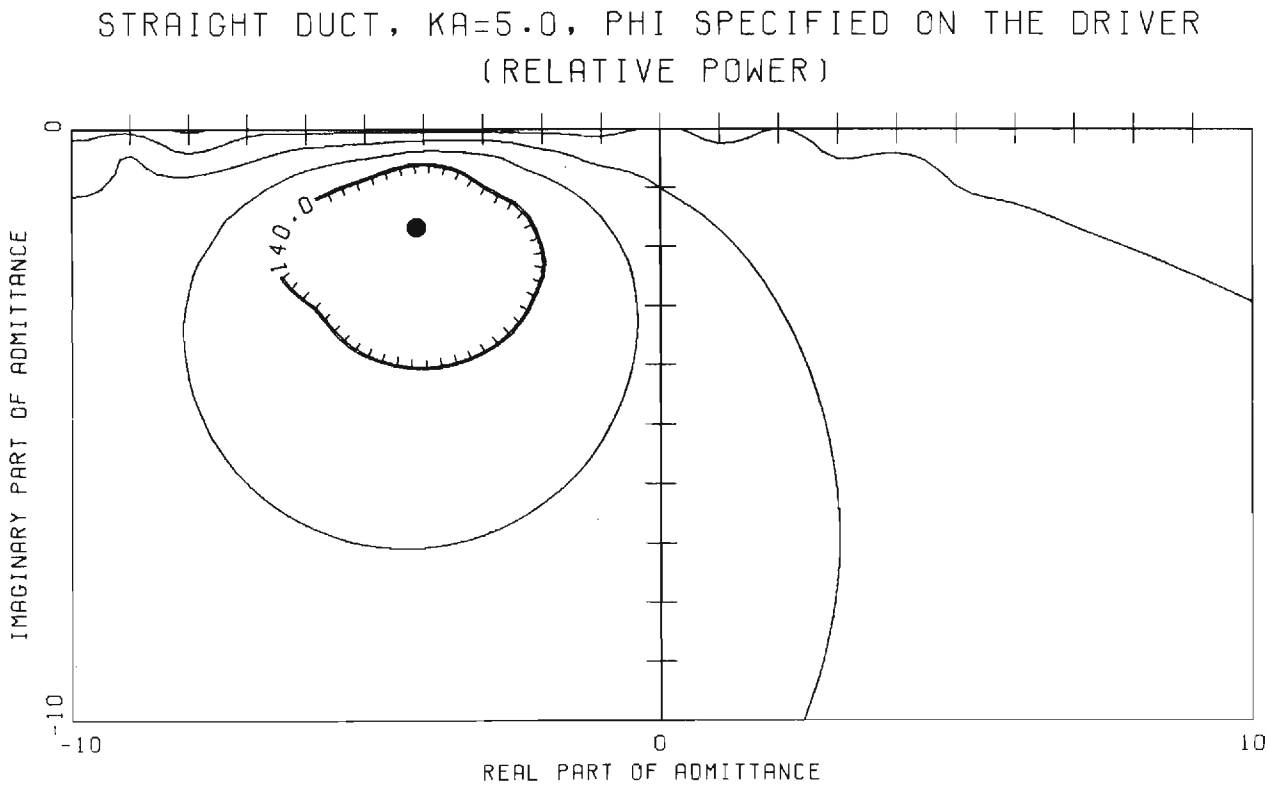
STRAIGHT DUCT, KA=5.0, PHI SPECIFIED ON THE DRIVER
(RELATIVE POWER)
IMAGINARY PART OF ADMITTANCE
0
-10
-10
0
10
REAL PART OF ADMITTANCE
-40.0

Figure 11c

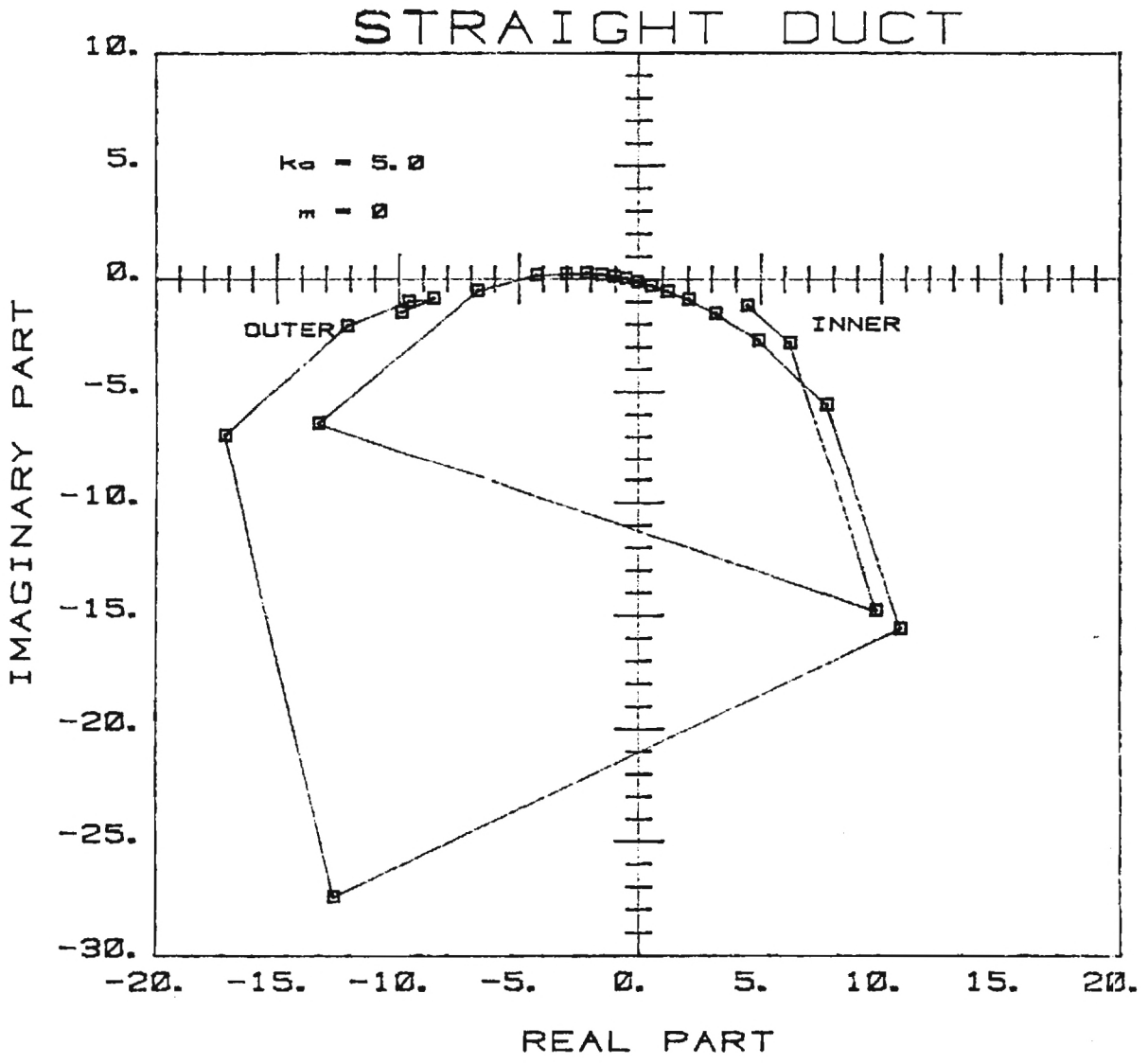

OPTIMUM ADMITTANCE DISTRIBUTION

Constant Velocity on the Driver

Figure 11d

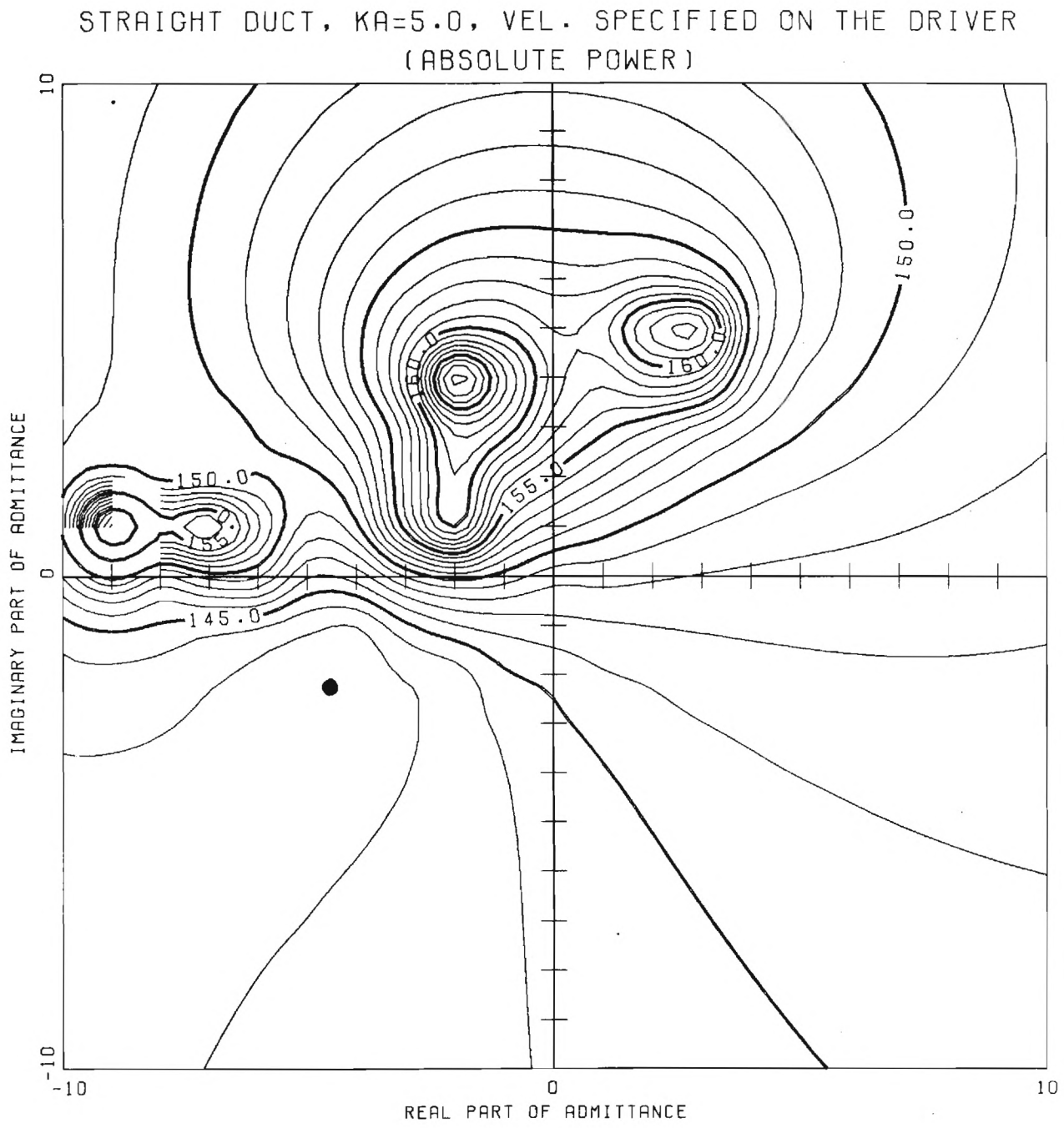
STRAIGHT DUCT, KA=5.0, VEL. SPECIFIED ON THE DRIVER
(ABSOLUTE POWER)
IMAGINARY PART OF ADMITTANCE
REAL PART OF ADMITTANCE
10
0
-10
-10
0
10
150.0
155.0
160.0
145.0

Figure 11e

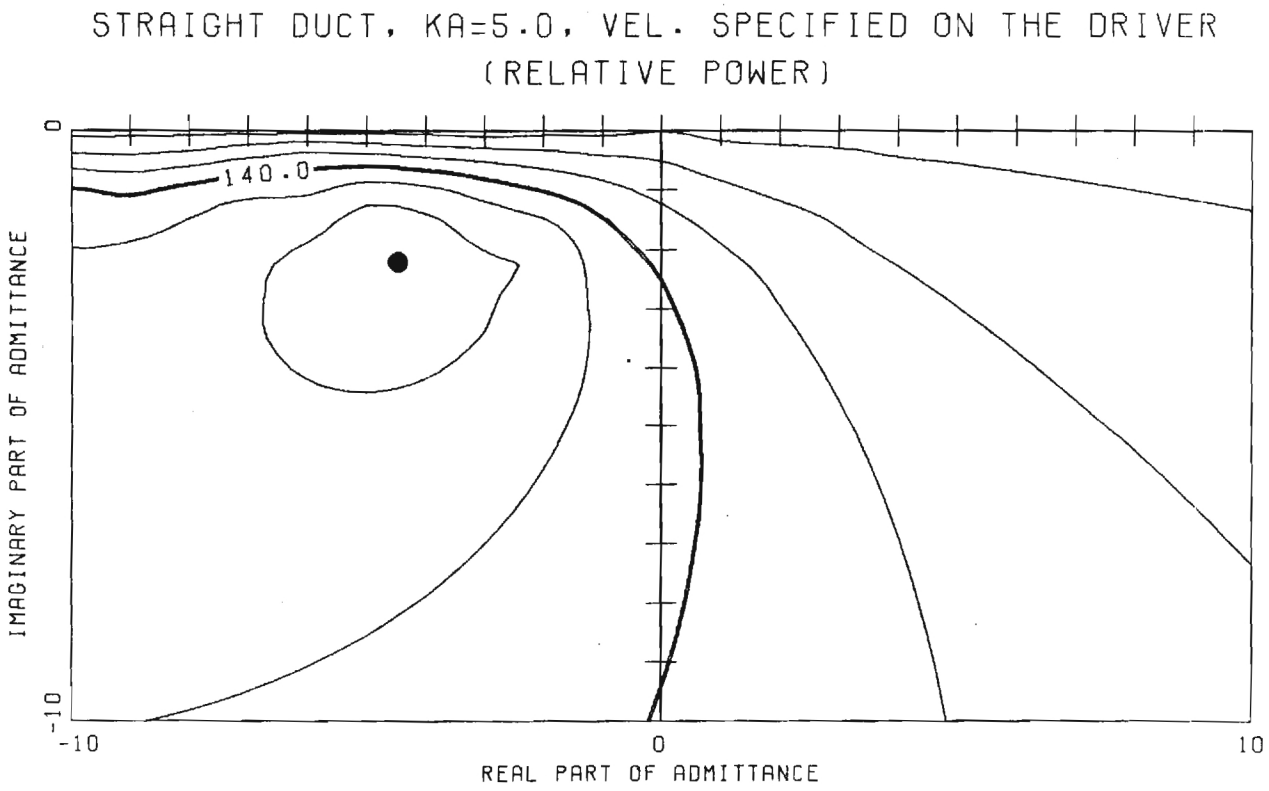
STRAIGHT DUCT, KA=5.0, VEL. SPECIFIED ON THE DRIVER
(RELATIVE POWER)
140.0
IMAGINARY PART OF ADMITTANCE
0
-10
-10
0
10
REAL PART OF ADMITTANCE

Figure 11f

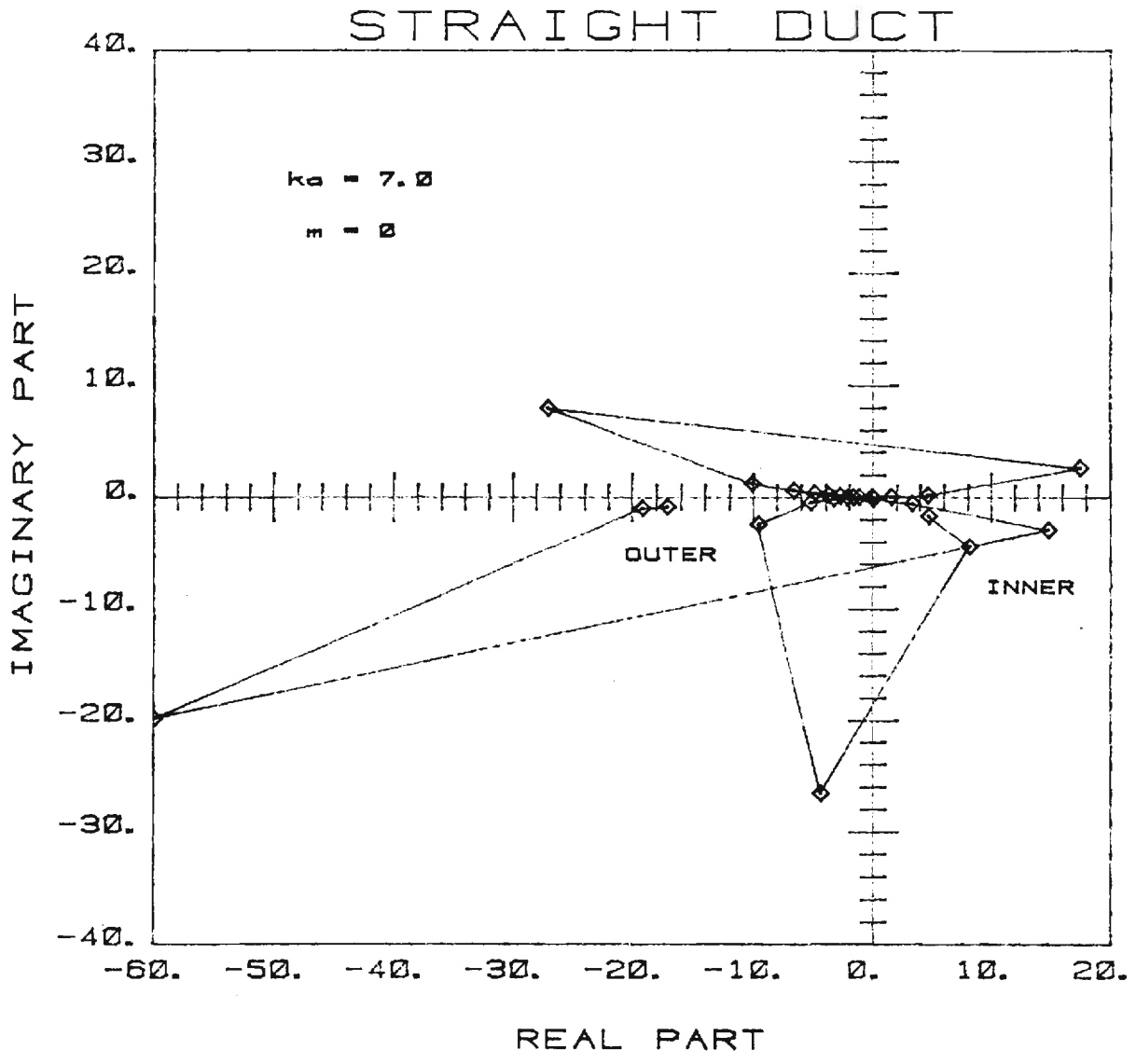

OPTIMUM ADMITTANCE DISTRIBUTION

Constant Phi on the Driver

Figure 12a

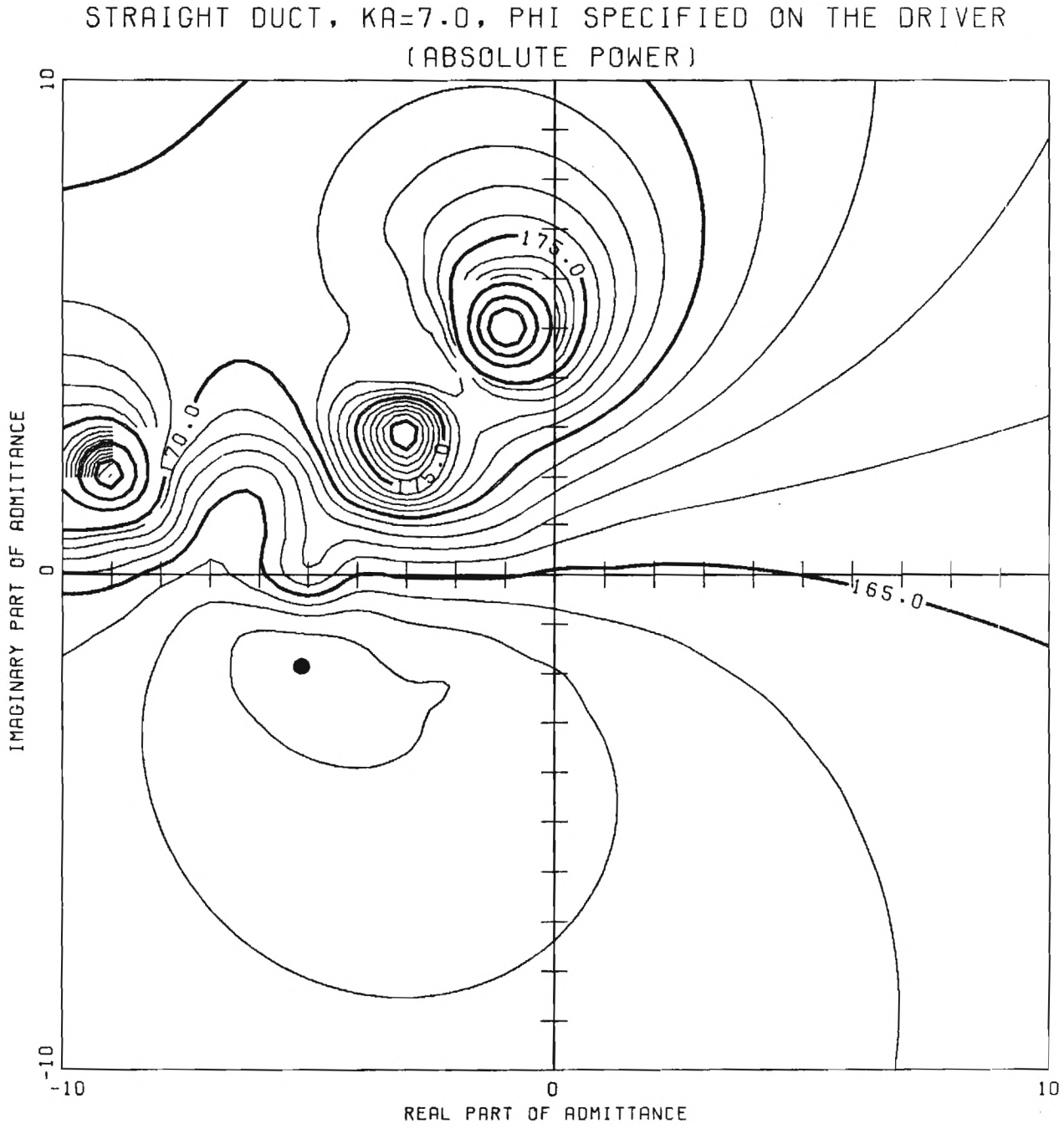
STRAIGHT DUCT, KA=7.0, PHI SPECIFIED ON THE DRIVER
(ABSOLUTE POWER)
IMAGINARY PART OF ADMITTANCE
REAL PART OF ADMITTANCE
10
0
-10
-10
0
10
175.0
170.0
165.0

Figure 12b

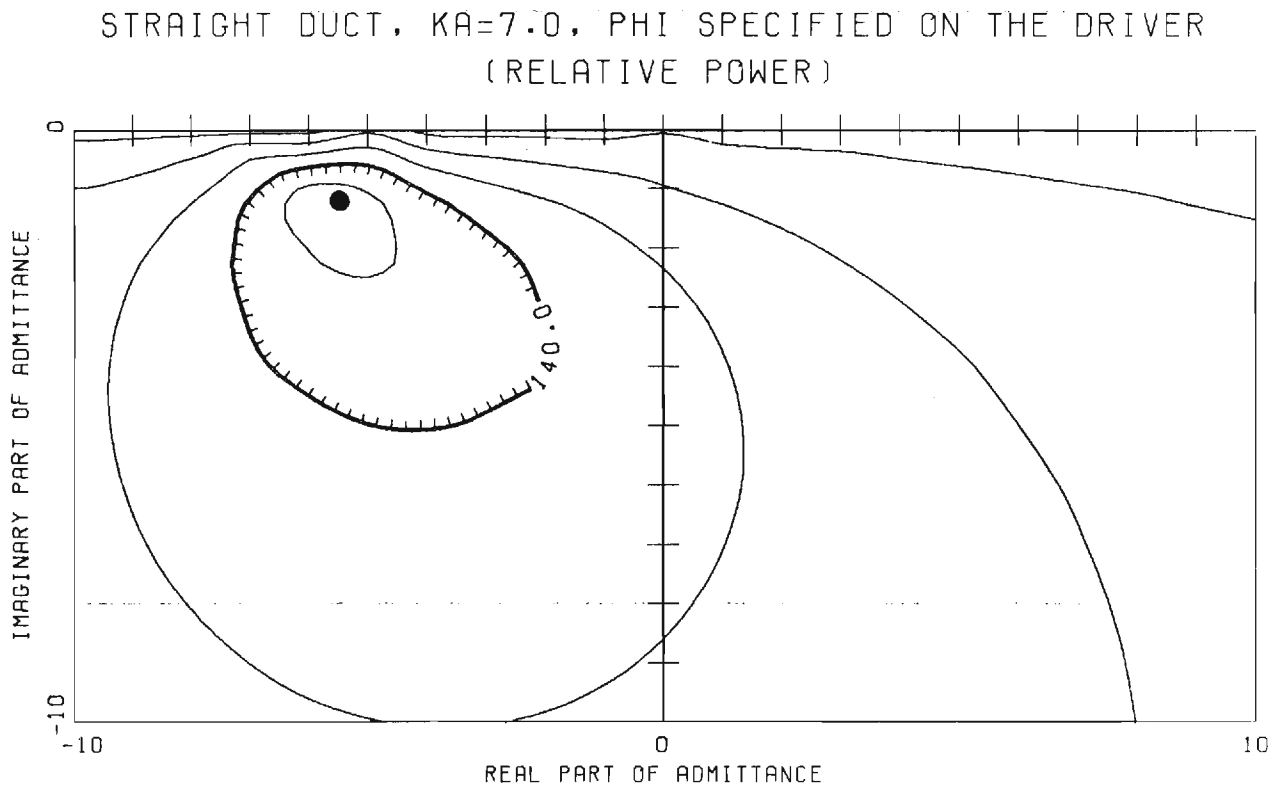
STRAIGHT DUCT, KA=7.0, PHI SPECIFIED ON THE DRIVER
(RELATIVE POWER)
0
-10
IMAGINARY PART OF ADMITTANCE
-10
0
10
REAL PART OF ADMITTANCE
0.
140.

Figure 12c

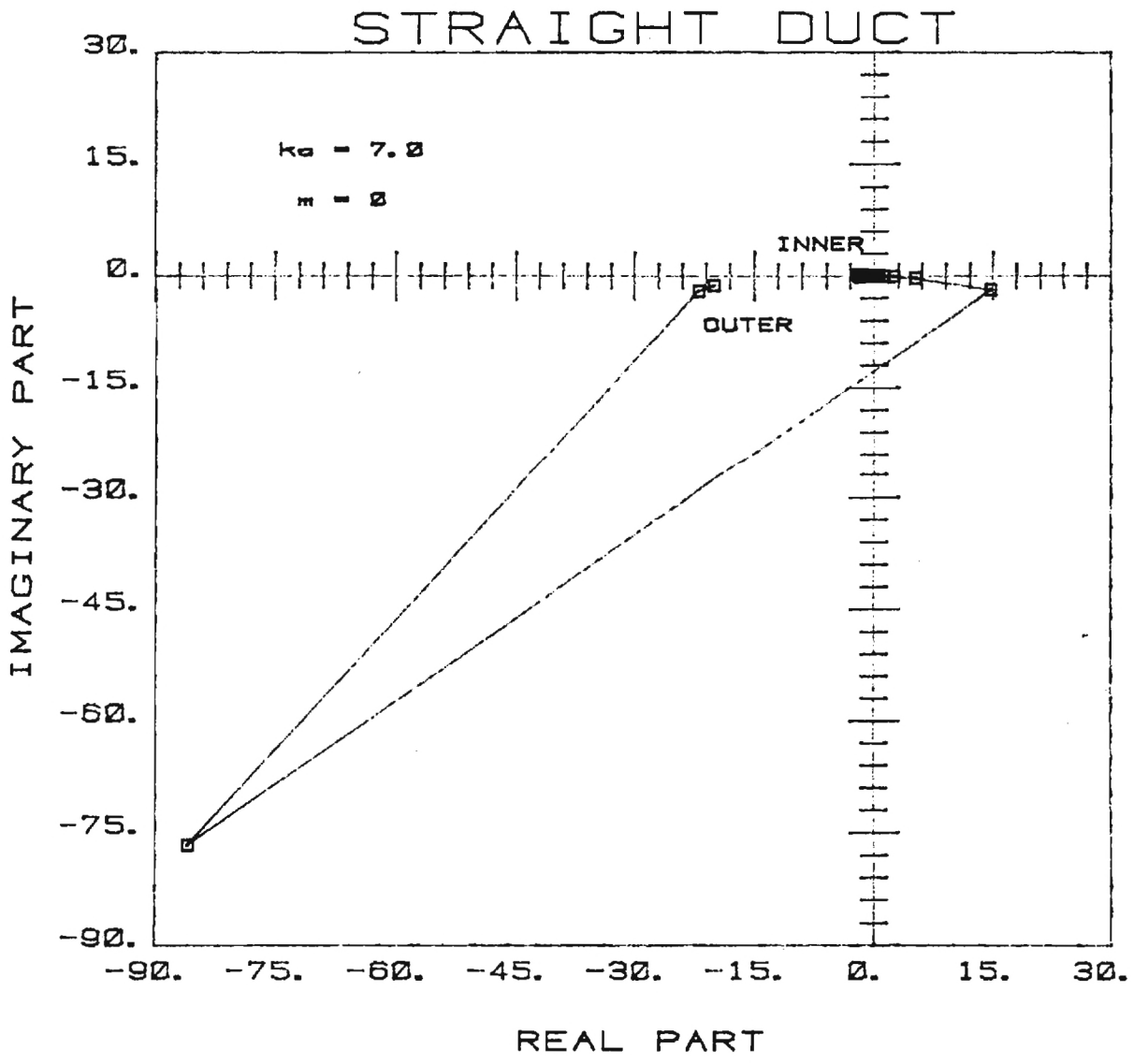

OPTIMUM ADMITTANCE DISTRIBUTION

Constant Velocity on the Driver

Figure 12d

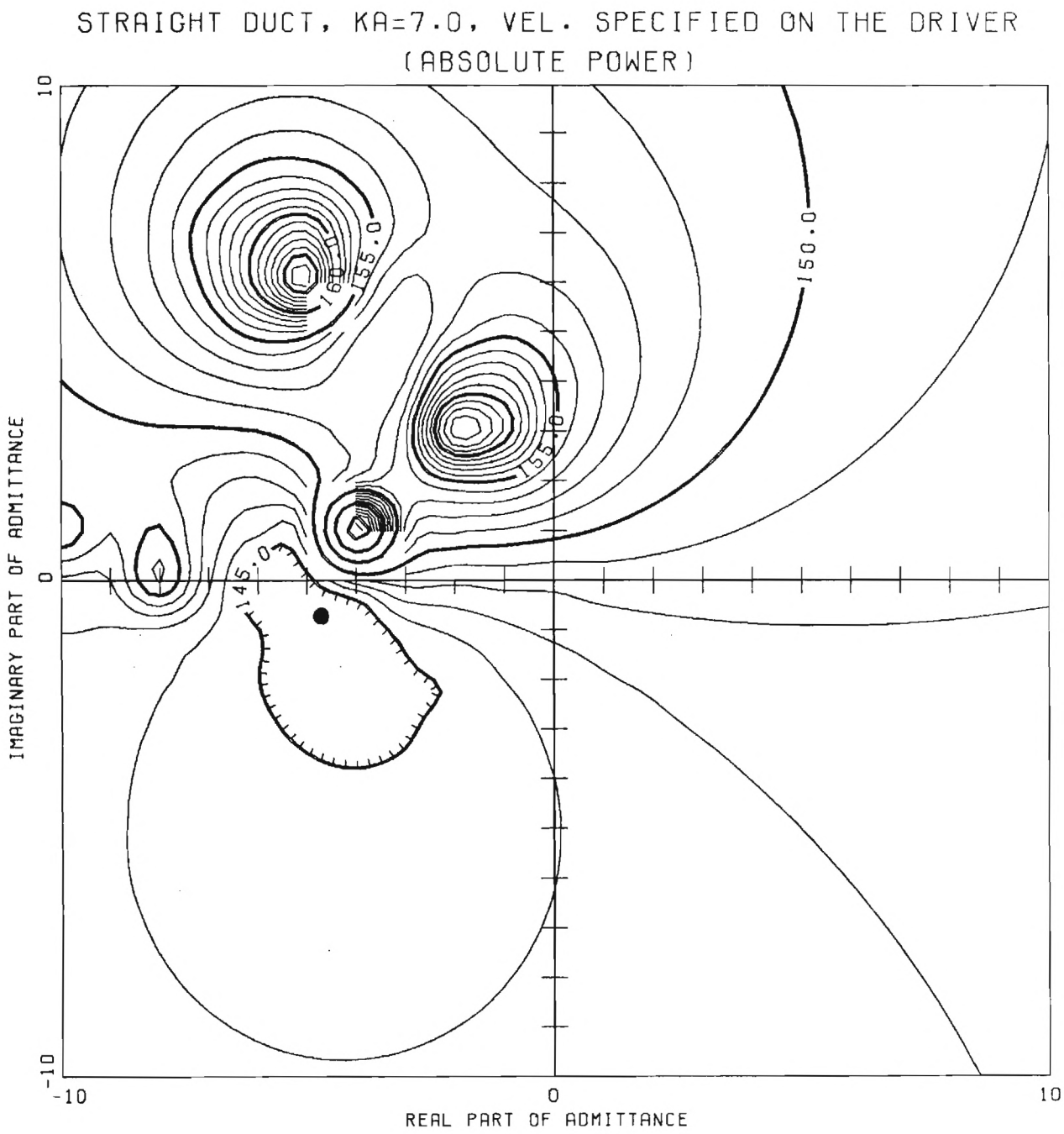
STRAIGHT DUCT, KA=7.0, VEL. SPECIFIED ON THE DRIVER
(ABSOLUTE POWER)
160.0
155.0
150.0
155.0
145.0
10
0
-10
-10
0
10
IMAGINARY PART OF ADMITTANCE
REAL PART OF ADMITTANCE

Figure 12e

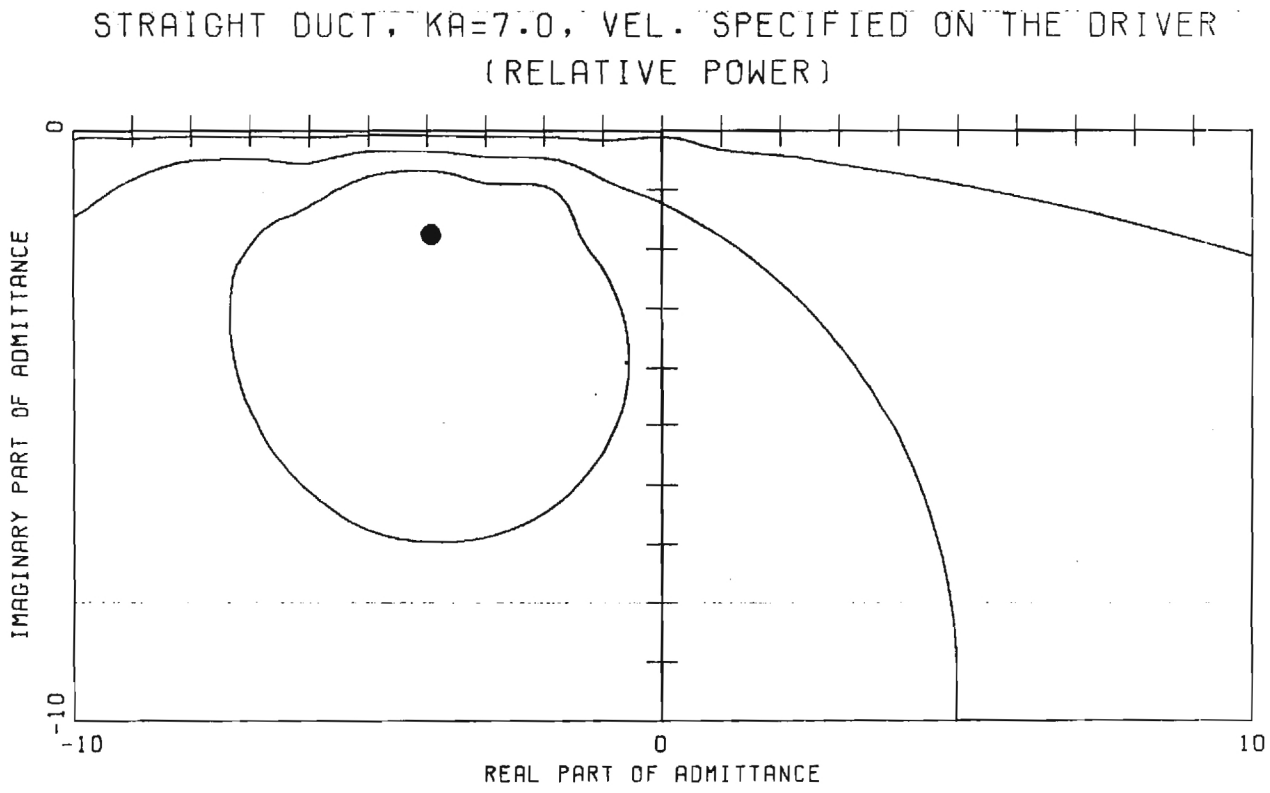
STRAIGHT DUCT, KA=7.0, VEL. SPECIFIED ON THE DRIVER
(RELATIVE POWER)
0
-10
IMAGINARY PART OF ADMITTANCE
-10
0
10
REAL PART OF ADMITTANCE

Figure 12f

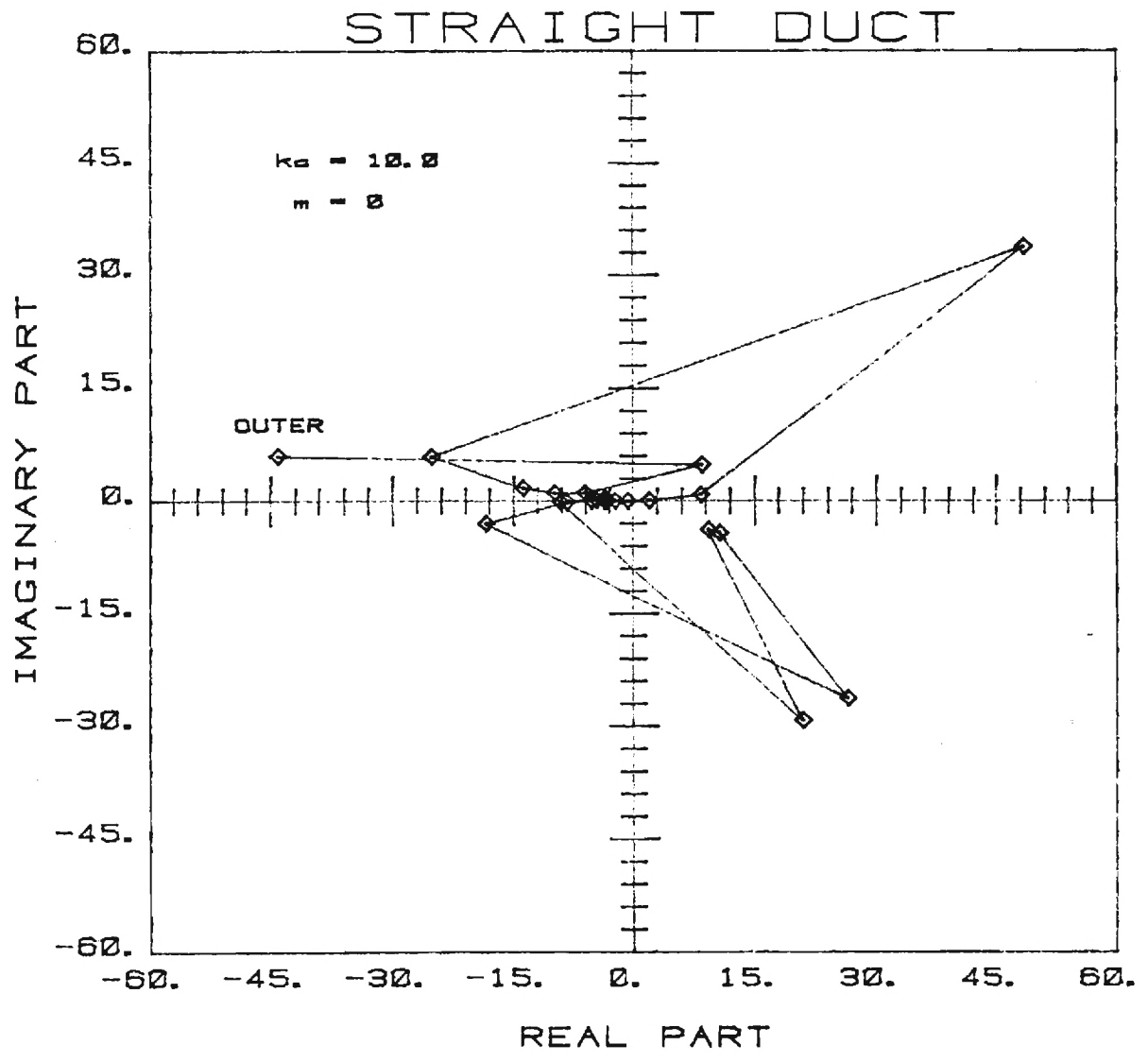

OPTIMUM ADMITTANCE DISTRIBUTION

Constant Phi on the Driver

Figure 13a

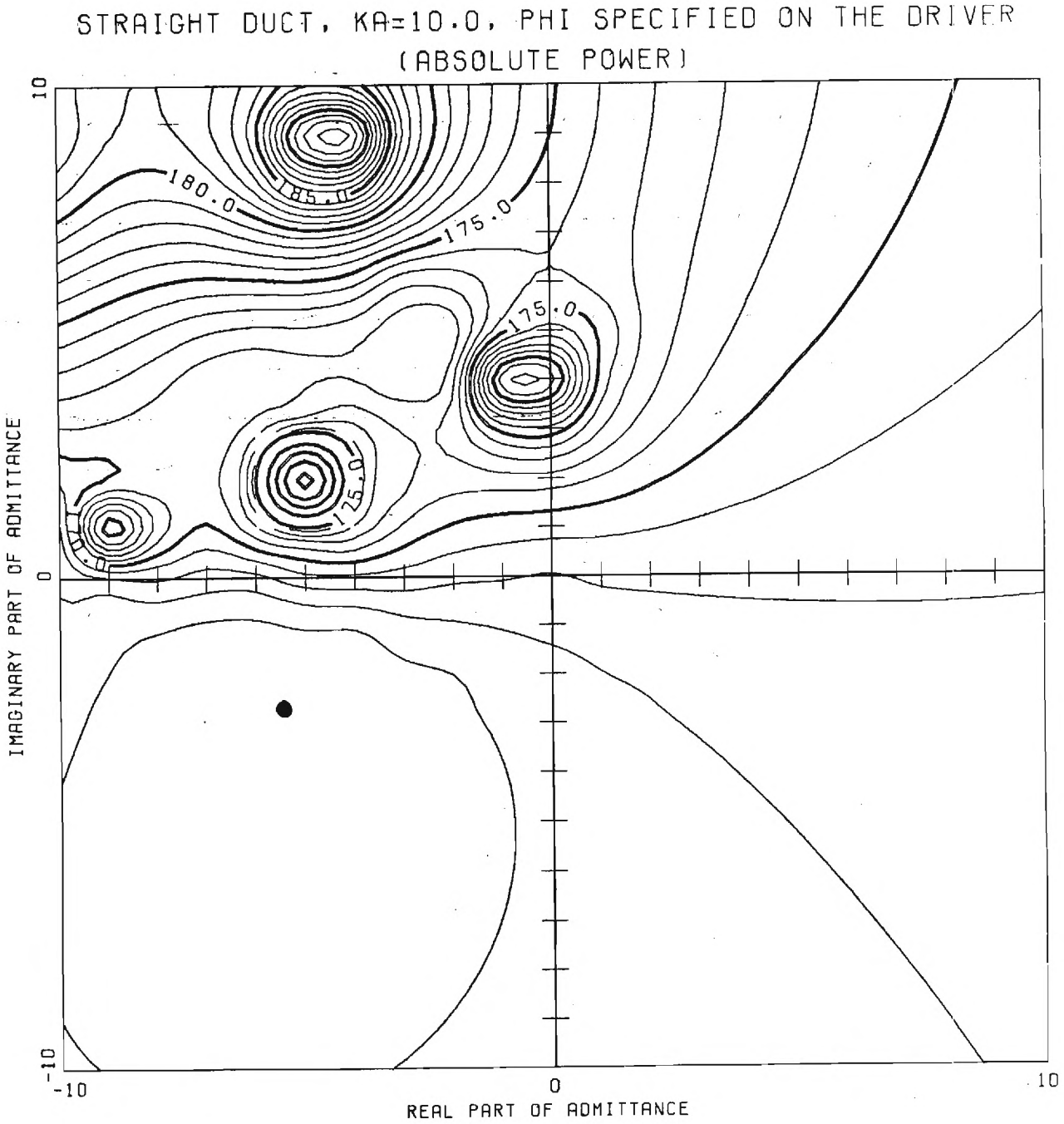
STRAIGHT DUCT, KA=10.0, PHI SPECIFIED ON THE DRIVER
(ABSOLUTE POWER)
180.0
185.0
175.0
175.0
125.0
10
0
-10
-10
0
10
IMAGINARY PART OF ADMITTANCE
REAL PART OF ADMITTANCE

Figure 13b

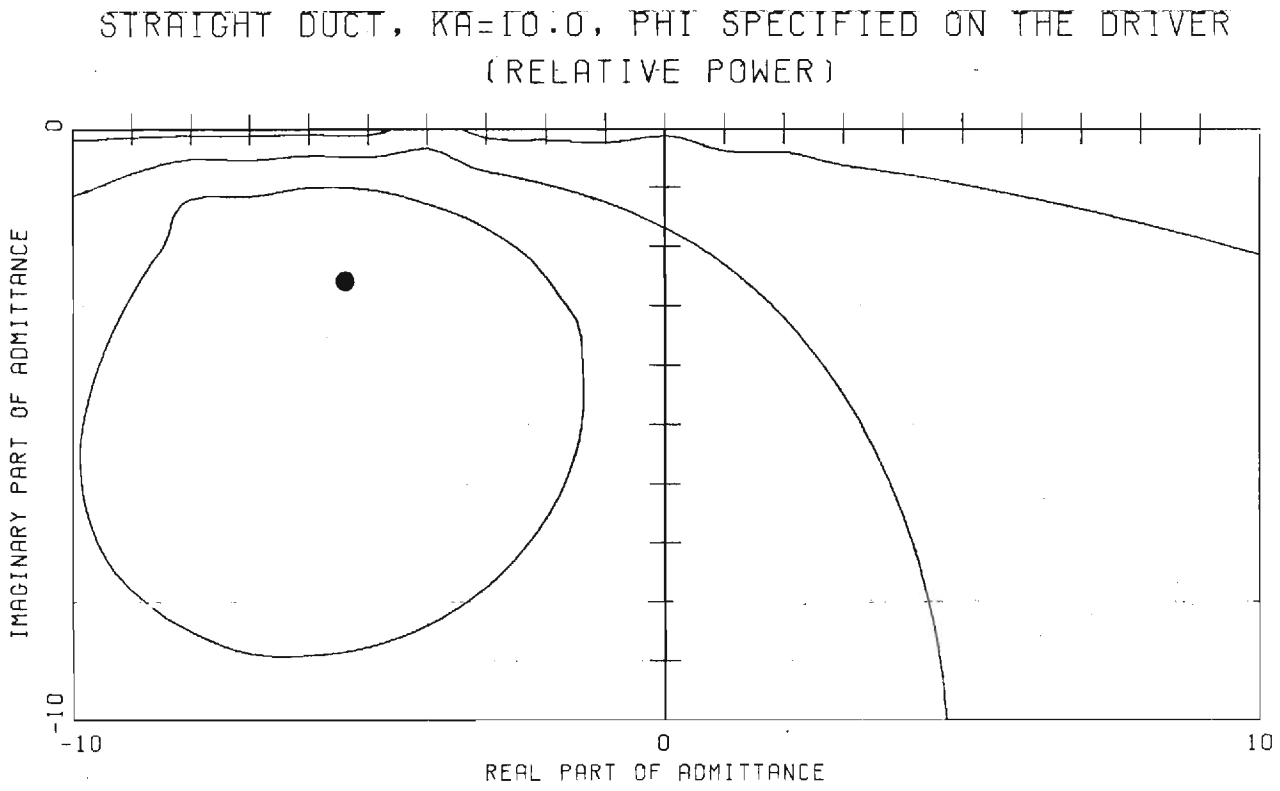
STRAIGHT DUCT, KA=10.0, PHI SPECIFIED ON THE DRIVER
(RELATIVE POWER)
IMAGINARY PART OF ADMITTANCE
0
-10
-10
0
10
REAL PART OF ADMITTANCE

Figure 13c

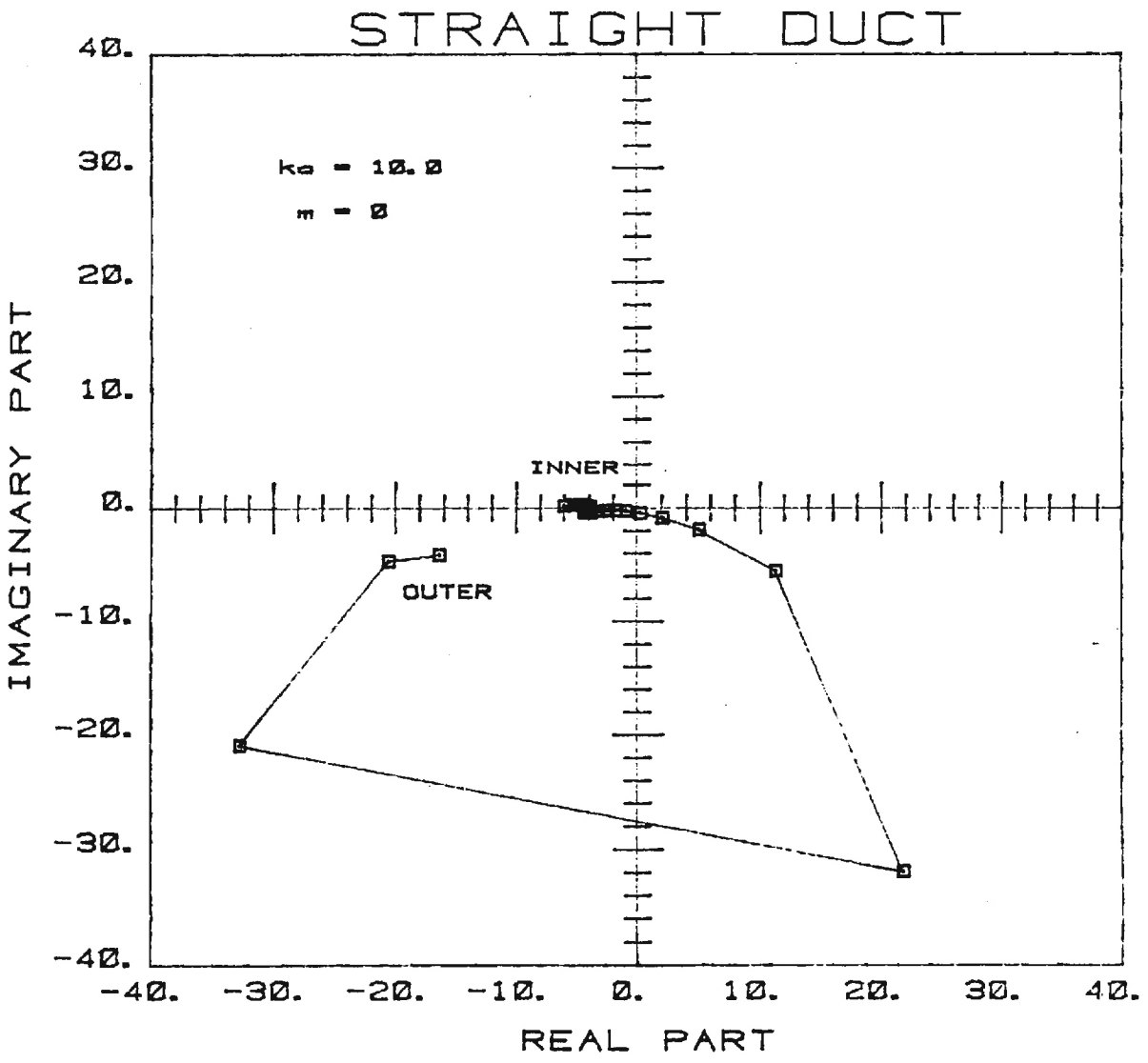

OPTIMUM ADMITTANCE DISTRIBUTION

Constant Velocity on the Driver

Figure 13d

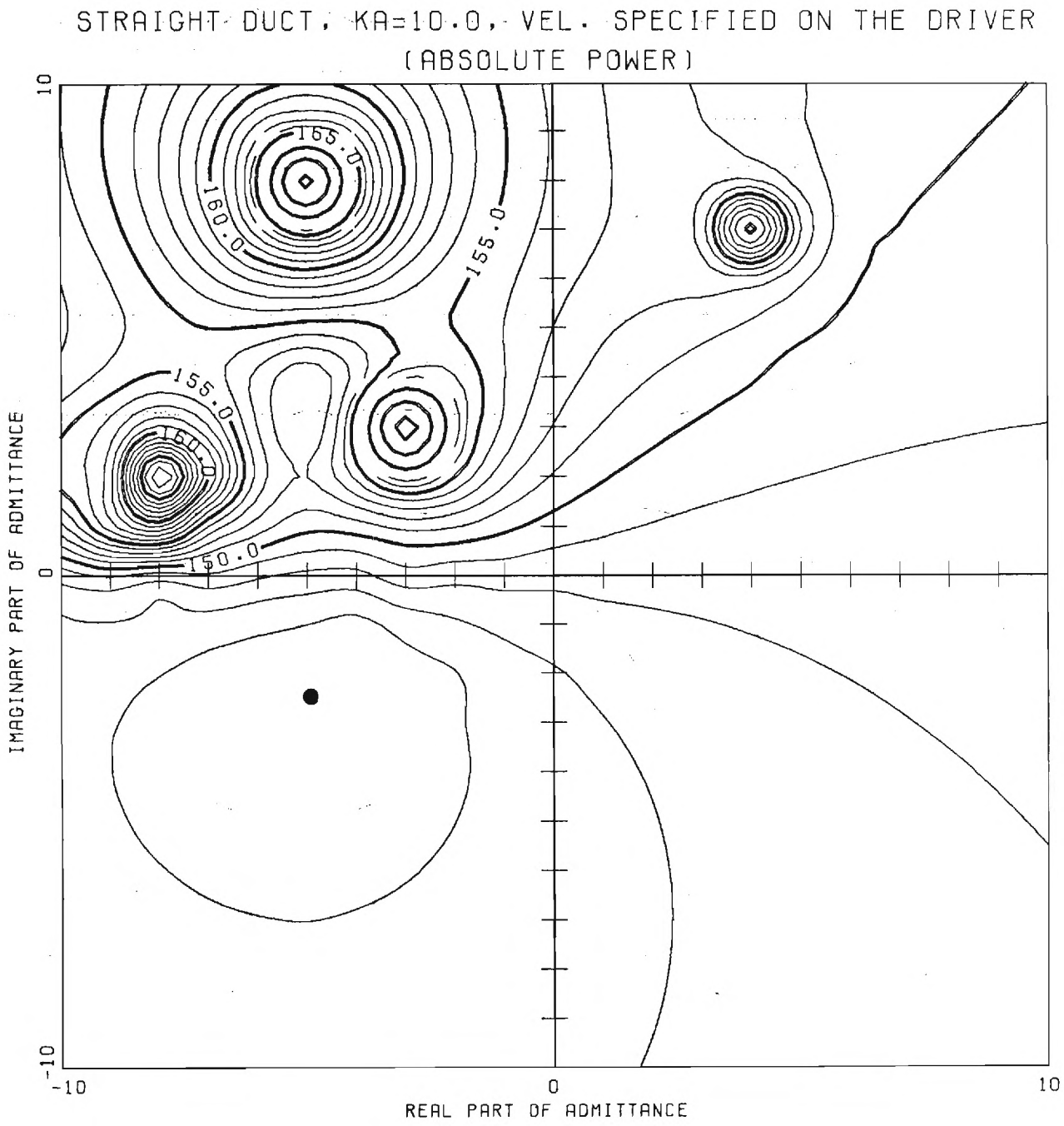
STRAIGHT DUCT, KA=10.0, VEL. SPECIFIED ON THE DRIVER
(ABSOLUTE POWER)
165.0
160.0
155.0
155.0
160.0
150.0
10
0
-10
-10
0
10
IMAGINARY PART OF ADMITTANCE
REAL PART OF ADMITTANCE

Figure 13e

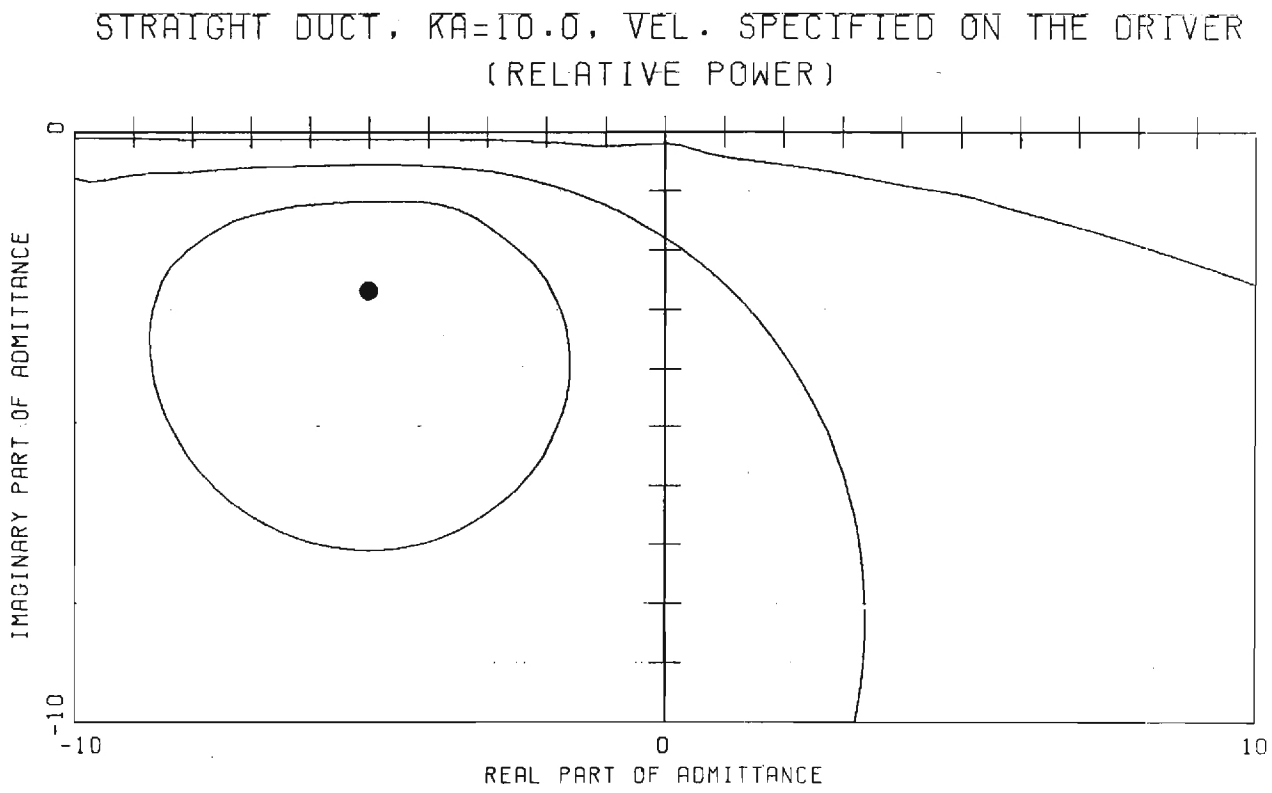
STRAIGHT DUCT, KA=10.0, VEL. SPECIFIED ON THE DRIVER
(RELATIVE POWER)
IMAGINARY PART OF ADMITTANCE
0
-10
-10
0
10
REAL PART OF ADMITTANCE

Figure 13f

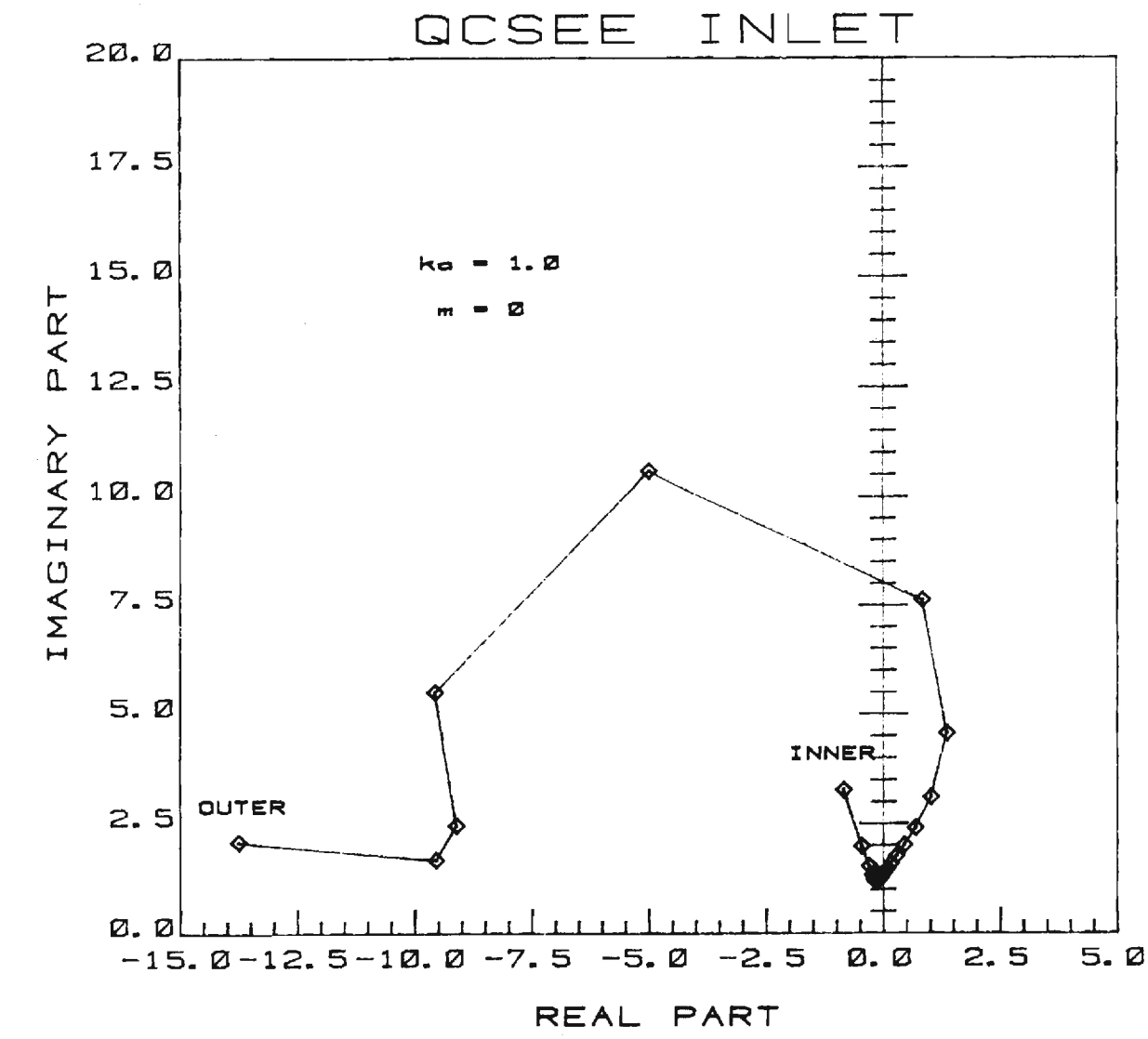
QCSEE INLET
20.0
17.5
15.0
12.5
10.0
7.5
5.0
2.5
0.0
IMAGINARY PART
ka = 1.0
m = 0
OUTER
INNER
-15.0 -12.5 -10.0 -7.5 -5.0 -2.5 0.0 2.5 5.0
REAL PART
OPTIMUM ADMITTANCE DISTRIBUTION
Constant Phi on the Driver

Figure 14a

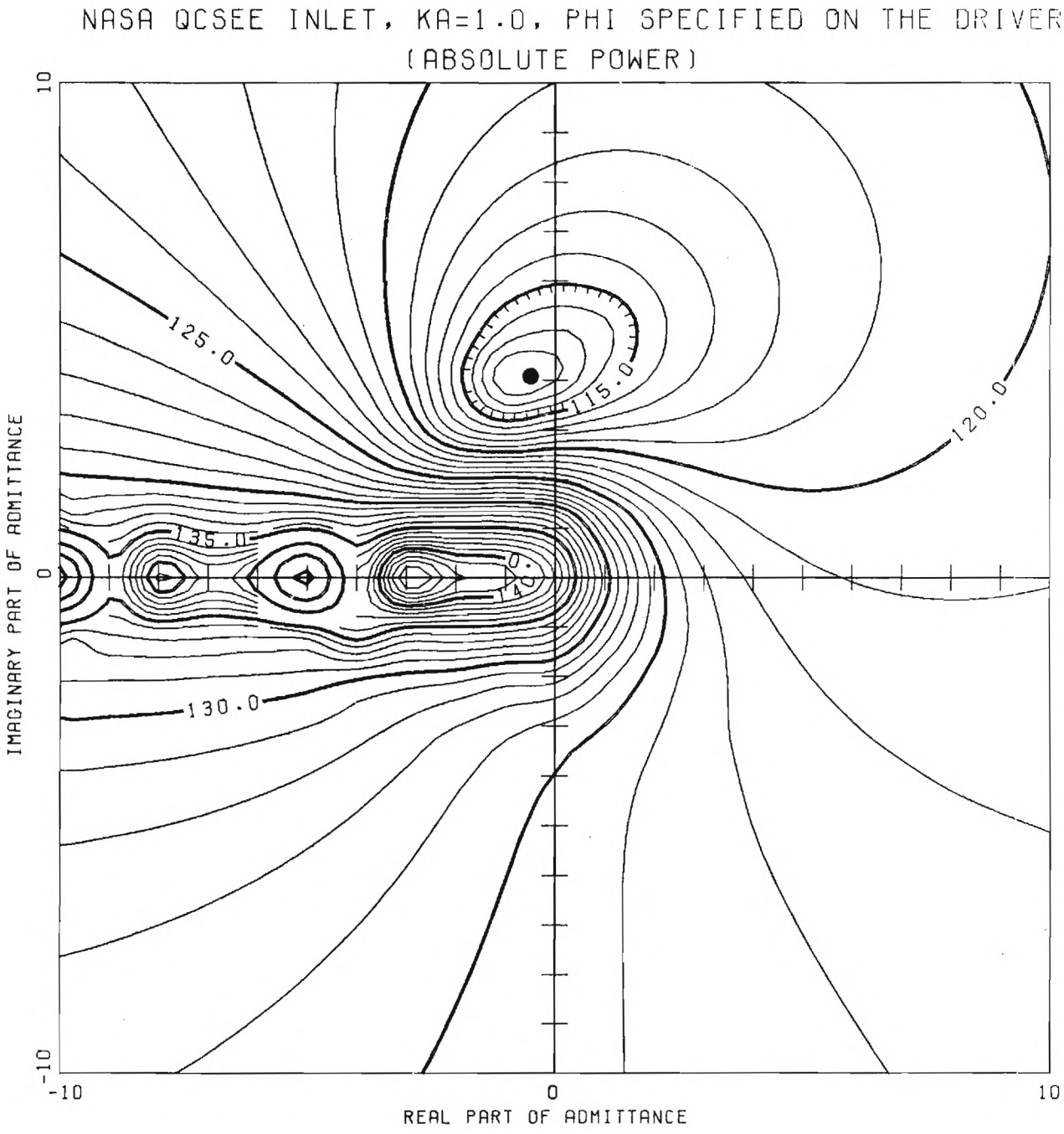
NASA QCSEE INLET, KA=1.0, PHI SPECIFIED ON THE DRIVER
(ABSOLUTE POWER)
IMAGINARY PART OF ADMITTANCE
REAL PART OF ADMITTANCE
10
0
-10
-10
0
10
125.0
115.0
120.0
135.0
0.0
130.0

Figure 14b

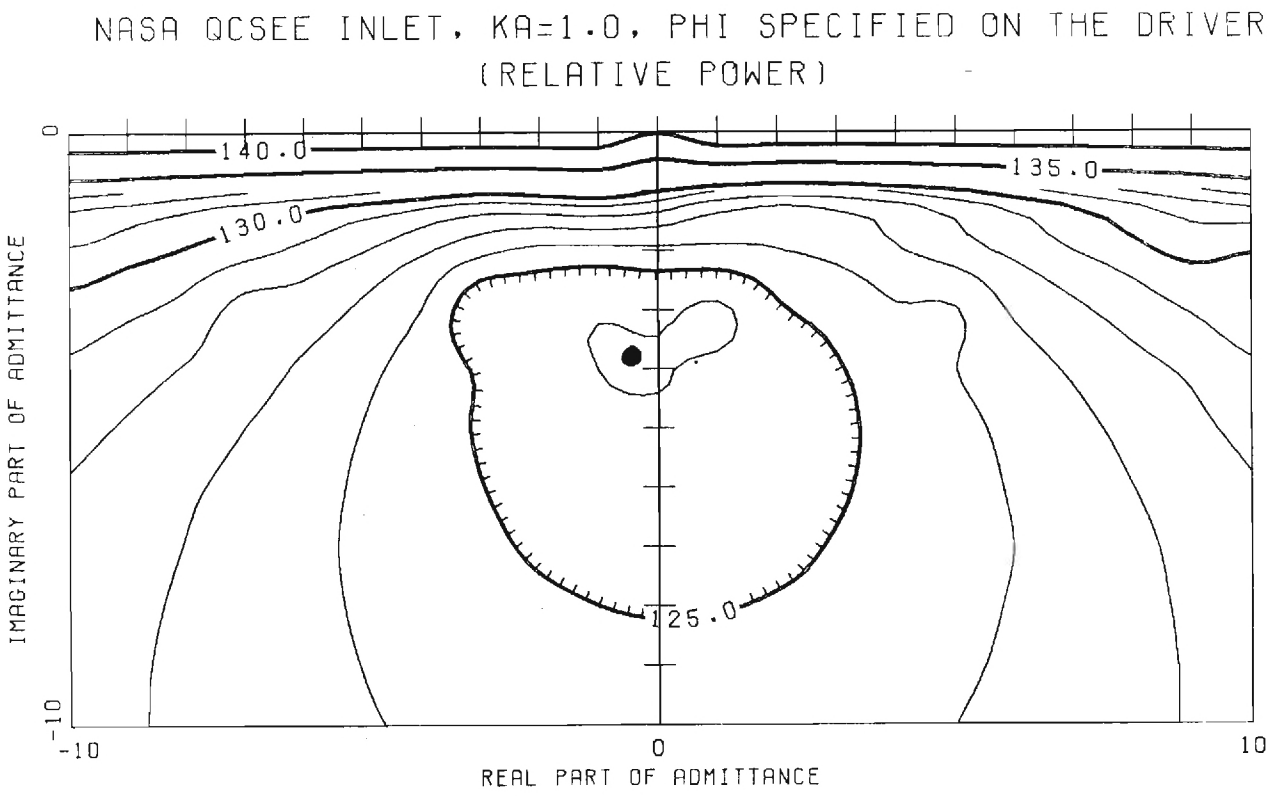
NASA QCSEE INLET, KA=1.0, PHI SPECIFIED ON THE DRIVER
(RELATIVE POWER)
140.0
135.0
130.0
125.0
0
-10
-10
0
10
IMAGINARY PART OF ADMITTANCE
REAL PART OF ADMITTANCE

Figure 14c

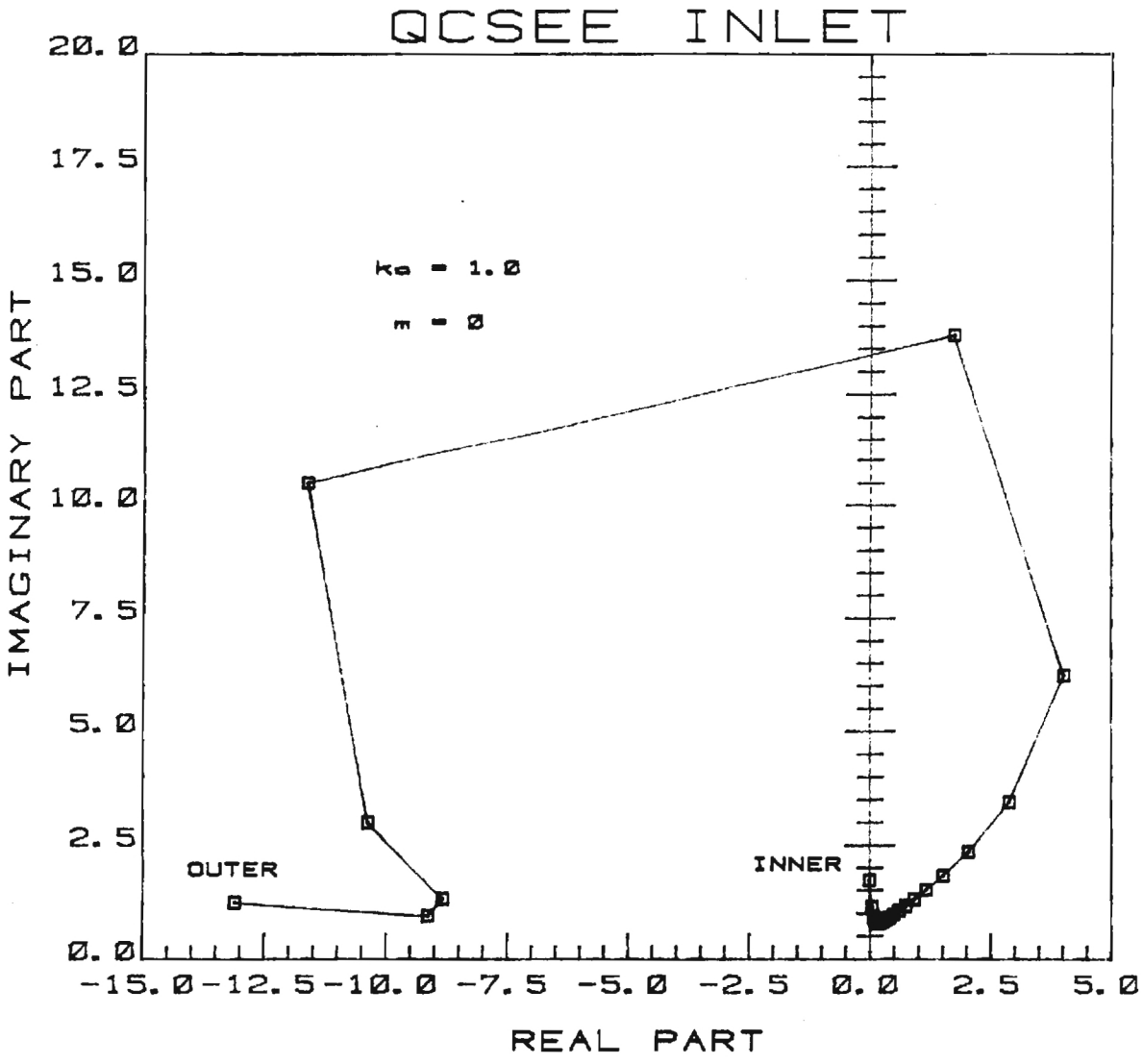

OPTIMUM ADMITTANCE DISTRIBUTION

Constant Velocity on the Driver

Figure 14d

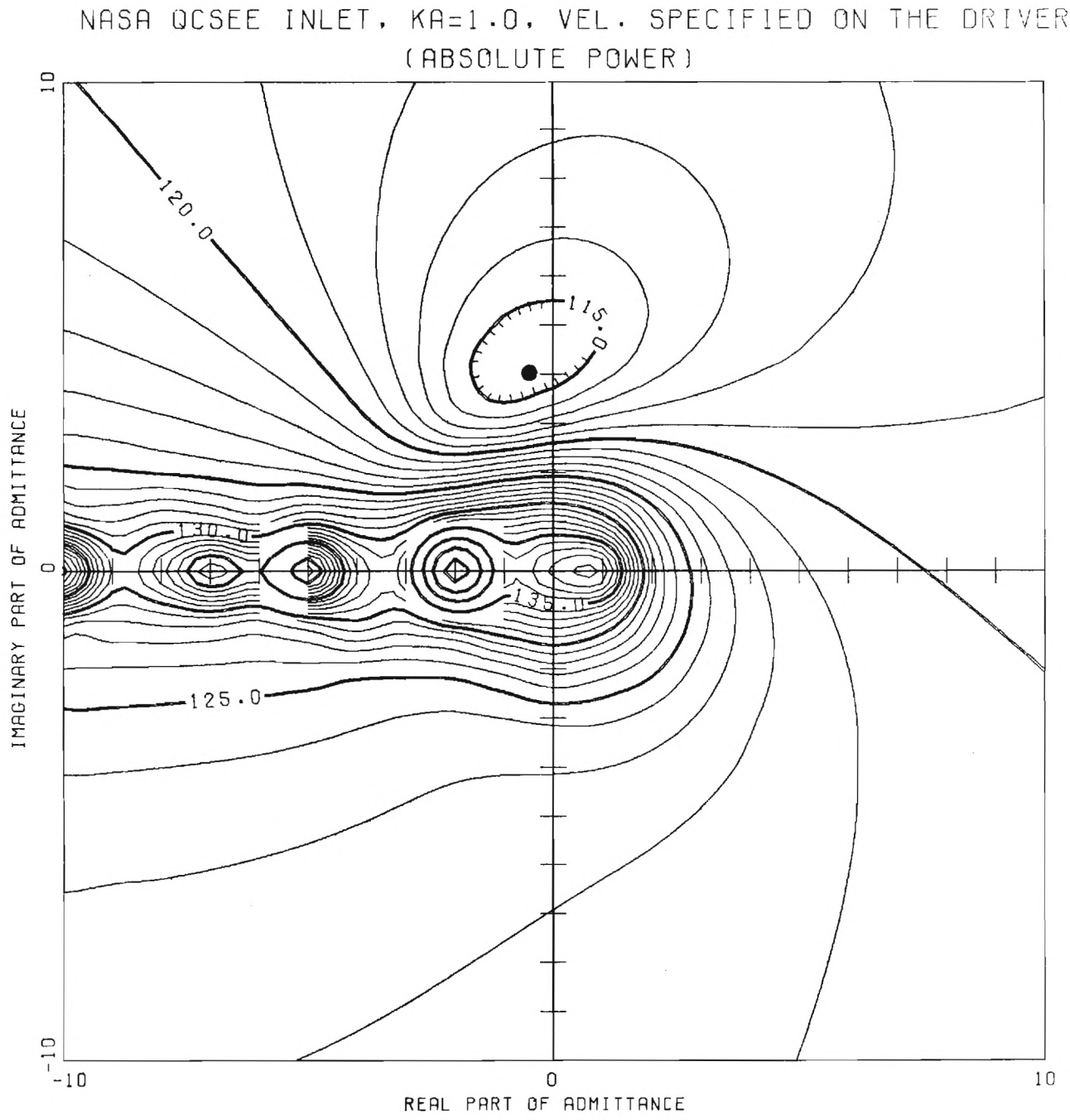
NASA QCSEE INLET, KA=1.0, VEL. SPECIFIED ON THE DRIVER
(ABSOLUTE POWER)
120.0
115.0
130.0
135.0
125.0
10
0
-10
-10
0
10
IMAGINARY PART OF ADMITTANCE
REAL PART OF ADMITTANCE

Figure 14e

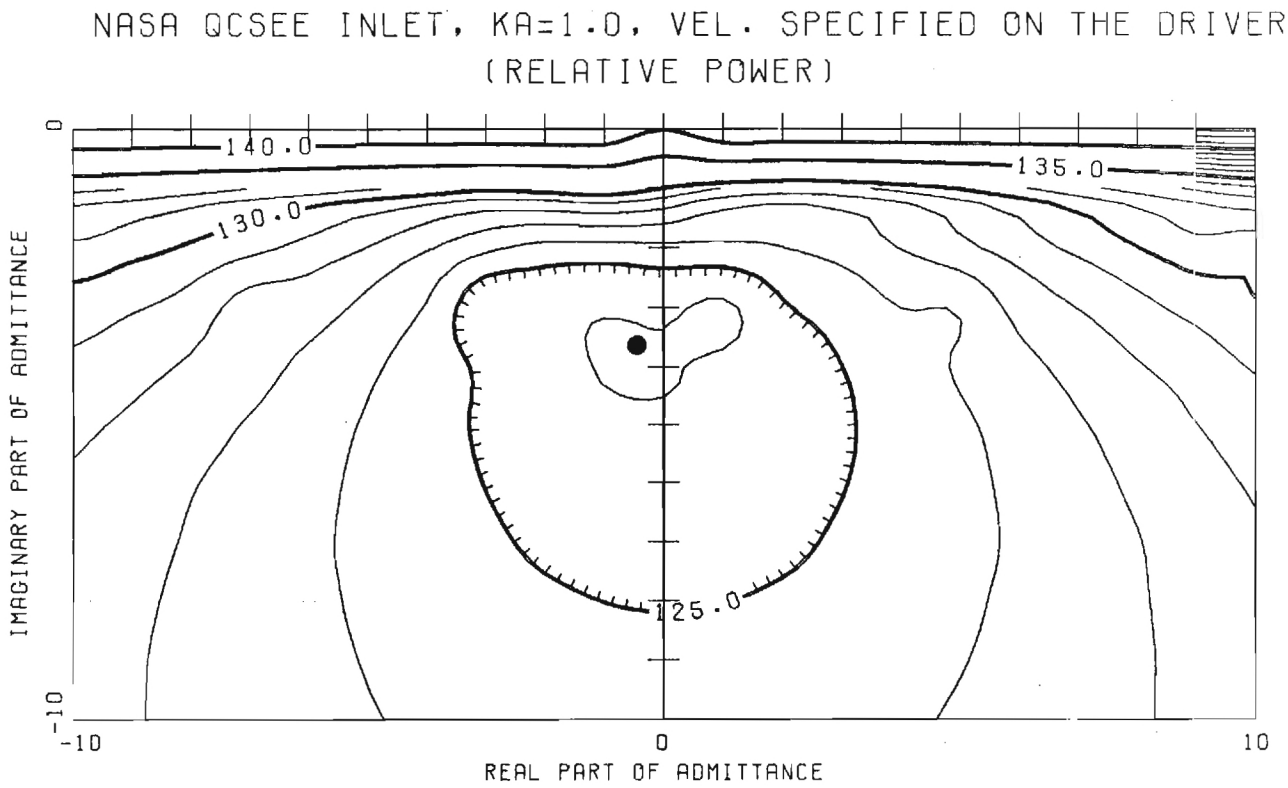
NASA QCSEE INLET, KA=1.0, VEL. SPECIFIED ON THE DRIVER
(RELATIVE POWER)
140.0
135.0
130.0
125.0
0
-10
-10
0
10
IMAGINARY PART OF ADMITTANCE
REAL PART OF ADMITTANCE

Figure 14f

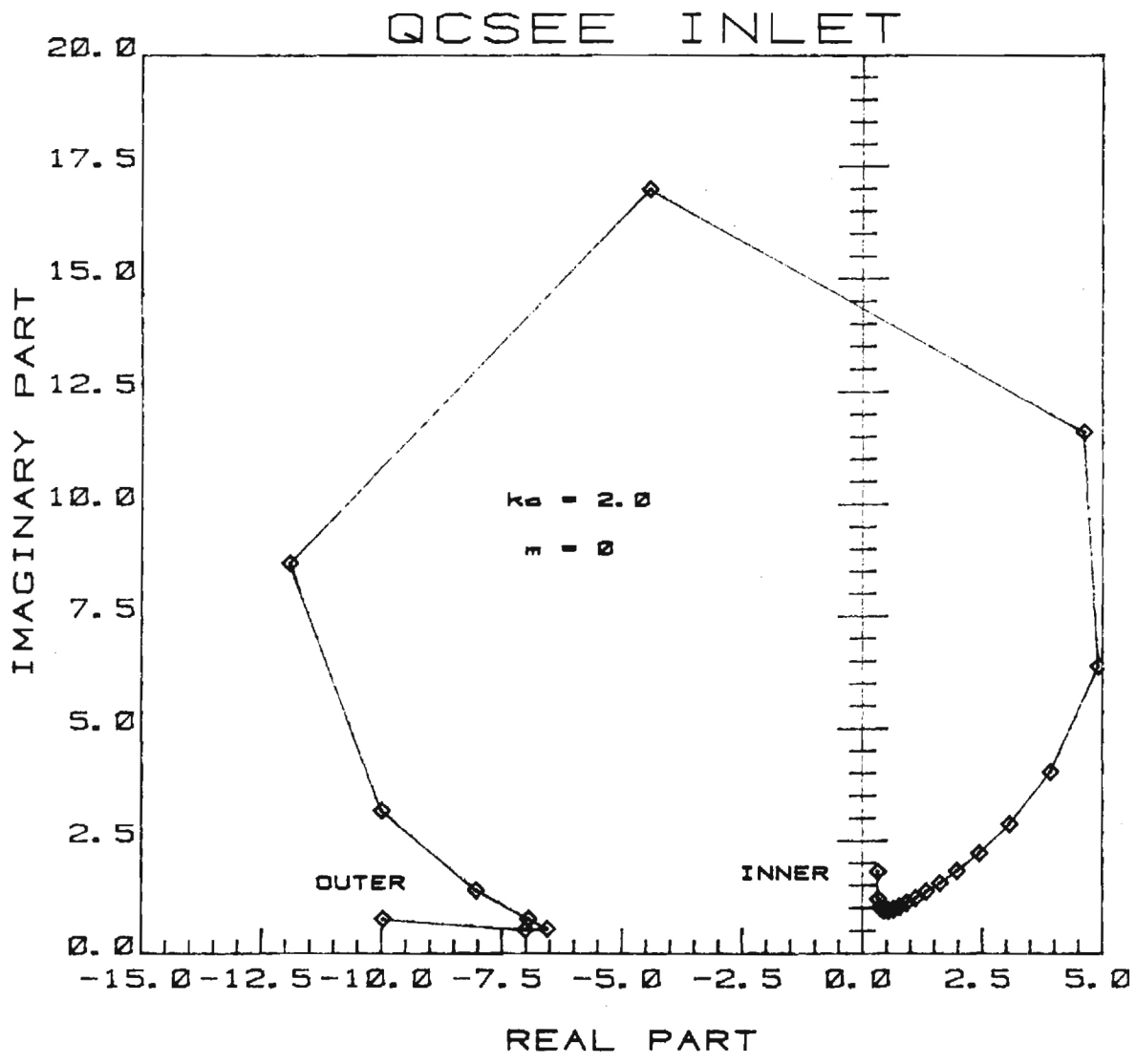

OPTIMUM ADMITTANCE DISTRIBUTION

Constant Phi on the Driver

Figure 15a

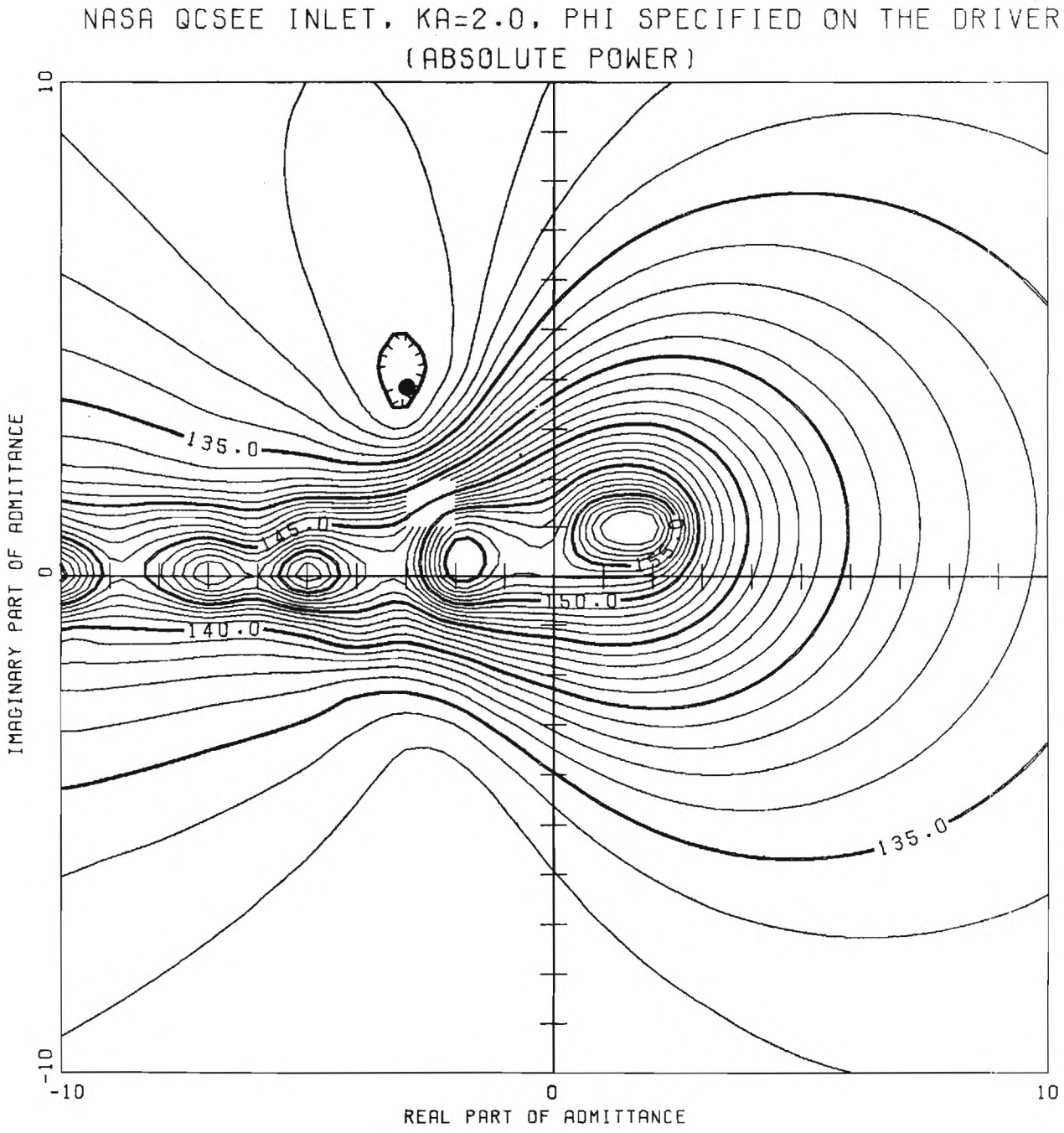
NASA QCSEE INLET, KA=2.0, PHI SPECIFIED ON THE DRIVER
(ABSOLUTE POWER)
IMAGINARY PART OF ADMITTANCE
REAL PART OF ADMITTANCE
10
0
-10
-10
0
10
135.0
145.0
150.0
140.0
135.0

Figure 15b

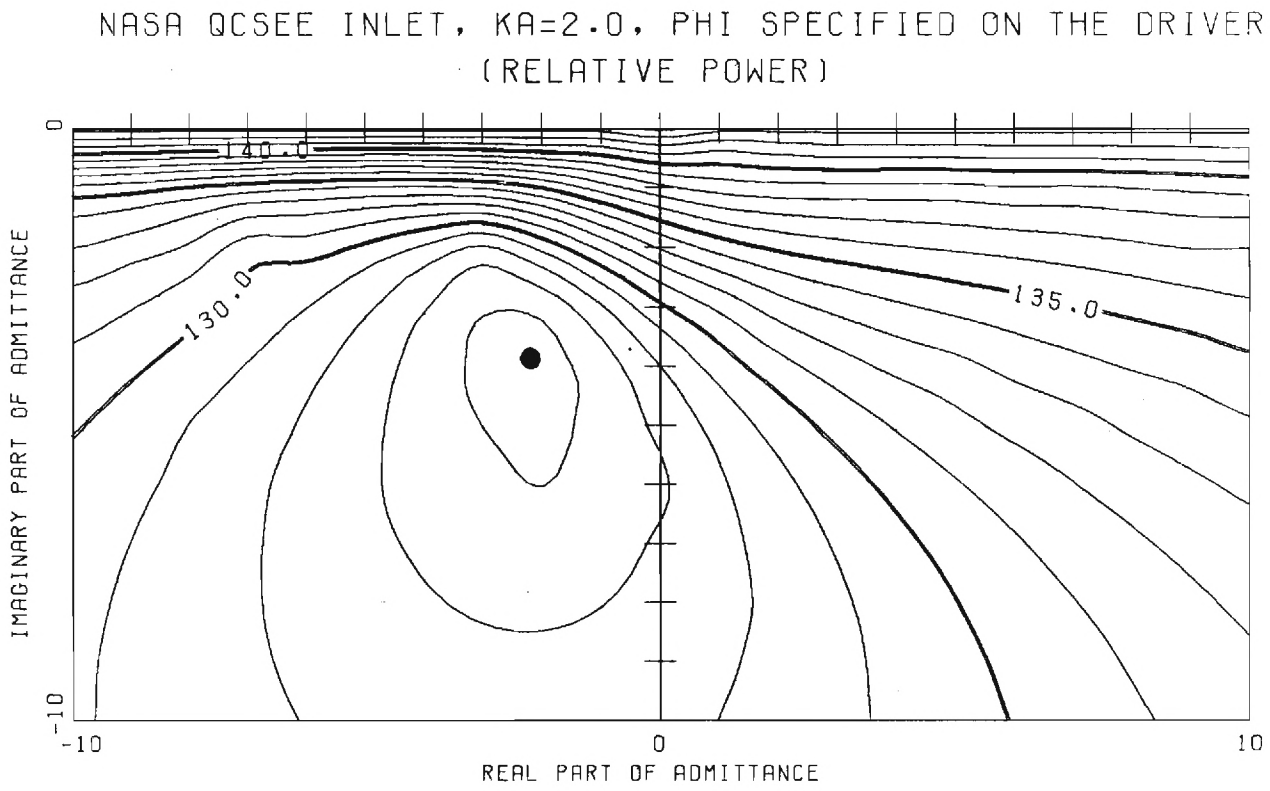
NASA QCSEE INLET, KA=2.0, PHI SPECIFIED ON THE DRIVER
(RELATIVE POWER)
140.0
130.0
135.0
0
-10
IMAGINARY PART OF ADMITTANCE
-10
0
10
REAL PART OF ADMITTANCE

Figure 15c

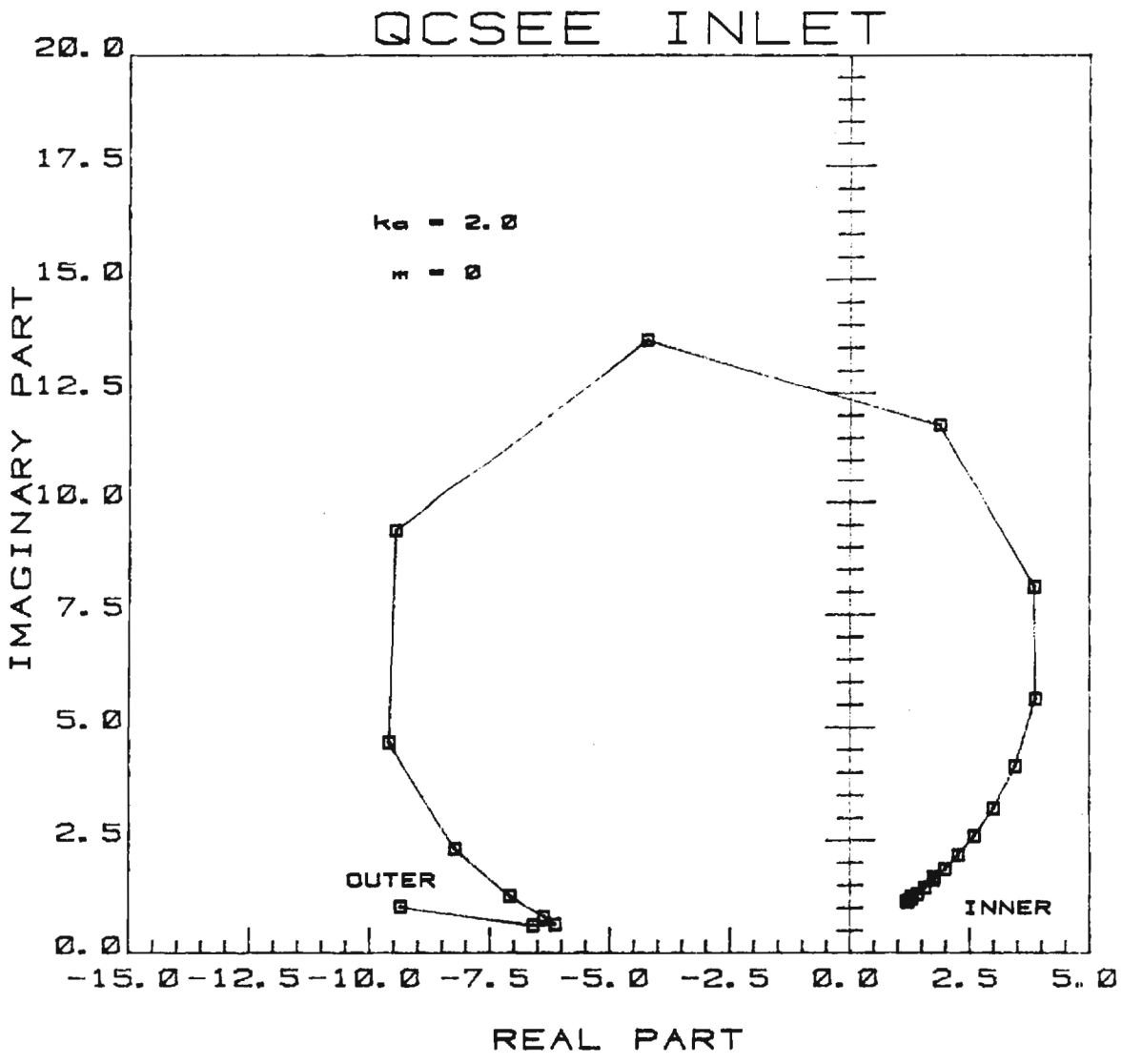

OPTIMUM ADMITTANCE DISTRIBUTION

Constant Velocity on the Driver

Figure 15d

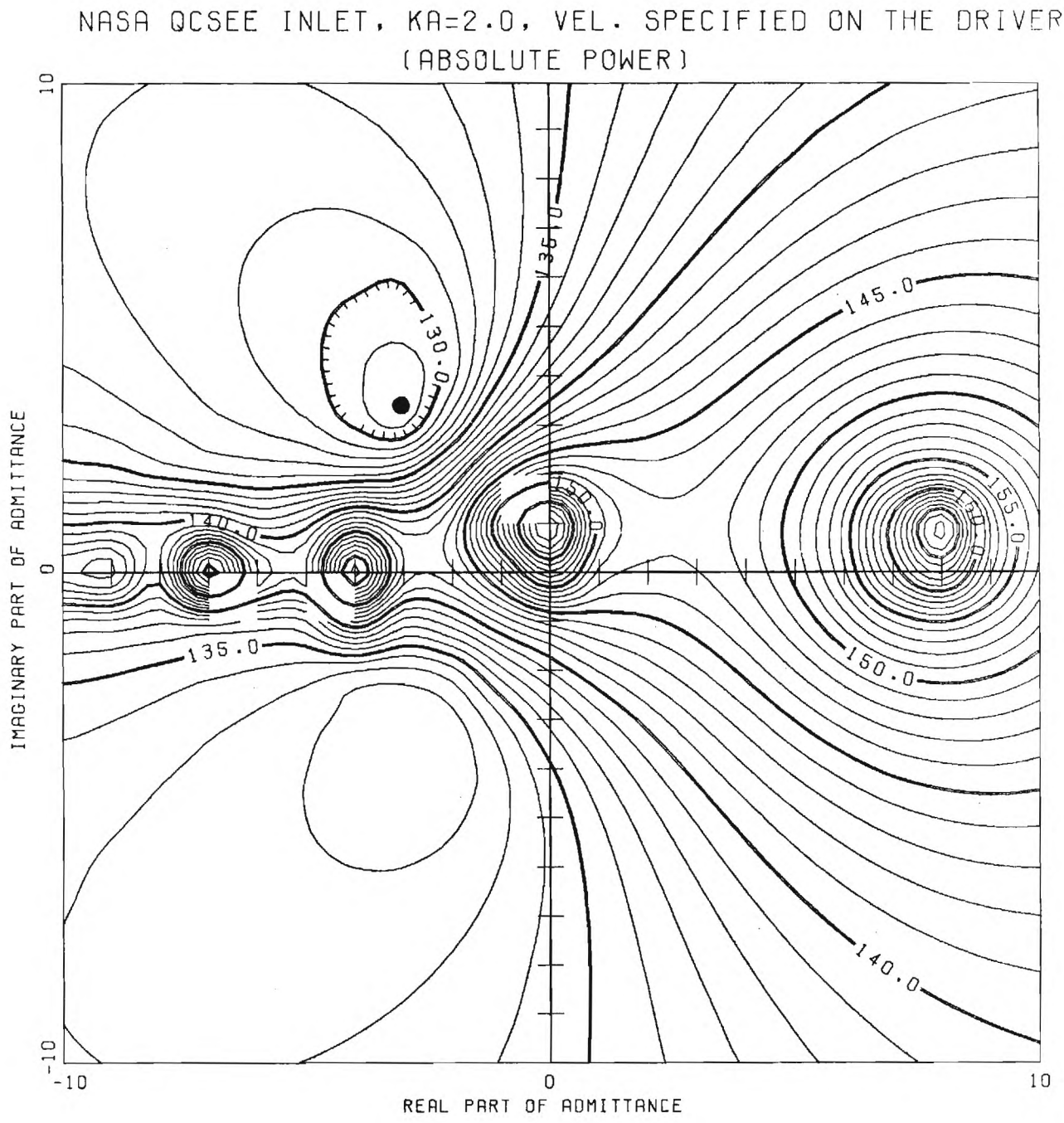
NASA QCSEE INLET, KA=2.0, VEL. SPECIFIED ON THE DRIVER
(ABSOLUTE POWER)
IMAGINARY PART OF ADMITTANCE
REAL PART OF ADMITTANCE
10
0
-10
-10
0
10
130.0
135.0
140.0
145.0
150.0
155.0

Figure 15e

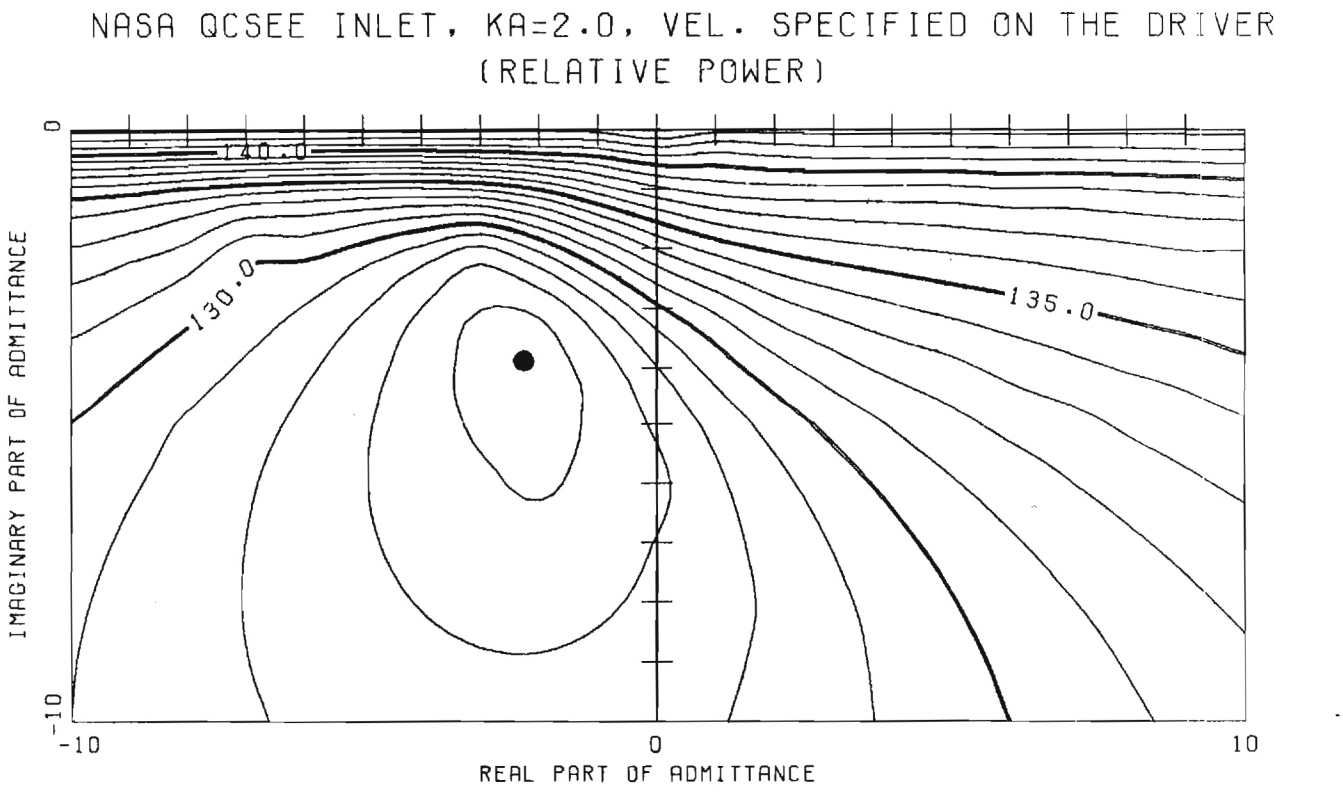
NASA QCSEE INLET, KA=2.0, VEL. SPECIFIED ON THE DRIVER
(RELATIVE POWER)
140.0
130.0
135.0
0
-10
-10
0
10
IMAGINARY PART OF ADMITTANCE
REAL PART OF ADMITTANCE

Figure 15f

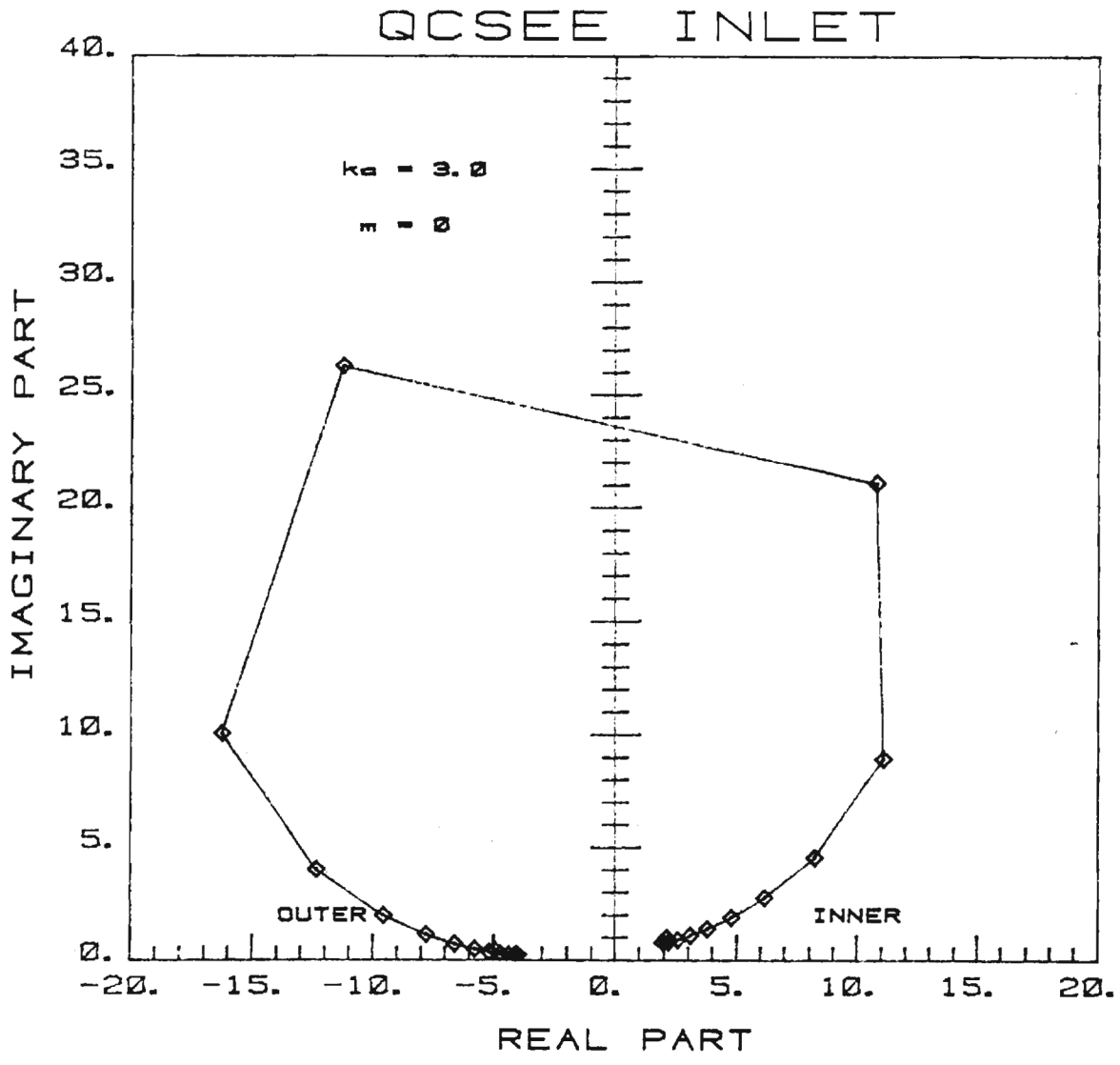

OPTIMUM ADMITTANCE DISTRIBUTION

Constant Phi on the Driver

Figure 16a

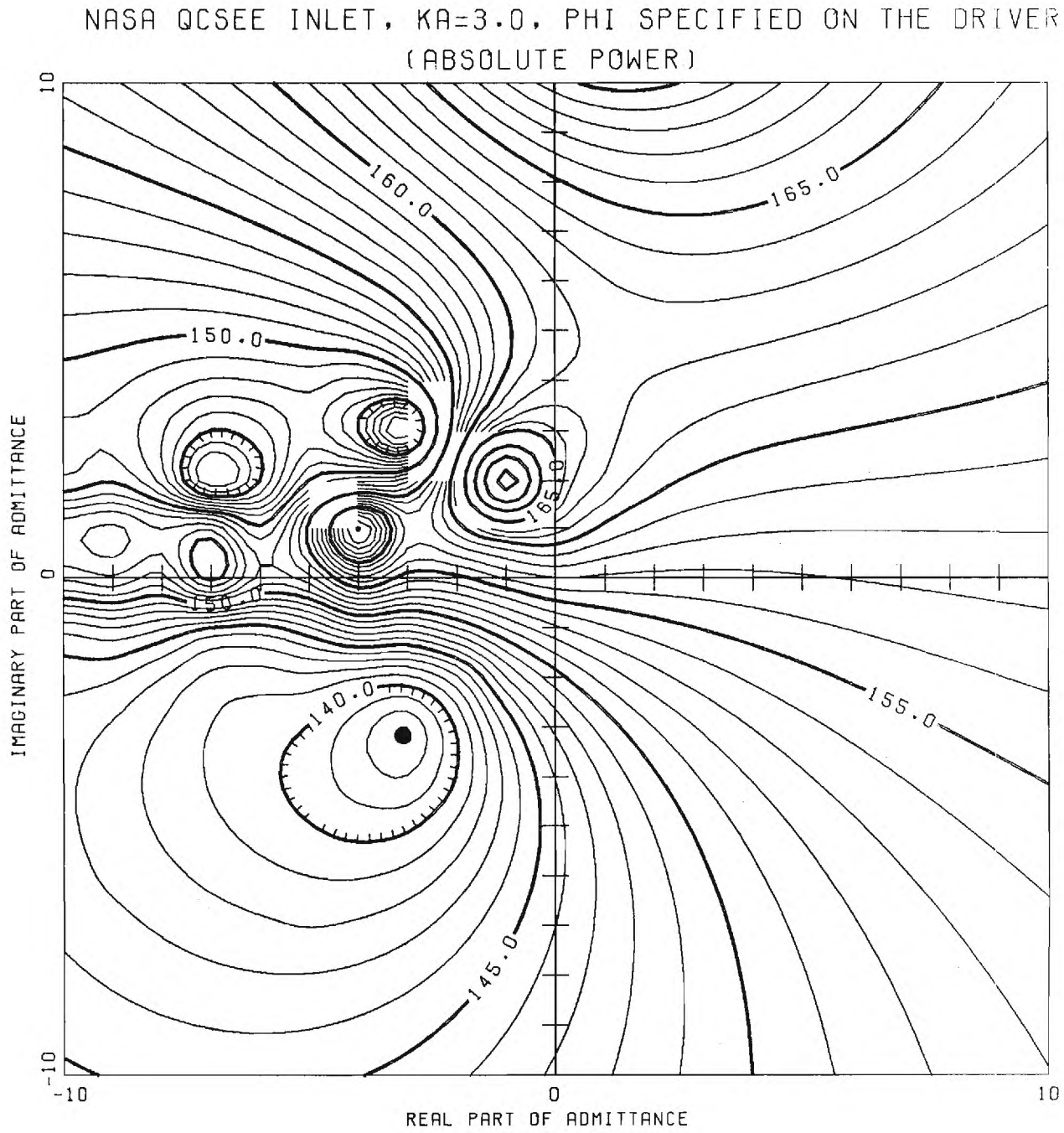
NASA QCSEE INLET, KA=3.0, PHI SPECIFIED ON THE DRIVER
(ABSOLUTE POWER)
160.0
165.0
150.0
165.0
150.0
140.0
155.0
145.0
10
0
-10
-10
0
10
IMAGINARY PART OF ADMITTANCE
REAL PART OF ADMITTANCE

Figure 16b

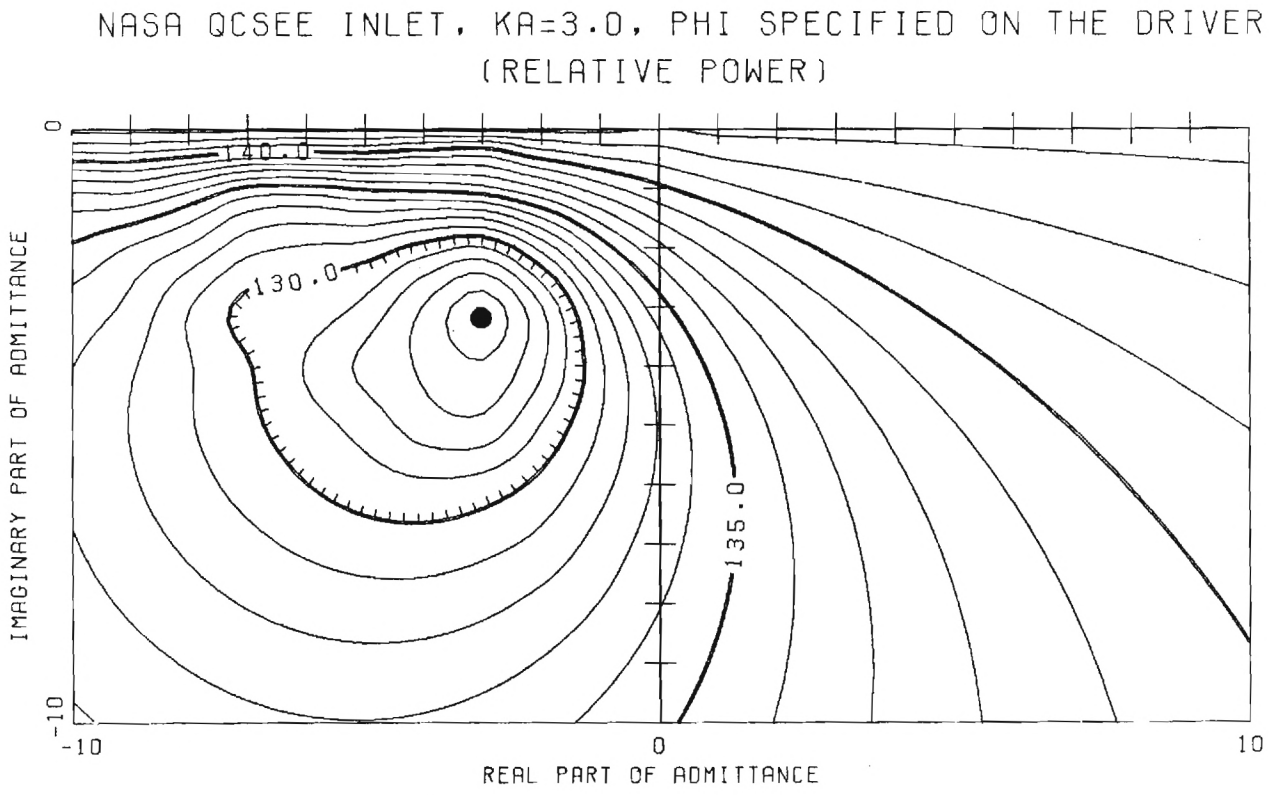
NASA QCSEE INLET, KA=3.0, PHI SPECIFIED ON THE DRIVER
(RELATIVE POWER)
140.0
130.0
135.0
0
-10
-10
0
10
IMAGINARY PART OF ADMITTANCE
REAL PART OF ADMITTANCE

Figure 16c

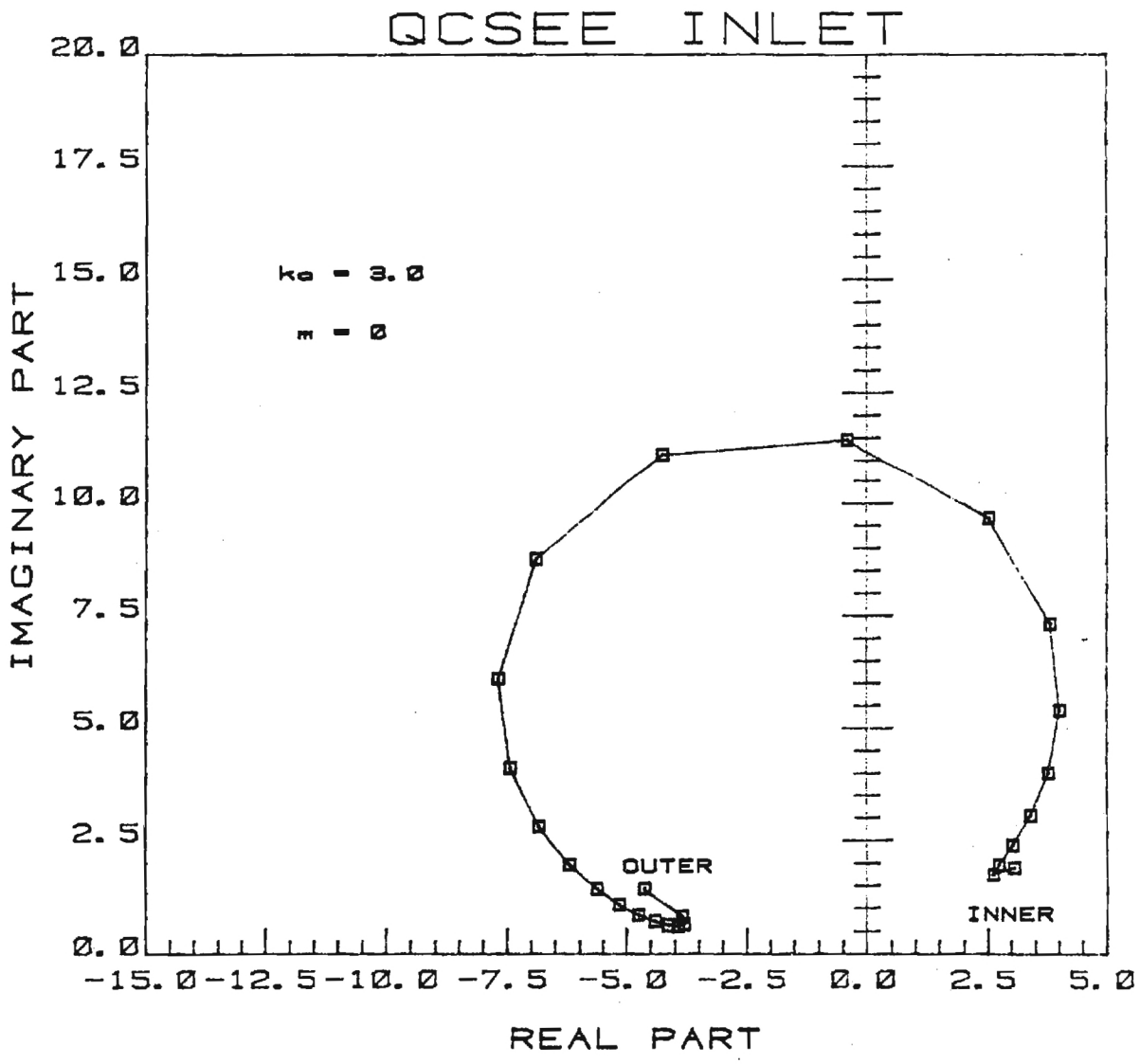

OPTIMUM ADMITTANCE DISTRIBUTION

Constant Velocity on the Driver

Figure 16d

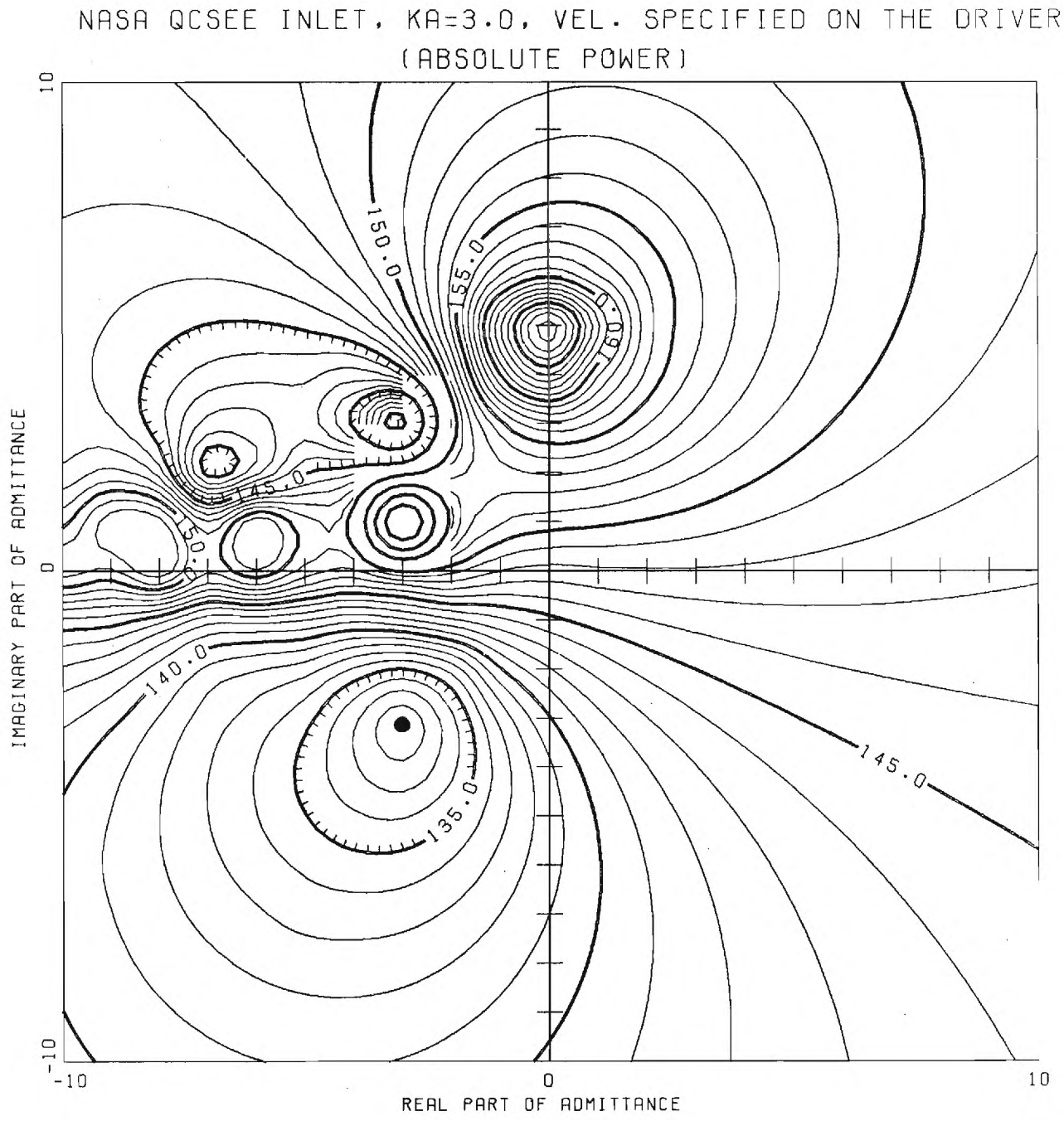
NASA QCSEE INLET, KA=3.0, VEL. SPECIFIED ON THE DRIVER
(ABSOLUTE POWER)
IMAGINARY PART OF ADMITTANCE
REAL PART OF ADMITTANCE
10
0
-10
-10
0
10
150.0
155.0
160.0
145.0
150.0
140.0
135.0
145.0

Figure 16e

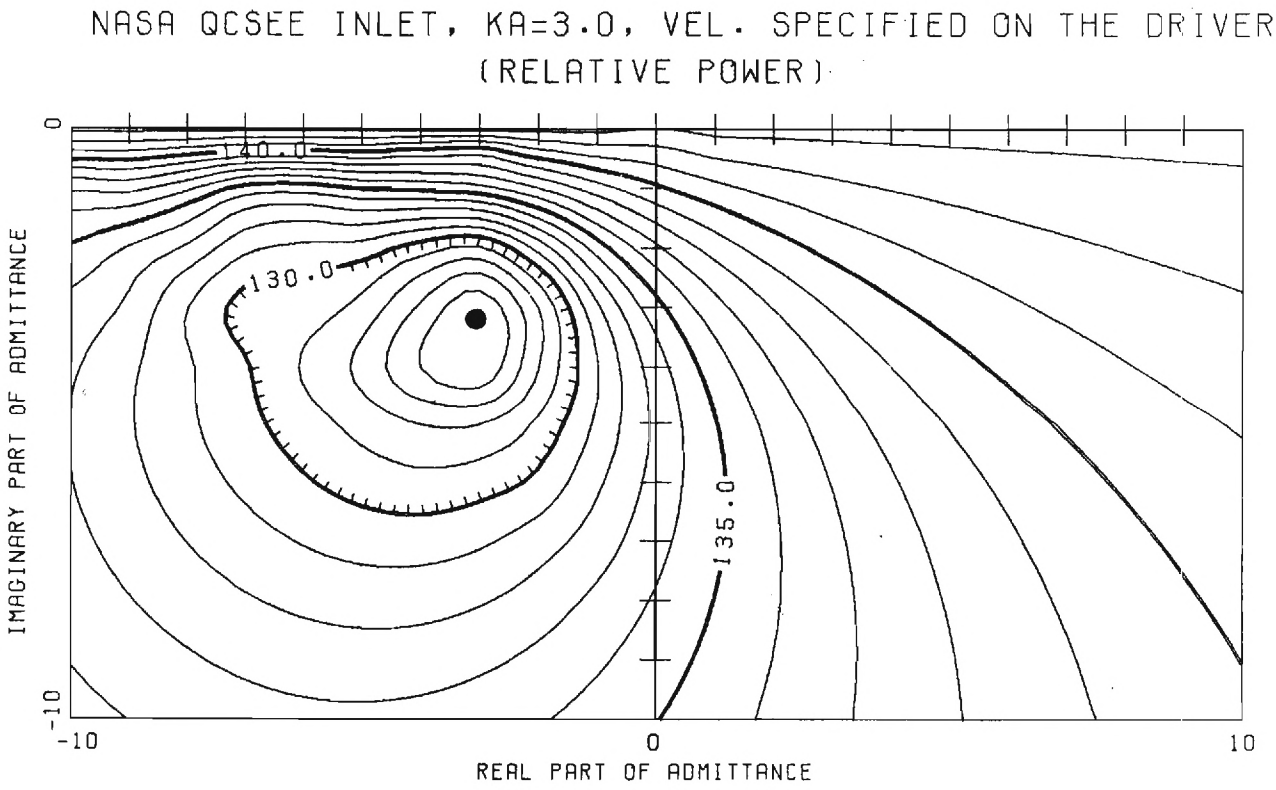
NASA QCSEE INLET, KA=3.0, VEL. SPECIFIED ON THE DRIVER
(RELATIVE POWER)
140.0
130.0
135.0
0
-10
-10
0
10
IMAGINARY PART OF ADMITTANCE
REAL PART OF ADMITTANCE

Figure 16f

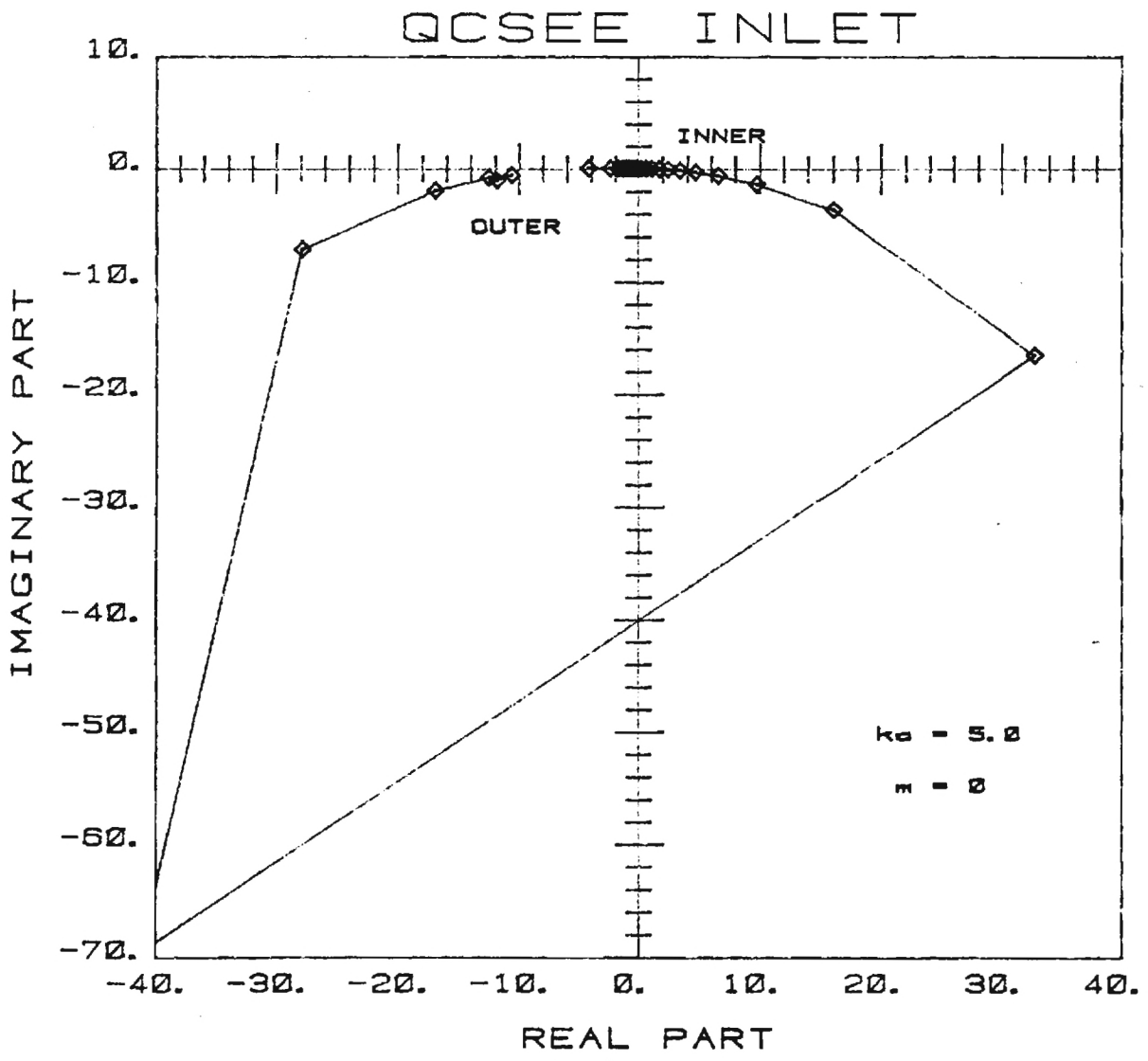

OPTIMUM ADMITTANCE DISTRIBUTION

Constant Phi on the Driver

Figure 17a

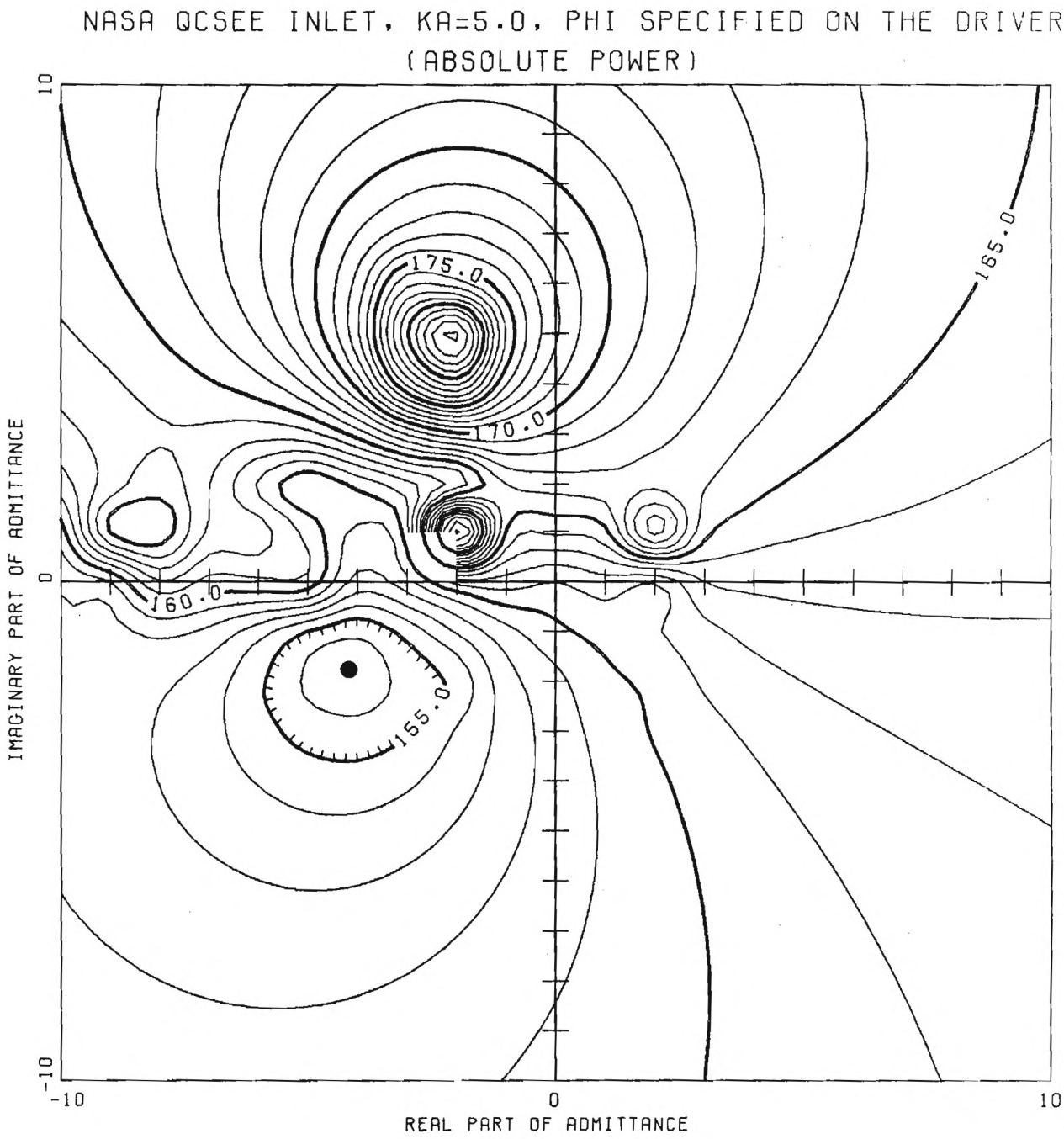
NASA QCSEE INLET, KA=5.0, PHI SPECIFIED ON THE DRIVER
(ABSOLUTE POWER)
175.0
170.0
165.0
160.0
155.0
10
0
-10
-10
0
10
IMAGINARY PART OF ADMITTANCE
REAL PART OF ADMITTANCE

Figure 17b

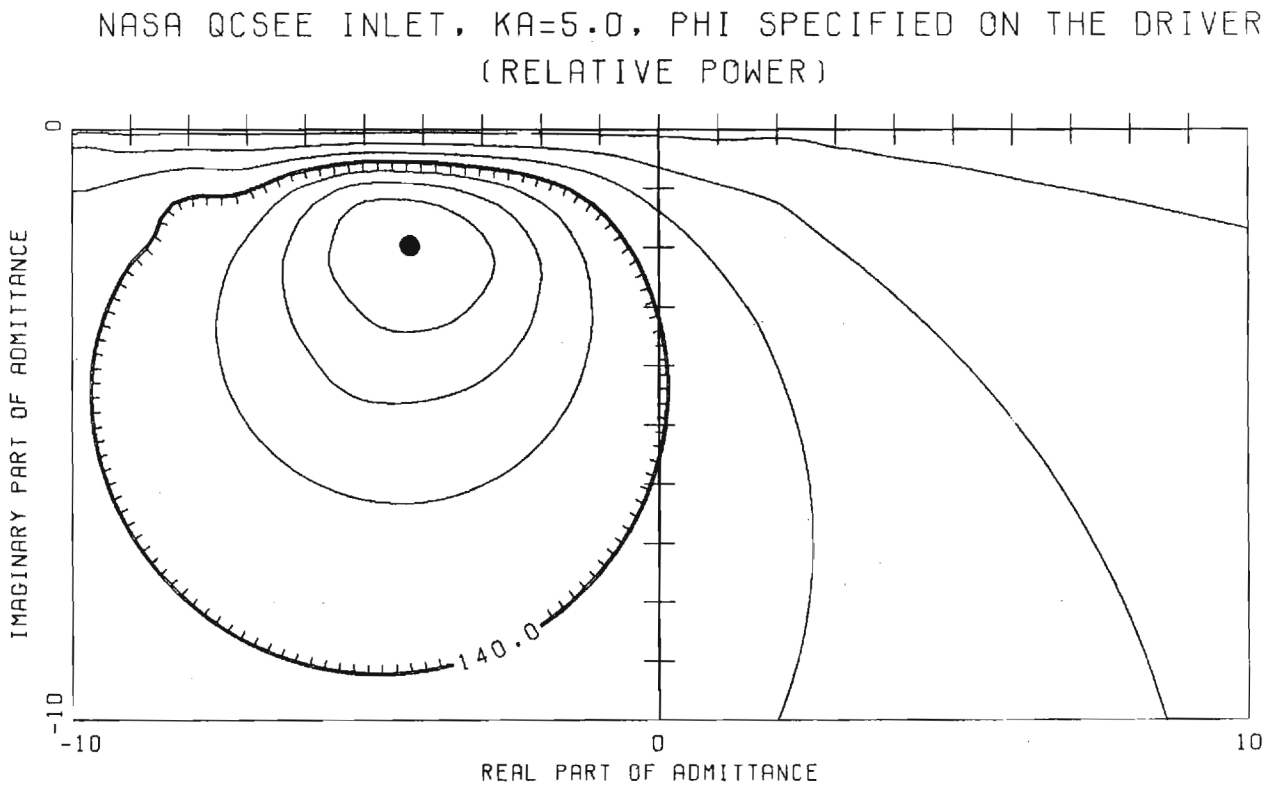
NASA QCSEE INLET, KA=5.0, PHI SPECIFIED ON THE DRIVER
(RELATIVE POWER)
IMAGINARY PART OF ADMITTANCE
0
-10
-10
0
10
REAL PART OF ADMITTANCE
140.0

Figure 17c

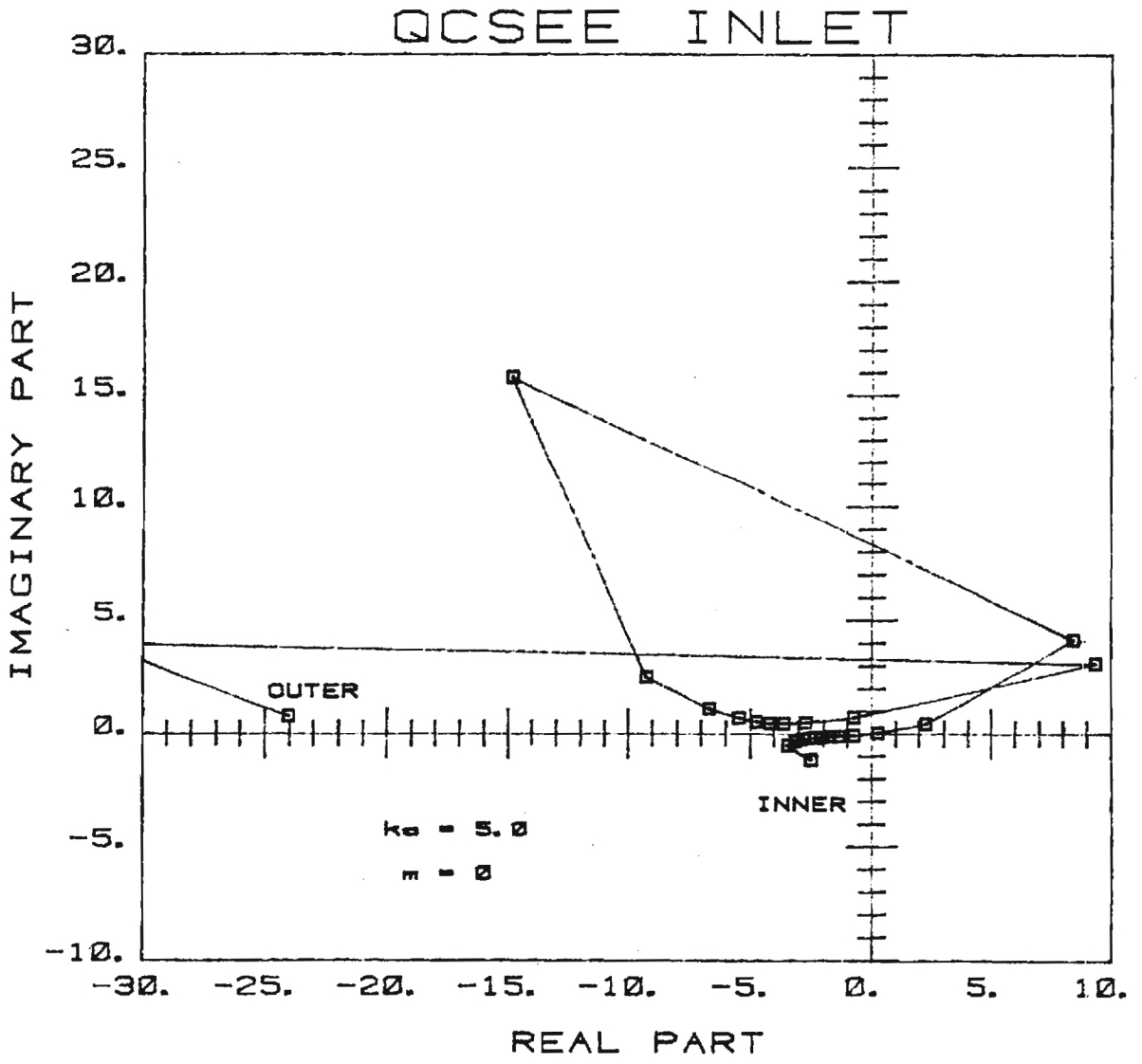

OPTIMUM ADMITTANCE DISTRIBUTION

Constant Velocity on the Driver

Figure 17d

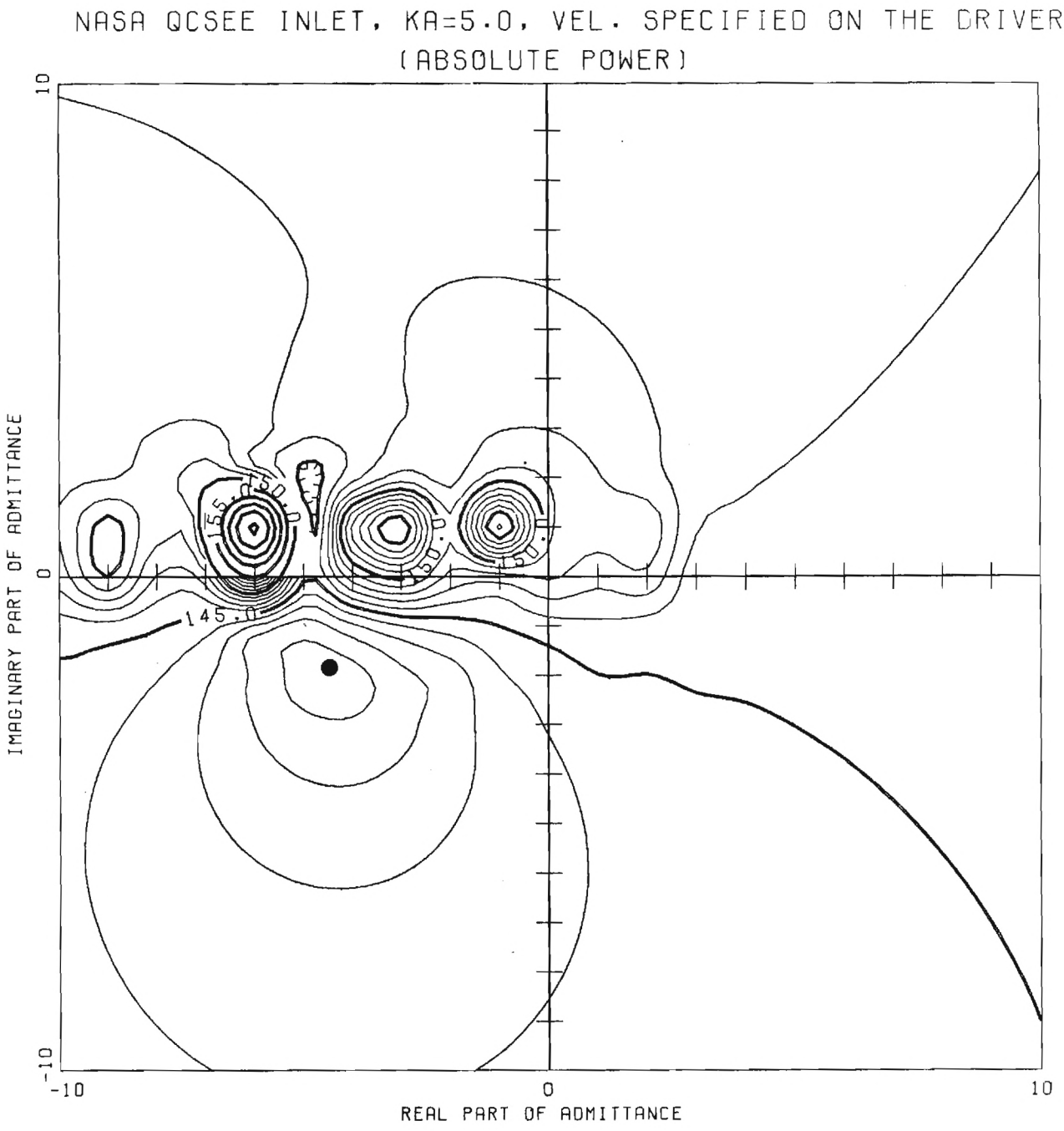
NASA QCSEE INLET, KA=5.0, VEL. SPECIFIED ON THE DRIVER
(ABSOLUTE POWER)
IMAGINARY PART OF ADMITTANCE
REAL PART OF ADMITTANCE
10
0
-10
-10
0
10
155.0
150.0
150.0
150.0
145.0

Figure 17e

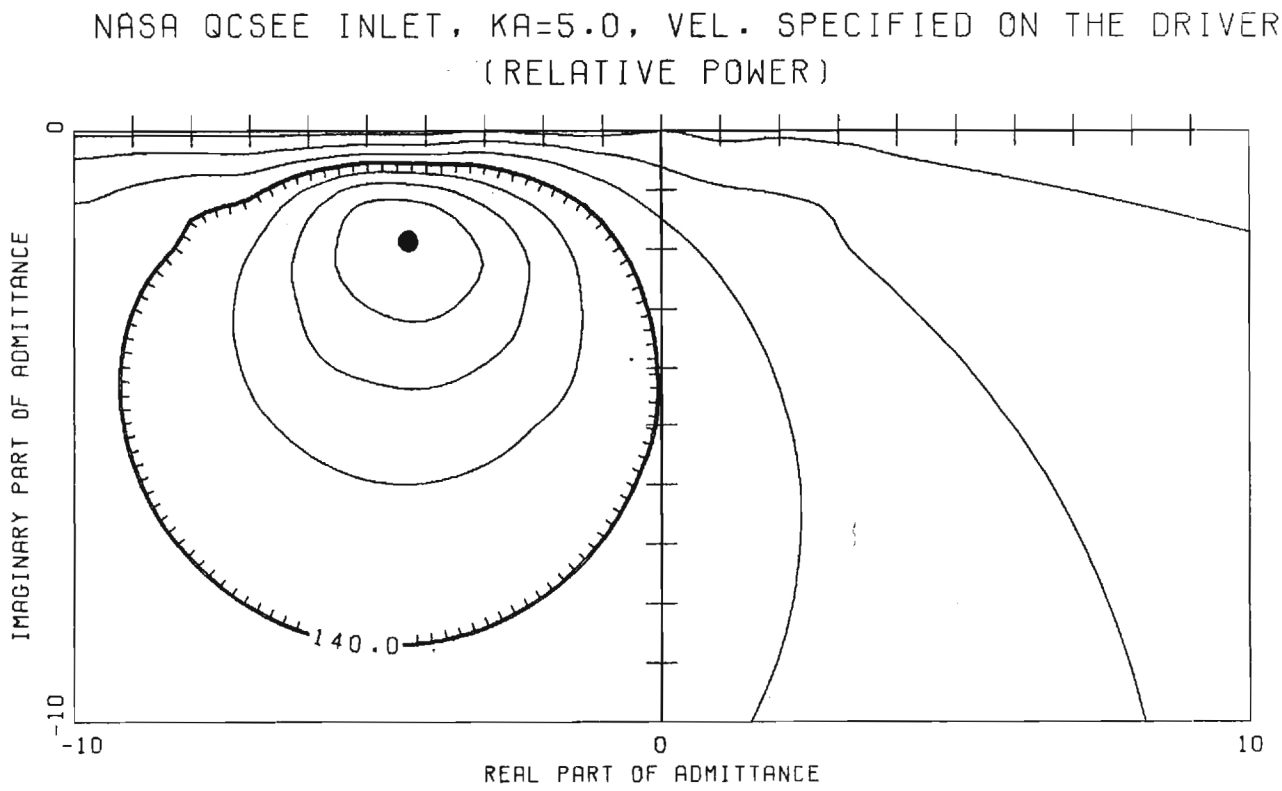
NASA QCSEE INLET, KA=5.0, VEL. SPECIFIED ON THE DRIVER
(RELATIVE POWER)
IMAGINARY PART OF ADMITTANCE
0
-10
-10
0
10
REAL PART OF ADMITTANCE
140.0

Figure 17f

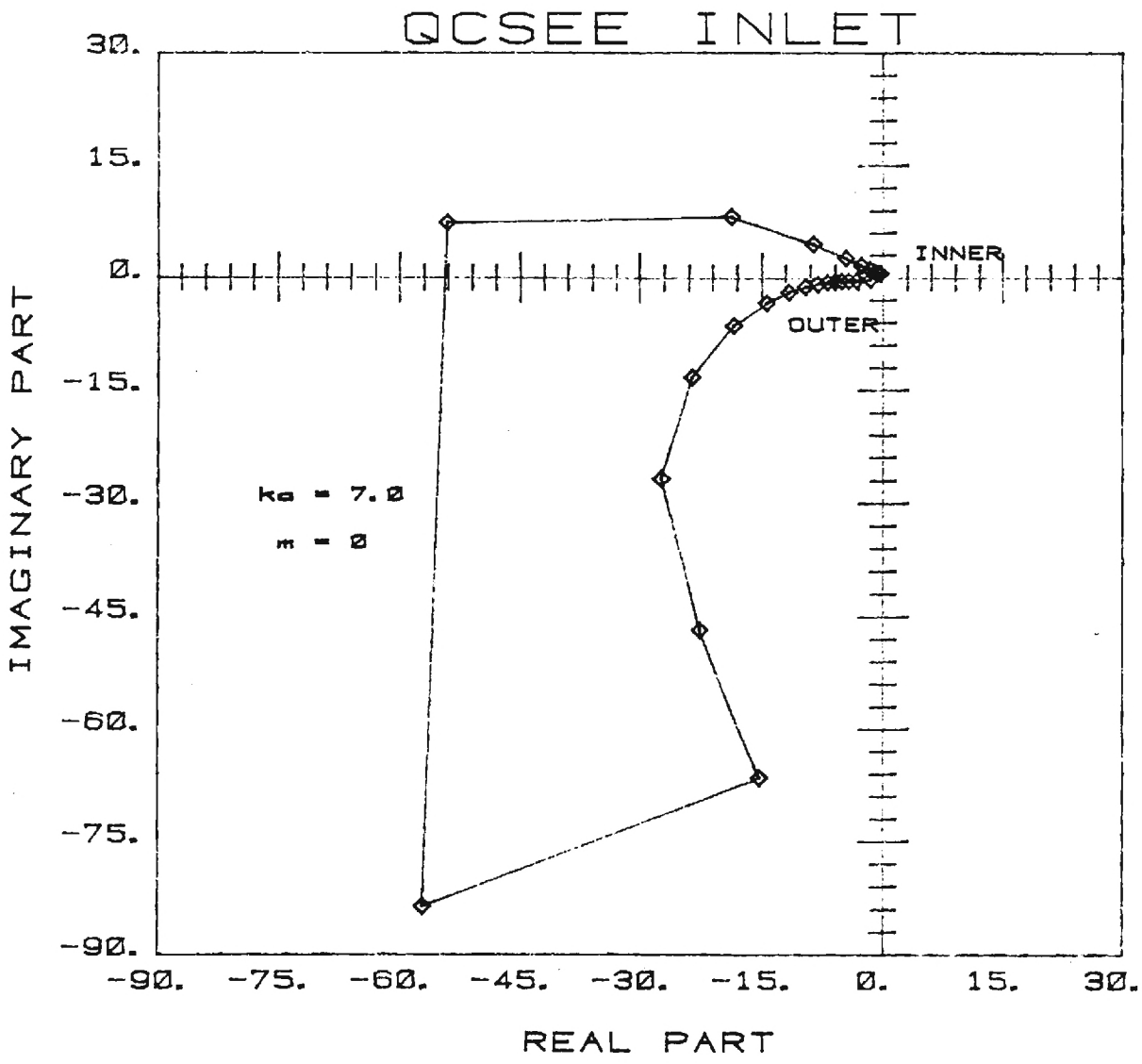

OPTIMUM ADMITTANCE DISTRIBUTION

Constant Phi on the Driver

Figure 18a

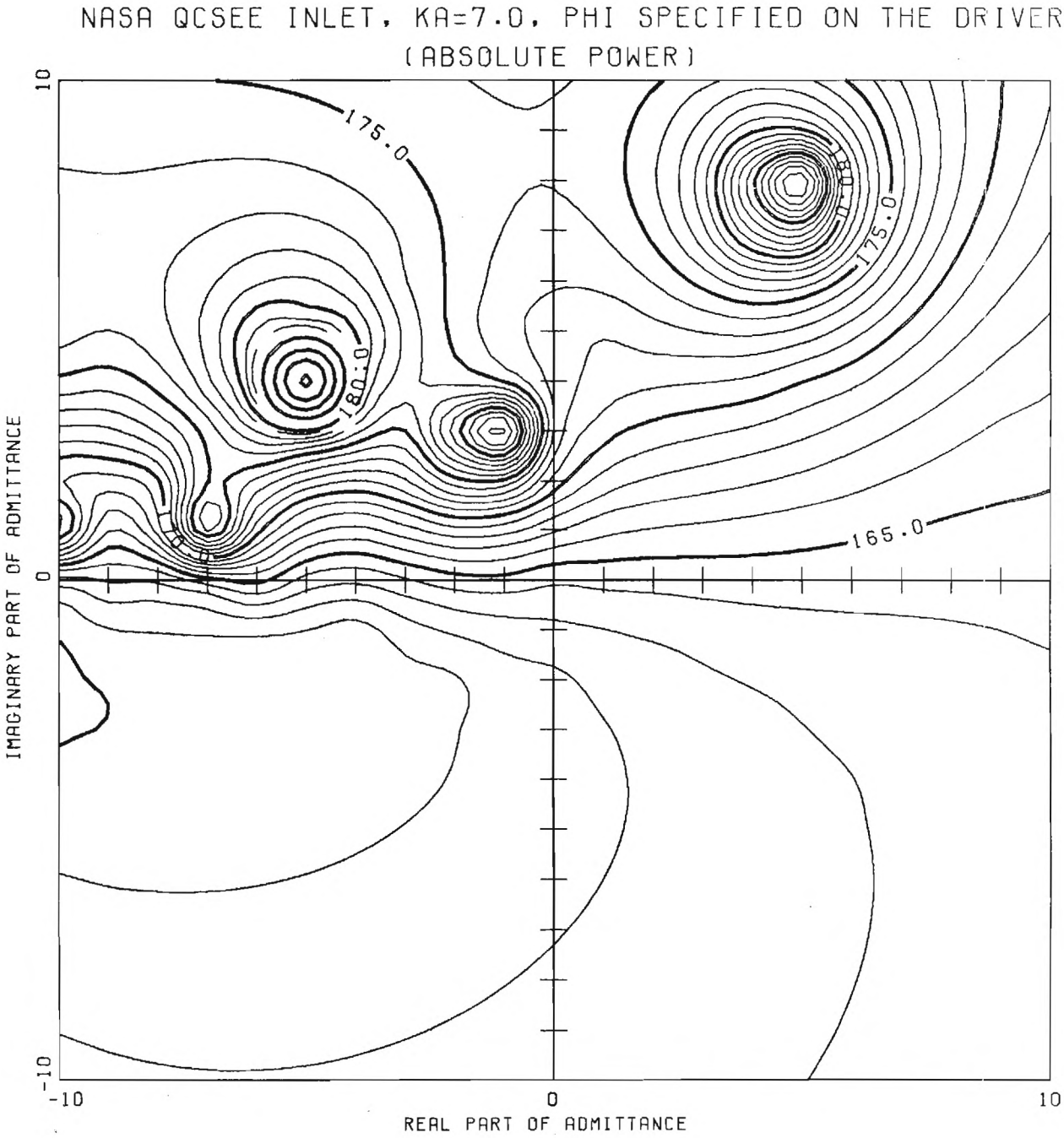
NASA QCSEE INLET, KA=7.0, PHI SPECIFIED ON THE DRIVER
(ABSOLUTE POWER)
175.0
180.0
165.0
IMAGINARY PART OF ADMITTANCE
REAL PART OF ADMITTANCE
10
0
-10
-10
0
10

Figure 18b

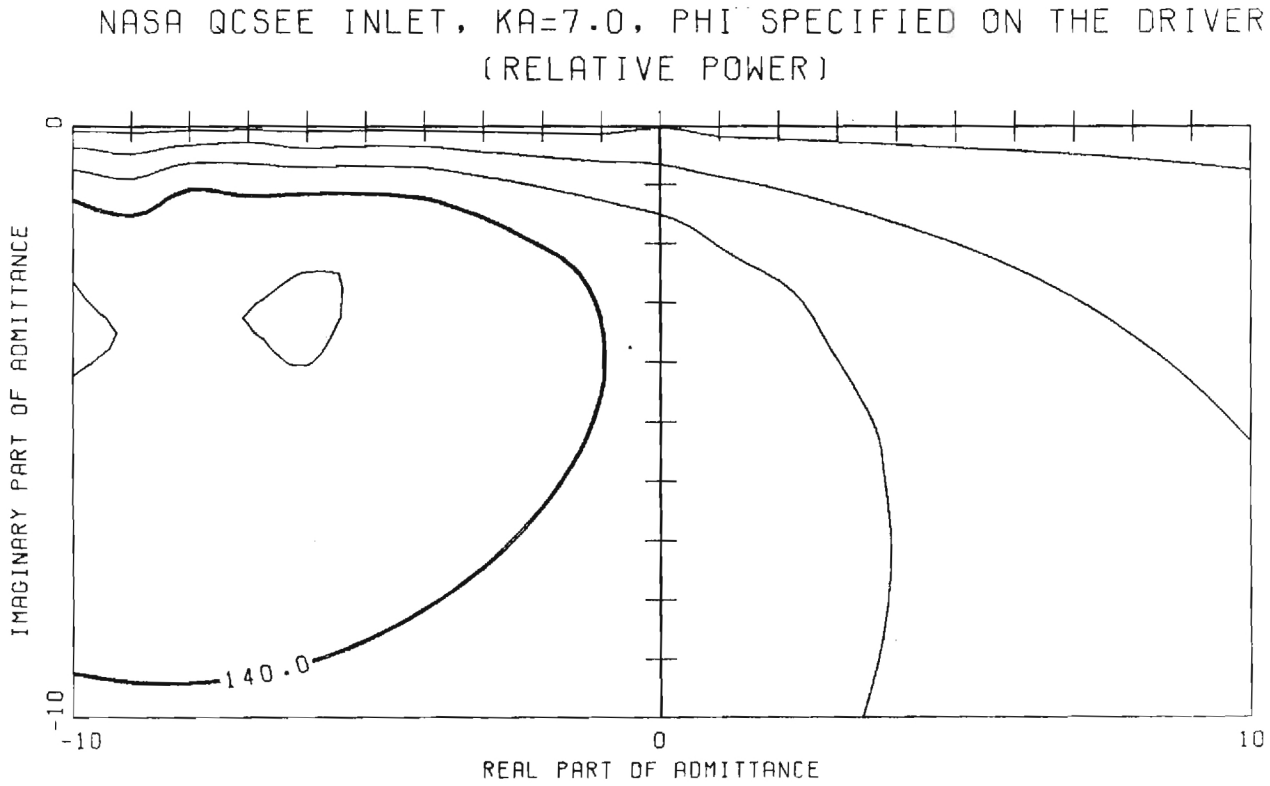
NASA QCSEE INLET, KA=7.0, PHI SPECIFIED ON THE DRIVER
(RELATIVE POWER)
IMAGINARY PART OF ADMITTANCE
0
-10
140.0
-10
0
10
REAL PART OF ADMITTANCE

Figure 18c

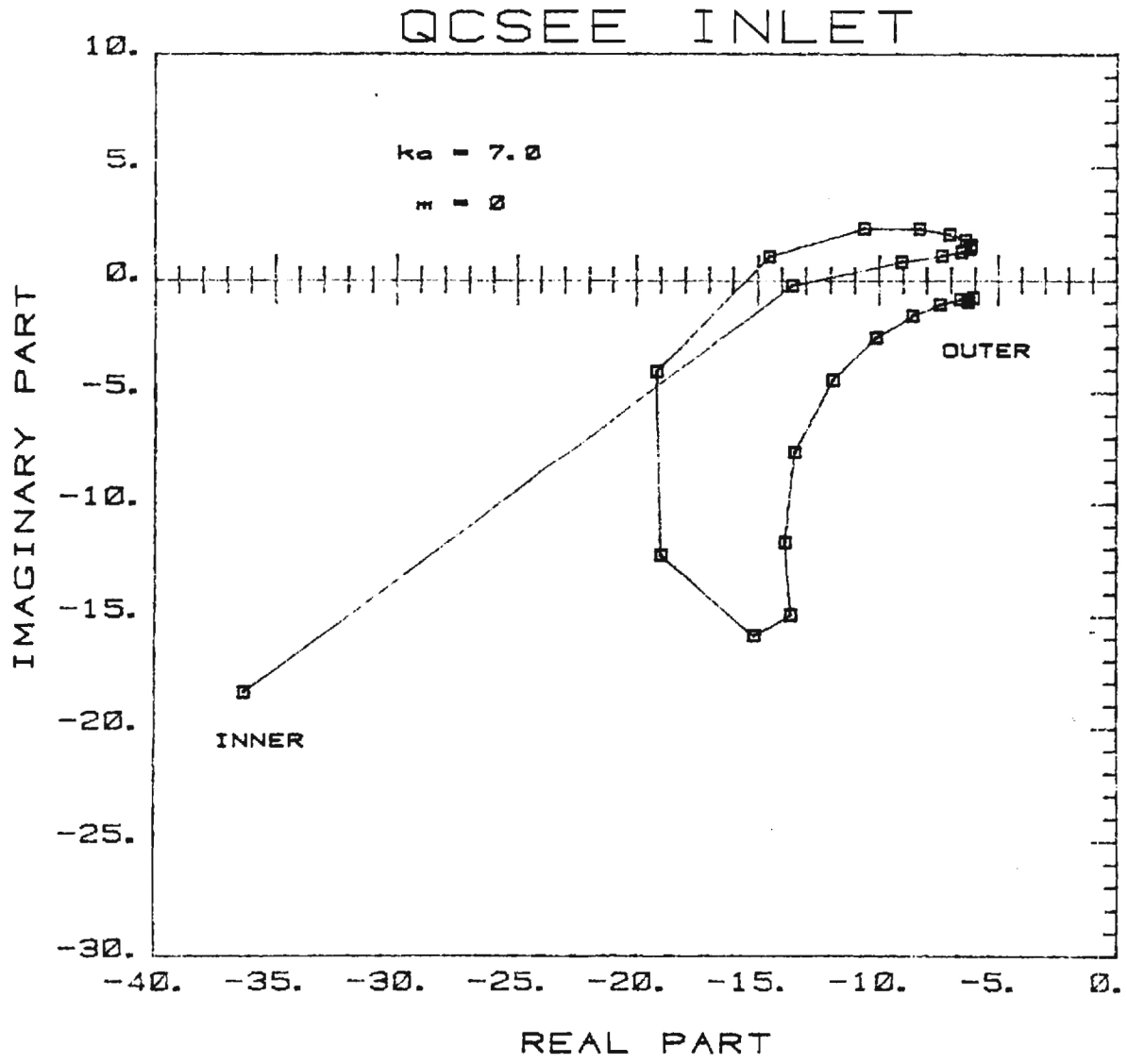

OPTIMUM ADMITTANCE DISTRIBUTION

Constant Velocity on the Driver

Figure 18d

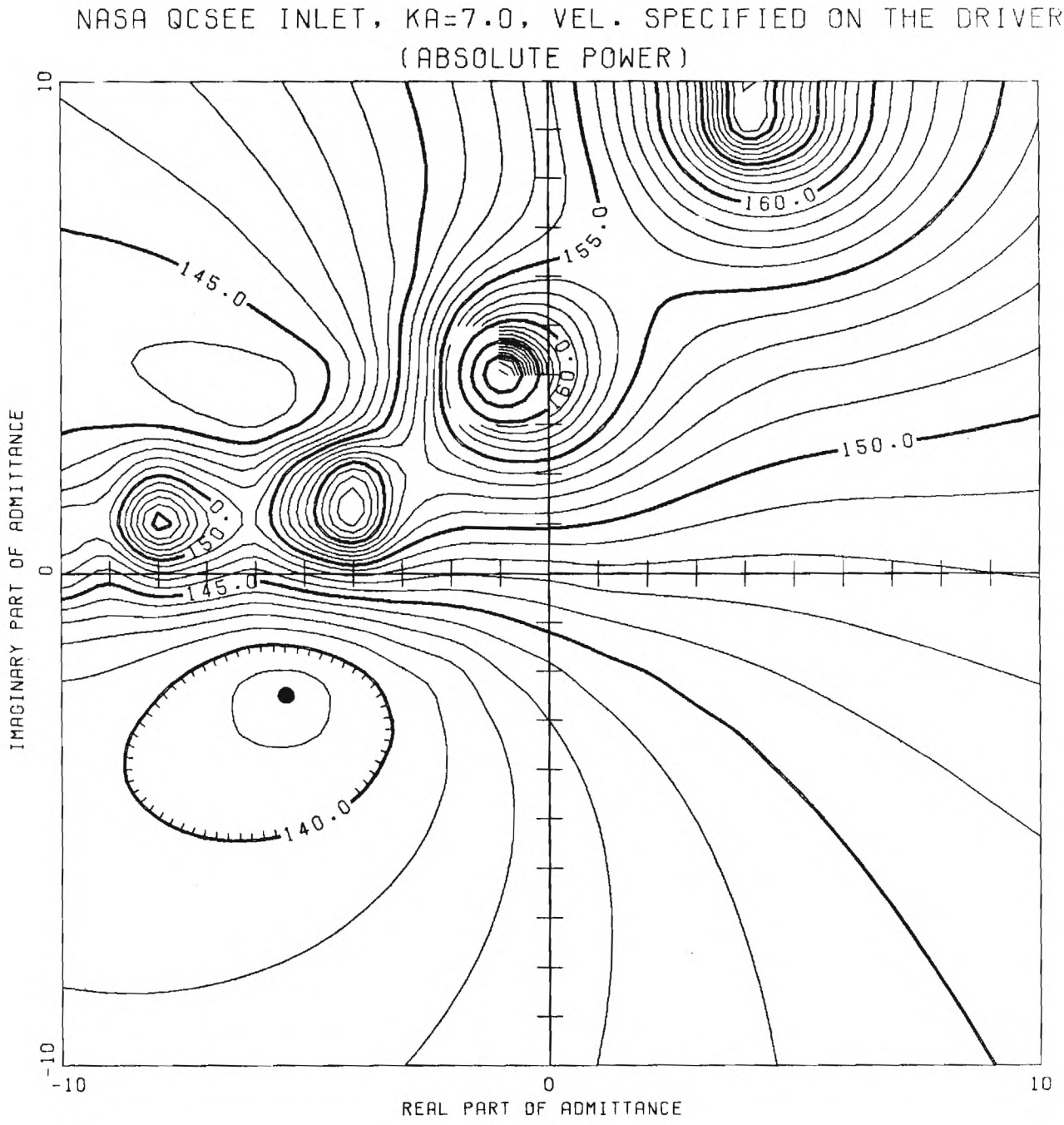
NASA QCSEE INLET, KA=7.0, VEL. SPECIFIED ON THE DRIVER
(ABSOLUTE POWER)
160.0
155.0
145.0
160.0
150.0
150.0
145.0
140.0
10
0
-10
-10
0
10
IMAGINARY PART OF ADMITTANCE
REAL PART OF ADMITTANCE

Figure 18e

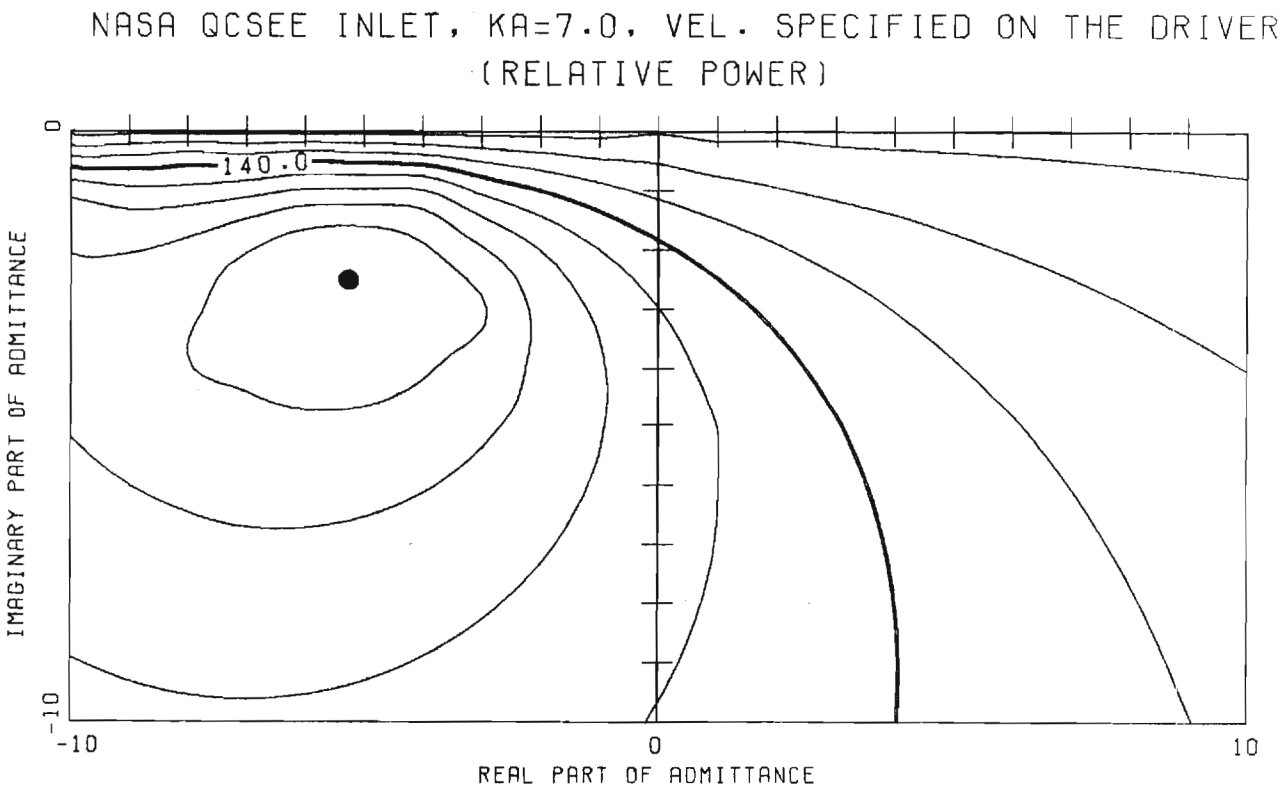
NASA QCSEE INLET, KA=7.0, VEL. SPECIFIED ON THE DRIVER
(RELATIVE POWER)
140.0
0
-10
IMAGINARY PART OF ADMITTANCE
-10
0
10
REAL PART OF ADMITTANCE

Figure 18f

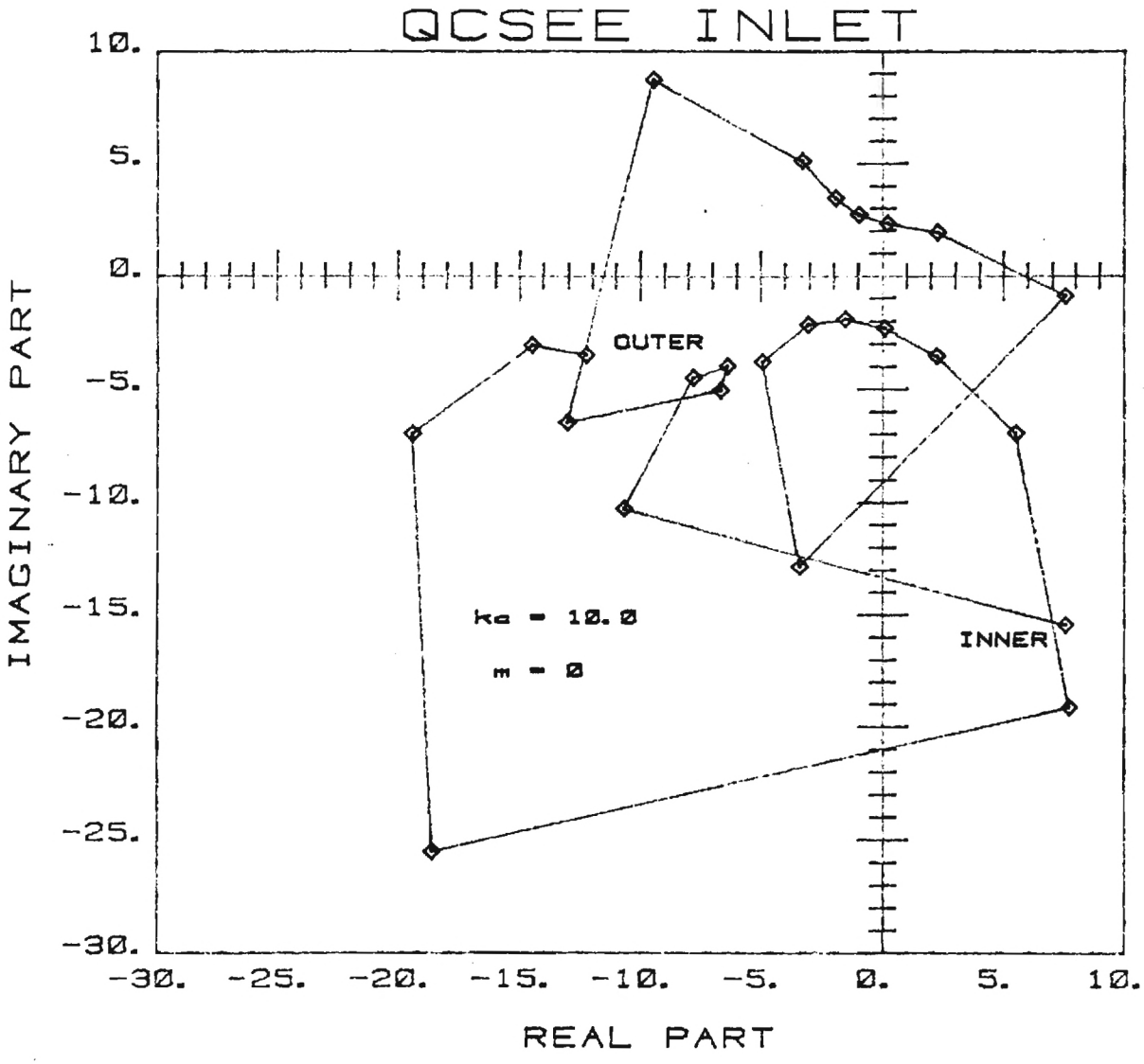

OPTIMUM ADMITTANCE DISTRIBUTION

Constant Phi on the Driver

Figure 19a

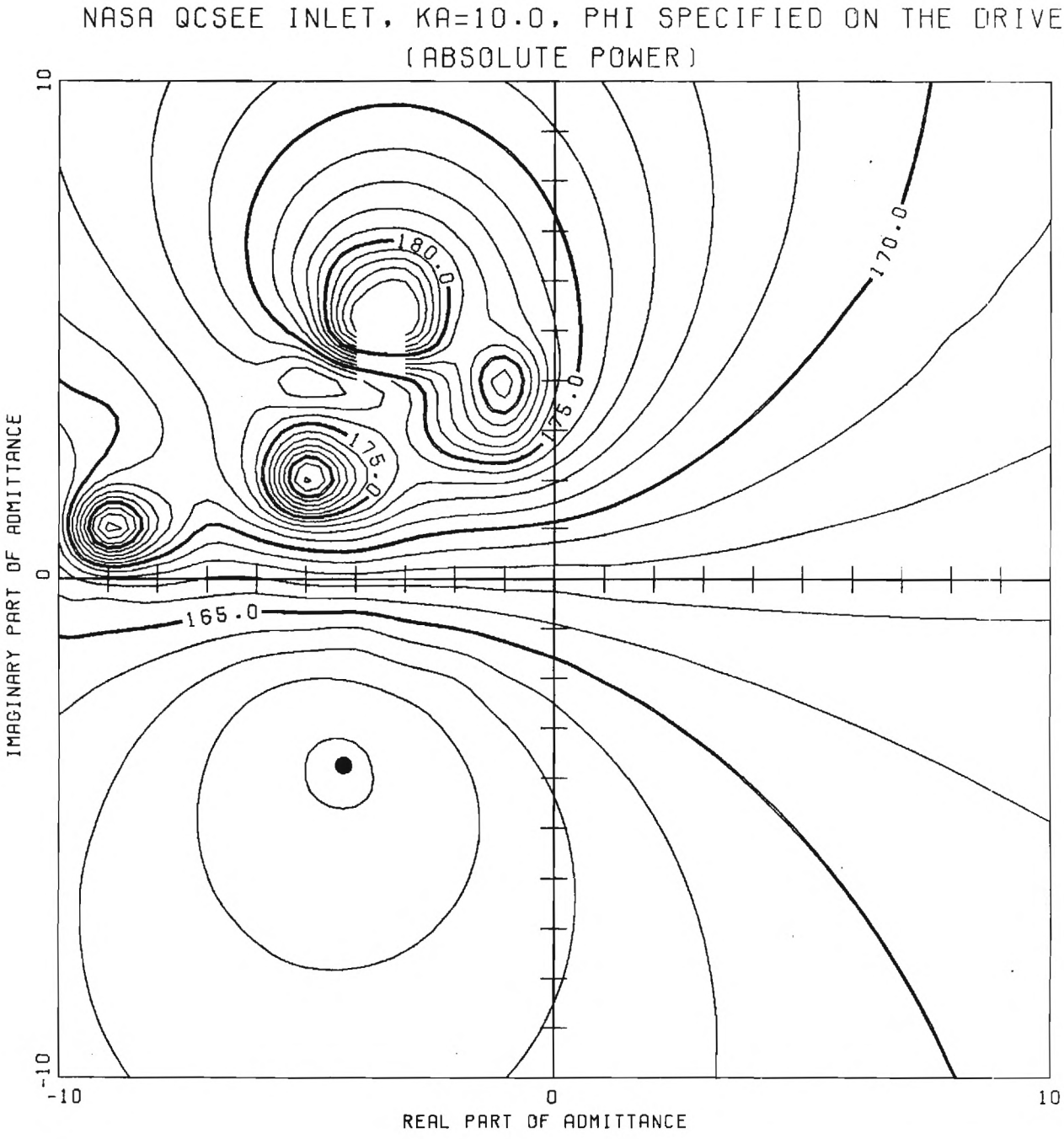
NASA QCSEE INLET, KA=10.0, PHI SPECIFIED ON THE DRIVER
(ABSOLUTE POWER)
IMAGINARY PART OF ADMITTANCE
REAL PART OF ADMITTANCE
10
0
-10
-10
0
10
180.0
175.0
175.0
170.0
165.0

Figure 19b

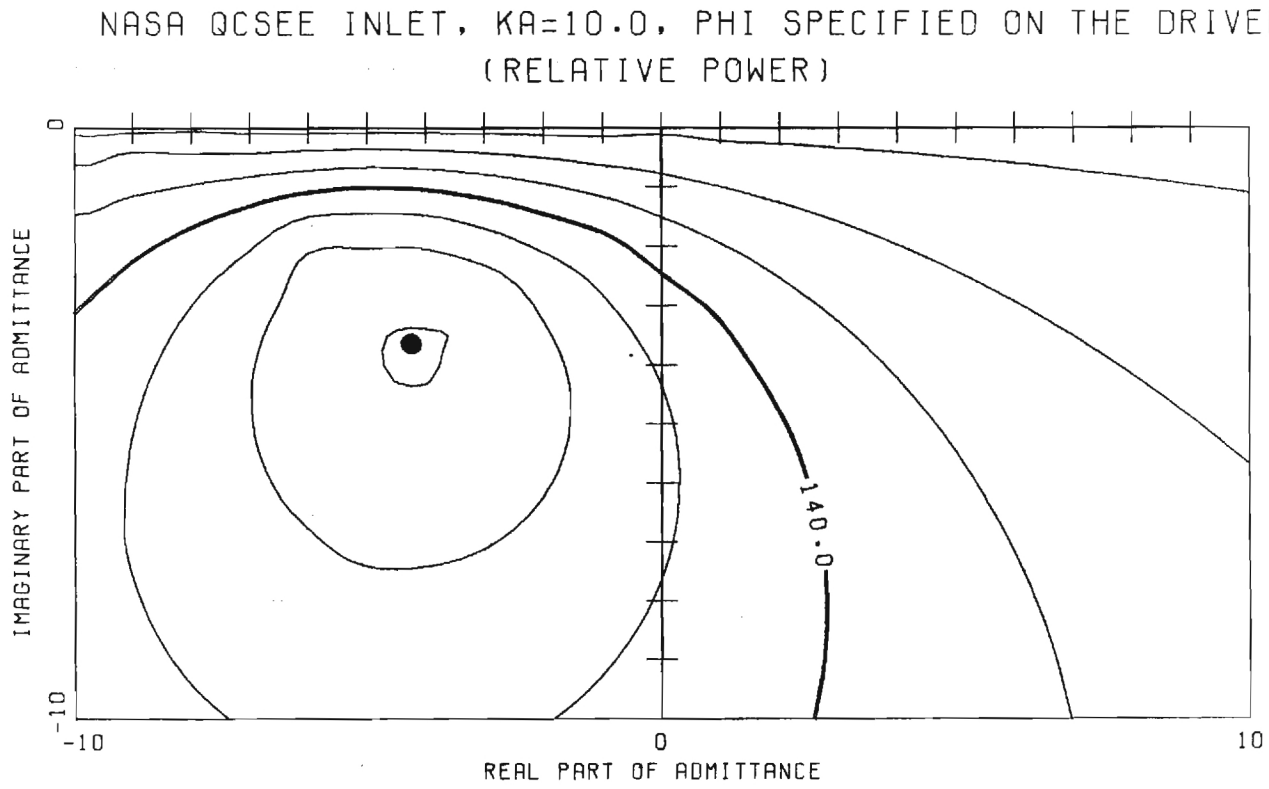
NASA QCSEE INLET, KA=10.0, PHI SPECIFIED ON THE DRIVER
(RELATIVE POWER)
IMAGINARY PART OF ADMITTANCE
0
-10
-10
0
10
REAL PART OF ADMITTANCE
140.0

Figure 19c

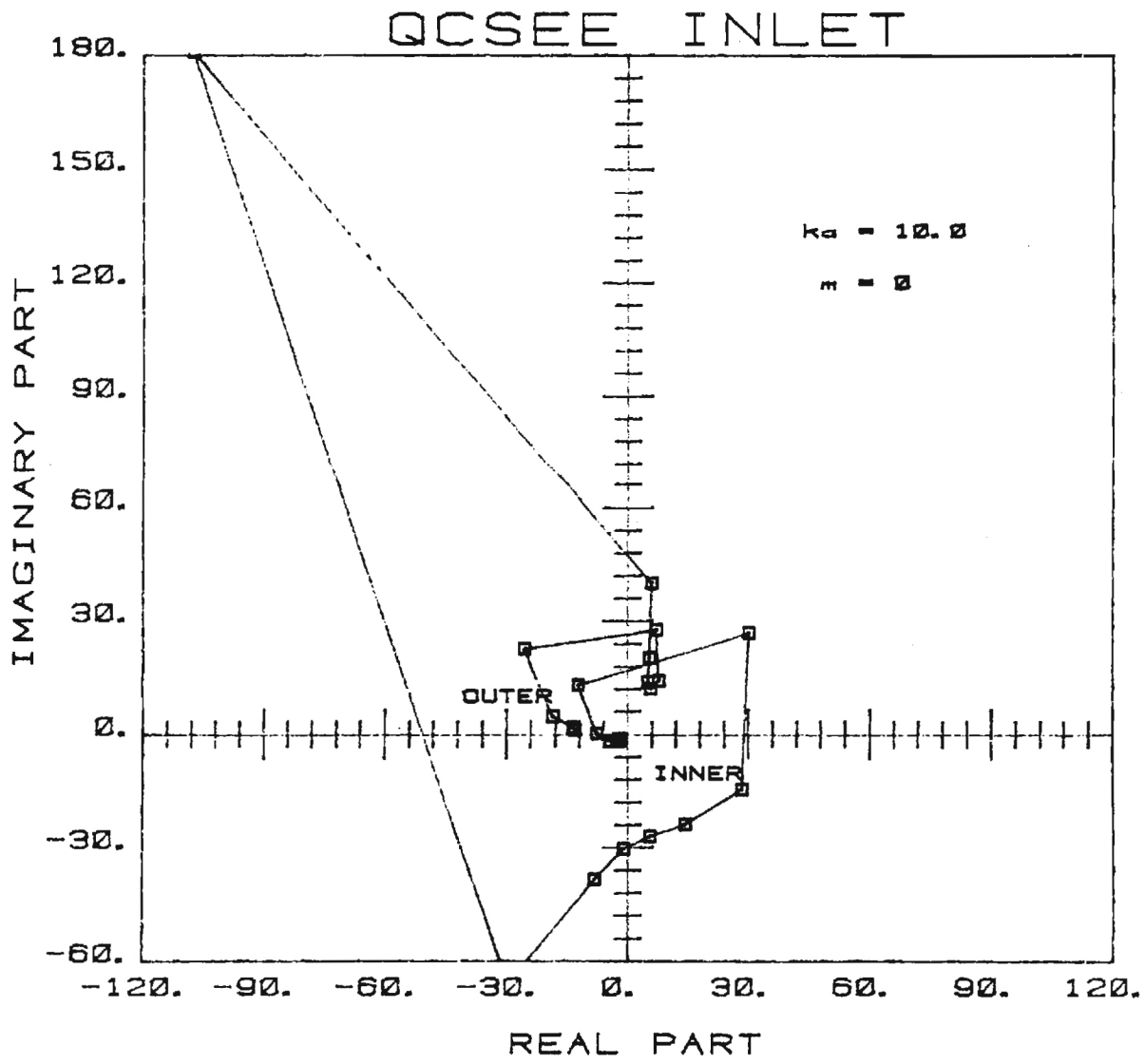

OPTIMUM ADMITTANCE DISTRIBUTION

Constant Velocity on the Driver

Figure 19d

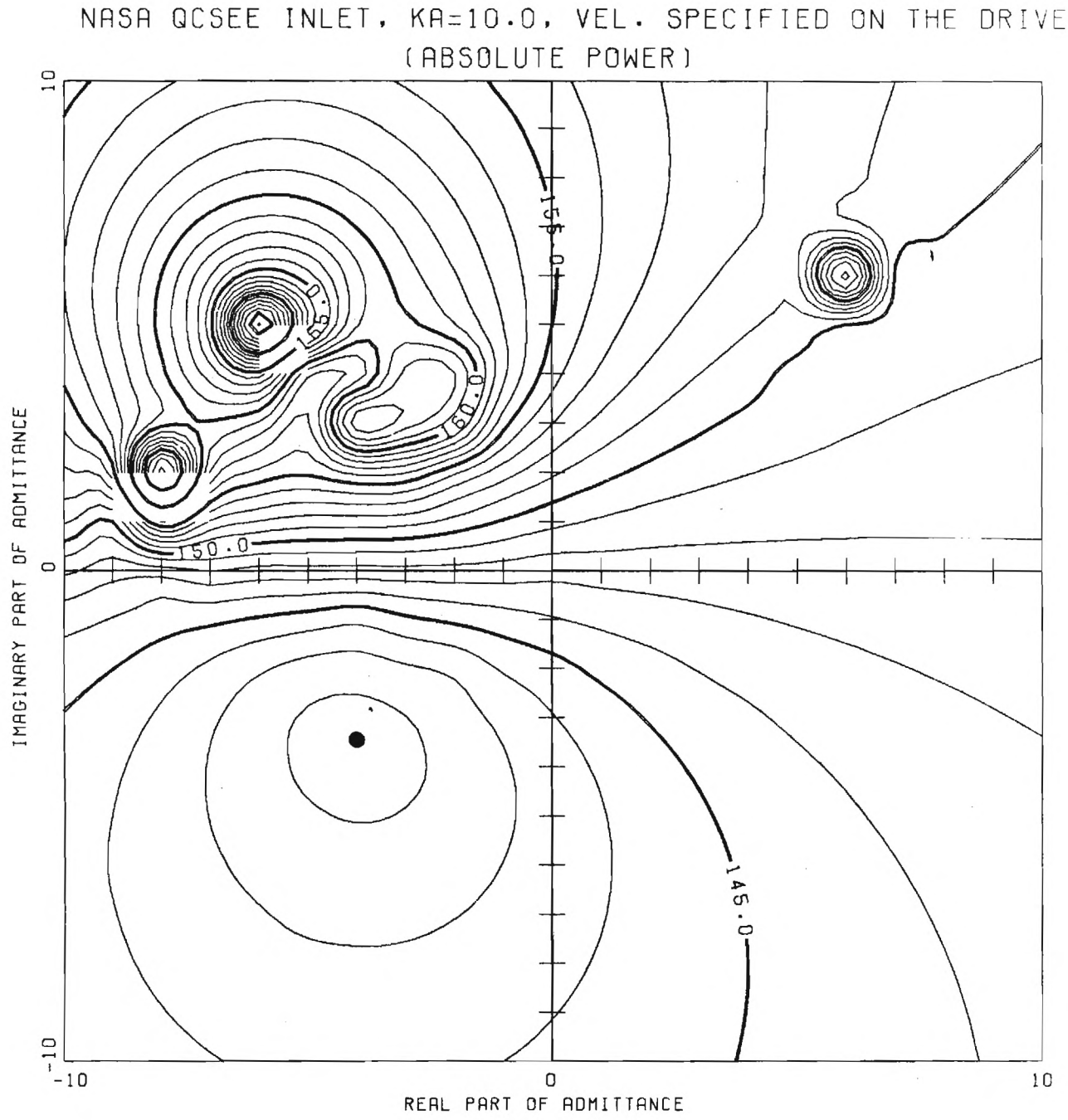
NASA QCSEE INLET, KA=10.0, VEL. SPECIFIED ON THE DRIVER
(ABSOLUTE POWER)
IMAGINARY PART OF ADMITTANCE
REAL PART OF ADMITTANCE
10
0
-10
-10
0
10
155.0
160.0
150.0
145.0

Figure 19e

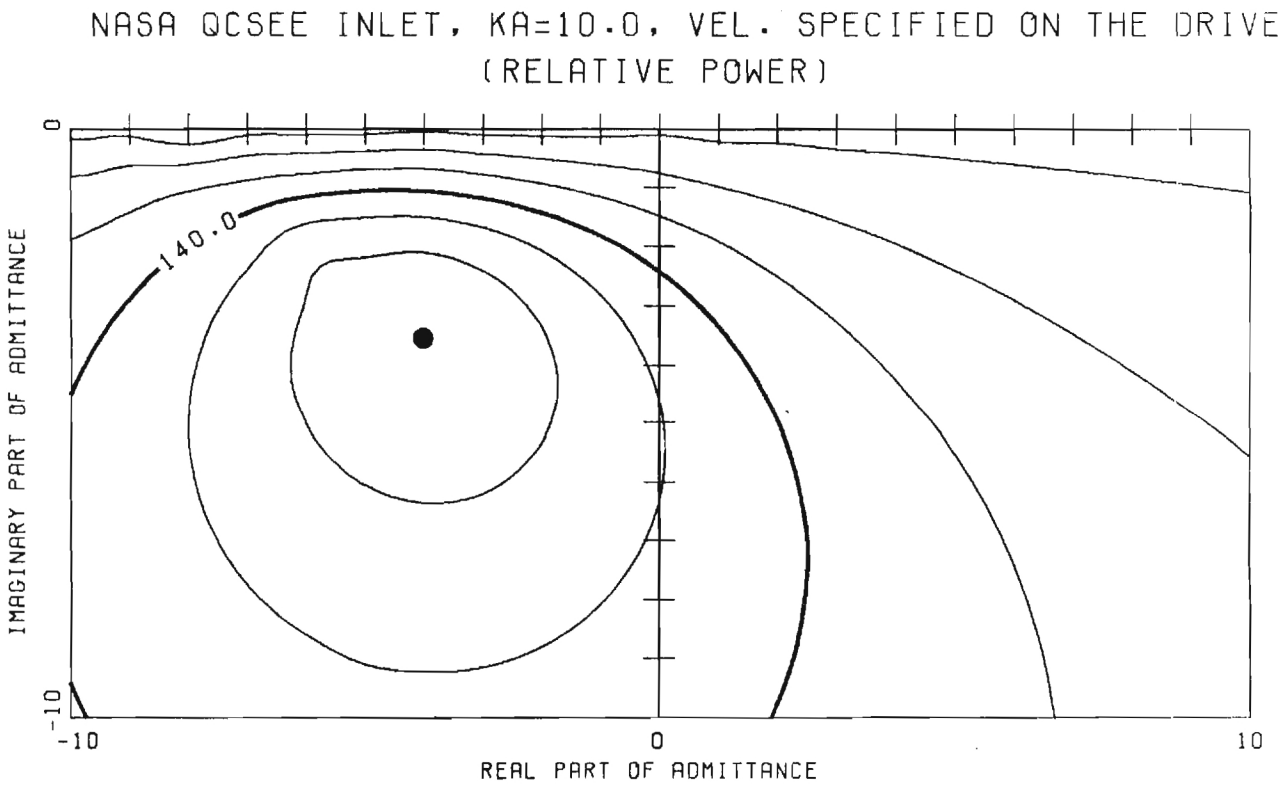
NASA QCSEE INLET, KA=10.0, VEL. SPECIFIED ON THE DRIVER
(RELATIVE POWER)
IMAGINARY PART OF ADMITTANCE
REAL PART OF ADMITTANCE
140.0
0
-10
-10
0
10

Figure 19f

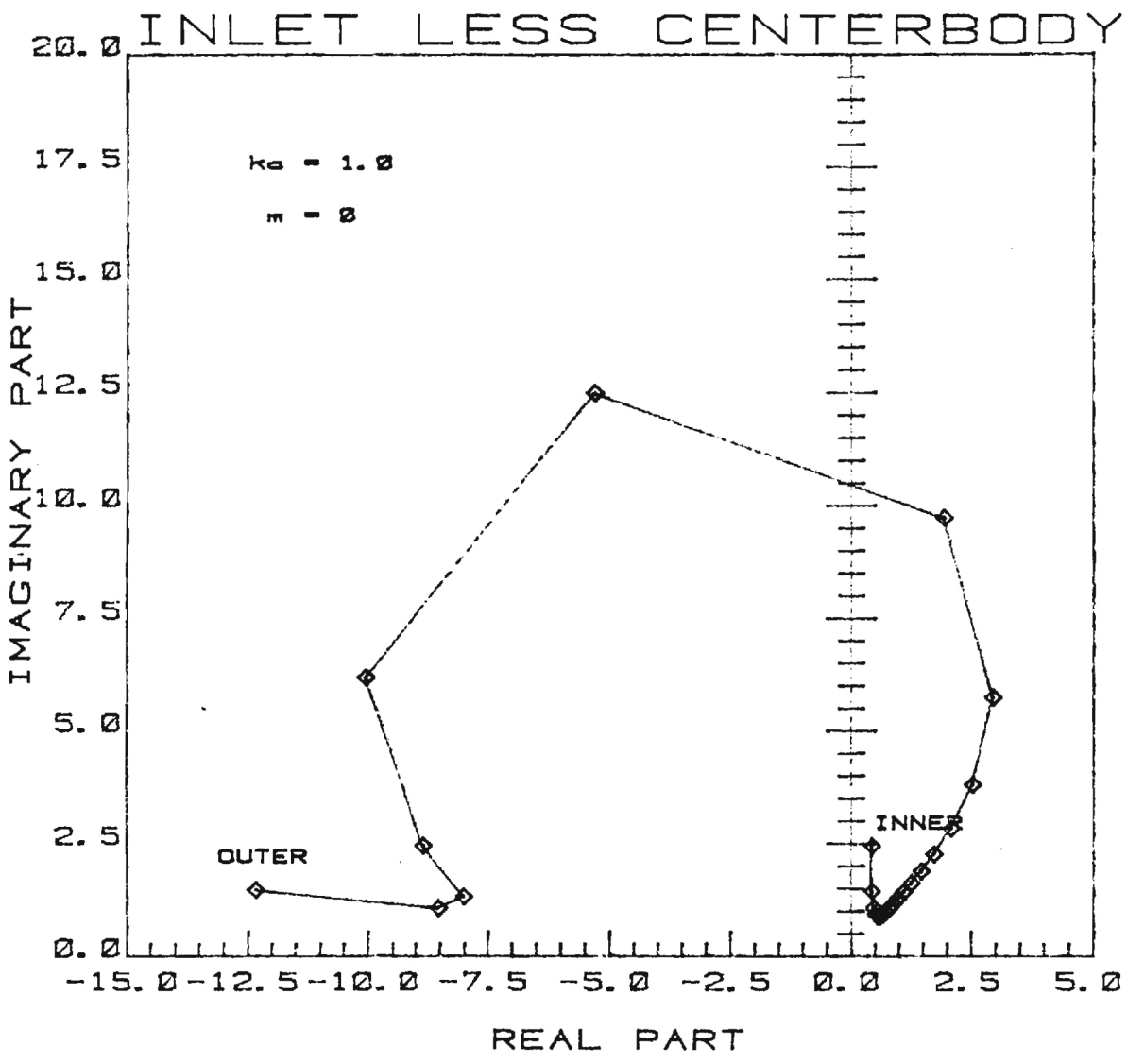

OPTIMUM ADMITTANCE DISTRIBUTION

Constant Phi on the Driver

Figure 20a

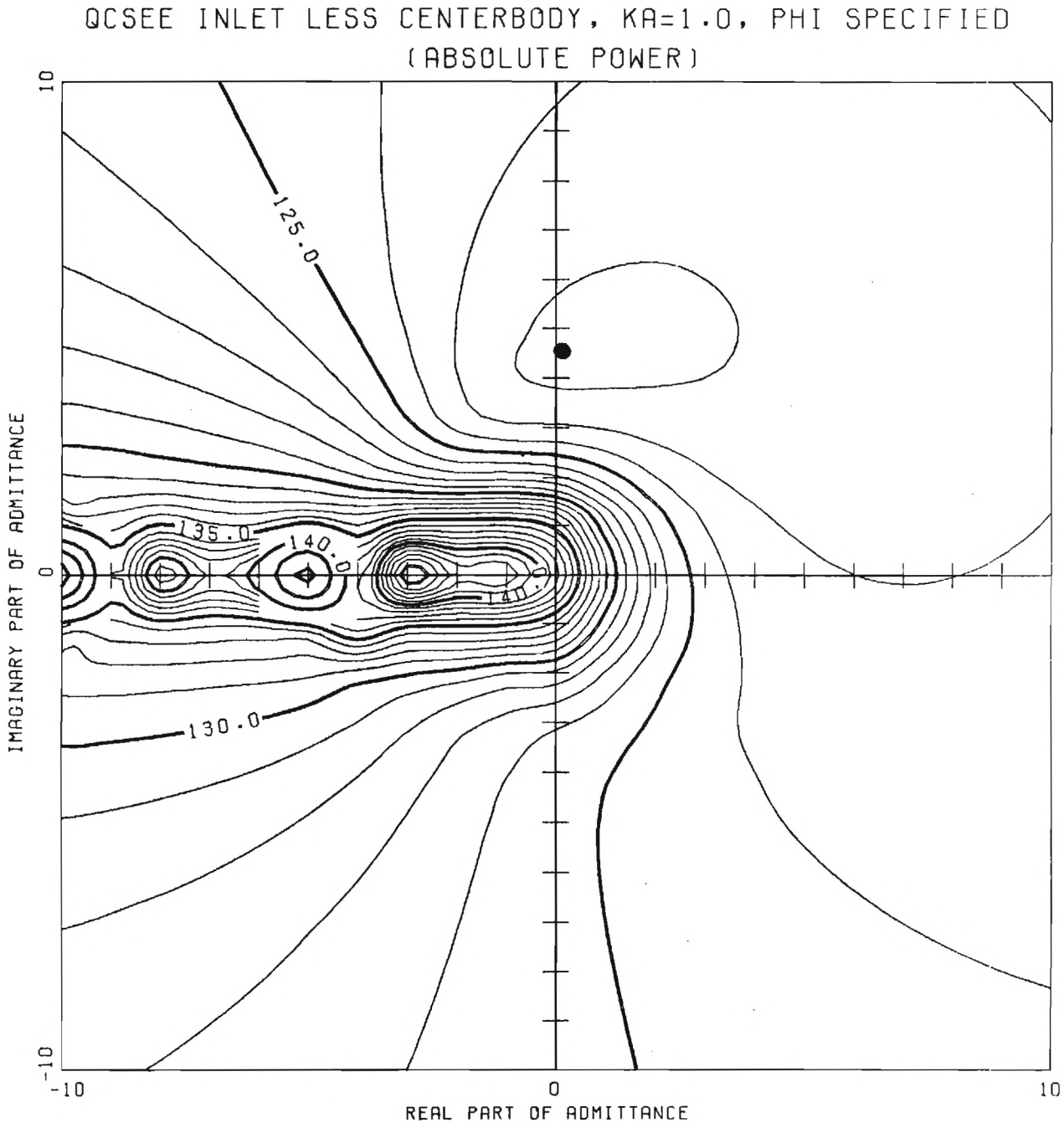
QCSEE INLET LESS CENTERBODY, KA=1.0, PHI SPECIFIED
(ABSOLUTE POWER)
125.0
135.0
140.0
145.0
130.0
10
0
-10
-10
0
10
IMAGINARY PART OF ADMITTANCE
REAL PART OF ADMITTANCE

Figure 20b

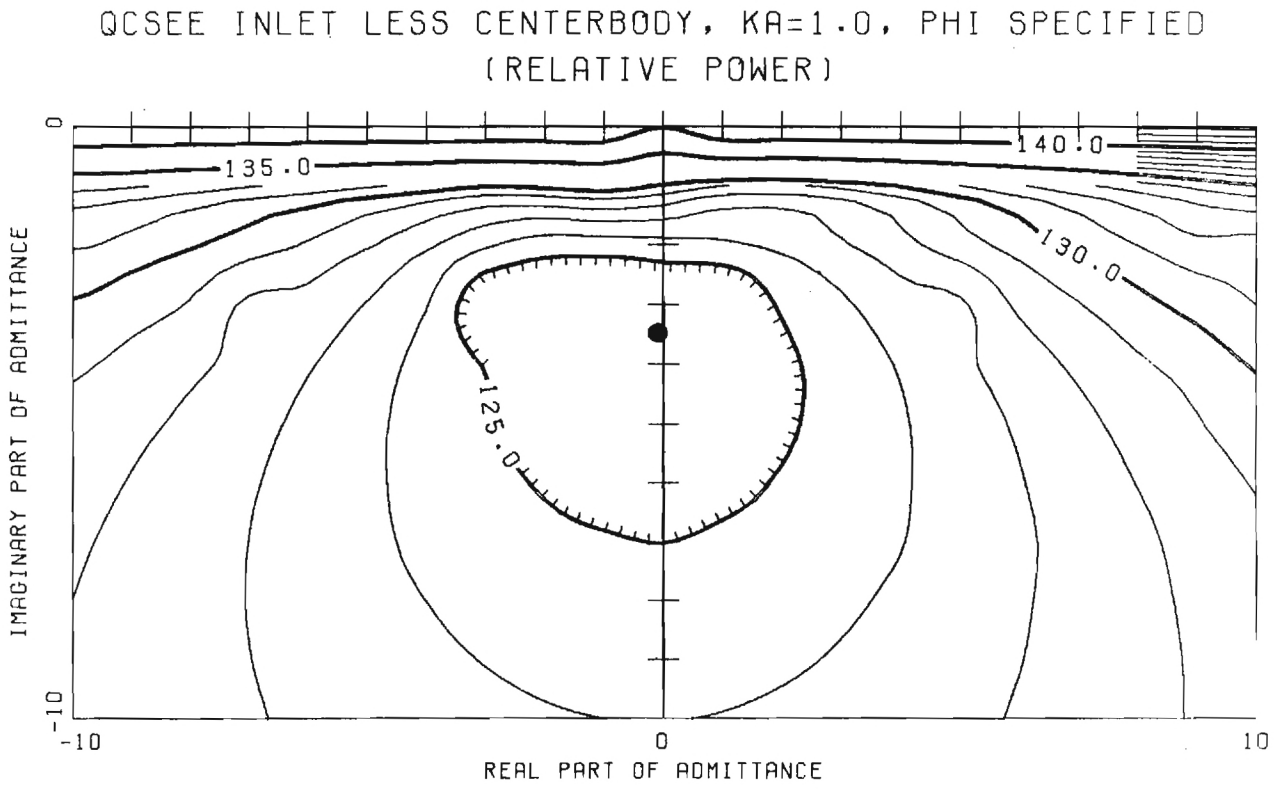
QCSEE INLET LESS CENTERBODY, KA=1.0, PHI SPECIFIED
(RELATIVE POWER)
140.0
135.0
130.0
125.0
0
-10
-10
0
10
IMAGINARY PART OF ADMITTANCE
REAL PART OF ADMITTANCE

Figure 20c

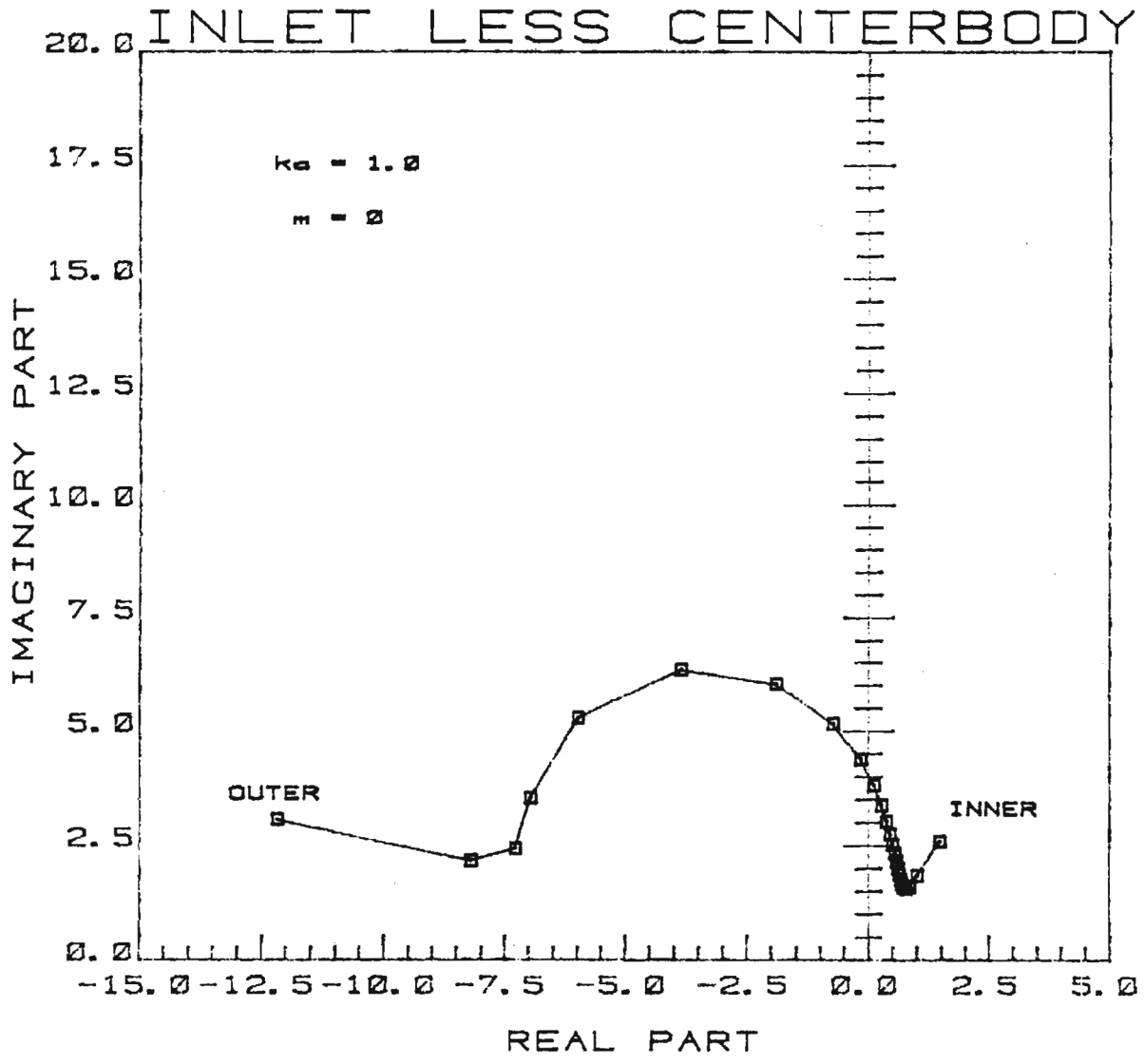

OPTIMUM ADMITTANCE DISTRIBUTION

Constant Velocity on the Driver

Figure 20d

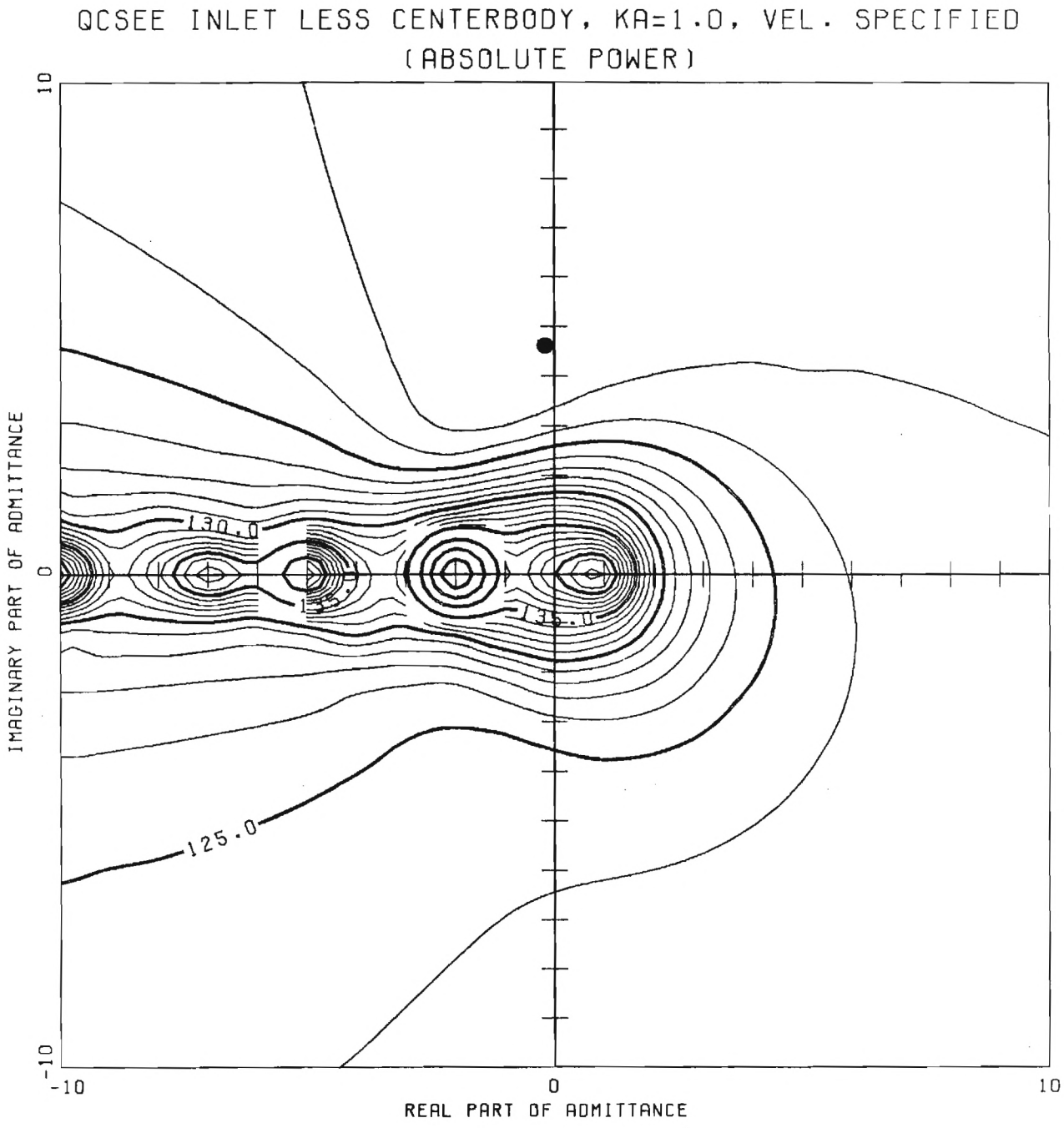
QCSEE INLET LESS CENTERBODY, KA=1.0, VEL. SPECIFIED
(ABSOLUTE POWER)
IMAGINARY PART OF ADMITTANCE
REAL PART OF ADMITTANCE
10
0
-10
-10
0
10
130.0
135.0
135.0
125.0

Figure 20e

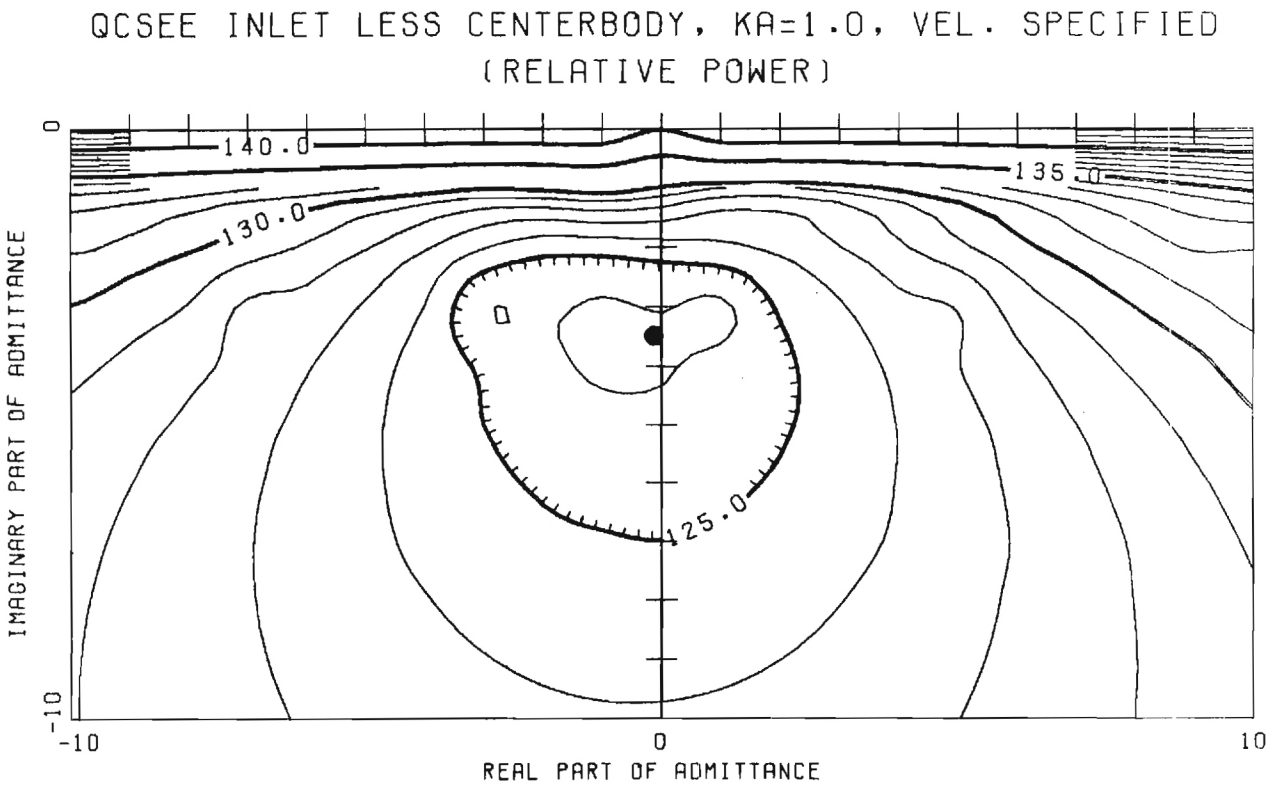
QCSEE INLET LESS CENTERBODY, KA=1.0, VEL. SPECIFIED
(RELATIVE POWER)
140.0
135.0
130.0
125.0
0
-10
IMAGINARY PART OF ADMITTANCE
-10
0
10
REAL PART OF ADMITTANCE

Figure 20f

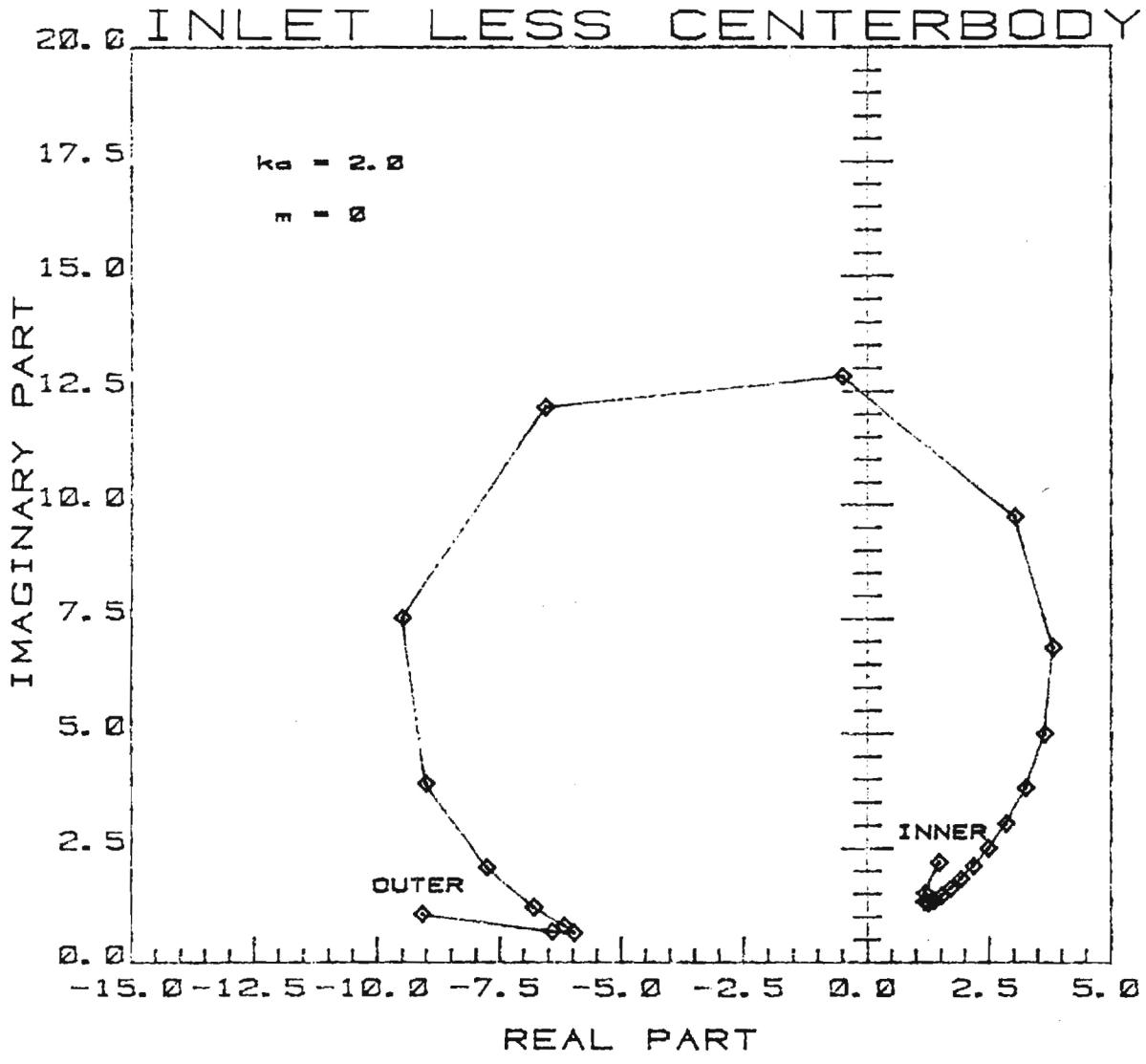

OPTIMUM ADMITTANCE DISTRIBUTION

Constant Phi on the Driver

Figure 21a

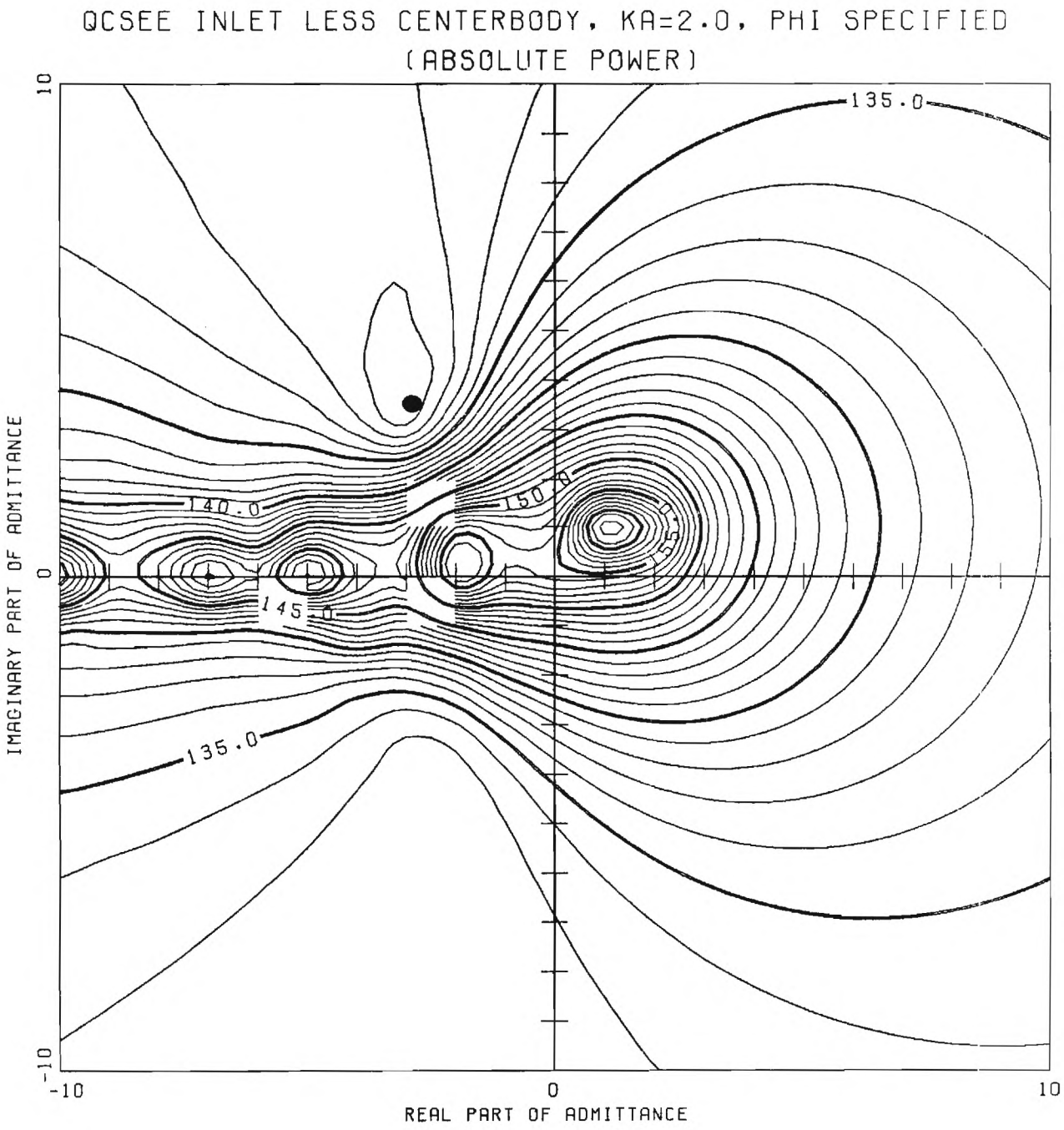
QCSEE INLET LESS CENTERBODY, KA=2.0, PHI SPECIFIED
(ABSOLUTE POWER)
135.0
140.0
150.0
145.0
135.0
10
0
-10
-10
0
10
IMAGINARY PART OF ADMITTANCE
REAL PART OF ADMITTANCE

Figure 21b

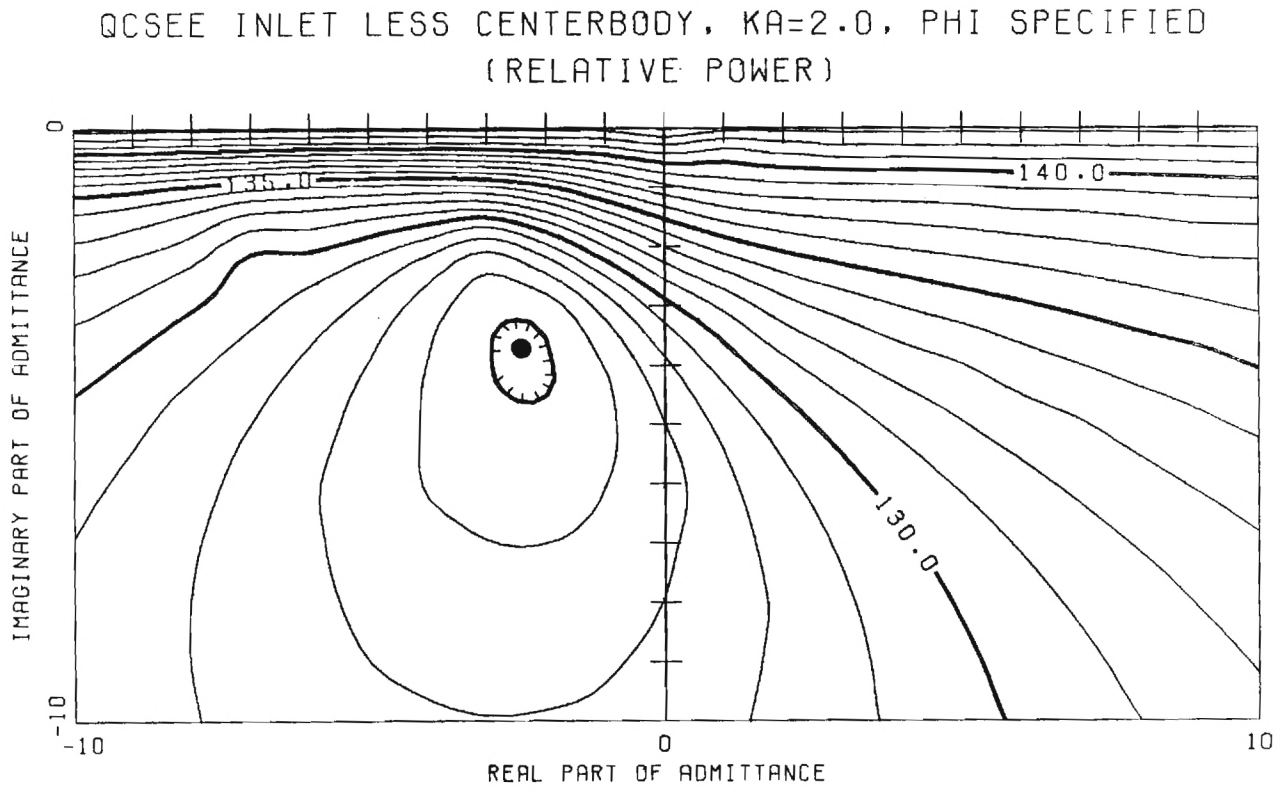
QCSEE INLET LESS CENTERBODY, KA=2.0, PHI SPECIFIED
(RELATIVE POWER)
0
-10
IMAGINARY PART OF ADMITTANCE
140.0
130.0
-10
0
10
REAL PART OF ADMITTANCE

Figure 21c

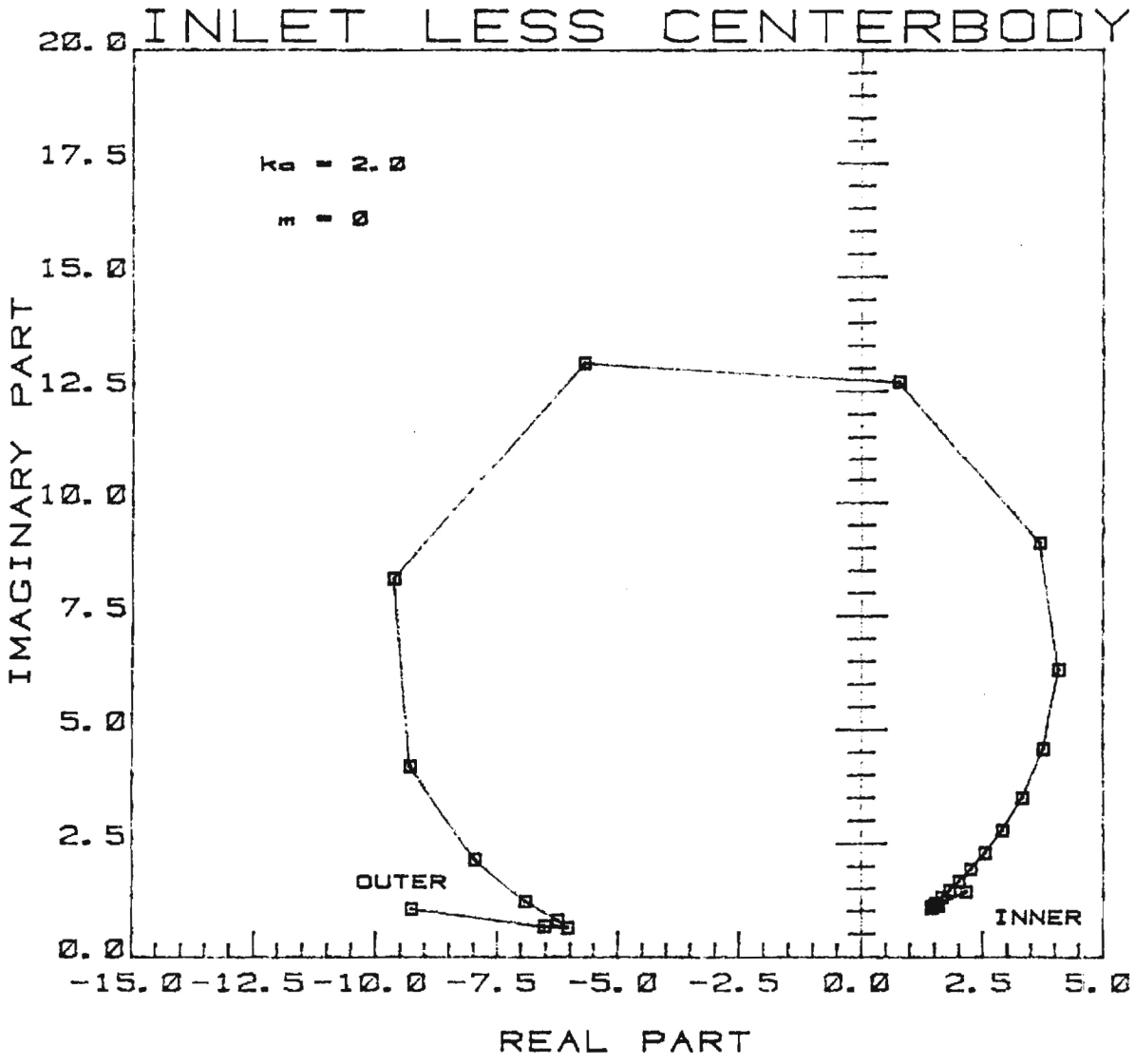

OPTIMUM ADMITTANCE DISTRIBUTION

Constant Velocity on the Driver

Figure 21d

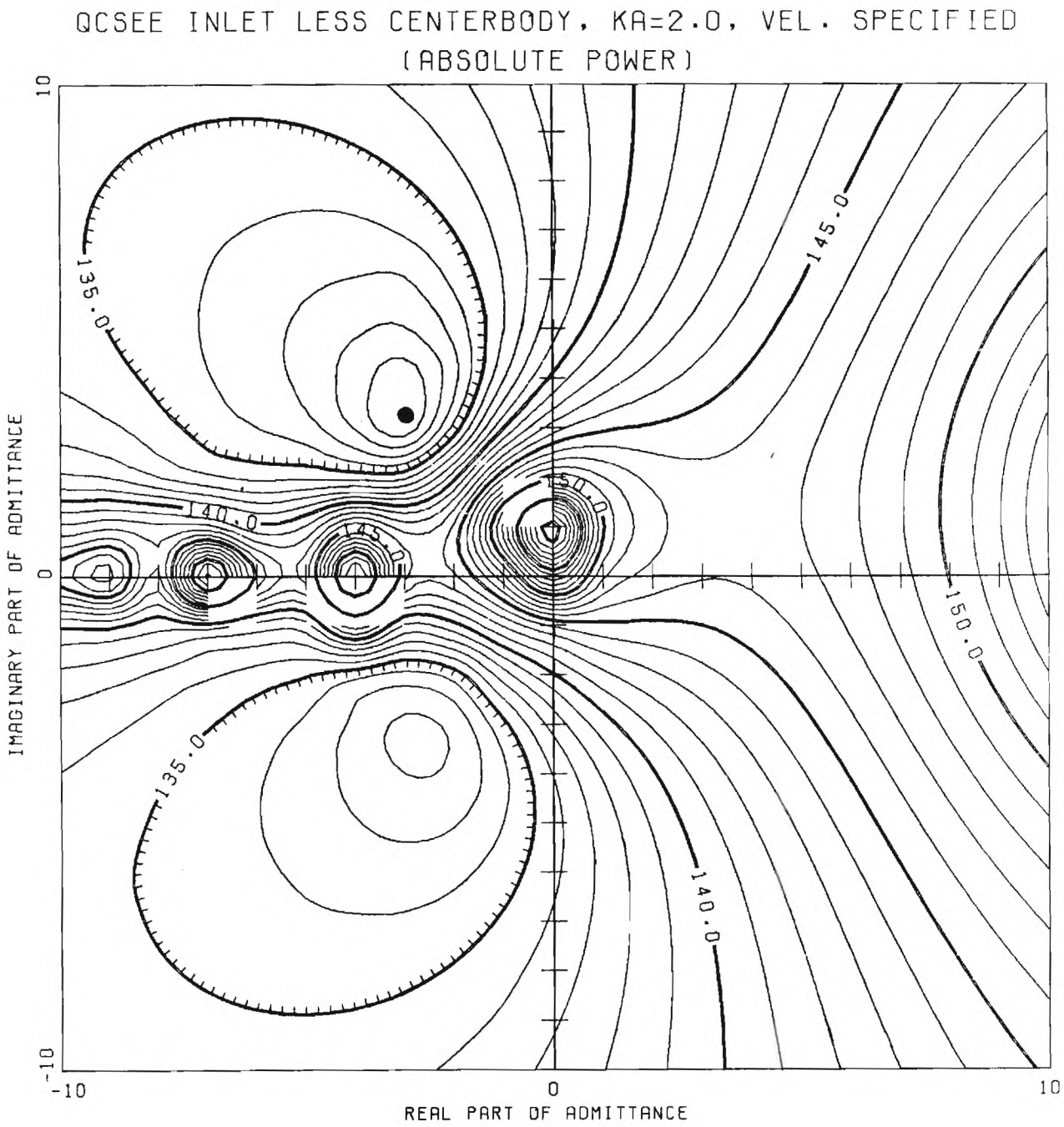
QCSEE INLET LESS CENTERBODY, KA=2.0, VEL. SPECIFIED
(ABSOLUTE POWER)
IMAGINARY PART OF ADMITTANCE
REAL PART OF ADMITTANCE
10
0
-10
-10
0
10
135.0
140.0
145.0
150.0

Figure 21e

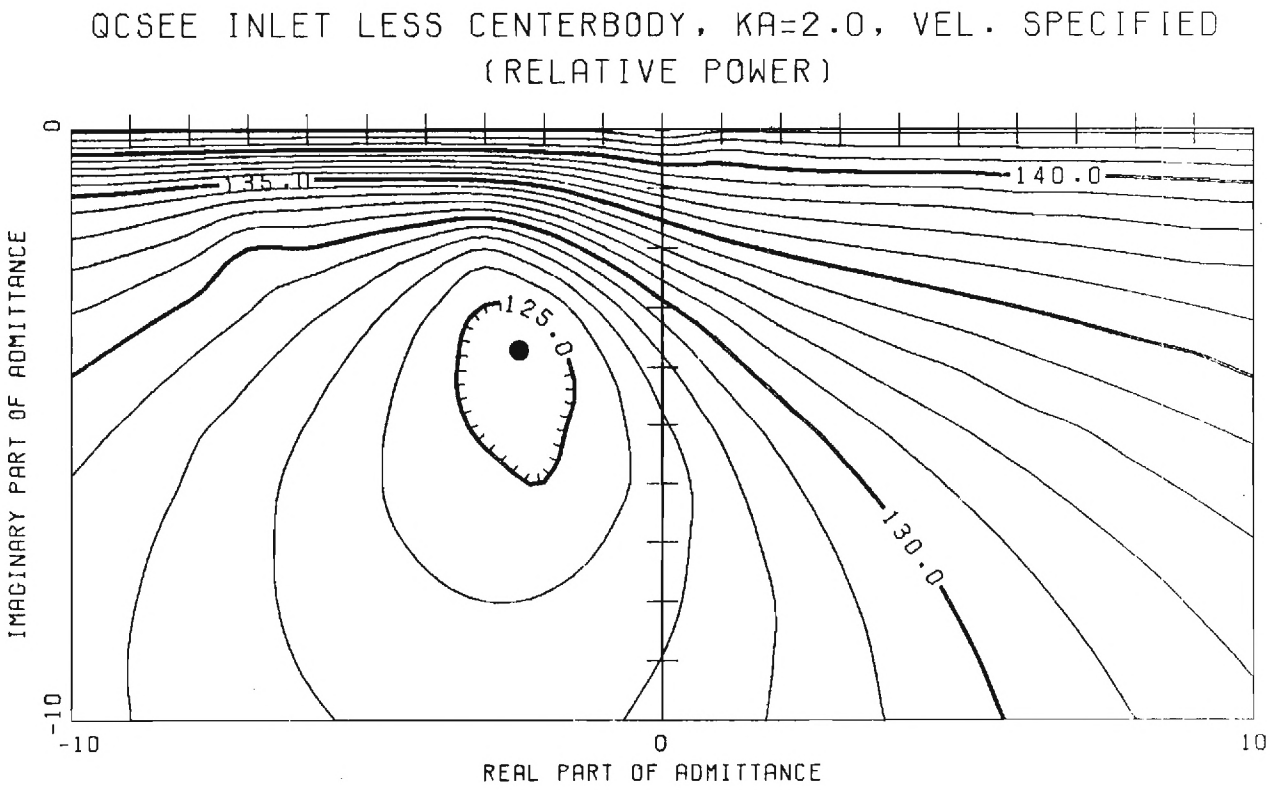
QCSEE INLET LESS CENTERBODY, KA=2.0, VEL. SPECIFIED
(RELATIVE POWER)
0
-10
IMAGINARY PART OF ADMITTANCE
135.0
140.0
125.0
130.0
-10
0
10
REAL PART OF ADMITTANCE

Figure 21f

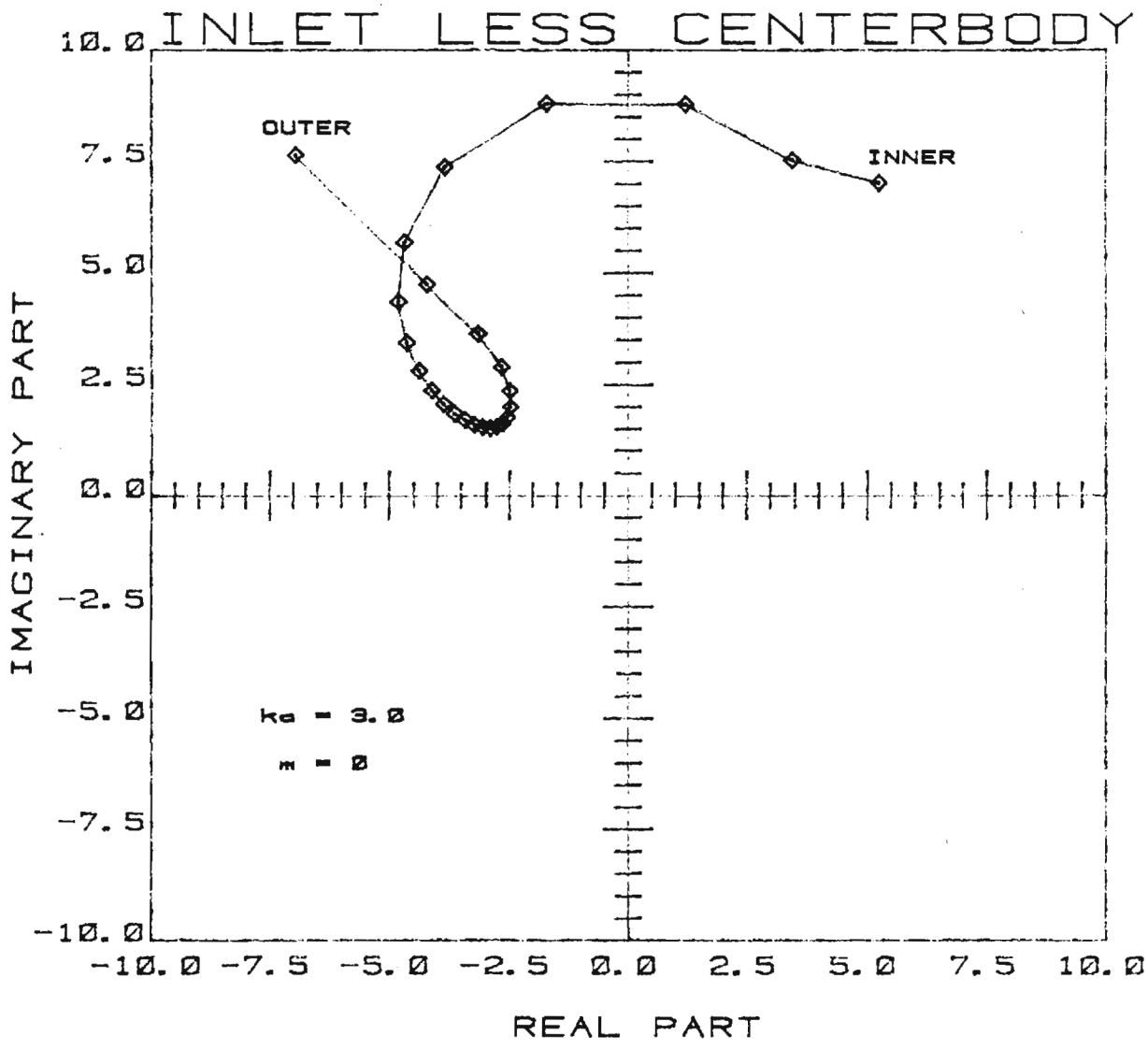

OPTIMUM ADMITTANCE DISTRIBUTION

Constant Phi on the Driver

Figure 22a

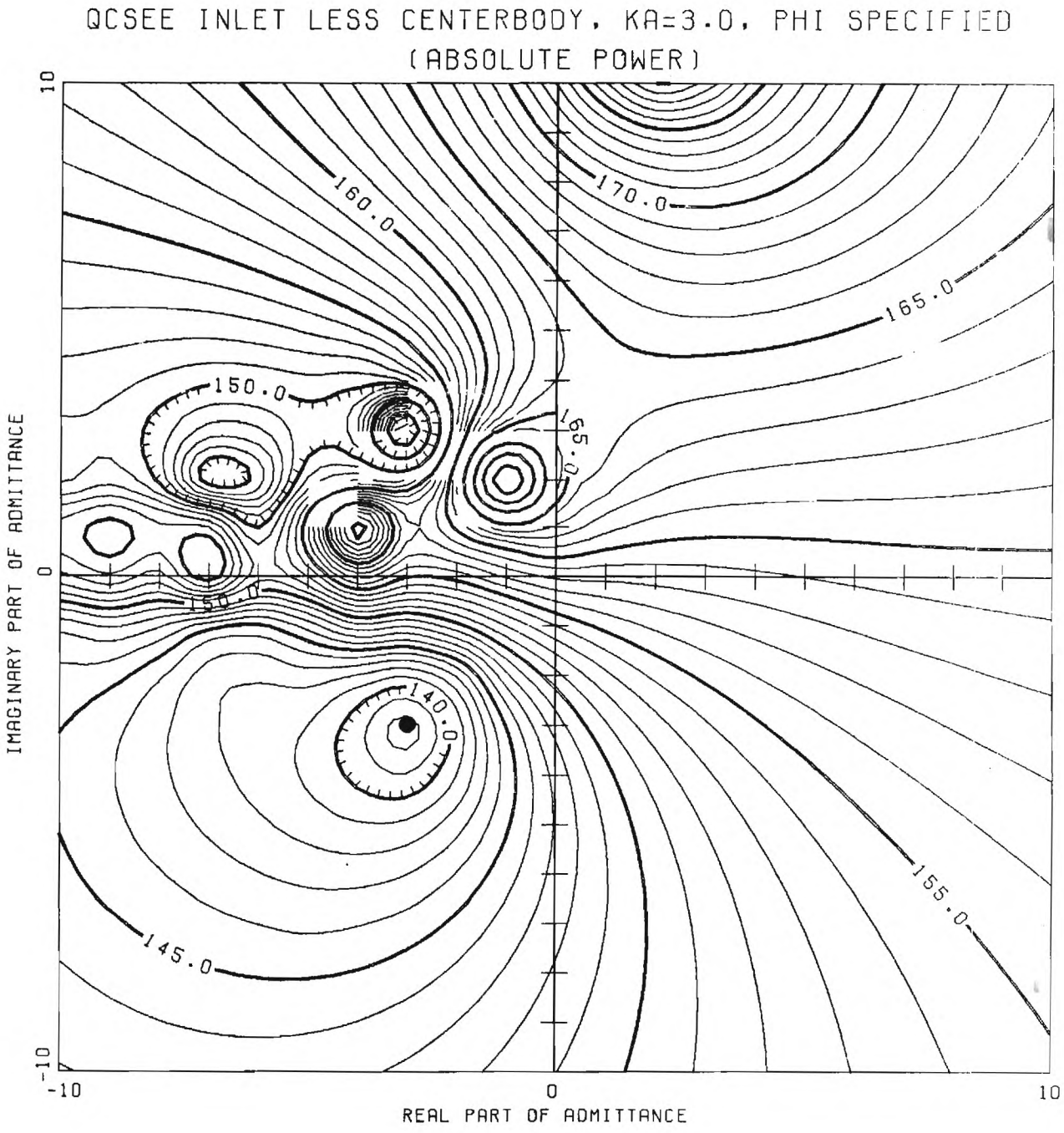
QCSEE INLET LESS CENTERBODY, KA=3.0, PHI SPECIFIED
(ABSOLUTE POWER)
IMAGINARY PART OF ADMITTANCE
REAL PART OF ADMITTANCE
10
0
-10
-10
0
10
160.0
170.0
165.0
150.0
165.0
150.0
140.0
155.0
145.0

Figure 22b

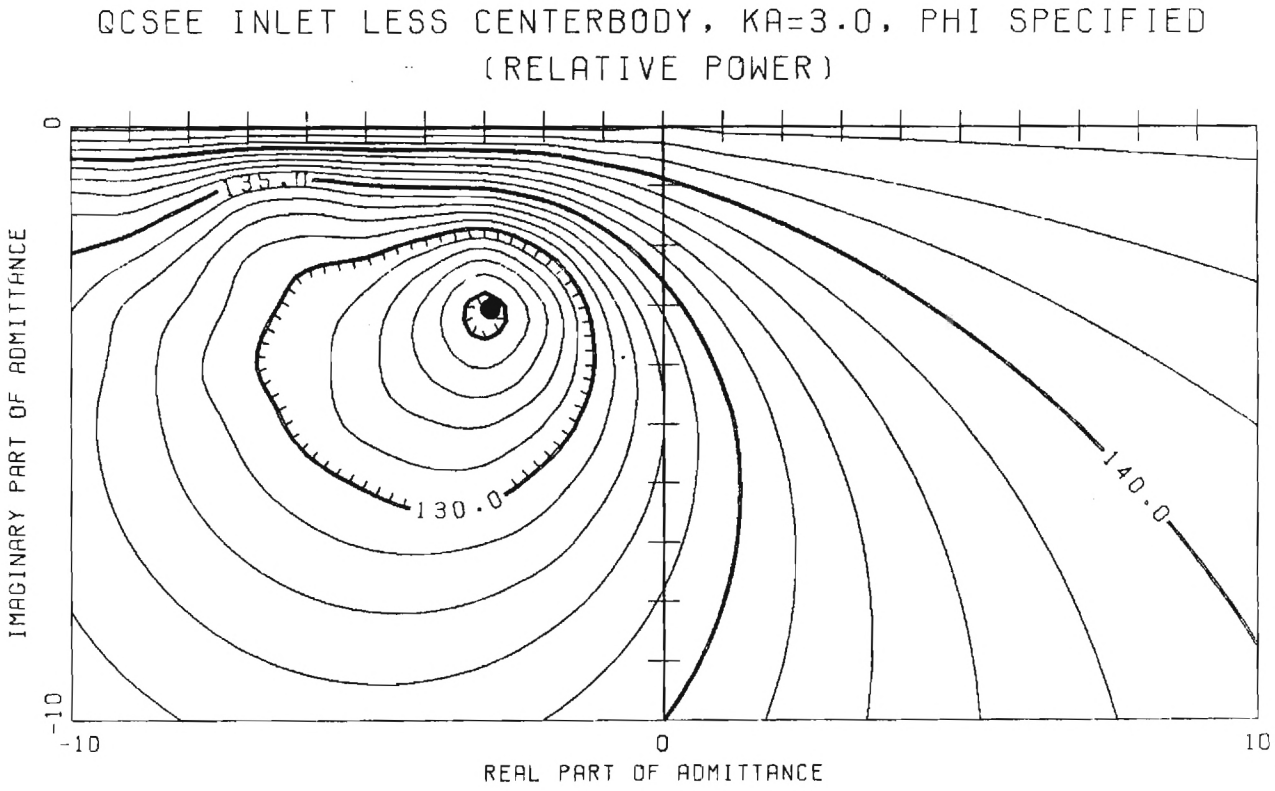
QCSEE INLET LESS CENTERBODY, KA=3.0, PHI SPECIFIED
(RELATIVE POWER)
IMAGINARY PART OF ADMITTANCE
0
-10
-10
0
10
REAL PART OF ADMITTANCE
135.0
130.0
140.0

Figure 22c

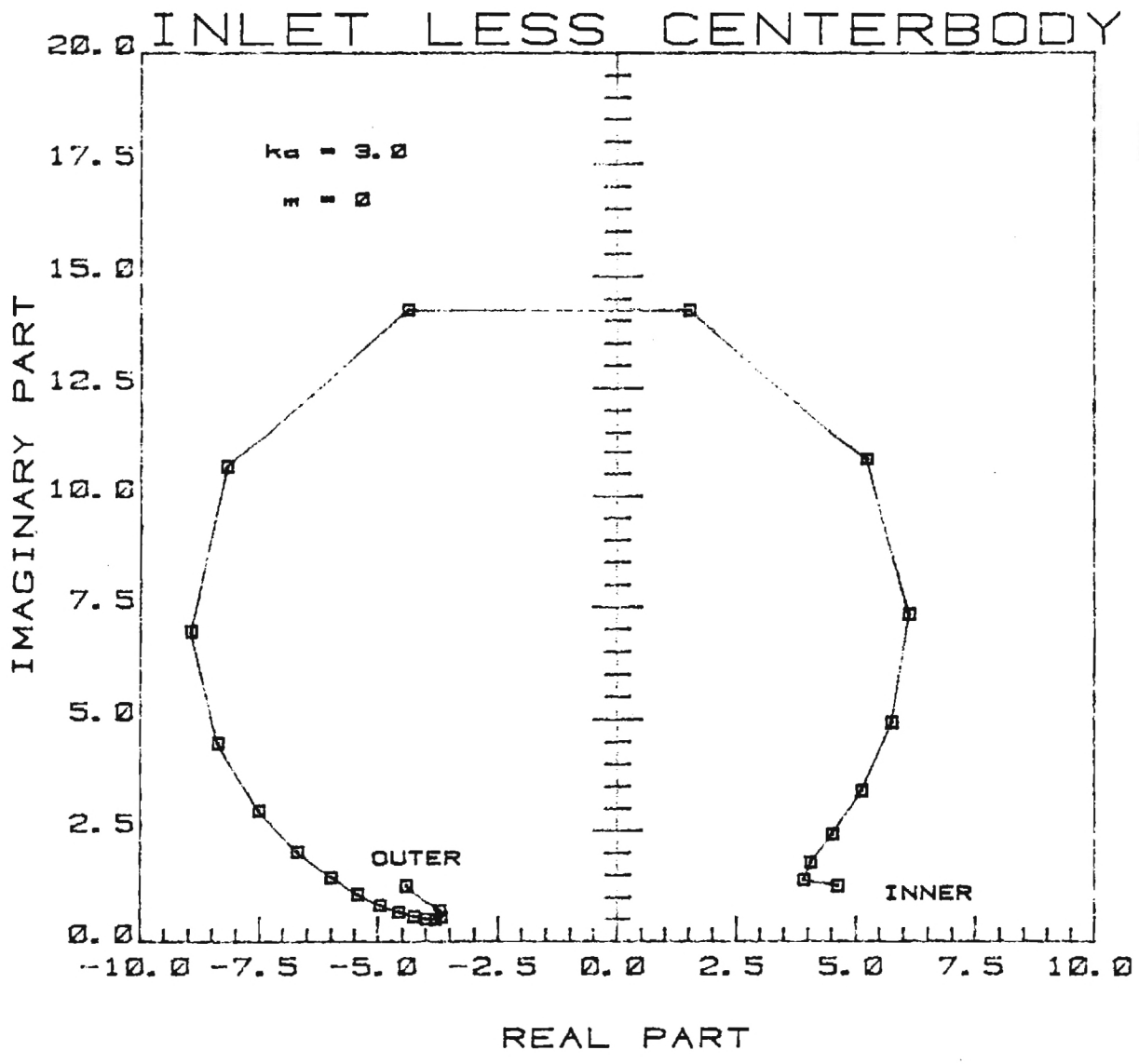

OPTIMUM ADMITTANCE DISTRIBUTION

Constant Velocity on the Driver

Figure 22d

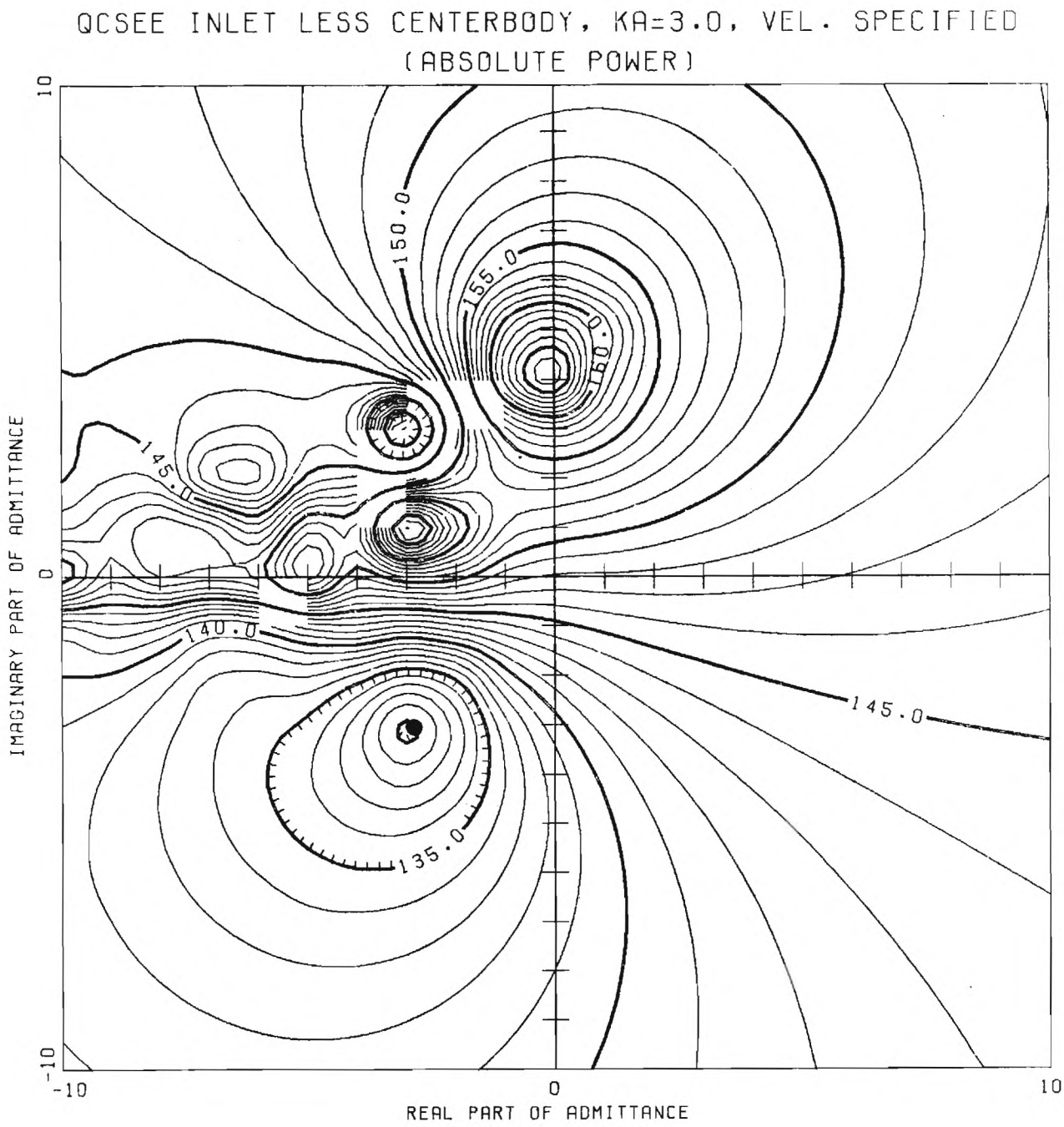
QCSEE INLET LESS CENTERBODY, KA=3.0, VEL. SPECIFIED
(ABSOLUTE POWER)
150.0
155.0
160.0
145.0
140.0
145.0
135.0
10
0
-10
-10
0
10
IMAGINARY PART OF ADMITTANCE
REAL PART OF ADMITTANCE

Figure 22e

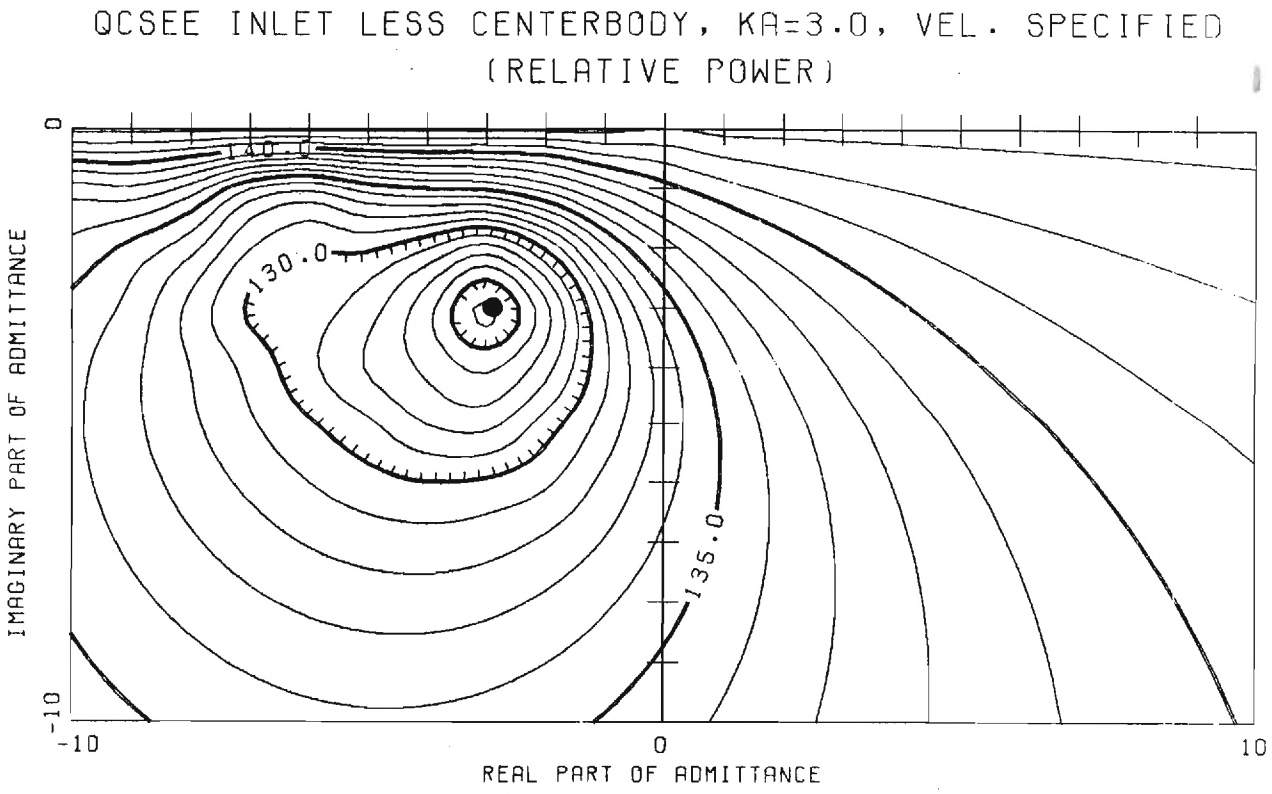
QCSEE INLET LESS CENTERBODY, KA=3.0, VEL. SPECIFIED
(RELATIVE POWER)
140.0
130.0
135.0
0
-10
-10
0
10
IMAGINARY PART OF ADMITTANCE
REAL PART OF ADMITTANCE

Figure 22f

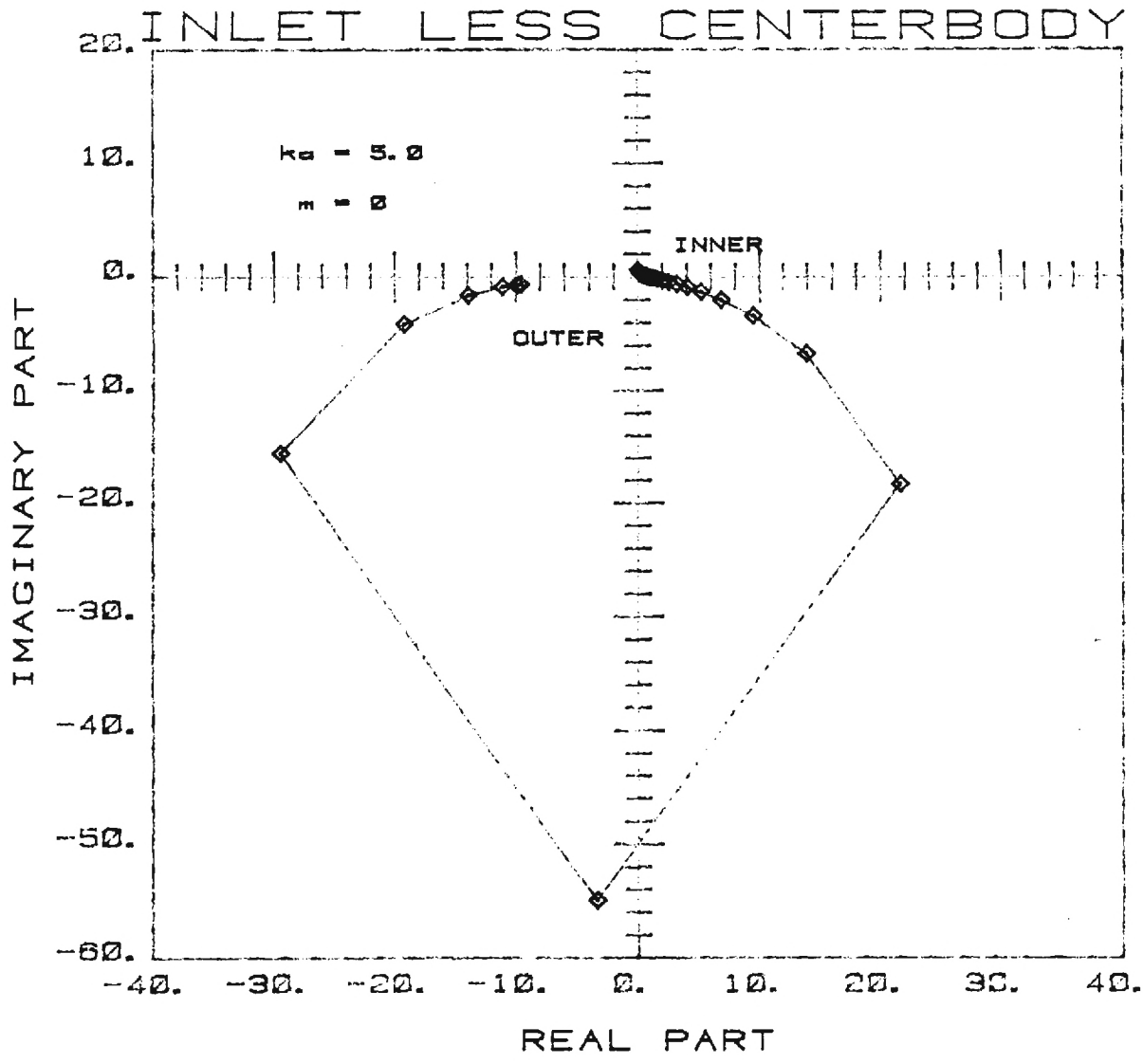

OPTIMUM ADMITTANCE DISTRIBUTION

Constant Phi on the Driver

Figure 23a

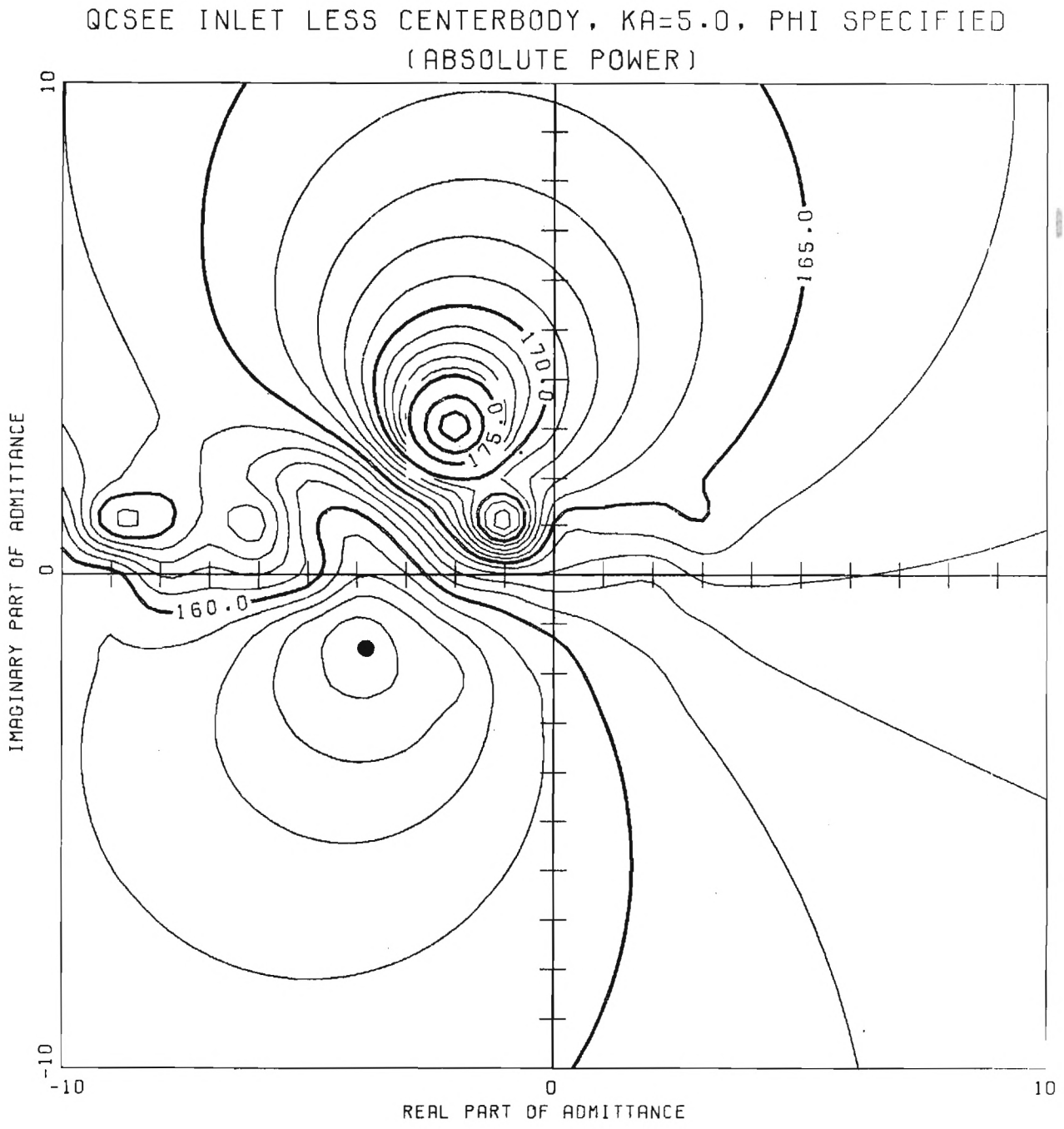
QCSEE INLET LESS CENTERBODY, KA=5.0, PHI SPECIFIED
(ABSOLUTE POWER)
IMAGINARY PART OF ADMITTANCE
REAL PART OF ADMITTANCE
10
0
-10
-10
0
10
165.0
170.0
175.0
160.0

Figure 23b

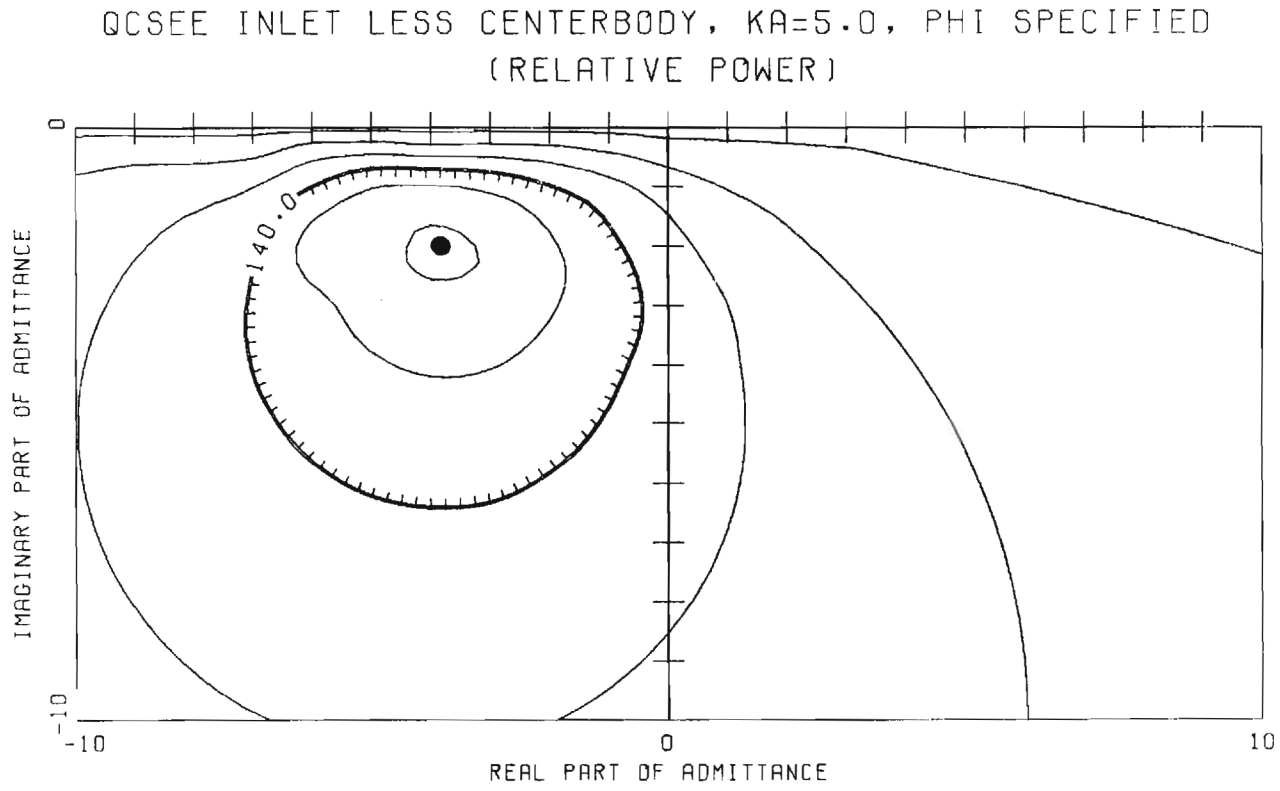
QCSEE INLET LESS CENTERBODY, KA=5.0, PHI SPECIFIED
(RELATIVE POWER)
IMAGINARY PART OF ADMITTANCE
REAL PART OF ADMITTANCE
0
-10
-10
0
10
40.0

Figure 23c

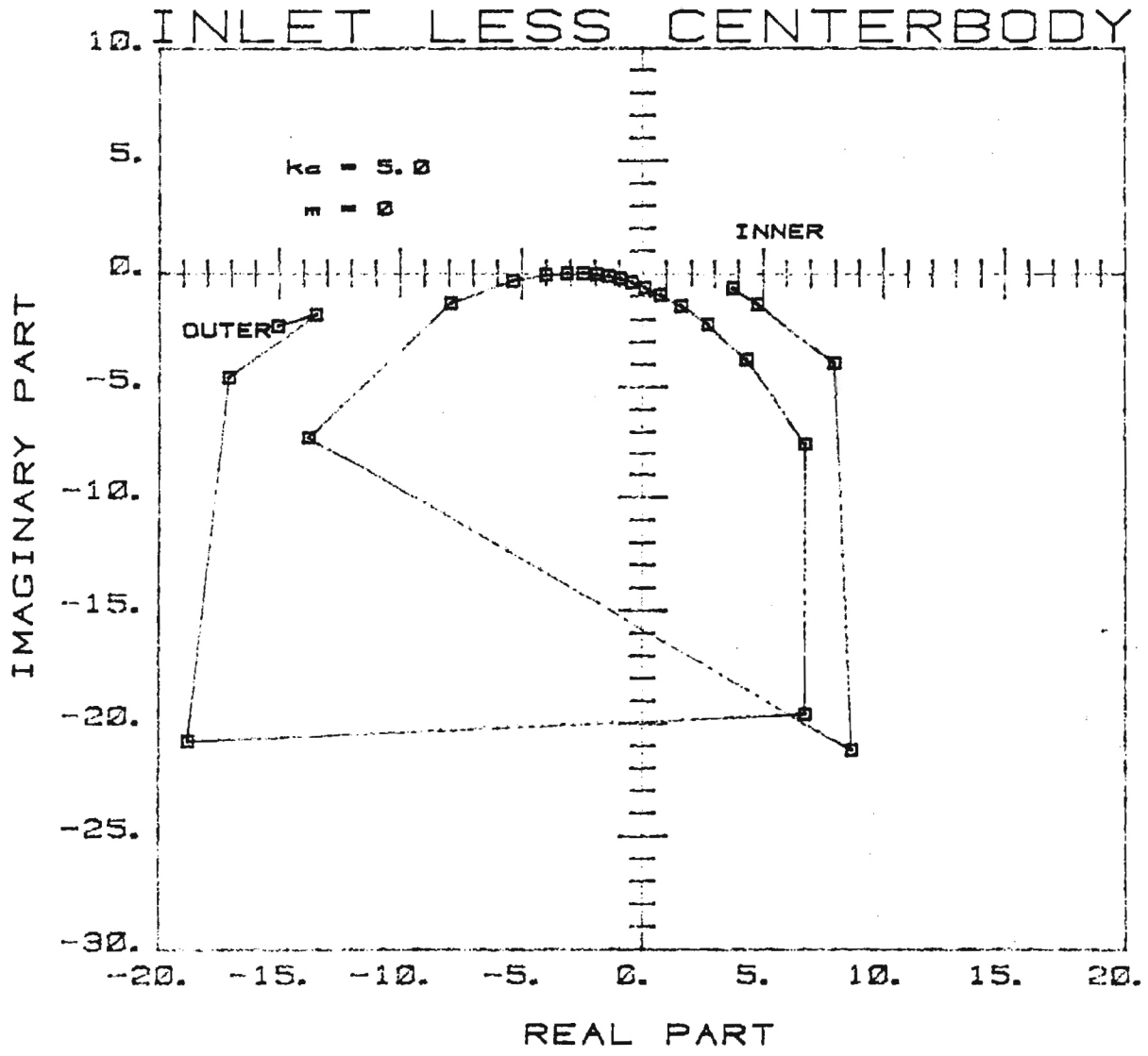

OPTIMUM ADMITTANCE DISTRIBUTION

Constant Velocity on the Driver

Figure 23d

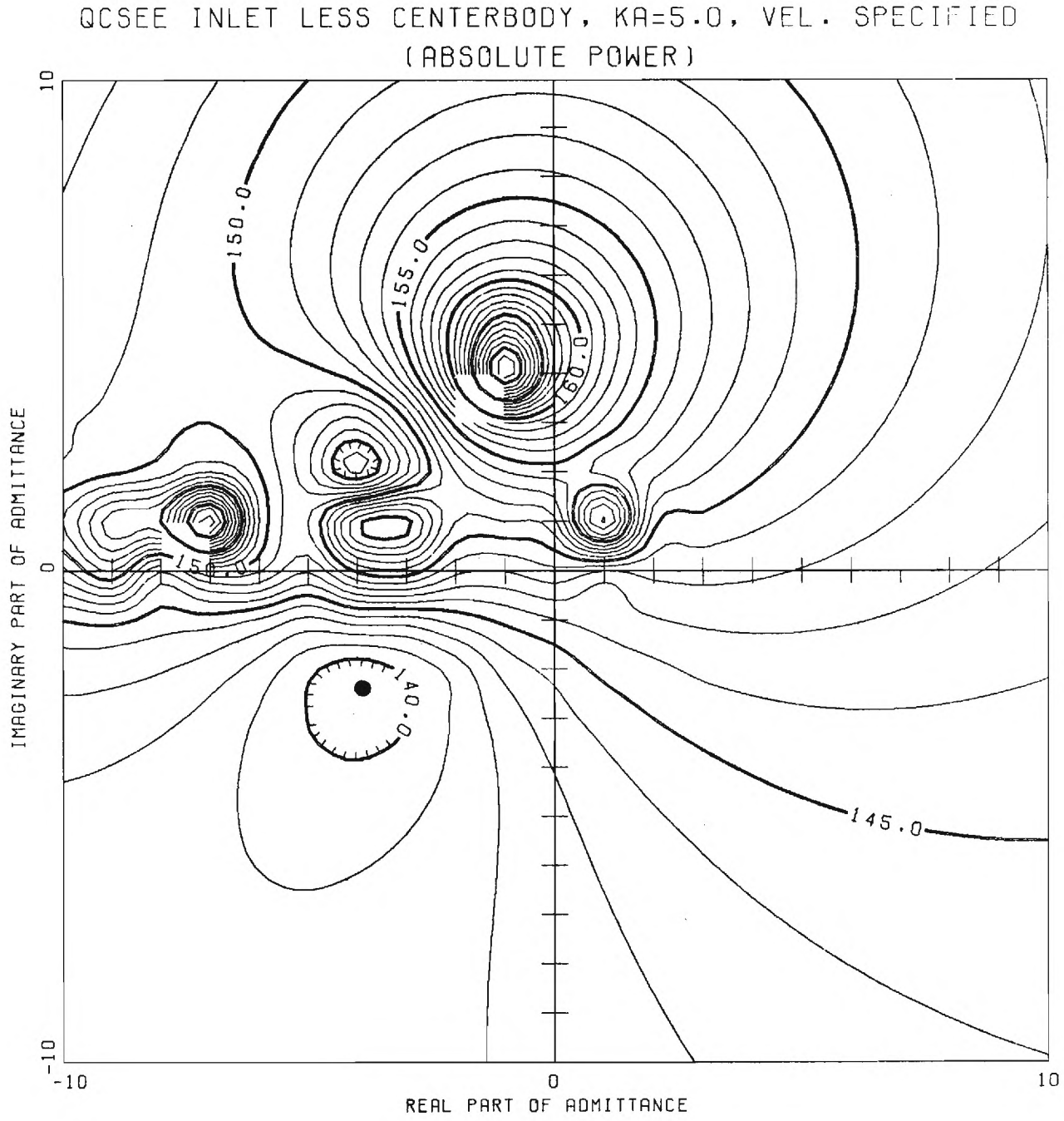
QCSEE INLET LESS CENTERBODY, KA=5.0, VEL. SPECIFIED
(ABSOLUTE POWER)
150.0
155.0
160.0
150.0
140.0
145.0
10
0
-10
-10
0
10
IMAGINARY PART OF ADMITTANCE
REAL PART OF ADMITTANCE

Figure 23e

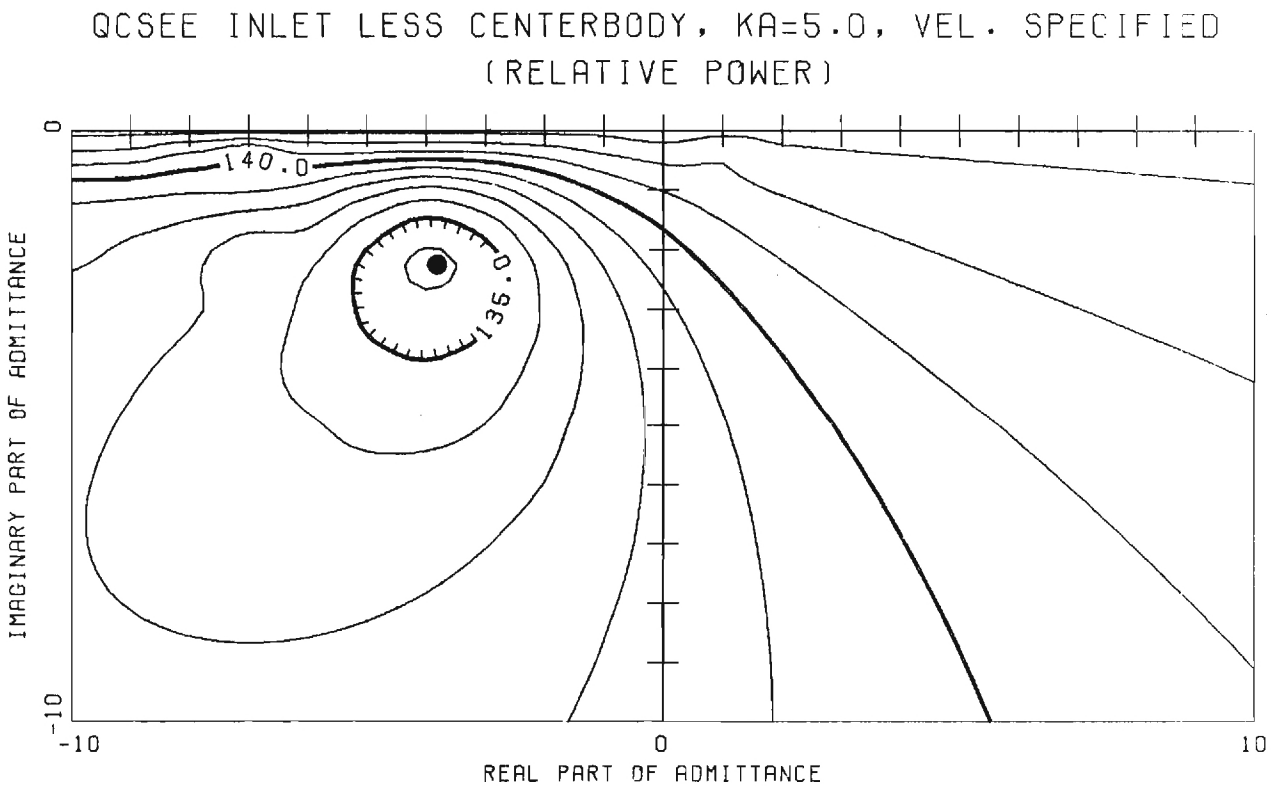
QCSEE INLET LESS CENTERBODY, KA=5.0, VEL. SPECIFIED
(RELATIVE POWER)
140.0
135.0
0
-10
IMAGINARY PART OF ADMITTANCE
-10
0
10
REAL PART OF ADMITTANCE

Figure 23f

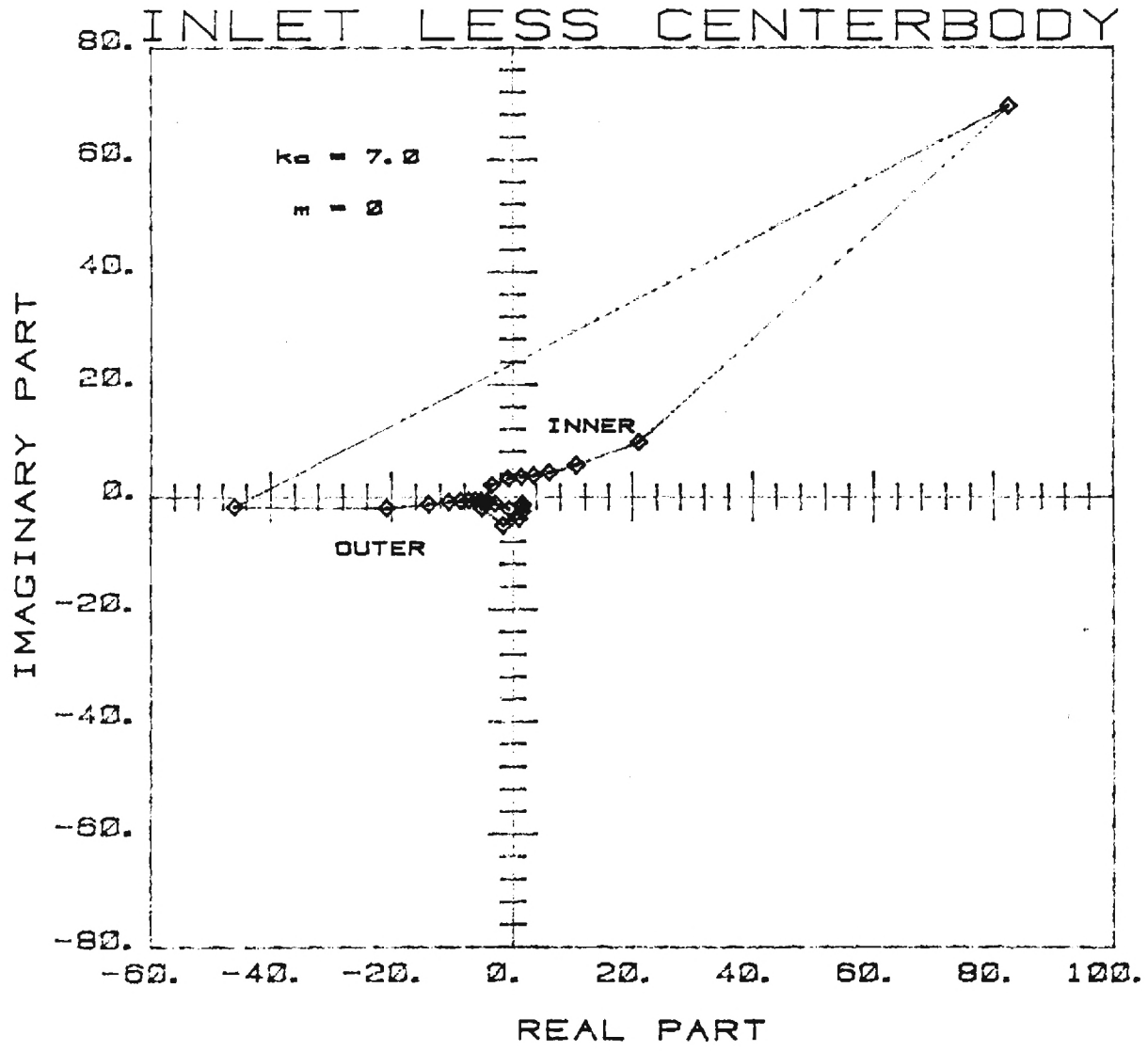

OPTIMUM ADMITTANCE DISTRIBUTION

Constant Phi on the Driver

Figure 24a

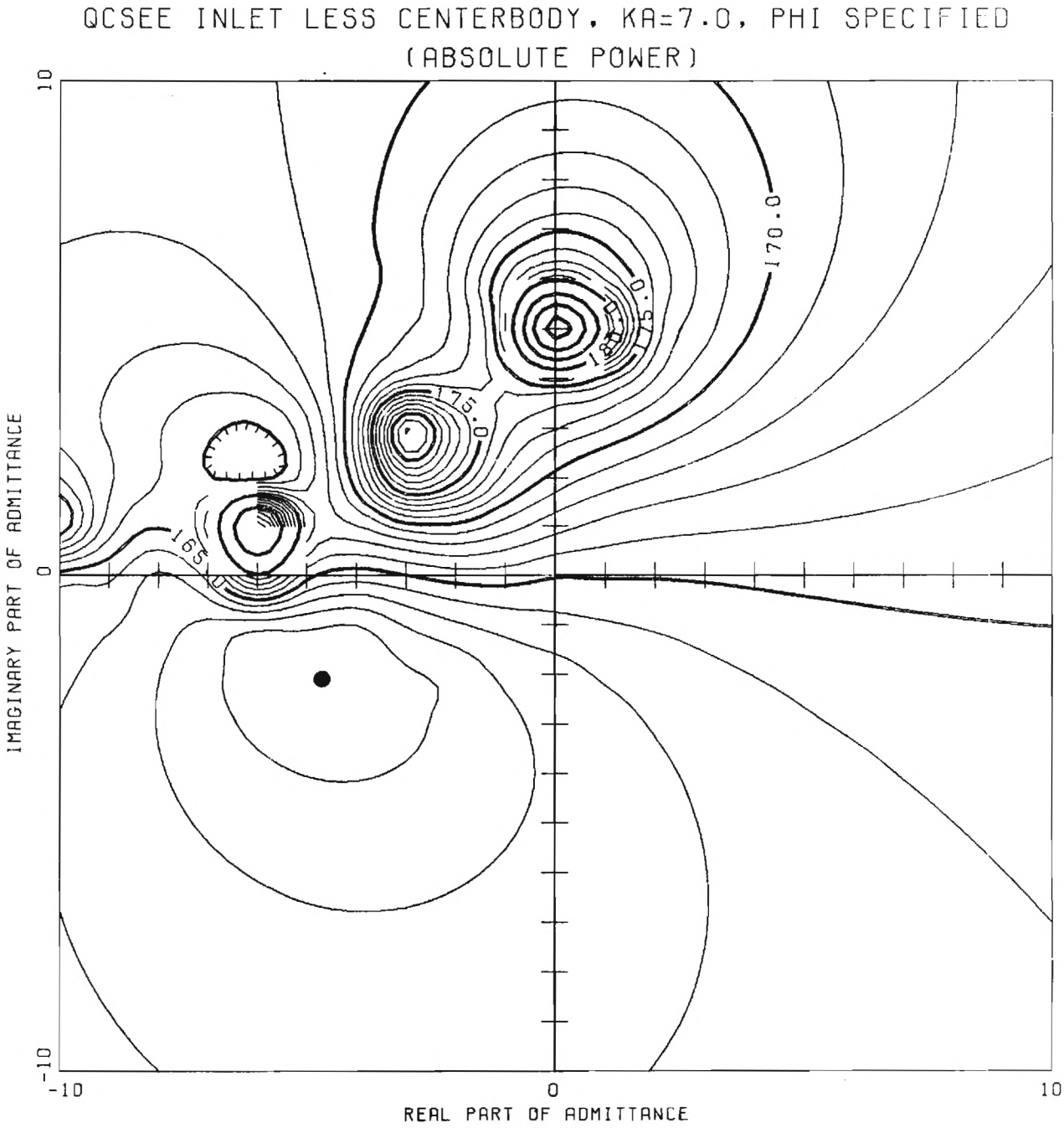
QCSEE INLET LESS CENTERBODY, KA=7.0, PHI SPECIFIED
(ABSOLUTE POWER)
IMAGINARY PART OF ADMITTANCE
REAL PART OF ADMITTANCE
10
0
-10
-10
0
10
170.0
175.0
180.0
165.0

Figure 24b

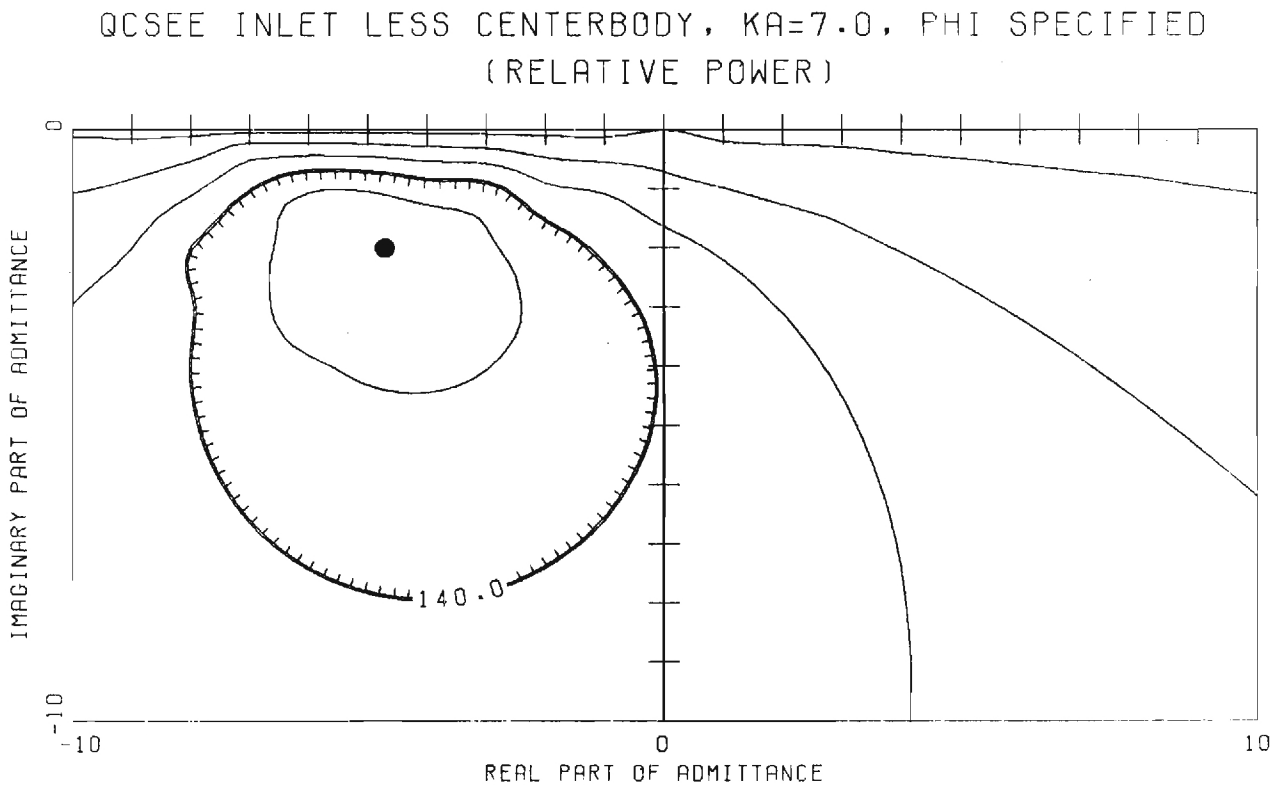
QCSEE INLET LESS CENTERBODY, KA=7.0, PHI SPECIFIED
(RELATIVE POWER)
IMAGINARY PART OF ADMITTANCE
0
-10
-10
0
10
REAL PART OF ADMITTANCE
140.0

Figure 24c

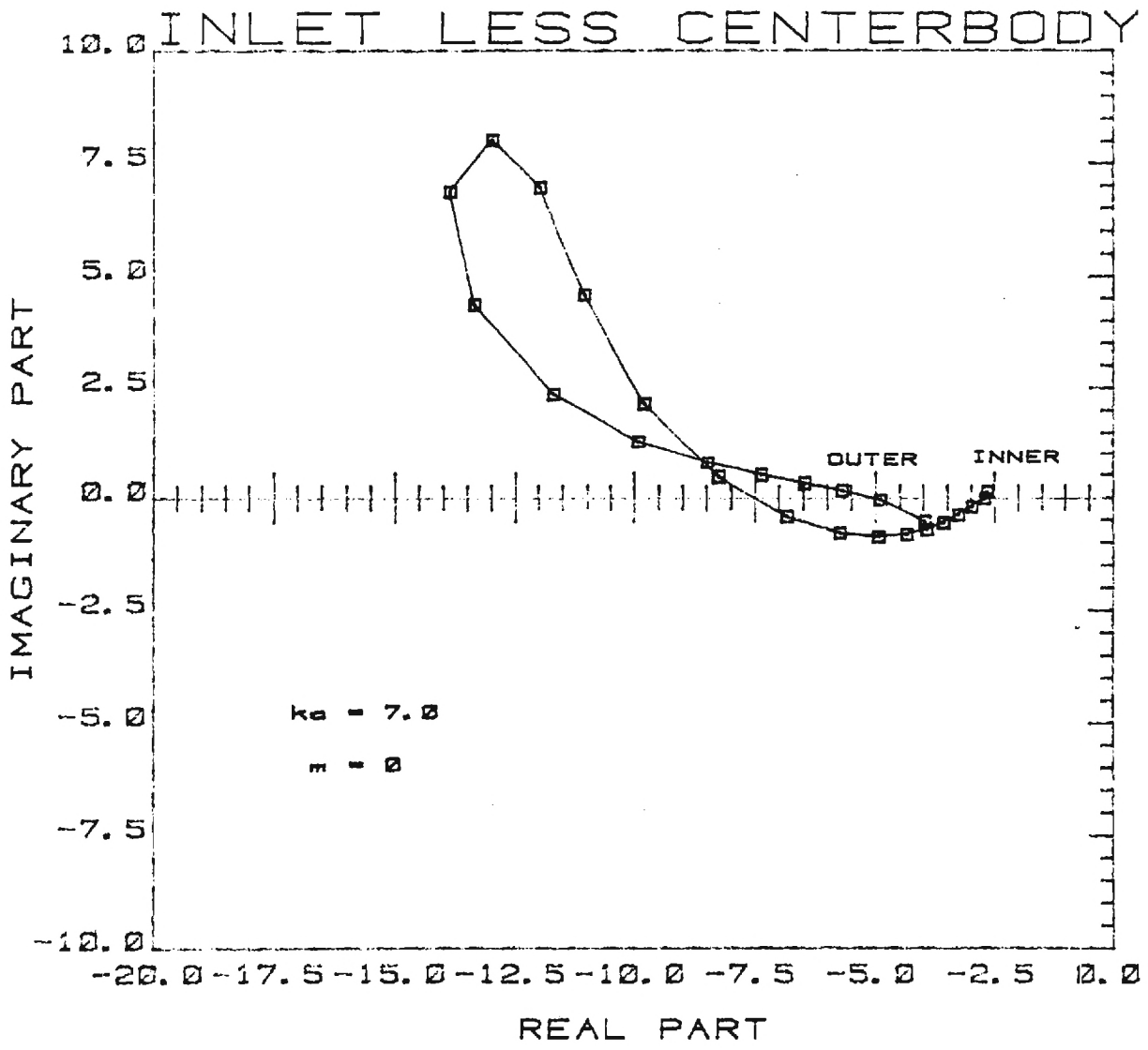

OPTIMUM ADMITTANCE DISTRIBUTION

Constant Velocity on the Driver

Figure 24d

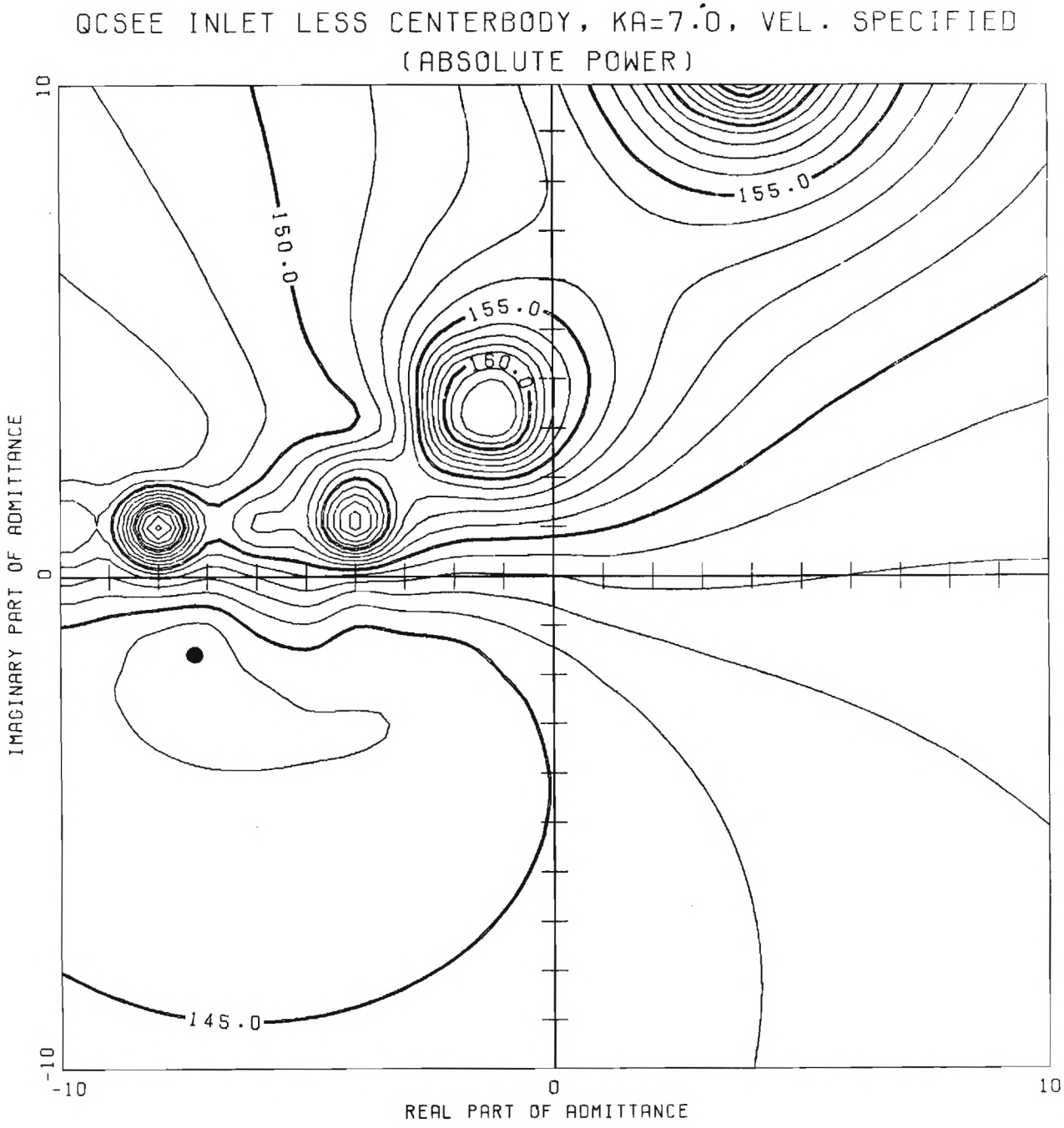
QCSEE INLET LESS CENTERBODY, KA=7.0, VEL. SPECIFIED
(ABSOLUTE POWER)
IMAGINARY PART OF ADMITTANCE
REAL PART OF ADMITTANCE
10
0
-10
-10
0
10
150.0
155.0
155.0
150.0
145.0

Figure 24e

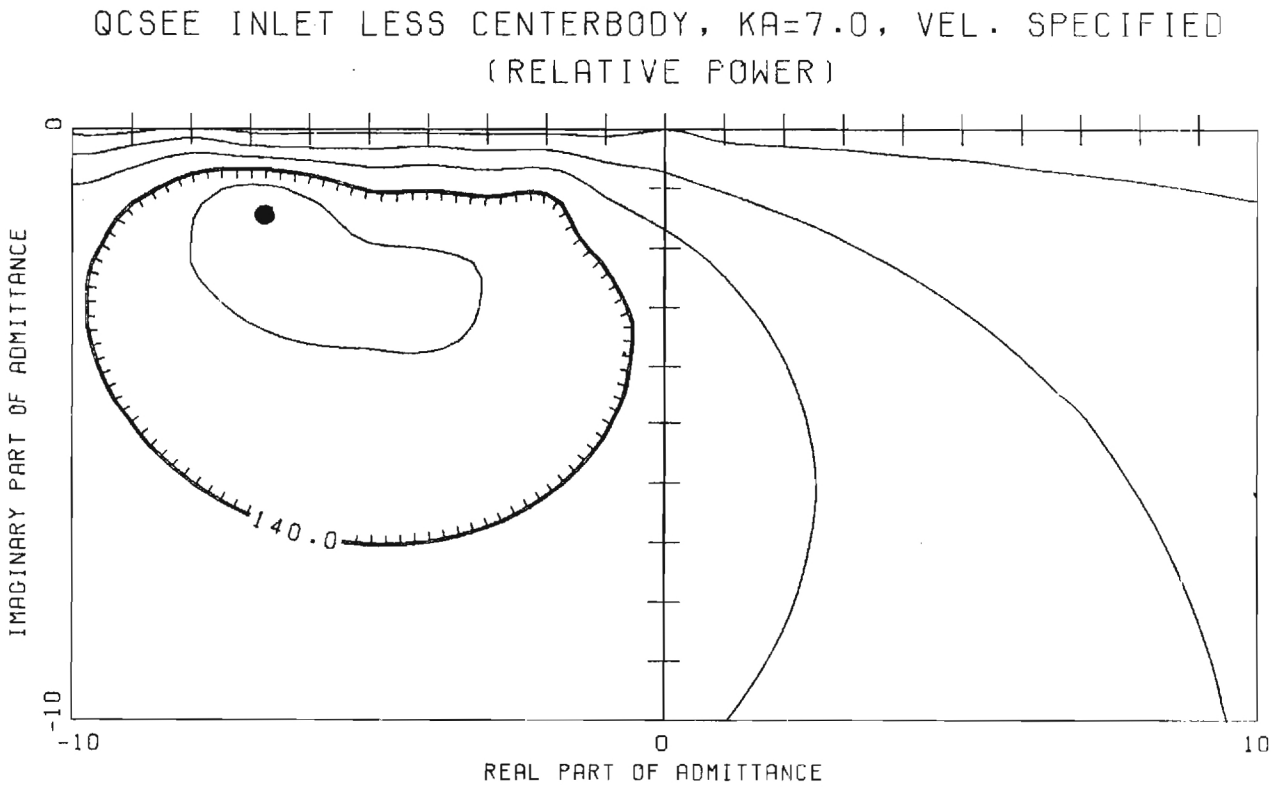
QCSEE INLET LESS CENTERBODY, KA=7.0, VEL. SPECIFIED
(RELATIVE POWER)
0
-10
IMAGINARY PART OF ADMITTANCE
140.0
-10
0
10
REAL PART OF ADMITTANCE

Figure 24f

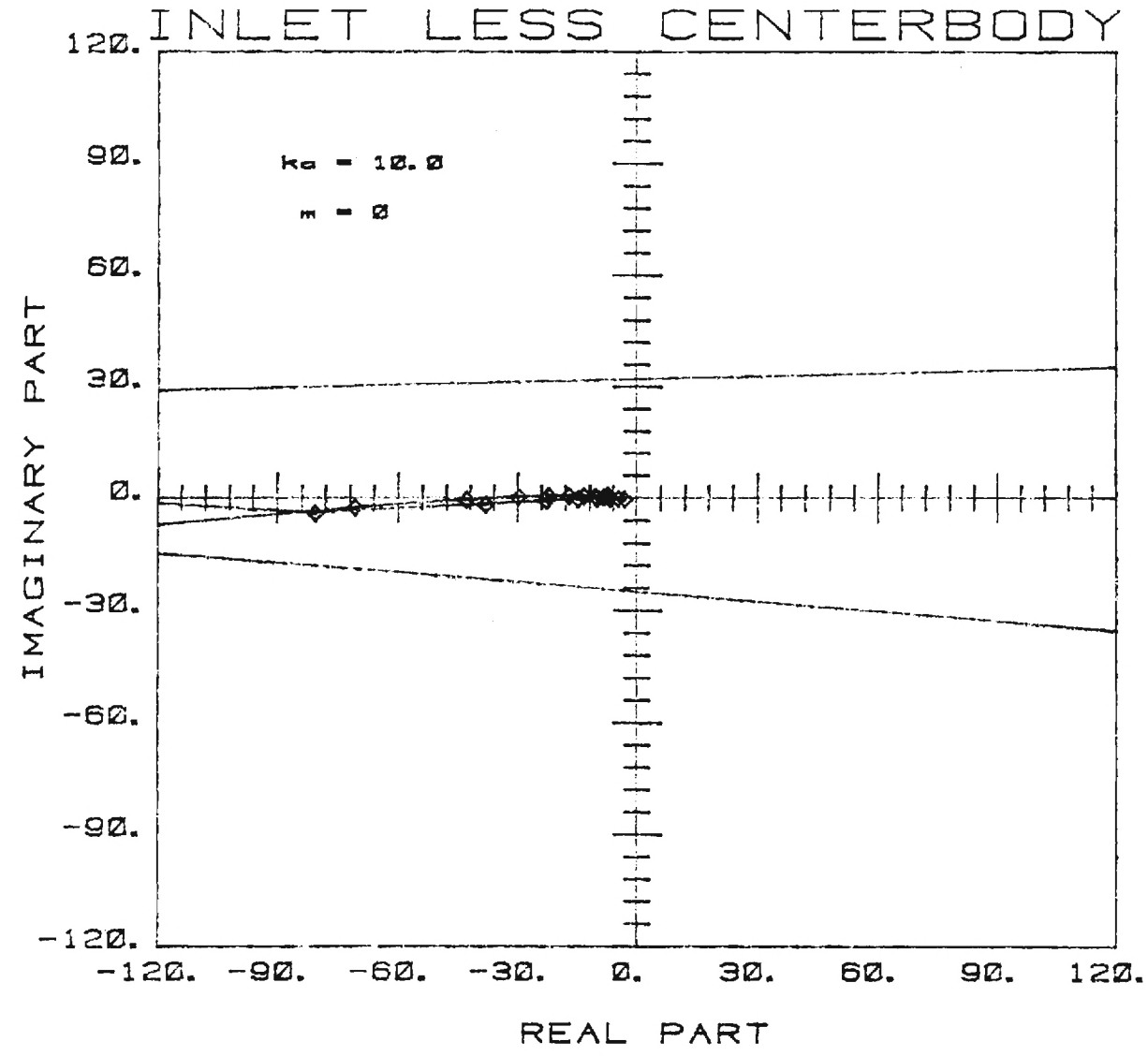

OPTIMUM ADMITTANCE DISTRIBUTION

Constant Phi on the Driver

Figure 25a

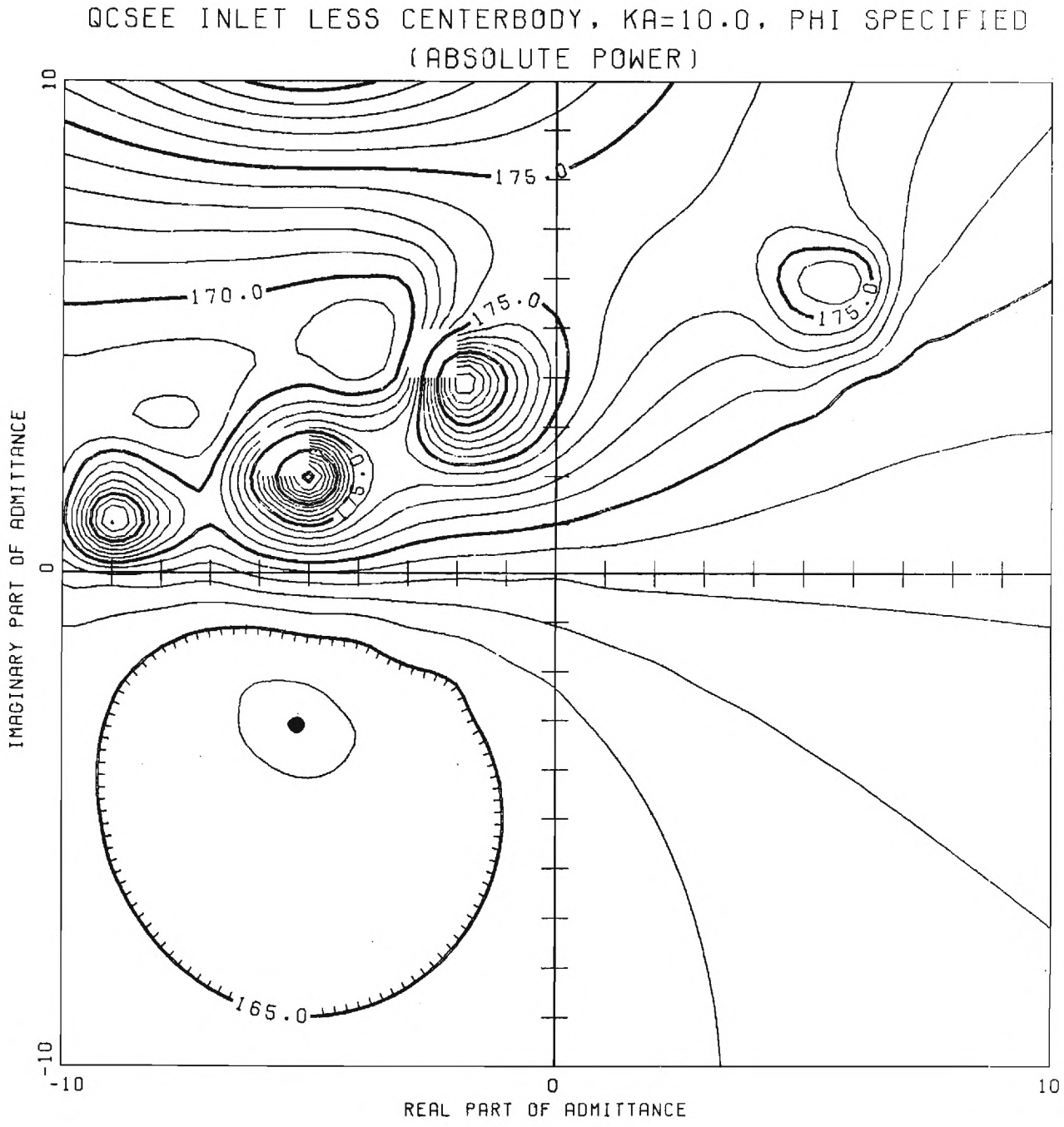
QCSEE INLET LESS CENTERBODY, KA=10.0, PHI SPECIFIED
(ABSOLUTE POWER)
175.0
170.0
175.0
175.0
165.0
IMAGINARY PART OF ADMITTANCE
REAL PART OF ADMITTANCE
10
0
-10
-10
0
10

Figure 25b

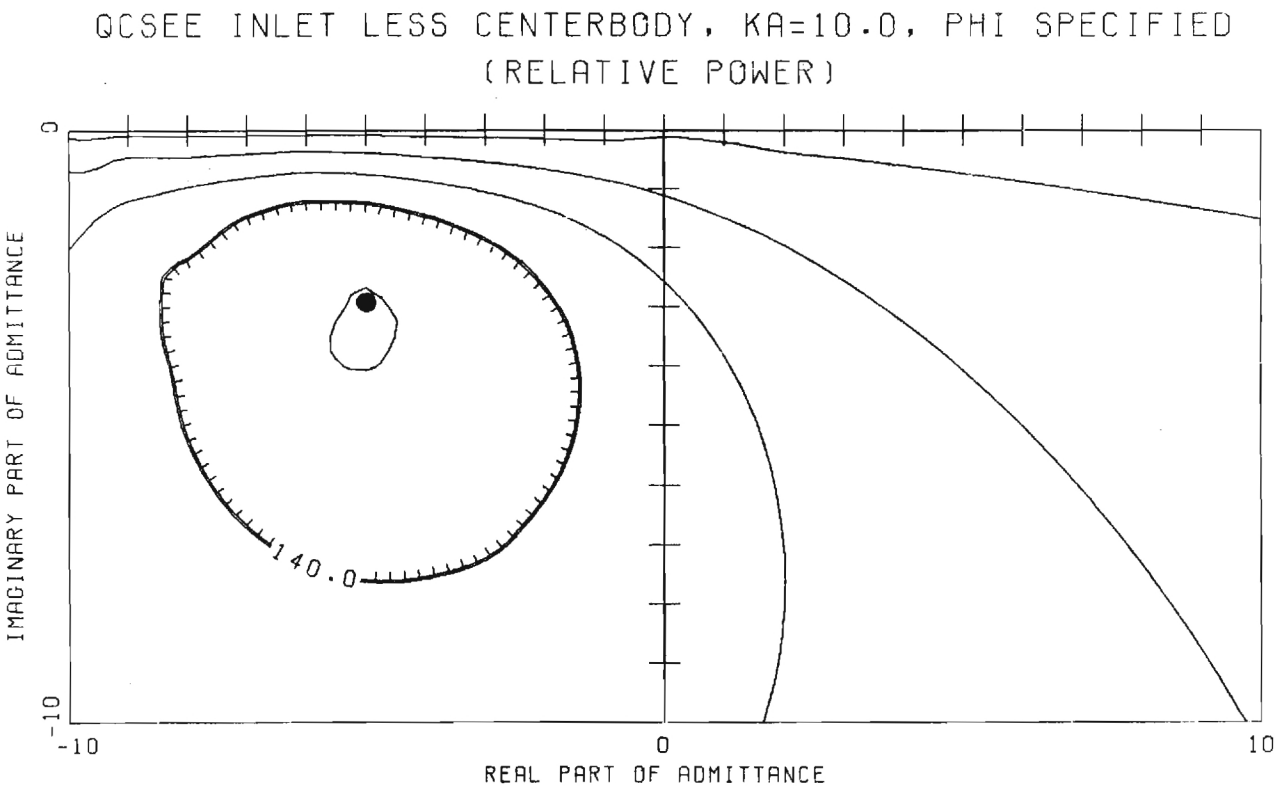
QCSEE INLET LESS CENTERBODY, KA=10.0, PHI SPECIFIED
(RELATIVE POWER)
IMAGINARY PART OF ADMITTANCE
REAL PART OF ADMITTANCE
0
-10
-10
0
10
140.0

Figure 25c

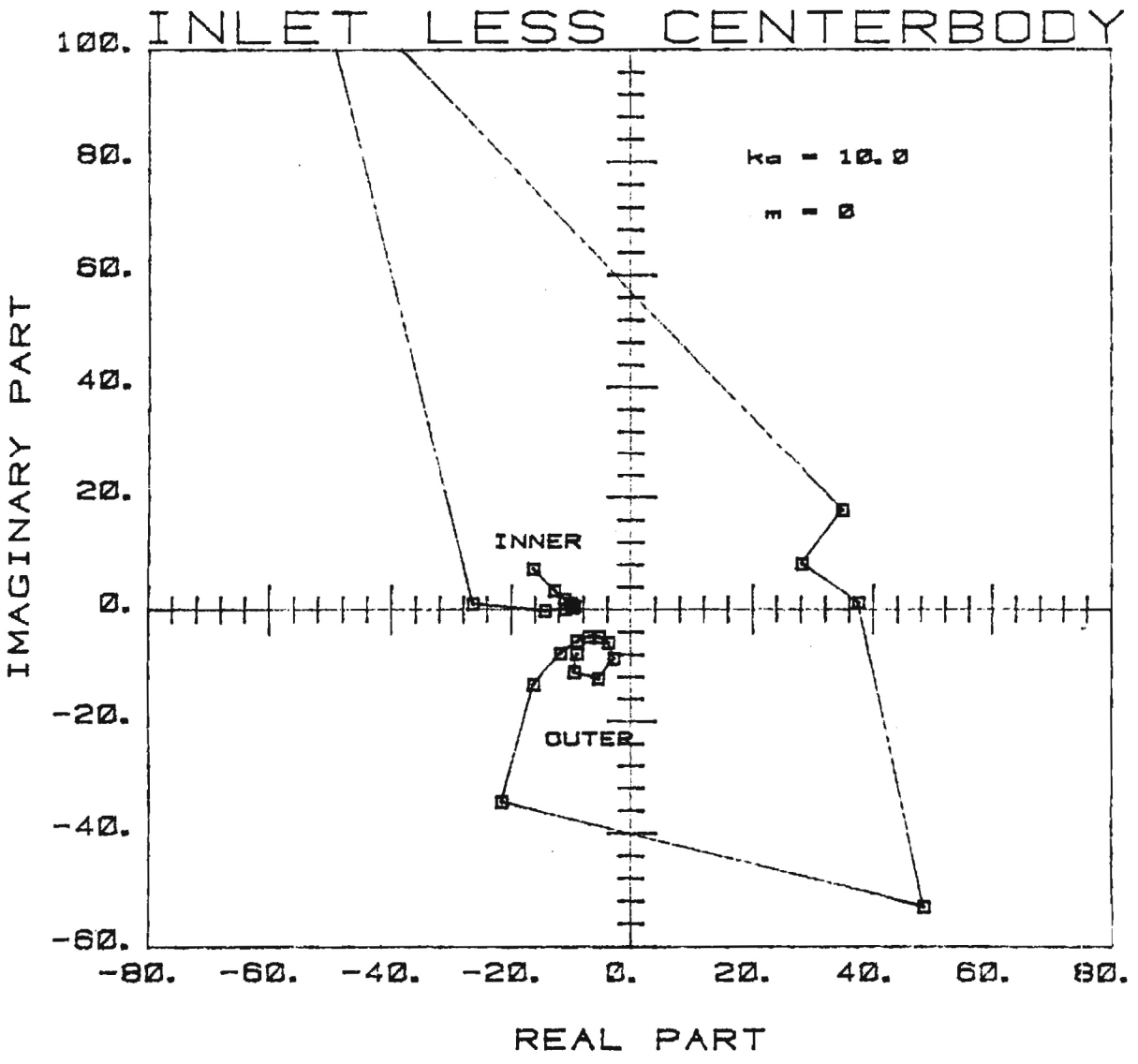

OPTIMUM ADMITTANCE DISTRIBUTION

Constant Velocity on the Driver

Figure 25d

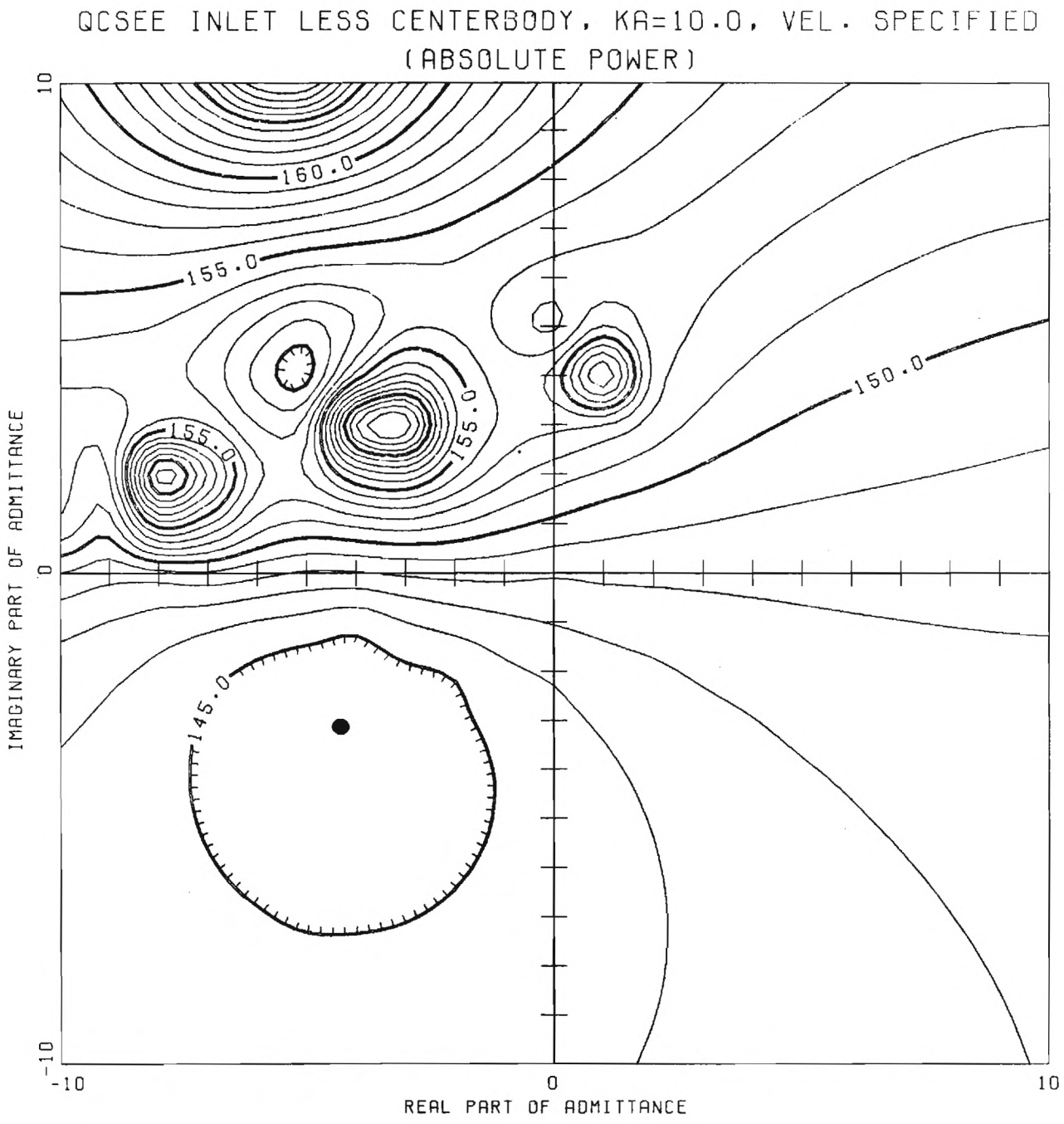
QCSEE INLET LESS CENTERBODY, KA=10.0, VEL. SPECIFIED
(ABSOLUTE POWER)
160.0
155.0
155.0
155.0
150.0
145.0
10
0
-10
-10
0
10
IMAGINARY PART OF ADMITTANCE
REAL PART OF ADMITTANCE

Figure 25e

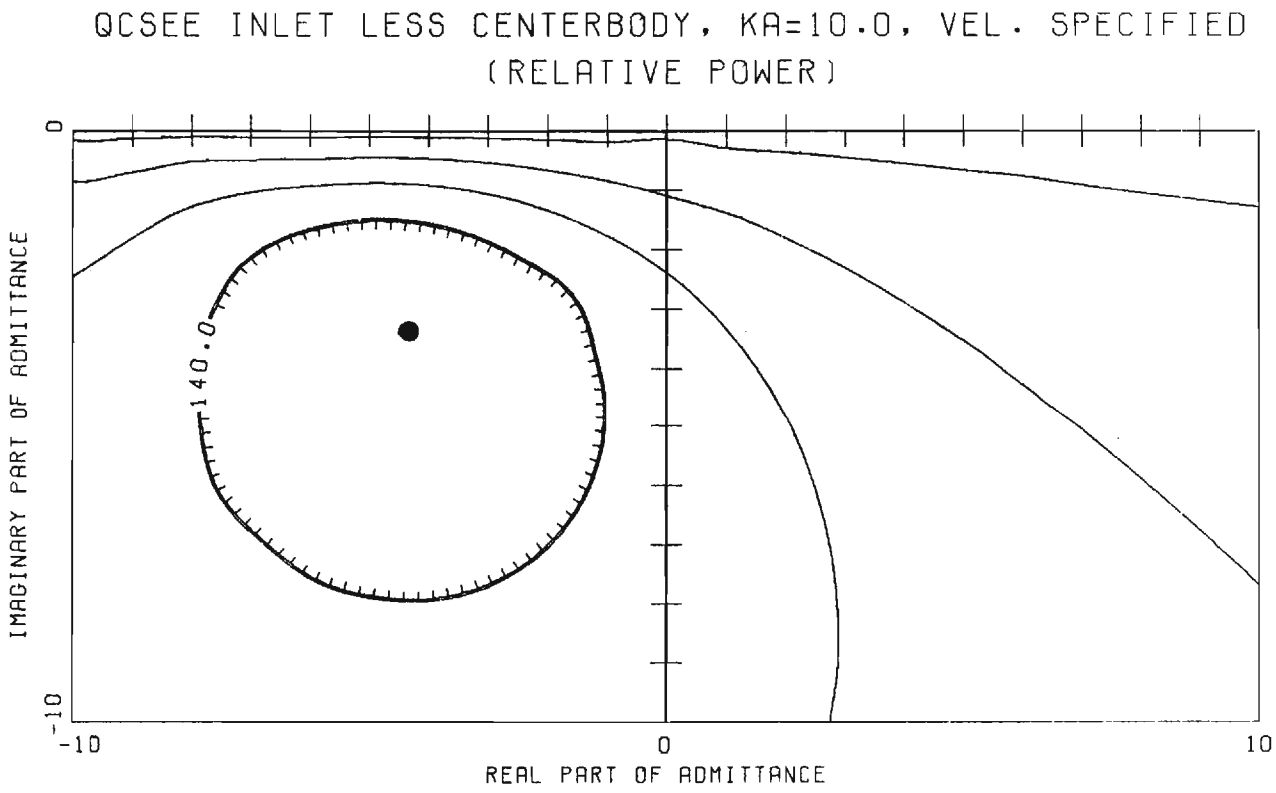
QCSEE INLET LESS CENTERBODY, KA=10.0, VEL. SPECIFIED
(RELATIVE POWER)
0
-10
IMAGINARY PART OF ADMITTANCE
140.0
-10
0
10
REAL PART OF ADMITTANCE

Figure 25f